JSCSEN 76(1)1–153(2011)

International Year of CHEMISTRY 2011

Journal of the Serbian Chemical Society

Electronic Version

VOLUME 76

No 1

BELGRADE 2011

Available on line at

www.shd.org.rs/JSCS/

The full search of JSCS is available through

DOAJ DIRECTORY OF OPEN ACCESS JOURNALS

www.doaj.org

Journal of the Serbian Chemical Society
JSCS-info@shd.org.rs • www.shd.org.rs/JSCS

J. Serb. Chem. Soc. Vol. 76, No. 1 (2011)

CONTENTS

Organic Chemistry

R. S. Kumar, *A. Idhayadhulla*, *A. J. A. Nasser* and *J. Selvin*: Synthesis and antimicrobial activity of a new series of 1,4-dihydropyridine derivatives 1

B. Mohtat, *H. Djahaniani*, *I. Yavari* and *K. Naderi*: A three-component synthesis of functionalized ketenimines by the reaction of alkyl isocyanides and dialkyl acetylenedicarboxylates in the presence of 2-quinolinol..... 13

A. Chaskar, *V. Vyavhare*, *V. Padalkar*, *K. Phatangare* and *H. Deokar*: An environmentally benign one-pot synthesis of 1,2-dihydro-1-aryl-3*H*-naphth[1,2-*e*][1,3]oxazin-3-one derivatives catalysed by phosphomolybdic acid 21

Biochemistry and Biotechnology

A. Ćirić, *A. Karioti*, *J. Glamočlija*, *M. Soković* and *H. Skaltsa*: Antimicrobial activity of secondary metabolites isolated from *Centaurea spruneri* Boiss. & Heldr. 27

I. E. Orhan, *F. Tosun*, *U. Tamer*, *A. Duran*, *B. Alan* and *A. F. Kök*: Quantification of genistein and daidzein in two endemic *Genista* species and their antioxidant activity ... 35

D. Jevremović, *V. Kojić*, *G. Bogdanović*, *T. Puškar*, *D. Eggbeer*, *D. Thomas* and *R. Williams*: A selective laser melted Co–Cr alloy used for the rapid manufacture of removable partial denture frameworks – initial screening of biocompatibility 43

Inorganic Chemistry

I. Ivanović, *S. Grgurić-Šipka*, *N. Gligorijević*, *S. Radulović*, *A. Roller*, *Ž. Lj. Tešić* and *B. K. Keppler*: X-Ray structure and cytotoxic activity of a picolinate ruthenium(II)–arene complex 53

M. Asadi, *H. Sepehrpour* and *K. Mohammadi*: Tetradentate Schiff base ligands of 3,4-diaminobenzophenone: Synthesis, characterization and thermodynamics of complex formation with Ni(II), Cu(II) and Zn(II) metal ions 63

A. S. Ramasubramanian, *B. R. Bhat*, *R. Dileep* and *S. Rani*: Transition metal complexes of 5-bromosalicylidene-4-amino-3-mercapto-1,2,4-triazine-5-one: synthesis, characterization, catalytic and antibacterial studies 75

Theoretical chemistry

D. M. Duda-Seiman, *S. Avram*, *S. Mancaş*, *V. Careja*, *C. Duda-Seiman*, *M. V. Putz* and *D. Ciubotariu*: MTD–CoMSIA modelling of HMG-CoA reductase inhibitors 85

Physical Chemistry

S. Lazarević, *I. Janković-Častvan*, *Ž. Radovanović*, *B. Potkonjak*, *Dj. Janaćković* and *R. Petrović*: Sorption of Cu^{2+} and Co^{2+} from aqueous solutions onto sepiolite: an equilibrium, kinetic and thermodynamic study 101

Electrochemistry

X. Liu, *B. Li* and *C. Li*: Sensitive determination of dihydronicotinamide adenine dinucleotide and ethanol with a nano-porous carbon electrode 113

S. Chen: In-line digital holography for the study of localized corrosion and dynamic processes of electrochemical reactions (Extended abstract)..... 125

Thermodynamics

K. Rajagopal and *S. S. Jayabalakrishnan*: A volumetric and viscometric study of 4-aminobutyric acid in aqueous solutions of metformin hydrochloride at 308.15, 313.15 and 318.15 K..... 129

Environmental

S. Đogo, *S. Ražić*, *D. Manojlović* and *L. Slavković*: Analysis of the bioavailability of Cr(III) and Cr(VI) based on the determination of chromium in *Mentha piperita* by graphite furnace atomic absorption spectrometry 143

Published by the Serbian Chemical Society
Karnegijeva 4/III, 11000 Belgrade, Serbia
Printed by the Faculty of Technology and Metallurgy
Karnegijeva 4, P.O. Box 35-03, 11120 Belgrade, Serbia
Available online at www.shd.org.rs/JSCS/

Journal of the Serbian Chemical Society
JSCS-info@shd.org.rs • www.shd.org.rs/JSCS
J. Serb. Chem. Soc. *76* (1) 1–11 (2011)
JSCS–4093
UDC 547.823+542.913:615.28–188
Original scientific paper

Synthesis and antimicrobial activity of a new series of 1,4-dihydropyridine derivatives

RADHAKRISHNAN SURENDRA KUMAR[1], AKBAR IDHAYADHULLA[1], ABDUL JAMAL ABDUL NASSER[1]* and JOSEPH SELVIN[2]

[1]*P. G. & Research, Department of Chemistry, Jamal Mohamed College, Tiruchirappalli-620 020, Tamil Nadu and* [2]*Department of Microbiology, Bharathidasan University, Tiruchirappalli-620024, Tamil Nadu, India*

(Received 27 November 2009, revised 21 July 2010)

Abstract: A series of 1,4-dihydropyridine derivatives (**1a**–**g**) were prepared from Hantzsch syntheses. The compounds **1a**–**g** were reacted with thiosemicarbazide to give the new series of compounds **2a**–**g**. IR, ^{1}H-NMR, ^{13}C-NMR, mass spectral and elemental analysis confirmed the synthesized compounds. The synthesized compounds were also screened for their antimicrobial activity.

Keywords: 1,4-dihydropyridine; thiosemicarbazide; condensation; antimicrobial activity.

INTRODUCTION

1,4-Dihydropyridine derivatives are of interest because of their biological activity, such as vasodilators, antihypertensive,[1–4] anti-inflammatory,[5] antihypoxic and anti-ischemic agents[6] and calcium channel modulators of the nifedipine type.[7] Recently, it was reported that the amide group was involved in the 3,5-position of 1,4-dihydropyridine derivatives and it exhibited pharmacological effects.[8,9] Basically thiosemicarbazone containing heterocyclics have significant biological activity, such as antitumour, fungicidal, bactericidal, anti-inflammatory and antiviral activities.[10–13] In view of these observations, it was decided to synthesize a new series of 1,4-dihydropyridine derivatives (**2a**–**g**) and screen them for their level of antimicrobial activity.

RESULTS AND DISCUSSION

Chemistry

The series of diethyl 2,6-dimethyl-4-substituted phenyl-1,4-dihydropyridine--3,5-dicarboxylate (**1a**–**f**) are already published in literature[14–19], but not their

* Corresponding author. E-mail: jamal_abdulchem@ymail.com
doi: 10.2298/JSC091127003K

antimicrobial screening. On the other hand the syntheses and antimicrobial screening of compound **1g** has not been published. The compounds **1a**–**g** were reacted with thiosemicarbazide to give 4-aryl-2,6-dimethyl-1,4-dihydropyridine--3,5-dicarboxylic acid, 3,5-bis[2-(aminothioxomethyl)hydrazide] (**2a**–**g**) by the hydrazinolysis method[20,21] (Scheme 1).

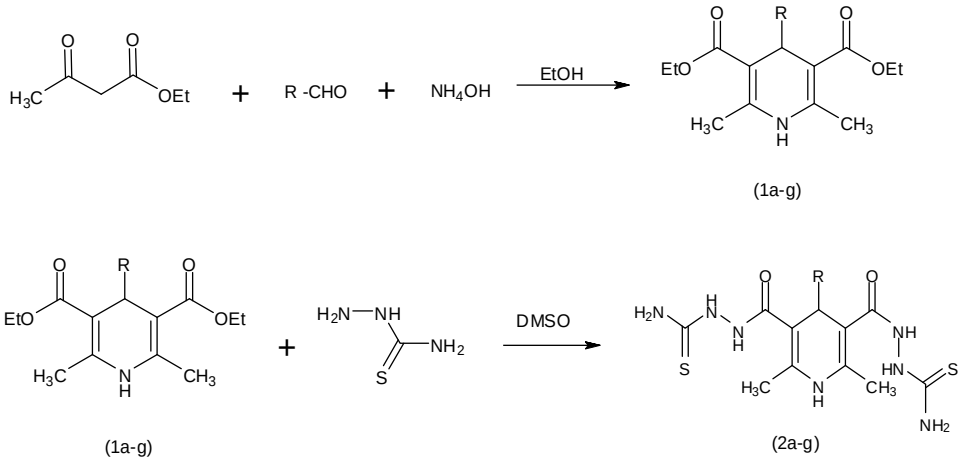

1a, 2a : R = 2-Furyl

1b, 2b : R = -Ph

1c, 2c : R = 4-Cl-C_6H_4

1d, 2d : R = 4-OH-C_6H_4

1e, 2e : R = 4-NO_2-C_6H_4

1f, 2f : R = 4-CH_3O-C_6H_4

1g, 2g : R = 4-$(CH_3)_2N$-C_6H_4

Scheme 1. Synthesis of the compounds **2a**–**g**.

Analytic and spectral data

*Diethyl 4-(furan-2-yl)-2,6-dimethyl-1,4-dihydropyridine-3,5-dicarboxylate (**1a**)*. Yield: 75 %; m.p.158 °C; Anal. Calcd. for $C_{17}H_{21}NO_5$: C, 63.94; H, 6.63; N, 4.39 %. Found: C, 63.98; H, 6.67; N, 4.35 %. IR (KBr, cm^{-1}): 3349 (N–H str), 3030 (Ar–H), 2940 (C–H str of CH_3), 1745 (C=O, ester), 812 (Ar–H). ^{1}H-NMR (300 MHz, DMSO-d_6, δ / ppm): 8.20 (1H, *s*, NH of pyridine ring), 7.27 (1H, *s*, furyl ring), 6.10–6.27 (2H, *d*, furyl ring), 4.72 (1H, *s*, C4–H), 4.20 (4H, *q*, C3––C**H**$_2$CH$_3$ and C5–OC**H**$_2$CH$_3$), 2.31 (6H, *s*, C2–CH$_3$ and C6–CH$_3$), 1.34 (6H, *t*, C2–OCH$_2$C**H**$_3$ and C6–OCH$_2$C**H**$_3$). ^{13}C-NMR (300 MHz, DMSO-d_6, δ / ppm): 142.1, 110.6, 106.7, 152.5 (furyl ring), 151.8 (C2,6), 33.2 (C4), 102.3 (3,5-

-**C**OOCH$_2$CH$_3$), 61.1(3,5-COO**C**H$_2$CH$_3$), 14.9 (3,5-COOCH$_2$**C**H$_3$), 18.1 (2,6--**C**H$_3$). MS (*m*/*z* (relative abundance, %)): 320.15 (M^++1, 40.2), 275.29, 231.24, 203.23, 173.22, 161.20, 147.2, 134.12, 82.10.

*Diethyl 2,6-dimethyl-4-phenyl-1,4-dihydropyridine-3,5-dicarboxylate (**1b**)*. Yield: 66 %; m.p. 253 °C; Anal. Calcd. for $C_{19}H_{23}NO_4$: C, 69.28; H, 7.04; N, 4.25 %. Found: C, 69.24; H, 7.07; N, 4.28 %. IR (KBr, cm^{-1}): 3350 (N–H str), 3034 (Ar–H), 2953 (C–H str of CH_3), 1755 (C=O, ester), 802 (Ar–H). ^{1}H-NMR (300 MHz, DMSO-d_6, δ / ppm): 8.25 (1H, *s*, NH of pyridine ring), 7.33–7.27 (5H, *m*, Ph-ring), 4.70 (2H, *s*, C4–H), 4.22 (4H, *q*, C3–OC**H**$_2$CH$_3$ and C5––OC**H**$_2$CH$_3$), 2.28 (6H, *s*, C2–CH$_3$ and C6-CH$_3$), 1.32 (6H, *t*, C2–OCH$_2$C**H**$_3$ and C6–OCH$_2$C**H**$_3$). ^{13}C-NMR (300 MHz, DMSO-d_6, δ / ppm): 125.1, 128.4, 127.1, 144.8 (phenyl ring), 150.7 (C2,6), 101.9 (3,5-**C**OOCH$_2$CH$_3$), 62.1 (3,5--COO**C**H$_2$CH$_3$), 44.1 (C4), 19.1 (2,6-**C**H$_3$), 15.4 (3,5-COOCH$_2$**C**H$_3$). MS (*m*/*z* (relative abundance, %)): 330.39 (M^++1, 38.9), 285.33, 241.28, 185.26, 171.23, 157.21, 81.11, 68.11.

Diethyl 4-(4-chlorophenyl)-2,6-dimethyl-1,4-dihydropyridine-3,5-dicarboxylate (**1c**). Yield: 57 %; m.p. 240 °C. Anal. Calcd. for $C_{19}H_{22}ClNO_4$: C, 62.72; H, 6.09; N, 3.85 %. Found: C, 62.75; H, 6.07; N, 3.81 %. IR (KBr, cm^{-1}): 3332 (N–H str), 3074 (Ar–H), 2942 (C–H str of CH_3), 1741 (C=O, ester), 812 (Ar–H), 610 (C–Cl), 787 (Ar–H). ^{1}H-NMR (300 MHz, DMSO-d_6, δ / ppm): 8.31 (1H, *s*, NH of pyridine ring), 7.36–7.19 (5H, *m*, Ph-ring), 4.76 (1H, *s*, C4–H), 4.18 (4H, *q*, 3C–OC**H**$_2$CH$_3$ and C5–OC**H**$_2$CH$_3$), 2.21 (6H, *s*, C2–CH$_3$ and C6–CH$_3$), 1.34 (6H, *t*, C2–OCH$_2$C**H**$_3$ and C6–OCH$_2$C**H**$_3$). ^{13}C-NMR (300 MHz, DMSO-d_6, δ / / ppm): 131.4, 128.1, 130.8, 142.5 (Ph–Cl), 152.5 (C2,6), 34.6 (C4), 103.9 (3,5--**C**OOCH$_2$CH$_3$), 60.3 (3,5-COO**C**H$_2$CH$_3$), 15.2 (3,5-COOCH$_2$**C**H$_3$), 18.6 (2,6--CH$_3$). MS (*m*/*z* (relative abundance, %)): 364.90 (M^++1, 21.2), 275.57, 219.70, 185.26, 171.23, 157.21, 144.21

*Diethyl 4-(4-hydroxyphenyl)-2,6-dimethyl-1,4-dihydropyridine-3,5-dicarboxylate (**1d**)*. Yield: 56 %; m.p. 240 °C; Anal. Calcd. for $C_{19}H_{23}NO_5$: C, 69.07; H, 6.71; N, 4.06 %. Found: C, 9.03; H, 6.75; N, 4.01 %. IR (KBr, cm^{-1}): 3342 (N–H str), 3024 (Ar–H), 2922 (C–H str of CH_3), 1764 (C=O, ester), 1447 (C–OH), 814 (Ar–H). ^{1}H-NMR (300 MHz, DMSO-d_6, δ / ppm): 9.47 (1H, *s*, C–OH), 8.41 (1H, *s*, NH of pyridine ring), 6.34–7.07 (4H, *m*, Ph-ring), 4.67 (1H, *s*, C4–H), 4.28 (4H, *q*, C3–OC**H**$_2$CH$_3$ and C5–OC**H**$_2$CH$_3$), 2.12 (6H, *s*, C2–CH$_3$ and C6–CH$_3$), 1.28 (6H, *t*, C2–OCH$_2$C**H**$_3$ and C6–OCH$_2$C**H**$_3$). ^{13}C-NMR (300 MHz, DMSO--d_6, δ / ppm): 155.6, 116.2, 131.2, 138.2 (Ph-OH), 151.4 (C2,6), 44.9 (C4), 101.4 (3,5-**C**OOCH$_2$CH$_3$), 62.3 (3,5-COO**C**H$_2$CH$_3$), 14.1(3,5-COOCH$_2$**C**H$_3$), 18.4 (2,6-CH$_3$). MS (*m*/*z* (relative abundance, %)): 346.81 (M^++1, 12.3), 310.45, 257.81, 201.48, 187.22, 173.28, 157.21.

*Diethyl 2,6-dimethyl-4-(4-nitrophenyl)-1,4-dihydropyridine-3,5-dicarboxylate (**1e**)*. Yield: 69 %; m.p.197 °C; Anal. Calcd. for $C_{19}H_{22}N_2O_6$: C, 60.95; H,

7.48; N, 7.48 %. Found: C, 60.91; H, 7.42; N, 7.41 %. IR (KBr, cm^{-1}): 3354 (N–H str), 3037 (Ar–H), 2973 (C–H str of CH_3), 1762 (C=O, ester), 1536 (C–NO_2), 812 (Ar–H). ^{1}H-NMR (300 MHz, DMSO-d_6, δ / ppm): 8.13–7.47 (4H, *m*, Ph--ring), 8.11 (1H, *s*, NH of pyridine ring), 4.79 (1H, *s*, C4–H), 4.25 (4H, *q*, C3––OC**H**$_2$CH$_3$ and C5–OC**H**$_2$CH$_3$), 2.31 (6H, *s*, C2–CH_3 and C6–CH_3), 1.37 (6H, *t*, C2–OCH$_2$C**H**$_3$ and C6–OCH$_2$C**H**$_3$); ^{13}C-NMR (300 MHz, DMSO-d_6, δ / / ppm): 144.8, 123.6, 126.9, 151.0 (Ph–NO_2), 152.2 (C2,6), 43.9 (C4), 103.2 (3,5-**C**OOCH$_2$CH$_3$), 60.8 (3,5-COO**C**H$_2$CH$_3$), 14.4 (3,5-COOCH$_2$**C**H$_3$), 18.8 (2,6-**C**H$_3$). MS (*m*/*z* (relative abundance, %)): 375.22 (M^++1, 21.2), 286.26, 185.26, 171.23, 157.21.

*Diethyl 4-(4-methoxyphenyl)-2,6-dimethyl-1,4-dihydropyridine-3,5-dicarboxylate (**1f**)*. Yield: 72 %; m.p. 197 °C; Anal. Calcd. for $C_{20}H_{25}NO_5$: C, 66.83; H, 7.01; N, 3.90 %. Found: C, 66.87; H, 7.07; N, 3.97 %. IR (KBr, cm^{-1}); 3352 (N–H str), 3026 (Ar–H), 2961 (C–H str of CH_3), 1742 (C=O, ester), 823 (Ar–H). ^{1}H--NMR (300 MHz, DMSO-d_6, δ / ppm): 8.21 (1H, *s*, NH of pyridine ring), 6.86––7.17 (5H, *m*, Ph-ring), 4.69 (1H, *s*, C4–H), 4.23 (4H, *q*, C3–OC**H**$_2$CH$_3$ and C5––OC**H**$_2$CH$_3$), 3.84 (3H, *s*, –OCH$_3$), 2.23 (6H, *s*, C2–CH_3 and C6–CH_3), 1.30 (6H, *t*, C2–OCH$_2$C**H**$_3$ and C6–OCH$_2$C**H**$_3$). ^{13}C-NMR (300 MHz, DMSO-d_6, δ / / ppm): 157.2, 114.6, 129.3, 135.9 (Ph), 158.3 (C2,6), 102.3 (3,5-**C**OOCH$_2$CH$_3$), 61.5 (3,5-COO**C**H$_2$CH$_3$), 55.7 (Ph–O**C**H$_3$), 43.6 (C4), 14.8 (3,5-COOCH$_2$**C**H$_3$), 18.0 (2,6-CH_3). MS (*m*/*z* (relative abundance, %)): 360.44 (M^++1, 41.2), 331.81, 287.31, 243.25, 187.23, 157.21.

*Diethyl 4-(4-(dimethylamino)phenyl)-2,6–dimethyl-1,4-dihydropyridine-3,5--dicarboxylate (**1g**)*. Yield: 56 %; m.p. 227 °C; Anal. Calcd. for $C_{21}H_{28}N_2O_4$: C, 67.72; H,7.58; N, 7.52 %. Found: C, 67.77; H, 7.52; N, 7.58 %. IR (KBr, cm^{-1}): 3348 (N–H str), 3027 (Ar–H), 2956 (C–H str of CH_3), 1761 (C=O, ester), 808 (Ar–H). ^{1}H-NMR (300 MHz, DMSO-d_6, δ / ppm): 8.37 (1H, *s*, NH of pyridine ring), 7.28–7.21 (5H, *m*, Ph-ring), 4.70 (2H, *s*, C4–H), 4.22 (4H, *q*, C3––OC**H**$_2$CH$_3$ and C5–OC**H**$_2$CH$_3$), 3.12 (6H, *s*, –N(CH$_3$)$_2$), 2.28 (6H, *s*, C2–CH_3 and C6–CH_3), 1.32 (6H, *t*, C2–OCH$_2$C**H**$_3$ and C6–OCH$_2$C**H**$_3$). ^{13}C-NMR (300 MHz, DMSO-d_6, δ / ppm): 128.3, 112.9, 148.5, 133.9 (Ph), 151.8 (C2,6), 43.8 (C4), 102.8 (3,5-**C**OOCH$_2$CH$_3$), 60.5 (3,5-COO**C**H$_2$CH$_3$), 40.8 (–N(**C**H$_3$)$_2$), 13.9 (3,5-COOCH$_2$**C**H$_3$), 18.9 (2,6-**C**H$_3$). MS (*m*/*z* (relative abundance, %)): 373.44 (M^++1, 51.8), 284.35, 228.33, 185.26, 171.23, 157.21.

*4-(Furan-2-yl)-2,6-dimethyl-1,4-dihydropyridine-3,5-dicarboxylic acid, 3,5--bis[2-(aminothioxomethyl)hydrazide] (**2a**)*. Yield: 63 %; m.p. 161 °C; Anal. Calcd. for $C_{15}H_{19}N_7O_3S_2$: C, 44.00; H, 4.68; N, 23.94 ; S, 15.66 %. Found: C, 44.06; H, 4.62; N, 23.97; S, 15.62 %. IR (KBr, cm^{-1}): 3372 (N–H), 3200 (NH––C=O), 3218 (NH_2), 3021 (Ar–H), 1260 (C=S), 1091 (N–C–N), 828 (Ar–H). ^{1}H--NMR (300 MHz, $CDCl_3$, δ / ppm): 9.62 (2H, *s*, NH_2), 8.43 (1H, *s*, NH of pyridine ring), 8.09 (1H, *d*, C3–CONH and C5–CONH), 7.51 (1H, *d*, 5'-H-furyl),

6.24 (1H, *d*, 4'-H-furyl), 6.24 (1H, *d*, 3'-H-furyl); 5.17 (2H, *s*, C4–H), 2.28 (6H, *s*, C2–CH_3 and C6–CH_3), 2.02 (1H, *d*, NHCS). ^{13}C-NMR (300 MHz, $CDCl_3$, δ / / ppm): 111.8, 108.3, 143.2, 152.8 (C4 in furyl ring), 105.3 (C3,5 in pyridine ring), 166.2 (C=O), 182.1 (C=S), 148.9 (C2,6 in pyridine ring), 35.3 (C4 in pyridine ring), 18.2 (C2,6–CH_3 in pyridine ring); MS (*m/z*, (relative abundance, %)): 410 (M^++1, 30.2), 291.30, 161.27, 175.22, 147.12, 81.11.

*2,6-Dimethyl-4-phenyl-1,4-dihydropyridine-3,5-dicarboxylic acid, 3,5-bis[2--(aminothioxomethyl)hydrazide] (**2b**)*. Yield: 53 %; m.p. 192 °C; Anal. Calcd. for $C_{17}H_{21}N_7O_2S_2$: C, 48.67; H, 5.50; N, 23.37; S, 15.29 %. Found: C, 48.64; H, 5.57; N, 23.31; S, 15.34 %. IR (KBr, cm^{-1}): 3370 (N–H), 3175 (NH–C=O), 3218 (NH_2), 3034 (Ar–H), 1718 (C=O), 1260 (C=S), 1091 (N–C–N), 808 (Ar–H). ^{1}H--NMR (300 MHz, $CDCl_3$, δ / ppm): 9.60 (2H, *s*, NH_2), 8.40 (1H, *s*, NH of pyridine ring), 8.11 (1H, *d*, C3–CONH and C5–CONH), 7.39–7.22 (5H, *m*, Ph--ring), 5.20 (2H, *s*, C4–H), 2.37 (6H, *s*, C2–CH_3 and C6–CH_3), 2.12 (1H, *d*, –NHCS); ^{13}C-NMR (300 MHz, $CDCl_3$, δ / ppm): 131.3, 128.5, 130.9, 141.8 (C4 in furyl ring), 106.8 (C3,5 in pyridine ring), 164.6 (C=O), 182.8 (C=S), 147.9 (C2,6 in pyridine ring), 34.6 (C4 in pyridine ring), 18.9 (2,6-CH_3 in pyridine ring); MS (*m/z*,(relative abundance, %)): 420.20 (M^++1, 20.1), 301.34, 241.28, 185.2, 157.21, 81.11.

*4-(4-Chlorophenyl)-2,6-dimethyl-1,4-dihydropyridine-3,5-dicarboxylic acid, 3,5-bis[2-(aminothioxomethyl)hydrazide] (**2c**)*. Yield: 68 %; m.p. 194 °C; Anal. Calcd. for $C_{17}H_{20}ClN_7O_2S_2$: C, 4.98; H, 4.40; N, 21.60; S, 14.14 %. Found: C, 44.92; H, 4.46; N, 21.64; S, 14.18 %. IR (KBr, cm^{-1}): 3325 (N–H), 3231 (NH_2), 3198 (NH–C=O), 3024 (Ar–H), 1265 (C=S), 1707(C=O), 1097 (N–C–N), 810 (Ar–H), 623 (C–Cl). ^{1}H-NMR (300 MHz, $CDCl_3$, δ / ppm): 9.41 (2H, *s*, NH_2), 8.41 (1H, *s*, NH of pyridine ring), 8.11 (1H, *d*, C3–CONH and C5–CONH), 7.38–7.14 (5H, *m*, Ph-ring), 5.10 (2H, *s*, C4–H), 2.45 (6H, *s*, C2–CH_3 and C6–CH_3), 2.08 (1H, *d*, –NHCS). ^{13}C-NMR (300 MHz, $CDCl_3$, δ / ppm): 128.7, 108.3, 143.2, 152.8 (C4 in furyl ring), 105.3 (C3,5 in pyridine ring), 166.2 (C=O), 182.1 (C=S), 148.9 (C2,6 in pyridine ring), 39.3 (C4 in pyridine ring), 18.2 (2,6–CH_3 in pyridine ring); MS (*m/z* (relative abundance, %)): 454.12 (M^++1, 12.3), 335.78, 275.73, 219.70, 157.21, 81.11.

*4-(4-Hydroxyphenyl)-2,6-dimethyl-1,4-dihydropyridine-3,5-dicarboxylic acid, 3,5-bis[2-(aminothioxomethyl)hydrazide] (**2d**)*. Yield: 74 %; m.p. 201 °C; Anal. Calcd. for $C_{17}H_{21}N_7O_3S_2$: C, 46.88; H, 22.51; N, 4.86; S, 14.72 %. Found: C, 46.81; H, 22.57; N, 4.81; S, 14.77 %. IR (KBr, cm^{-1}): 3342 (N–H), 3220 (NH_2), 3192 (NH–C=O), 3028 (Ar–H), 1472 (C–OH), 1717 (C=O), 1242 (C=S), 1091 (N––C–N). ^{1}H-NMR ($CDCl_3$, δ / ppm): 9.71 (2H, *s*, NH_2), 9.41 (1H, *s*, OH), 8.64 (1H, *s*, NH of pyridine ring), 8.01 (1H, *d*, C3–CONH and C5–CONH), 7.33––7.27 (5H, *m*, Ph-ring), 5.11 (2H, *s*, C4–H), 2.25 (6H, *s*, C2–CH_3 and C6–CH_3), 2.02 (1H, *d*, –NHCS). ^{13}C-NMR (300 MHz, $CDCl_3$, δ / ppm): 155.8, 137.1,

130.3, 114.2 (C4 in 4-OH-phenyl ring), 102.9 (3,5-C in pyridine ring), 164.9 (C=O), 184.6 (3,5 C=S), 148.1(C2,6 in pyridine ring), 43.8 (C4 in pyridine ring), 19.2 (2,6–CH_3 in pyridine ring). MS (*m*/*z* (relative abundance, %)): 435.52 (M^++1, 27.2), 257.28, 201.26, 173.21, 157.21, 81.11.

*2,6-Dimethyl-4-(4-nitrophenyl)-1,4-dihydropyridine-3,5-dicarboxylic acid, 3,5-bis[2-(aminothioxomethyl)hydrazide] (**2e**)*. Yield: 76 %; m.p. 190 °C; Anal. Calcd. for $C_{17}H_{20}N_8O_4S_2$: C, 43.96; H, 4.34; N, 24.12; S, 15.81 %. Found: C, 43.91; H, 4.38; N, 24.17; S, 15.87 %. IR (KBr, cm^{-1}): 3310 (N–H), 3241 (NH_2), 3218 (NH–C=O), 3041 (Ar–H), 1710 (C=O), 1530 (C–NO_2), 1272 (C=S), 1094 (N–C–N). ^{1}H-NMR (300 MHz, $CDCl_3$, δ / ppm): 9.77 (2H, *s*, NH_2), 8.60 (1H, *s*, NH of pyridine ring), 8.15 (1H, *d*, C3–CONH and C5–CONH), 7.42–7.18 (5H, *m*, Ph-ring), 5.17 (2H, *s*, C4–H), 2.31 (6H, *s*, C2–CH_3 and C6–CH_3), 2.08 (1H, *d*, –NHCS). ^{13}C-NMR (300 MHz, $CDCl_3$, δ / ppm): 143.2, 123.7, 126.7 (C4 in 4--NO_2-phenyl ring), 102.9 (3,5-C in pyridine ring), 164.9 (C=O), 181.9 (C=S), 149.9 (2,6-C in pyridine ring), 44.5 (4-C in pyridine ring), 19.7(2,6-C–**C**H_3 in pyridine ring). MS (*m*/*z* (relative abundance, %)): 465.52 (M^++1, 12.78), 346.34, 286.20, 258.23, 230.21, 202.20, 81.11.

*4-(4-Methoxyphenyl)-2,6-dimethyl-1,4-dihydropyridine-3,5-dicarboxylic acid, 3,5-bis[2-(aminothioxomethyl)hydrazide] (**2f**)*. Yield: 66 %; m.p. 210 °C; Anal. Calcd. for $C_{18}H_{23}N_7O_3S_2$: C, 48.09; H, 5.16; N, 21.81; S, 14.27 %. Found: C, 48.05; H, 5.19; N, 21.88; S,14.21 %. IR (KBr, cm^{-1}): 3323 (N–H), 3251 (NH–C=O), 3231 (NH_2), 3034 (Ar–H), 1717 (C=O), 1251 (C=S), 1091 (N-C-N), 808 (Ar–H). ^{1}H-NMR (300 MHz, DMSO-d_6, δ / ppm): 9.82 (2H, *s*, NH_2), 8.57 (1H, *s*, N–H of pyridine ring), 8.05 (1H, *d*, C3–CONH and C5–CONH), 7.33–7.27 (5H, *m*, Ph-ring), 5.21 (2H, *s*, C4–H), 3.81 (3H, *s*, –OCH_3), 2.25 (6H, *s*, C2–CH_3 and C6–CH_3), 2.10 (1H, *d*, –NHCS). ^{13}C-NMR (300 MHz, $CDCl_3$, δ / ppm): 111.8, 108.3, 143.2, 152.8 (C4 in 4-CH_3O-phenyl ring), 105.3 (3,5-C in pyridine ring), 166.2 (3,5-C=O), 181.7 (3,5-C=S), 147.7 (2,6-C in pyridine ring), 44.7 (C4 in pyridine ring), 18.8 (2,6-CH_3 in pyridine ring), 55.9 (–OCH_3); MS (*m*/*z*, (relative abundance, %)): 450.21 (M^++1, 29.12), 331.36, 271.31, 243.25, 215.29, 185.26, 157.21.

*4-[4-(Dimethylaminophenyl]-2,6-dimethyl-1,4-dihydropyridine-3,5-dicarboxylic acid, 3,5-bis[2-(aminothioxomethyl)hydrazide] (**2g**)*. Yield: 61 %; m.p. 205 °C; Anal. Calcd. for $C_{19}H_{26}N_8O_2S_2$: C, 49.33; H, 5.67; N, 24.22; S, 13.86 %. Found: C, 49.37; H, 5.69; N, 24.27; S, 13.82 %. IR (KBr, cm^{-1}): 3320 (N–H), 3211 (NH_2), 3118 (NH–C=O), 3021 (Ar–H), 1712 (C=O), 1248 (C=S), 1091 (N––C–N), 812 (Ar–H). ^{1}H-NMR (300 MHz, DMSO-d_6, δ / ppm): 9.66 (2H, *s*, NH_2), 8.52 (1H, *s*, NH of pyridine ring), 8.03 (1H, *d*, C3–CONH and C5––CONH), 6.62–7.07 (4H, *m*, Ph-ring), 5.13 (2H, *s*, C4–H), 3.06 (1H, *s*, –N(CH_3)$_2$), 2.19 (6H, *s*, C2–CH_3 and C6–CH_3), 2.07 (1H, *d*, NHCS). ^{13}C-NMR (300 MHz, $CDCl_3$, δ / ppm) 112.8, 134.8, 128.3, 148.2, 152.8 (C4 in 4-(CH_3)$_2$N-phenyl ring),

106.3 (3,5-C in pyridine ring), 165.2 (C=O), 181.1 (C=S), 147.9 (2,6-C in pyridine ring), 39.3 (C4 in pyridine ring), 40.8 ($N(CH_3)_2$), 46.5 (C4 in pyridine ring), 18.2 (2,6-CH_3 in pyridine ring). MS (*m*/*z* (relative abundance, %)): 463.22 (M^++1, 16.24), 432.56, 344.41, 284.35, 256.29, 213.23, 199.24, 185.26.

Spectroscopy

The IR spectra of compounds **1a**–**g** showed an absorption band at 3332 to 3354 cm^{-1} due to N–H stretching, another absorption band at 1741–1764 cm^{-1} due to the keto group in the ester groups. Compound **1c** showed an absorption band at 610 cm^{-1} corresponding the to Cl–C bonds, compound **1d** showed an absorption band at 1447 cm^{-1} corresponding to the HO–C bonds and compound **1e** showed an absorption band at 1536 cm^{-1} corresponding the O_2N–C groups. The ^{1}H-NMR spectra of compounds **1a**–**g** showed a singlet at δ 8.11–8.41 ppm, attributable to the NH protons present in the 1,4-dihydropyridine ring, and another important singlet at δ 4.67–4.79 ppm, which was attributable to the C4–H proton present in the 1,4-dihydropyridine ring. The ^{13}C-NMR spectra of compounds **1a**–**g** showed peaks at δ 33.2–44.9 ppm, corresponding to C4 in the pyridine ring, δ 101.4–103.9 ppm, corresponding to the 3,5-position of C–**C**OOEt, and δ 150.7––152.8 ppm, corresponding to the 2,6-position of **C**–CH_3 in the pyridine ring. The mass spectral analysis of compounds **1a**–**g** showed molecular ion peaks, which confirmed the molecular mass of these compounds. The IR spectra of compounds **2a**–**g** showed an absorption band obtained at 3320–3372 cm^{-1} corresponding to the NH group present in the 1,4-dihydropyridine ring and another absorption band at 3118–3200 cm^{-1} which was due to NH–C=O stretching. An absorption band for the C=S group was observed at 1242–1272 cm^{-1}. The ^{1}H--NMR spectra of **2a**–**g** showed as a singlet a band at δ 8.41–8.64 ppm, attributable to the NH protons present in the 1,4-dihydropyridine ring. The C4–H, CONH, NHCS and NH_2 protons resonated as singlets at δ 5.10–5.21, 8.01–8.15, 2.02––2.12 and 9.14–9.82 ppm, respectively. The ^{13}C-NMR spectra of compounds **2a**–**g** showed peaks at δ 163.1–166.2, 181.1–184.6, 34.6–46.5 and 18.2–19.7 ppm, corresponding to the 3,5-position of CO-NH group in the pyridine ring, the 3,5--position of CS in the pyridine ring, the 4-position of carbon in the pyridine ring and the 2,6-position of CH_3 in the pyridine ring, respectively. Mass spectral analysis of compounds **2a**–**g** showed molecular ion peaks, which confirmed the molecular masses of these compounds.

Antibacterial screening

The bacterial zones of inhibition values (mm) are given in Table I. The antimicrobial activities of compounds **1a**–**g** and **2a**–**g** were screened. The structure activity relationship (SAR) analysis of the base compounds **1a**–**g** was compared with that of the thiosemicarbazone-containing compounds **2a**–**g**. Ciprofloxacin

was used as a standard at 100 μg ml^{-1}. Compounds **1a**–**g** showed low activity compared with compounds **2a**–**g** towards all the tested organisms.

TABLE I. Antibacterial activity of the synthesized compounds **1a**–**g** and **2a**–**g** (disk diameter: 7 cm)

Compound	*S. aureus*	*K. pneumoniae*	*E. coli*	*P. aeruginosa*
1a	–	–	10	14
1b	6	7	5	6
1c	10	–	8	10
1d	–	8	–	–
1e	5	5	6	12
1f	–	6	5	15
1g	5	–	10	6
2a	9	–	16	30
2b	17	18	12	18
2c	25	15	13	10
2d	15	16	25	–
2e	13	12	16	20
2f	11	18	15	22
2g	10	7	18	16
Ciprofloxacin	22	19	27	32

Compounds **2a**–**g** were screened for *Staphylococcus aureus* and compound **2c** was found to be highly active compared with the standard ciprofloxacin because it contained an amide group in the 3,5-position with C=S and a 4-chlorophenyl group in the fourth position. On the other hand, compounds **2a**, **2b** and **2d**–**g** had low activities compared with the standard ciprofloxacin.

Compounds **2a**–**g** were screened for *Klebsiella pneumoniae*, whereby compounds **2b** and **2f** showed equipotent activity with the standard ciprofloxacin. On the other hand, compounds **2a**, **2d**–**e** and **2g** had low activities compared with the standard ciprofloxacin.

Compounds **2a**–**g** were screened for *Escherichia coli* and the compound **2d** was found to have an equipotent activity compared with the standard ciprofloxacin. On the other hand, compounds **2a**–**c** and **2e**–**g** had low activities compared with the standard ciprofloxacin.

Compounds **2a**–**g** were screened for *Pseudomonas aeruginosa*, whereby the compound **2a** exhibited equipotent activity compared with the standard ciprofloxacin, while the other compounds **2b**–**g** had low activities compared with the standard ciprofloxacin.

Antifungal screening

The fungacidal zones of inhibition, mm, values are given in Table II. Compounds **2a**–**g** were screened for *Aspergillus niger*; the compounds **2b**–**g** were less active compared with the standard clotrimazole, while compound **2a** had no activity.

Compounds **2a**–**g** were screened for *Candida albicans*. Compound **2d** was highly active compared with the standard clotrimazole because it contained an amide group in the 3,5-position with C=S and 4-hydroxyphenyl in the fourth position, while the other compounds **2a**–**c** and **2e**–**g** had lower activities than the standard clotrimazole.

TABLE II. Antifungal activity of the synthesized compounds **1a**–**g** and **2a**–**g** (disk diameter: 7 cm)

Compound	*A. niger*	*C. albicans*	*M. audouinii*	*C. neoformans*
1a	–	8	10	–
1b	9	10	8	9
1c	10	16	–	8
1d	14	–	12	–
1e	8	–	–	–
1f	12	15	11	9
1g	5	16	12	–
2a	–	8	6	7
2b	10	–	–	6
2c	15	20	14	13
2d	16	26	18	15
2e	8	11	15	15
2f	16	10	18	24
2g	14	17	16	–
Clotrimazole	22	24	26	25

Compounds **2a**–**g** were screened for *Microsporum audouinii*. The compounds **2a** and **2c**–**g** had lower activity than the standard clotrimazole, while compound **2b** was inactive.

Compounds **2a**–**g** were screened for *Cryptococcus neoformans*, the compound **2f** had equipotent activity with the standard clotrimazole, while the other compounds **2a**–**d** and **2e** had lower activities compared with the standard clotrimazole and compound **2g** exhibited no activity.

EXPERIMENTAL

Chemistry

The melting points were recorded in open capillary tubes and are reported uncorrected. The IR spectra were recorded in KBr on a Shimadzu 8201pc FTIR specrometer (4000–400 cm^{-1}). The ^{1}H-NMR and ^{13}C-NMR spectra were recorded on a Bruker DRX-300 MHz instrument. The mass spectra (EI) were obtained on a Jeol JMS D-300 spectrometer operating at 70 eV. Elemental analyses (C, H, N and S) were realized using an Element Analyzer, model Vario EL III. The purity of the compounds was checked by thin layer chromatography (TLC).

*Synthesis of diethyl 4-(furan-2-yl)-2,6-dimethyl-1,4-dihydropyridine-3,5-dicarboxylate (**1a**)*

The reaction mixture consisting of ethyl acetoacetate (0.2 mol), furfural (0.1 mol) and ammonium hydroxide (0.1 mol) in methanol (20 mL) was heated at reflux for 4 h. The ob-

tained solid was filtered off, washed with water and recrystallized using absolute ethanol. The above procedure was followed for the synthesis of compounds **1b**–**g**.

*Synthesis of 4-(furan-2-yl)-2,6-dimethyl-1,4-dihydropyridine-3,5-dicarboxylic acid, 3,5-bis[2-(aminothioxomethyl)hydrazide] (**2a**)*

The reaction mixture consisting of compound **1a** (0.1 mol), thiosemicarbazide (0.2 mol) dissolved in ethanol (30 mL) and a few drops DMSO was heated under reflux for 10 h. The obtained solid was allowed to cool and then poured into crushed ice. The solid was collected by filtration, washed with water and recrystallised using ethanol. The above procedure was followed for the synthesis of compounds **2b**–**g**.

In vitro *antibacterial screening*

The compounds **1a**–**g** and **2a**–**g** were evaluated for their *in vitro* antibacterial activity against *S. aureus* (ATCC-25923), *K. pneumoniae* (recultured), *E. coli* (ATCC-25922) and *P. aeruginosa* (ATCC-27853) by the agar diffusion method[22,23] using Mueller–Hinton agar (Hi--Media) medium. Each compound was tested at a concentration of 100 μg mL^{-1} in DMSO. Ciprofloxacin was used as the standard. The zone of inhibition (mm) was measured after 24 h incubation at 37 ºC.

In vitro *antifungal screening*

The compounds **1a**–**g** and **2a**–**g** were evaluated for their *in vitro* antifungal activity against *A. niger*, *C. albicans*, *M. audouinii* and *C. neoformans* (recultured) using an agar diffusion method[24,25] with Sabouraud's dextrose agar (Hi-Media). Each compound was tested at a concentration of 100 μg mL^{-1} in DMSO. Clotrimazole was used as the standard. The zone of inhibition (mm) was measured after 24 h incubation at 37 °C.

CONCLUSIONS

A new series of 1,4-dihydropyriodine derivatives (**2a**–**g**) was synthesized. The synthesized compounds were screened for their antibacterial activity, whereby compound **2c** was more active than ciprofloxacin against *S. aureus* organism. When the synthesized compounds were screened for their antifungal activity, a compound **2d** showed higher activity than clotrimazole against *C. albicans*. These findings could be of importance for further studies in this field.

Acknowledgments. We wish to thank for State Government of Tamil Nadu for providing financial support through a state government fellowship. We wish to thank one of the authors Dr. J. Selvin, Department of Microbiology for help in the antimicrobial studies. We sincerely thank the management of Jamal Mohamed College for providing the Laboratory Facilities.

ИЗВОД

СИНТЕЗА И АНТИМИКРОБНА АКТИВНОСТ НОВЕ СЕРИЈЕ ДЕРИВАТА 1,4-ДИХИДРОПИРИДИНА

R. SURENDRA KUMAR[1], A. IDHAYADHULLA[1], A. JAMAL ABDUL NASSER[1] и J. SELVIN[2]

[1]*P. G. & Research Department of Chemistry, Jamal Mohamed College, Tiruchirappalli-620 020, Tamil Nadu и* [2]*Department of Microbiology, Bharathidasan University.Tiruchirappalli–620024, Tamil Nadu, India*

Ханчовом синтезом добијена је нова серија деривата 1,4-дихидропиридина (**1a**–**g**). Једињења **1a**–**g** реаговала су са тиосемикарбазидима и добијена је нова серија једињења **2a**–**g**.

Структура синтетисаних једињења је потврђена ИЦ, 1H-NMR, 13C-NMR и масеним спектрима и елементалном анализом. Синтетисаним једињењима је одређена антибикробна активност.

(Примљено 27. новембра 2009, ревидирано 21. јула 2010)

REFERENCES

1. C. Gaudio, A. Korolkovas, Y. Takahata, *J. Pharm. Sci.* **83** (1994) 1110
2. K .J. Chleifer, *J. Med .Chem*. **42** (1999) 2204
3. S. Visentin, P. Amiel, R. Frittero, D. Boschi, C. Roussel, L. Giusta, E. Carbone, Gasco, *J. Med. Chem*. **42** (1999) 1422
4. J.-L. Jiang, A.-H. Li, S.-Y. Jang, L. Chang, N. Melman, S. Moro, X.-D. Ji, E. B. Lobkovsky, J. C. Clardy, K. A. Jacobson, *J. Med. Chem*. **42** (1999) 3055
5. T. Godfraid, R. Miller, M. Wibo, *Pharmocol. Rev*. **38** (1986) 321
6. B. Khadilkar, S. Borkar, *Synth. Commun*. **28** (1998) 207
7. B. Schnell, W. Krenn, K. Faber, C. O. Kappe, *J. Chem. Soc. Perkin Trans. 1* **24** (2000) 4382
8. S. R. Pattan, V. B. Rasal, N. Venkatramana, A. B. Khade, S. R. Butle, S. G .Jadhav, B .G. Desai, F. V. Manvi, *Indian J. Chem*. **46B** (2007) 698
9. T .Suresh, S. K. Swamy, V. M. Reddy, *Indian J. Chem*. **46B** (2007) 115
10. A. Bhavik, A. Dinesh Sureja, A. Yogesh Naliapara, A. Anamik Shaha, A. K. Saxenab, *Bioorg. Med. Chem.* **91** (2001) 993
11. M. Amini, L. Navidpour, A. Shafiee, *Daru* **16** (2008) 9
12. K. Nandi, S .Chaudhri, S. K. Mazumdah, S. Ghosh, E. Ect, *J. Chem. Soc. Perkin Trans 2* **11** (1984) 1729
13. M. A. Ali, M. A. Chowdhary, M. Naziruddin, *Polyhedron* **3** (1984) 595
14. D. Suresh, D. Kumar, S. Jagir, S. Sandhu, *Synth. Commun*. **39** (2009) 1957
15. M.-S. Bai, Y.-Y. Chen, D.-L. Niu, L. Peng, *Acta Crystallogr*. **E65** (2009) o799
16. P. P. Reddy, V. Vijayakumar, J. Suresh, T. Narasimhamurthyc, P. L. Nilantha Lakshmand, *Acta Crystallogr*. **E66** (2010) o363
17. A. Debache, R. Boulcina, A. Belfaitah, S. Rhouati, B. Carboni, *Synlett* **4** (2008) 509
18. V. Sivamurugan, R. Suresh Kumar, M. Palanichamy, V. Murugesan, *J. Heterocycl. Chem.* **42** (2009) 969
19. J. S. Yadav, B. V. Subha-Reddy, P. T. Reddy, *Synth. Commun*. **31** (2000) 425
20. S. K. Srivastava, S. Srivastava, S. D. Srivastava, *Indian J. Chem.* **41B** (2002)2357
21. S. Ojha, U. Ameta, N. Dhakar, G. L. Talesara, *Indian J. Chem*. **46B** (2007) 860
22. W. Bauer, W. M. Kirby, J. C. S. Harris, J. C. Turck, *Am. Clin. Pathol*. **39** (1966) 493
23. R. G. Petersdorf, J. C. Sherris, *Am. J. Med*. **39** (1965) 766
24. S. H. Gillespie, *Medical Microbiology-Illustrated*, Butterworth Heinemann, London, 1994, p. 234
25. R. S. Varma, *Antifungal Agents: Past, Present and Future prospects*, National Academy of Chemistry and Biology, Lucknow, 1998.

Journal of the Serbian Chemical Society
JSCS-info@shd.org.rs • www.shd.org.rs/JSCS
J. Serb. Chem. Soc. *76* (1) 13–20 (2011)
JSCS–4094
UDC 547.48+547.467+547.313+547.239+547.421:542.9
Original scientific paper

A three-component synthesis of functionalized ketenimines by the reaction of alkyl isocyanides and dialkyl acetylenedicarboxylates in the presence of 2-quinolinol

BITA MOHTAT[1]*, HOORIEH DJAHANIANI[2], ISSA YAVARI[3] and KOBRA NADERI[1]

[1]Chemistry Department, Islamic Azad University, Karaj Branch, Karaj, [2]Chemistry Department, Islamic Azad University, East Branch, Qiamdasht, Tehran and [3]Chemistry Department, Islamic Azad University, Science and Research Branch, Tehran, Iran

(Received 18 February, revised 21 June 2010)

Abstract: The 1:1 reactive intermediates generated by the addition of alkyl isocyanides to dialkyl acetylenedicarboxylates were trapped by 2-quinolinol to yield highly functionalized ketenimines and, in some cases, minor amounts of 1-azabuta-1,3-dienes.

Keywords: ketenimines; 1-azadienes; alkyl isocyanides; acetylenic esters; NH-acids; multi-component reaction.

INTRODUCTION

Ketenimines are important reactive intermediates that occur as transient compounds in many thermal and photochemical reactions.[1] There has been intense interest in their reactions, such as cycloaddition,[2] nucleophilic[3,4] and electrophilic addition.[5] They have also found widespread use as reactive starting materials for the formation of four-, five-, and six-membered heterocyclic ring systems.[5–7] Methods for the synthesis of ketenimines have been extensively reviewed.[8] The addition of nucleophilic carbenes, such as isocyanides, to dialkyl acetylenedicarboxylates was investigated in detail.[9] The trapping of the 1:1 intermediate formed between dialkyl acetylenedicarboxylates and isocyanides with OH, NH, and CH acids has been widely studied.[10–14] In continuation of our interest in the application of isocyanides in multi-component reactions, MCR,[15–18] an efficient synthesis of ketenimine **4** from alkyl isocyanides **1** and dialkyl acetylenedicarboxylates **2** in the presence of a strong NH-acid, such as quinolin-2-ol, is reported herein. In some cases, minor amounts (13–25 %) of 1-azadienes **5** were obtained (Scheme 1).

* Corresponding author. E-mail: B.mohtat@jooyan.org
doi: 10.2298/JSC100218011M

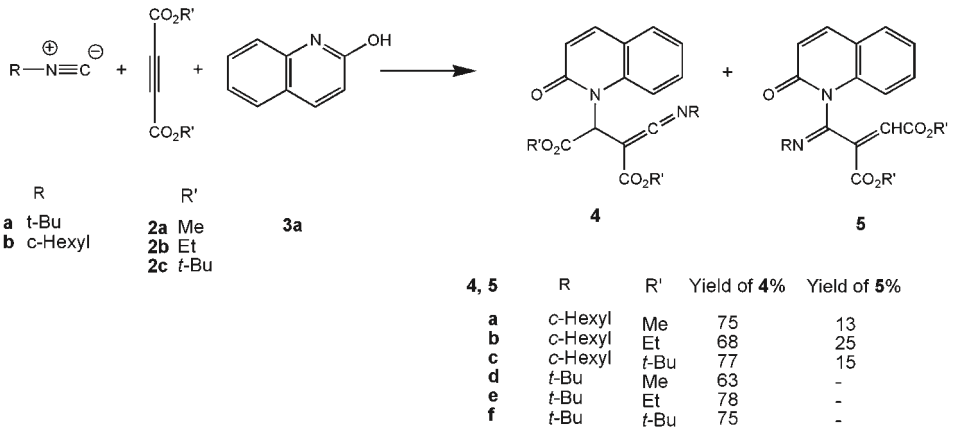

4, 5	R	R'	Yield of 4%	Yield of 5%
a	*c*-Hexyl	Me	75	13
b	*c*-Hexyl	Et	68	25
c	*c*-Hexyl	*t*-Bu	77	15
d	*t*-Bu	Me	63	-
e	*t*-Bu	Et	78	-
f	*t*-Bu	*t*-Bu	75	-

Scheme 1. Typical procedure for the synthesis of compounds **4** and **5**.

RESULTS AND DISCUSSION

The reaction of alkyl isocyanides **1** with acetylenic esters **2** in the presence of an NH-acid, such as quinolin-2-ol, afforded the isomeric highly functionalized ketenimines **4** in fairly good yields.

The structures of **4** and **5** were deduced from their elemental analyses, mass spectrometric data, and their ^{1}H- and ^{13}C-NMR, DEPT and IR spectral data, given below.

*Dimethyl 2-(cyclohexylcarbonimidoyl)-3-(2-oxo-1(2*H*)-quinolinyl)succinate (**4a**)*. Yellow oil; yield: 63 %; Anal. Calcd. for $C_{22}H_{24}N_2O_5$: C, 66.65; H, 6.10; N, 7.07 %. Found: C, 66.70; H, 6.07; N, 7.05 %. IR (KBr, cm^{-1}): 2077 (–C=C=N stretching), 1745 (–C=O stretching of –COOR group), 1651 (–C=O stretching of amide group). ^{1}H-NMR (300 MHz, $CDCl_3$, δ / ppm): 1.20–2.07 (10H, *m*, 5 CH_2), 3.72 (6H, *s*, 2 OCH_3), 3.86 (1H, *m*, H–CN), 6.17 (1H, *s*, CH), 6.64 (1H, *d*, aromatic, J = 9.4 Hz, CH), 7.26 (1H, *t*, aromatic, J = 7.5 Hz, CH), 7.58 (1H, *d*, aromatic, J = 7.5 Hz, CH), 7.62 (1H, *t*, aromatic, J = 8.6 Hz, CH), 7.72 (1H, *d*, aromatic, J = 9.4 Hz, CH), 7.86 (1H, *d*, aromatic, J = 8.6 Hz, CH). ^{13}C-NMR (75.4 MHz, $CDCl_3$, δ / ppm): 24.4 (CH_2), 25.0 (CH_2), 25.6 (CH_2) 33.0 (CH_2), 33.4 (CH_2), 52.0 (OCH_3), 53.2 (OCH_3), 55.4 (C–H), 59.7 (**C**=C=N), 60.8 (C–N), 115.3 (CH=), 121.4 (CH=), 122.8 (CH=), 123.0 (CH=), 129.3 (CH=), 131.4 (CH=), 139.7 (C=), 140.6 (C=), 162.5 (C=O), 164.8 (C=O), 168.8 (C=O), 171.5 (C=**C**=N). DEPT (125.7 MHz, $CDCl_3$, δ / ppm): 24.4 (CH_2), 25.7 (CH_2), 25.9 (CH_2) 32.8 (CH_2), 33.4 (CH_2), 52.0 (OCH_3), 53.2 (OCH_3), 55.4 (C–H), 60.8 (C–N), 115.3 (CH=), 121.4 (CH=), 122.9 (CH=), 123.4 (CH=), 129.3 (=CH), 131.4 (=CH), 139 (C=), 140.5 (C=), 160.4 (C=O), 162.7 (C=O), 167.4 (C=O), 170.6 (C=**C**=N). MS (*m*/*z*, (relative abundance, %)): 396 (M^+, 18), 270 (24), 237 (32), 171 (58), 156 (39), 145 (47), 83 (100), 55 (58), 41(56).

*Dimethyl 2-[(*E*)-(cyclohexylimino)(2-oxo-1(2*H*)-quinolinyl)methyl]but-2-enedioate (**5a**)*. Yellow oil; yield: 26 %; Anal. Calcd. for $C_{22}H_{24}N_2O_5$: C, 66.65; H, 6.10; N, 7.07 %. Found: C, 66.69; H, 6.13; N, 7.02 %. IR (KBr, cm^{-1}): 1732 (–C=O stretching of –COOR group), 1668 (–C=O stretching of amide group), 1594 (–C=N stretching of imine group). ^{1}H-NMR (300 MHz, $CDCl_3$, δ / ppm): 1.10–1.90 (10H, *m*, 5 CH_2), 3.10 (1H, *m*, HC–N), 3.67 (3H, *s*, OCH_3), 3.95 (3H, *s*, OCH_3), 5.71 (1H, *s*, CH), 6.70 (1H, *d*, aromatic, *J* = 9.6 Hz, CH), 7.02 (1H, *d*, aromatic, *J* = 8.4 Hz, CH), 7.27 (1H, *t*, aromatic, *J* = 7.8 Hz, CH), 7.50 (1H, *t*, aromatic, *J* = 8.4 Hz, CH), 7.62 (1H, *d*, aromatic, *J* = 7.8 Hz, CH), 7.81 (1H, *d*, aromatic, *J* = 9.6 Hz, CH). ^{13}C-NMR (75.4 MHz, $CDCl_3$, δ / ppm): 23.4 (CH_2), 23.5 (CH_2), 25.5 (CH_2) 32.04 (CH_2), 32.4 (CH_2), 52.3 (OCH_3), 52.7 (OCH_3), 60.9 (C–N), 114.5 (CH=), 119.8 (CH=), 121.4 (CH=), 122.9 (CH=), 123.4 (CH=), 128.9 (C=), 131.4 (CH=), 137.5 (CH=), 141.0 (C=), 144.3 (C=), 144.8 (C=N), 160.1 (C=O), 164.6(C=O), 165.8 (C=O). MS (*m*/*z*, (relative abundance, %)): 396 (M^+, 10), 280 (37), 227 (100), 170 (55), 83 (45), 55 (38).

*Diethyl 2-(cyclohexylcarbonimidoyl)-3-(2-oxo-1(2*H*)-quinolinyl)succinate (**4b**)*. Yellow oil; yield: 71 %; Anal. Calcd. for $C_{24}H_{28}N_2O_5$: C, 67.91; H, 6.65; N, 6.60 %. Found: C, 67.82; H, 6.68; N, 6.69 %. IR (KBr, cm^{-1}): 2093 (–C=C=N stretching), 1741 (–C=O stretching of –COOR group), 1672 (–C=O stretching of amide group). ^{1}H-NMR (300 MHz, $CDCl_3$, δ / ppm): 1.11–1.99 (10H, *m*, 5 CH_2), 1.19 (3H, *t*, *J* = 7.1 Hz, CH_2–C**H**$_3$), 1.23 (3H, *t*, *J* = 7.1 Hz, CH_2–C**H**$_3$), 3.89 (1H, *m*, HC–N), 4.19 (2H, *q*, *J* = 7.1 Hz, OC**H**$_2$–CH_3), 4.29 (2H, *m*, OC**H**$_2$–CH_3), 6.13 (1H, *s*, CH), 6.60 (1H, *d*, aromatic, *J* = 9.4 Hz, CH), 7.24 (1H, *t*, aromatic, *J* = 7.8 Hz, CH), 7.56–7.60 (2H, *m*, aromatic, 2 CH), 7.70 (1H, *d*, aromatic, *J* = 9.4 Hz, CH), 7.88 (1H, *d*, aromatic, *J* = 8.6 Hz, CH). ^{13}C-NMR (75.4 MHz, $CDCl_3$, δ / ppm): 14.0 (CH_3), 14.4 (CH_3), 23.8 (CH_2), 25.3 (2 CH_2), 32.9 (2 CH_2), 55.1 (C–H), 59.7 (**C**=C=N), 60.2 (OCH_2), 60.3 (OCH_2), 61.9 (C–N), 115.0 (=CH), 120.9 (=CH), 121.0 (=CH), 122.3 (=CH), 128.9 (=CH), 130.9 (=CH), 139.4 (C=), 140.2 (C=), 160.2 (C=O), 162.1 (C=O), 167.9 (C=O), 170.8 (C=**C**=N). MS (*m*/*z*, (relative abundance, %)): 424 (M^+, 7), 341 (76), 280 (71), 144 (100), 97 (38), 29 (44).

*Diethyl 2-[(*E*)-(cyclohexylimino)(2-oxo-1(2*H*)-quinolinyl)methyl]but-2-enedioate (**5b**)*. Yellow oil; yield: 19 %; Anal. Calcd. for $C_{24}H_{28}N_2O_5$: C, 67.91; H, 6.65; N, 6.60 %. Found: C, 67.88; H, 6.68; N, 6.63 %. IR (KBr, cm^{-1}): 1741 (–C=O stretching of –COOR group), 1672 (–C=O stretching of amide group), 1590 (–C=N stretching of imine group); ^{1}H-NMR (300 MHz, $CDCl_3$, δ / ppm): 1.06––1.97 (10H, *m*, 5 CH_2), 1.32 (3H, *t*, *J* = 7.1 Hz, CH_2–C**H**$_3$), 1.40 (3H, *t*, *J* = 7.1 Hz, CH_2–C**H**$_3$), 3.09 (1H, *m*, H–CN), 4.15 (2H, *q*, *J* = 7.1 Hz, OC**H**$_2$–CH_3), 4.44 (2H, *m*, OC**H**$_2$–CH_3), 5.71 (1H, *s*, CH), 6.70 (1H, *d*, aromatic, *J* = 9.6 Hz, CH), 7.05 (1H, *d*, aromatic, *J* = 8.5 Hz, CH), 7.29 (1H, *t*, aromatic, *J* = 8.5 Hz, CH), 7.50 (1H, *t*, aromatic, *J* = 7.5 Hz, CH), 7.78 (1H, *d*, aromatic, *J* = 7.8 Hz, CH),

7.80 (1H, *d*, aromatic, *J* = 9.6 Hz, CH). ^{13}C-NMR (75.4 MHz, $CDCl_3$, δ / ppm): 13.6 (CH_3), 13.9 (CH_3), 23.5 (CH_2), 25.1 (CH_2), 25.5 (CH_2), 32.4 (CH_2), 32.6 (CH_2), 60.7 (C–N), 61.3 (OCH_2), 61.7 (OCH_2), 114.7 (=CH), 119.8 (=CH), 121.5 (=CH), 123.2 (=CH), 123.4 (=CH), 128.8 (C=), 131.3 (=CH), 137.5 (C=), 141 (=CH), 144.3 (C=), 144.6 (C=N), 163.8 (C=O), 164.0 (C=O), 165.3 (C=O). MS (*m*/*z*, (relative abundance, %)): 424 (M^+, 7), 280 (31), 253 (56), 227 (100), 171 (48), 83 (41), 29 (35).

Di-tert-*butyl 2-(cyclohexylcarbonimidoyl)-3-(2-oxo-1(2*H*)-quinolinyl)succinate (**4c**)*. Yellow oil; yield: 55 %; Anal. Calcd. for $C_{28}H_{36}N_2O_5$: C, 69.98; H, 7.55; N, 5.83 %. Found; C, 69.51; H, 7.60; N, 5.79 %. IR (KBr, cm^{-1}): 2073 (–C=C=N stretching), 1721 (–C=O stretching of –COOR group), 1673 (–C=O stretching of amide group). ^{1}H-NMR (300 MHz, $CDCl_3$, δ / ppm): 1.06–2.01 (10H, *m*, 5 CH_2), 1.41 (9H, *s*, $C(CH_3)_3$), 1.46 (9H, *s*, $C(CH_3)_3$), 3.85 (1H, *m*, H–CN), 6.04 (1H, *s*, CH), 6.64 (1H, *d*, aromatic, *J* = 9.2 Hz, CH), 7.28 (1H, *t*, aromatic, *J* = 7.5 Hz, CH), 7.55–7.62 (2H, *m*, aromatic, 2 CH), 7.69 (1H, *d*, aromatic, *J* = 9.4 Hz, CH), 7.82 (1H, *d*, aromatic, *J* = 8.4 Hz, CH). ^{13}C-NMR (75.4 MHz, $CDCl_3$, δ / ppm): 24.3 (CH_2), 25.1 (CH_2), 25.8 (CH_2), 28.2 ($C(\mathbf{C}H_3)_3$), 28.9 ($C(\mathbf{C}H_3)_3$), 33.46 (2 CH_2), 57.5 (C–H), 62.5 (**C**=C=N), 68.9 (C–N), 80.5 (C–O), 82.3 (C–O), 115.7 (CH), 121.6 (=CH), 122.5 (=CH), 129.1 (=CH), 130.2 (=CH), 131.1 (=CH), 139.9 (C=), 140.2 (C=), 162.4 (C=O), 165.1 (C=O), 167.9 (C=O), 176.5 (C=**C**=N). MS (*m*/*z*, (relative abundance, %)): 480 (M^+, 11), 336 (47), 202 (74), 158 (100), 122 (36), 83 (49), 57 (100).

Di-tert-*butyl 2-[(*E*)-(cyclohexylimino)(2-oxo-1(2*H*)-quinolinyl)methyl] but-2--enedioate (**5c**)*. Yellow oil; yield: 16 %; Anal. Calcd. for $C_{28}H_{36}N_2O_5$: C, 69.98; H, 7.55; N, 5.83 %. Found; C, 69.94; H, 7.58; N, 5.79 %. IR (KBr, cm^{-1}): 1732 (–C=O stretching of –COOR group), 1660 (–C=O stretching of amide group), 1595 (–C=N stretching of imine group). ^{1}H-NMR (300 MHz, $CDCl_3$, δ / ppm): 1.08–2.00 (10H, *m*, 5 CH_2), 1.42 (9H, *s*, $C(CH_3)_3$), 1.60 (9H, *s*, $C(CH_3)_3$), 3.08 (1H, *m*, H–CN), 5.70 (1H, *s*, CH), 6.72 (1H, *d*, aromatic, *J* = 9.5 Hz, CH), 7.15 (1H, *d*, aromatic, *J* = 8.2 Hz, CH), 7.28 (1H, *t*, aromatic, *J* = 8.2 Hz , CH), 7.50 (1H, *t*, aromatic, *J* = 7.4 Hz, CH), 7.62 (1H, *d*, aromatic, *J* = 7.4 Hz, CH), 7.81 (1H, *d*, aromatic, *J* = 9.5 Hz, CH). ^{13}C-NMR (75.4 MHz, $CDCl_3$, δ / ppm): 23.8 (CH_2), 23.9 (CH_2), 25.9 (CH_2), 28.3 ($C(\mathbf{C}H_3)_3$), 28.5 ($C(\mathbf{C}H_3)_3$), 32.4 (CH_2), 32.6 (CH_2), 60.9 (C–N), 82.1 (C–O), 83.0 (C–O), 115.4 (=CH), 120.2 (=CH), 121.9 (=CH), 123.6 (=CH), 125.0 (=CH), 129.0 (=CH), 131.7 (C=), 138.3 (=CH), 141.2 (C=), 144.0 (C=), 144.9 (C=N), 160.6 (C=O), 163.8 (C=O), 165.4 (C=O). MS (*m*/*z*, (relative abundance, %)):480 (M^+, 11), 336 (37), 253 (48), 227 (100), 144 (45), 83 (47), 57 (35).

*Dimethyl 2-(*tert-*butylcarbonimidoyl)-3-(2-oxo-1(2*H*)-quinolinyl)succinate (**4d**)*. Yellow oil; yield: 87 %; Anal. Calcd. for $C_{20}H_{22}N_2O_5$: C, 64.85; H, 5.99; N, 7.56 %. Found: C, 64.89; H, 5.94; N, 7.60 %. IR (KBr, cm^{-1}): 2079 (–C=C=N

stretching), 1750 (–C=O stretching of –COOR group), 1670 (–C=O stretching of amide group). ^{1}H-NMR (300 MHz, $CDCl_3$, δ / ppm): 1.43 (9H, *s*, $C(CH_3)_3$), 3.70 (3H, *s*, $–OCH_3$), 3.72 (3H, *s*, $–OCH_3$), 6.12 (1H, *s*, CH), 6.63 (1H, *d*, aromatic, *J* = 9.4 Hz, CH), 7.24 (1H, *t*, aromatic, *J* = 7.5 Hz, CH), 7.51–7.62 (2H, *m*, aromatic, 2 CH), 7.70 (1H, *d*, aromatic, *J* = 8.9 Hz, CH), 7.80 (1H, *d*, aromatic, *J* = 8.6 Hz, CH). ^{13}C NMR (75.4 MHz, $CDCl_3$, δ / ppm): 30.0 ($C(\mathbf{C}H_3)_3$), 51.7 (OCH_3), 52.8 (OCH_3), 54.8 (C–H), 60.9 (**C**=C=N), 68.1 (C–N), 114.8 (=CH), 121.1 (=CH), 122.5 (=CH), 128.9 (=CH), 131.0 (=CH), 132.4 (=CH), 139.2 (C=), 140.3 (C=), 162.0 (C=O), 167.7 (C=O), 168.3 (C=O), 171.0 (**C**=C=N). MS (*m*/*z*, (relative abundance, %)):370 (M^+, 4), 313 (31), 226 (29), 143 (85), 57 (100), 41 (34).

*Diethyl 2-(*tert*-butylcarbonimidoyl)-3-(2-oxo-1(2*H*)-quinolinyl)succinate (**4e**)*. Yellow powder; yield: 73 %; m.p. 93–97 °C; Anal. Calcd. for $C_{22}H_{26}N_2O_5$: C, 68.71; H, 7.56; N, 6.14; found: C, 68.73; H, 7.50; N, 6.12. IR (KBr, cm^{-1}): 2073 (–C=C=N stretching), 1747 (–C=O stretching of –COOR group), 1646 (–C=O stretching of amide group). ^{1}H-NMR (300 MHz, $CDCl_3$, δ / ppm): 1.18 (3H, *t*, *J* = 7.1 Hz, $CH_2–C\mathbf{H}_3$), 1.24 (3H, *t*, *J* = 7.1 Hz, $CH_2–C\mathbf{H}_3$), 1.43 (9H, *s*, $C(CH_3)_3$), 4.20 (2H, *q*, *J* = 7.1 Hz, $OC\mathbf{H}_2–CH_3$), 4.29 (2H, *m*, $OC\mathbf{H}_2–CH_3$), 6.09 (1H, *s*, CH), 6.63 (1H, *d*, aromatic, *J* = 9.4 Hz, CH), 7.24 (1H, *t*, aromatic, *J* = 7.8 Hz, CH), 7.51–7.56 (2H, *m*. aromatic, 2 CH), 7.70 (1H, *d*, aromatic, *J* = 9.4 Hz, CH), 7.83 (1H, *d*, aromatic, *J* = 8.6 Hz, CH). ^{13}C-NMR (75.4 MHz, $CDCl_3$, δ / / ppm): 14.1 (CH_3), 14.3 (CH_3), 30.1 ($C(\mathbf{C}H_3)_3$), 51.9 (C–H), 54.8 (**C**=C=N), 60.3 (C–N), 61.9 (OCH_2), 62.2 (OCH_2), 114.9 (=CH), 121.0 (=CH), 122.4 (=CH), 128.9 (=CH), 130.7 (=CH), 133.7 (=CH), 136.6 (C=), 139.4 (C=), 162.0 (C=O), 164.8 (C=O), 167.8 (C=O), 170.7 (C=**C**=N). MS (*m*/*z*, (relative abundance, %)): 398 (M^+, 21), 342 (57), 269 (50), 254 (61), 223 (42), 195 (31), 145 (100), 57 (76), 41(42).

Di-tert-*butyl 2-(*tert*-butylcarbonimidoyl)-3-(2-oxo-1(2*H*)-quinolinyl)succinate (**4f**)*. Yellow powder; yield: 79 %; m.p. 94–98 °C; Anal. Calcd. for $C_{26}H_{34}N_2O_5$: C, 68.70; H, 7.54; N, 6.16 %. Found: C, 68.73; H, 7.50; N, 6.12 %. IR (KBr, cm^{-1}): 2073 (–C=C=N stretching), 1743 (–C=O stretching of –COOR group), 1666 (–C=O stretching of amide group). ^{1}H-NMR (300 MHz, $CDCl_3$, δ / / ppm): 1.40 (18H, *s*, 2 $C(CH_3)_3$), 1.46 (9H, *s*, $C(CH_3)_3$), 5.99 (1H, *s*, CH), 6.63 (1H, *d*, aromatic, *J* = 9.4 Hz, CH), 7.22 (1H, *t*, aromatic, *J* = 7.4 Hz, CH), 7.55––7.60 (2H, *m*, aromatic, 2 CH), 7.67 (1H, *d*, aromatic, *J* = 9.4 Hz, CH), 7.75 (1H, *d*, aromatic, *J* = 8.6 Hz, CH). ^{13}C-NMR (75.4 MHz, $CDCl_3$, δ / ppm): 27.8 ($C(\mathbf{C}H_3)_3$), 28.4 ($C(\mathbf{C}H_3)_3$), 30.0 ($C(\mathbf{C}H_3)_3$), 51.6 (C–H), 55.3 (**C**=C=N), 61.7 (C–N), 80.0 (C–O), 81.9 (C–O), 115.0 (CH=), 120.8 (CH=), 121.2 (CH=), 122.1 (CH=), 128.7 (CH=), 130.8 (CH=), 139.6 (C=), 139.5 (C=), 161.7 (C=O), 161.9 (C=O), 166.7 (C=O), 169.5 (C=**C**=N). MS (*m*/*z*, (relative abundance, %)): 454 (M^+, 2), 310 (24), 254 (23), 198 (35), 145 (82), 57 (100), 41 (30).

The ^{1}H-NMR spectrum of **4a** exhibited three sharp lines for methoxy (δ 3.72 and 3.86 ppm) and methine (δ 6.17 ppm) protons. The cyclohexyl and quinolinol moiety appeared at δ 1.20–2.07 ppm and 6.63–7.80 ppm. The ^{13}C-NMR spectrum of **4a** exhibited distinct resonances in agreement with the proposed structure. The DEPT spectrum of **4a** exhibited fifteen sharp lines in agreement with dimethyl 2-(cyclohexylcarbonimidoyl)-3-(2-oxo-1(2*H*)-quinolinyl)succinate. Partial assignments of these resonances are given above. The ^{1}H-NMR spectra of **4b**–**f** are similar to that of **4a**, except for the signals of the cyclohexyl and ester moiety. The ^{1}H-NMR spectrum of **5a** displayed sharp signals for the methoxy (δ 3.67 and 3.95 ppm), and vinyl (δ 5.71 ppm) protons. The ^{13}C-NMR spectrum of **5a** exhibited distinct resonances in agreement with dimethyl 2-[(*E*)-(cyclohexylimino)(2-oxo-1(2*H*)-quinolinyl)methyl]but-2-enedioate. A partial assignment of these resonances is given above. The structural assignments of **5a**–**c** made on the basis of their NMR spectra were supported by their IR spectra. Of special interest is the strong ketenimine absorption band at about 2079 cm^{-1}. Based on the well-established chemistry of isocyanides,[19–22] it is reasonable to assume that **4** and **5** result from an initial addition of the alkyl isocyanide to the acetylenic ester and subsequent protonation of the 1:1 adduct by the NH-acid. Then, the positively charged ion **7** can be attacked at two positions by the nitrogen atom of the anion of the NH-acid. Conjugate addition produces the ketenimines **4** and direct addition leads to the 1-azadienes **5** (Scheme 2).

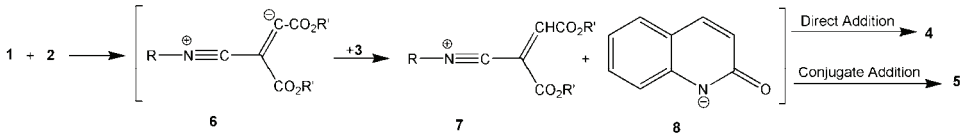

Scheme 1. A possible mechanism for the preparation of **4** and **5**.

EXPERIMENTAL

Melting points were measured on an Electrothermal 9100 apparatus. Elemental analyses for C, H, and N were performed using a Heraeus CHNO-Rapid analyzer. The IR spectra were measured on a Shimadzu IR-460 spectrometer. The ^{1}H- and ^{13}C-NMR spectra were recorded on a Bruker DRX-300 Avance instrument with $CDCl_3$ as the solvent at 300 and 75 MHz, respectively. The mass spectra were recorded on a Finnigan-Matt 8430 mass spectrometer operating at an ionization potential of 70 eV. The alkyl isocyanides, dialkyl acetylenedicaboxylates and 2-quinolinol were obtained from Fluka and were used without further purification.

*Typical procedure for the synthesis of ketenimines and 1-azadienes (**4** and **5**)*

To a stirred solution of dialkyl acetylenedicarboxylate (2 mmol) and alkyl isocyanide (2 mmol) in 10 mL of CH_2Cl_2, 2-quinolinol (2 mmol) was added dropwise at 0 °C over 10 min. The reaction mixture was then allowed to warm to room temperature and stand for 24 h. The solvent was removed under reduced pressure and the residual solid was recrystallized from diethyl ether. The oily products were purified by preparative TLC on silica gel (Merck silica

gel DC-Fertigplatten 60/Kieselguhr F254) 20 cm×20 cm plates using *n*-hexane-AcOEt (2:1) as the eluent.

CONCLUSIONS

In conclusion, a method for the preparation of highly functionalized ketenimines and 1-azadienes has once more been demonstrated. The present method carries the advantage that not only is the reaction performed under neutral conditions, but also the starting materials and reagents can be mixed without any activation or modification.

ИЗВОД

ТРОКОМПОНЕНТНА СИНТЕЗА ФУНКЦИОНАЛИЗОВАНИХ КЕТЕНИМИНА ДОБИЈЕНИХ РЕАКЦИЈОМ АЛКИЛ-ИЗОЦИЈАНИДА И ДИАЛКИЛ-АЦЕТИЛЕНДИКАРБОКСИЛАТА У ПРИСУСТВУ 2-ХИНОЛИНОЛА

БИТА МОНТАТ[1], HOORIEH DJAHANIANI[2], ISSA YAVARI[3] и KOBRA NADERI[1]

[1]Chemistry Department, Islamic Azad University, Karaj Branch, Karaj, [2]Chemistry Department, Islamic Azad University, Tehran Shargh Branch, Tehran и [3]Chemistry Department, Islamic Azad University, Science and Research Branch, Tehran, Iran

Смеша интермедијера, добијених у односу 1:1 адицијом алкил-изоцијанида на диалкил-ацетилендикарбоксилате, трапована је 2-хинолином, и као производ су добијени функционализовани кетенимини у високом приносу, а у неким примерима добијене су мале количине 1-азабута-1,3-диена.

(Примљено 18. фебруара, ревидирано 21. јуна 2010)

REFERENCES

1. T. T. Tidwell, *Acc. Chem. Res.* **23** (1990) 273
2. M. H. Mosslemin, I. Yavari, M. Anary-Abbasinejad, M. R. Nateghi, *J. Fluorine Chem.* **125** (2004) 1497
3. K. Sung, T. T. Tidwell, *J. Am. Chem. Soc.* **120** (1998) 3043
4. C. Fromont, S. Masson, *Tetrahedron* **55** (1999) 5405
5. R. Aumann, *Angew. Chem. Int. Ed. Eng.* **27** (1988) 1456
6. R. Aumann, B. Jasper, M. Lage, B. Krebs, *Organometallics* **13** (1994) 3502
7. R. Gertzmann, M. H. Moller, U. Rodewald, R. Frohlich, M. Grehl, E.-U. Wurthwein, *Tetrahedron* **51** (1995) 3767
8. J. P. Michael, C. B. D. Koning, in *Comprehensive organic functional group transformations*, A. R. Katritzky, O. Meth-Cohn, C. W. Rees, Eds., Elsevier, Cambridge, 1995, p. 555
9. H. Junjappa, M. K. Saxena, D. Ramaiah, B. B. Loharay, N. P. Rath, M. V. George, *J. Org. Chem.* **63** (1998) 9801
10. I. Yavari, M. Anary-Abbasinejad, A. Alizadeh, Z. Hossaini, *Tetrahedron* **59** (2003) 1289
11. I. Yavari, H. Zare, B. Mohtat, *Mol. Diversity* **10** (2006) 24
12. I. Yavari, F. Nasiri, H. Djahaniani, *Mol. Diversity* **8** (2004**)** 431
13. M. Anary-Abbasinejad, H. Anaraky-Ardakani, F. Rastegari, A. Hassanabadi, *J. Chem. Res.* **10** (2007) 602
14. M. Adib, M. H. Sayahi, B. Behnam, E. Sheibani, *Monatsh. Chem.* **137** (2006) 191

15. I. Yavari, H. Djahaniani, F. Nassiri, *Monatsh. Chem.* **134** (2004) 543
16. I. Yavari, H. Djahaniani, F. Nassiri, *Collect. Czech. Chem. Commun.* **69** (2004) 1499
17. I. Yavari, L. Moradi, F. Nasiri, H. Djahaniani, *Mendeleev Commun.* **15** (2006) 156
18. I. Yavari, M. Davar-Panah, M. Heydari, K. Najafian, A. Zonouzi, *Monatsh. Chem.* **127** (1996) 963
19. I. Ugi, *Angew. Chem. Int. Ed. Eng*. **21** (1982) 810
20. A. Domling, *Chem. Rev*. **106** (2006) 17
21. H. M. Walborsky, M. P. Periasamy, in *The Chemistry of Functional Groups*, C. Suppl, S. Patai, Z. Rappoport, Eds., Wiley, New York, 1983, p. 835
22. V. Nair, A. U. Viond, J. S. Nair, A. R. Sreekanth, N. P. Rath, *Tetrahedron Lett.* **41** (2000) 6675.

Journal of the Serbian Chemical Society
JSCS-info@shd.org.rs • www.shd.org.rs/JSCS
J. Serb. Chem. Soc. *76* (1) 21–26 (2011)
JSCS–4095
UDC 546.18–32+546.77–32+
547.867:544.4:547–316
Original scientific paper

An environmentally benign one-pot synthesis of 1,2-dihydro-1--aryl-3*H*-naphth[1,2-*e*][1,3]oxazin-3-one derivatives catalysed by phosphomolybdic acid

ATUL CHASKAR[1,2]*, VIMAL VYAVHARE[1], VIKAS PADALKAR[1], KIRAN PHATANGARE[1] AND HRUSHIKESH DEOKAR[1]

[1]*C. K. Thakur Research Centre, Navi Mumbai-410206, India and* [2]*Dipartimento di chimica, materiali ed ingegneria chimica "Giulio Natta" Politecnico di Milano, Milan, Italy*

(Received 10 April, revised 29 June 2010)

Abstract: A phosphomolybdic acid catalysed novel method for the synthesis of 1,2-dihydro-1-aryl-3*H*-naphth[1,2-*e*][1,3]oxazin-3-one derivatives by a one-pot, three-component reaction of *β*-naphthol, aromatic aldehydes and urea in excellent yields is described.

Keywords: MCRs; phosphomolybdic acid; naphtho-oxazine; catalysis; aldehydes.

INTRODUCTION

Oxazinone, benzoxazinone and their derivatives are an important class of heterocyclic compounds. These heterocyclic systems exhibit biological activities, such as HIV-1 reverse transcriptase inhibitors[1] (Fig. 1). Naphthalene-condensed 1,3-oxazin-2-ones have been reported to act as antibacterial agents.[2] They have been used as precursors in the preparation of phosphinic ligands for asymmetric catalysis.[3] Hitherto, only few reports for the synthesis of naphthalene-condensed oxazinone derivatives have been documented in the literature. Aromatic oxazines were first synthesized in 1944 by Holly and Cope through Mannich reactions from phenols, formaldehyde, and amines.[4] From the 1950s to the 1960s, many benzoxazines and naphthoxazines were synthesized by Burke and co-workers.[5] Fulop *et al*. reported the condensation of amino alkylnaphthols as precursors with phosgene in the presence of triethylamine giving naphthalene-condensed 1,3--oxazin-2-one derivatives in moderate yields.[6] Cimarelli and co-workers used carbonyl di-imidazole instead of phosgene for the synthesis of these compounds.[7]

* Corresponding author. E-mail: achaskar@rediffmail.com
doi: 10.2298/JSC100410016C

Recently, Bazgir *et al*. reported the synthesis of naphthoxazine derivatives using *p*-TSA and microwave radiation under solvent-free conditions.[8]

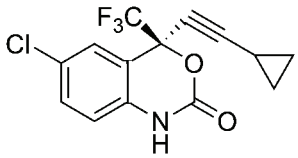

Fig. 1. Efavirenz (Sustiva™).

However, some difficulties still exist, such as unsatisfactory yields, long reaction times, strong acidic conditions, highly expensive reagents. The required solvents or the reagents used are toxic and hazardous which causes environmental pollution. Therefore, to overcome these limitations, the discovery and development of a new, simple, green, one pot and efficient protocol with a highly active catalyst for the preparation of 1,2-dihydro-1-aryl-3*H*-naphth[1,2-*e*][1,3]-oxazin-3-one derivatives under neutral, mild and practical conditions is of prime interest.

In recent decades, considerable attention has been devoted to heterogeneous organic transformations using heteropolyacids. Due to the super acidic properties of solid heteropolyacids (HPAs), they have been employed in numerous applications as useful and versatile acid catalysts over the last three decades.[9] They are usually solids that are insoluble in non-polar solvents but highly soluble in polar ones. They can be used in bulk or supported forms in both homogeneous and heterogeneous systems. They are more active catalysts than conventional inorganic and organic acids for various reactions in solution;[10] phosphomolybdic acid as a HPA catalyst has become important in industries related to fine chemicals.[11] Furthermore, heteropolyacids have several advantages, such as mild reaction conditions, easy work-up procedures and high selectivity including high flexibility in the modification of the acid strength, ease of handling, environmental compatibility, non-toxicity and experimental simplicity. They are non-corrosive and environmentally benign, as they can be reused and recycled.[12]

Our group has been working extensively on the development of novel methodologies under mild reaction conditions using phosphomolybdic acid.[13] In this study, the convenient and practical synthesis of 1,2-dihydro-1-aryl-3*H*--naphth[1,2-*e*][1,3]oxazin-3-one derivatives *via* the simple and efficient, one-pot multi-component condensation reaction of *β*-naphthol, aldehydes and urea in the presence of a catalytic amount of phosphomolybdic acid in DMF was realised (Scheme 1). The products were synthesized in good to excellent yields and characterized by ^{1}H-NMR, ^{13}C-NMR and mass spectroscopy, as well as by their physical constants. The physical and spectral data of known compounds are in agreement with those reported in the literature.[6–8]

EXPERIMENTAL

All commercial reagents were used as received without purification and all solvents were of reagent grade. The reaction was monitored by TLC using 0.25 mm Merck silica gel 60 F254 pre-coated plates, which were visualized with UV light. The melting points were determined in open capillaries. The IR spectra were recorded on a PerkinElmer 257 spectrometer using KBr discs. The ^{1}H-NMR and ^{13}C-NMR spectra were recorded on a VXR-300 MHz instrument using TMS as the internal standard.

General experimental procedure

A mixture of *β*-naphthol (0.01 mol), aldehyde (0.01 mol), urea (0.015 mol), phosphomolybdic acid (0.001 mol) and dimethylformamide (5 mL) was heated at 100 °C for an appropriate time (see later). After completion of reaction, as monitored by TLC, the reaction mixture was poured onto crushed ice, extracted with ethyl acetate and washed with water. The ethyl acetate extract was dried over anhydrous sodium sulphate and concentrated under reduced pressure. The crude product was crystallized by using 2-propanol.

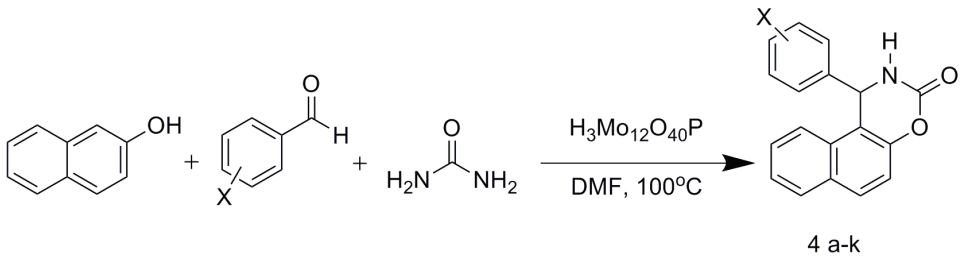

Scheme 1. Synthesis of 1,2-dihydro-1-aryl-3*H*-naphth[1,2-*e*][1,3]oxazin-3-ones.

RESULTS AND DISCUSSION

A preliminary experiment was performed to determine the suitable reaction conditions. The reaction of *β*-naphthol, benzaldehyde and urea in presence of phosphomolybdic acid was investigated. The best result was obtained in the presence of phosphomolybdic acid at 100 °C in DMF (Table I).

TABLE I. Effect of solvents on the preparation of 1,2-dihydro-l-phenyl-3*H*-naphth[1,2-*e*]-[1,3]oxazin-3-one (reaction conditions: *β*-naphthol (0.01 mol), benzaldehyde (0.01 mol), urea (0.015 mol), phosphomolybdic acid (0.001 mol), solvent (5 mL))

Entry	Solvent	*t* / °C	Time, h	Isolated yield, %
1	Ethanol	75	6.5	72
2	Methanol	55	6	75
3	Dimethylformamide	100	3	87
4	Acetonitrile	75	7	48
5	IPA	100	6.5	70
6	Chloroform	55	8	52
7	Toluene	110	7.5	48
8	Dichloromethane	38	10	40

To investigate the feasibility of this synthetic methodology for the synthesis of 1,2-dihydro-1-aryl-3*H*-naphth[1,2-*e*][1,3]oxazin-3-one derivatives, the reaction of *β*-naphthol with a variety of aromatic aldehydes and urea in presence of a catalytic amount of phosphomolybdic acid was performed, furnishing thereby the respective 1,2-dihydro-1-aryl-3*H*-naphth[1,2-*e*][1,3]oxazin-3-one derivatives in high yields. The optimized results are summarized in Table II, from which it can be observed that the results were excellent in terms of yields and product purity using aromatic aldehydes carrying electron-donating as well as electron-withdrawing substituents. When the reactions were conducted without the catalyst, the product yields were only 15–20 %, therefore phosphomolybdic acid provokes a considerable enhancement in the conversion.

In this protocol, phosphomolybdic acid was used as a recyclable catalyst. After completion of the reaction, the catalyst was recovered as follows: the reaction mixture was poured into ice-cold water and extracted with ethyl acetate. The ethyl acetate layer was then washed with water, dried over sodium sulphate and evaporated under reduced pressure to obtain the product. The aqueous layer was evaporated under reduced pressure to recover the phosphomolybdic acid, which was further reused for two more processes. The average percentage yield of recovery of phosphomolybdic acid is given in Table III.

TABLE II. Synthesis of 1,2-dihydro-1-aryl-3*H*-naphth[1,2-*e*][1,3]oxazin-3-one derivatives (reaction conditions: *β*-naphthol (0.01 mol), aldehyde (0.01 mol), urea (0.015 mol) phosphomolybdic acid (0.001 mol), dimethylformamide (5 mL), *t* = 100 °C)

Entry	Product	Aldehyde (X)	Time, h	Isolated yield, %
1	**4a**	2-OH	3	85
2	**4b**	2-Cl		89
3	**4c**	4-Cl		89
4	**4d**	4-OMe		86
5	**4e**	4-Me	2.5	87
6	**4f**	4-NO_2		92
7	**4g**	3-NO_2		92
8	**4h**	H	3	87
9	**4i**	2,5-OH	3.5	85
10	**4k**	2-OH, 5-OMe		84

TABLE III. Recyclability of the system using phosphomolybdic acid for the preparation of 1,2-dihydro-1-aryl-3*H*-naphth[1,2-*e*][1,3]oxazin-3-one derivatives

Run	Yield, %
1	87
2	87
3	86

Representative spectral data

1,2-Dihydro-l-(4-chlorolphenyl)-3H-*naphth[1,2-e][1,3]oxazin-3-one (**4c**)*. M.p. 209 °C. IR (KBr, cm^{-1}): 3224, 3146, 1734, 1600, 850, 730. ^{1}H-NMR (300 MHz, DMSO-d_6, δ, ppm): 6.21(1H, *s*, CH), 7.30–8.12 (10H, *m*, Ar-H), 8.89 (1H, *s*, NH). ^{13}C-NMR (300 MHz, DMSO-d_6, δ, ppm): 53, 114, 117, 123, 125, 127, 128, 129, 130, 129.5, 129.6, 130.5, 133, 142, 147, 149 ppm. MS (*m*/*z*): 309 (M^+).

1,2-Dihydro-l-(4-methylphenyl)-3H-*naphth[1,2-e][1,3]oxazin-3-one (**4e**)*. M.p. 167 °C. IR (KBr, cm^{-1}): 3225, 3127, 7210, 1658, 1580, 830. ^{1}H-NMR (300 MHz, DMSO-d_6, δ, ppm): 2.23 (3H, *s*, CH_3), 6.15 (1H, *d*, CH), 7.05–7.88 (10H, *m*, Ar-H), 8.78 (1H, *s*, NH). ^{13}C-NMR (300 MHz, DMSO-d_6, δ, ppm): 22, 52, 113, 116, 122, 126, 126, 128, 130, 129, 131, 132, 133, 137, 140, 148, 150. MS (*m*/*z*): 290 (M^+).

CONCLUSIONS

In conclusion, a novel method with judicious choice of the solvent and catalyst for the synthesis of 1,2-dihydro-1-aryl-3*H*-naphth[1,2-*e*][1,3]oxazin-3-one derivatives has been developed. This new protocol has enormous potential for the preparation of a large library of 1,3-oxazin-2-ones in an expeditious and environmentally friendly way in good to excellent yields from readily accessible starting materials. A variety of functional groups are compatible with the reaction conditions.

Acknowledgements. The authors are grateful to University Grand Commission, New Delhi and to the University of Mumbai for financial support. Thanks to Dr. S.T. Gadade, Principal, C. K. Thakur College, for providing the laboratory and other facilities.

ИЗВОД

ЕКОЛОШКИ БЕНИГНА СИНТЕЗА ДЕРИВАТА 1,2-ДИХИДРО-1-АРИЛ-3*H*-НАФТ-[1,2-*e*][1,3]ОКСАЗИН-3-ОНА, У ЈЕДНОМ РЕАКЦИОНОМ КОРАКУ, КАТАЛИЗОВАНА ФОСФОМОЛИБДЕНСКОМ КИСЕЛИНОМ

ATUL CHASKAR[1,2], VIMAL VYAVHARE[1], VIKAS PADALKAR[1], KIRAN PHATANGARE[1] и HRUSHIKESH DEOKAR[1]

[1]C. K. Thakur Research Centre, Navi Mumbai-410206, India и [2]Dipartimento di chimica, materiali ed ingegneria chimica "Giulio Natta" Politecnico di Milano, Milan, Italy

Описан је нов поступак за синтезу 1,2-дихидро-1-арил-3*H*-нафт[1,2-*e*][1,3]оксазин-3--она у једном реакционом кораку и високом приносу, реакцијом β-нафтола, ароматичних алдехида и урее у присуству фосфомолибденске киселине као катализатора.

(Примљено 10. априла, ревидирано 29. јуна 2010)

REFERENCES

1. M. Patel, R. J. McHugh Jr., B. C. Cordova, R. M. Klabe, S. Erickson-Viitanen, G. L. Trainor, S. S. Ko, *Bioorg. Med. Chem. Lett.* **9** (1999) 3221
2. N. Latif, N. Mishriky, F. M. Assad, *Aust. J. Chem.* **35** (1982) 1037
3. Y. Wang, X. Li, K. Ding, *Tetrahedron Asym.* **13** (2002) 1291

4. F. W. Holly, A. C. Cope, *J. Am. Chem. Soc.* **66** (1944) 1875
5. a) W. J. Burke, *J. Am. Chem. Soc.* **71** (1949) 609; b) W. J. Burke, M. J. Kolbezen, C. W. Stephens, *J. Am. Chem. Soc.* **74** (1952) 3601; c) W. J. Burke, K. C. Murdock, G. J. Ec, *J. Am. Chem. Soc.* **76** (1954) 1677; d) W. J. Burke, R. P. Smith, C. Weatherbee, *J. Am. Chem. Soc.* **74** (1952) 602; e) W. J. Burke, E. M. Glennie, C. Weatherbeee, *J. Org. Chem.* **29** (1964) 909; f) W. J. Burke, C. R. Hammer, C. Weatherbee, *J. Org. Chem.* **26** (1961) 4403; g) W. J. Burke, W. A. Nasatuvicus, C. Weatherbee, *J. Org. Chem.* **29** (1964) 407; h) W. J. Burke, C. Weatherbee, *J. Am. Chem. Soc.* **72** (1950) 4691; i) W. J. Burke, R. J. Reynolds, *J. Am. Chem. Soc.* **76** (1954) 1291
6. I. Szatmari, A. Hetenyi, L. Lazar, F. Fulop, *J. Heterocyc. Chem.* **41 (**2004) 367
7. C. Cimarelh, G. Palmieri, E. Volpini, *Can. J. Chem.* **82** (2004) 1314
8. M. Dabiri, A. Delbari, A. Bazgir, *Synlett* **5** (2007) 821
9. a) I. Kozhevnikov, *Chem. Rev*. **98** (1998) 171; b) C. Izumi, Y. Urabe, M. Onaka, *Zeolite, Clay and Heteropolyacid in Organic Reactions*, Ch. 3, Kodansha/VCH, New York, 1993; c) *Catalysis for Fine Chemical Synthesis, Catalysis by Polyoxometalates 2*, I. Kozhevnikov, E. Derouane, Eds., Wiley, New York, 2002
10. a) M. Tiofeeva, A. Dimidov, I. Kozhevnikov, *J. Mol. Catal*. **79** (1993) 21; b) R. S. Drago, J. A. Dias, T. Maier, *J. Am. Chem. Soc*. **119** (1997) 7702
11. T. Okuhara, N. Mizuno, M. Misono, *Adv. Catal*. **41** (1996) 113
12. M. A. Schwegler, H. Van Bekkum, N. Munck, *Appl. Catal*. **74** (1991) 191
13. a) A. Chaskar, V. Padalkar, K. Phatangare, K. Patil, A. Bodkhe, B. Langi, *Appl. Catal. A* **359** (2009) 84; b) K. Phatangare, V. Padalkar, D, Mhatre, K. Patil, A. Chaskar, *Synth. Commun*. **39** (2009) 4117; c) P. Gawand, H. Deokar, B. Langi, A. Yadav, A. Chaskar, *Synth. Commun*. **39** (2009) 4171.

Journal of the Serbian Chemical Society
JSCS-info@shd.org.rs • www.shd.org.rs/JSCS
J. Serb. Chem. Soc. *76* (1) 27–34 (2011)
JSCS–4096
UDC **Centaurea spruneri*:577.121:547.565:615.281/.282–188
Original scientific paper

Antimicrobial activity of secondary metabolites isolated from *Centaurea spruneri* Boiss. & Heldr.

ANA ĆIRIĆ[1], ANASTASIA KARIOTI[2,3], JASMINA GLAMOČLIJA[1], MARINA SOKOVIĆ[1] and HELEN SKALTSA[2]*

[1]*Department of Plant Physiology, Mycological Laboratory, Institute for Biological Research "S. Stanković", University of Belgrade, Bul. despota Stefana 142, 11 000 Belgrade, Serbia,* [2]*Department of Pharmacognosy and Chemistry of Natural Products, School of Pharmacy, University of Athens, Panepistimiopolis, Zografou, 157 71, Athens, Greece and* [3]*Department of Pharmaceutical Sciences, University of Florence, via Ugo Schiff 6, Polo Scientifico, Sesto Fiorentino, 50019 Florence, Italy*

(Received 27 January, revised 19 May 2010)

Abstract: Two coumarins, scopoletin (**1**) and isoscopoletin (**2**), two simple phenolic acids, protocatechuic acid (**3**) and isovanillic acid (**4**) and one flavonoid, eriodictyol (**5**) were isolated from the aerial parts of *Centaurea spruneri*. The structure of the compounds was established by spectroscopic methods. The *in vitro* antimicrobial activity of the isolated compounds was tested against eight bacteria and eight fungal species, using a microdilution method. All compounds tested showed moderate antibacterial and antifungal activities. Their minimum inhibitory concentrations were in the range 0.655–2.38 μmol ml^{-1} and their minimal bactericidal concentrations ranged from 0.694 to 4.15 μmol ml^{-1} against the tested bacterial species. All compounds showed fungistatic activity at 0.259–2.38 μmol ml^{-1} and fungicidal at 0.69–2.6 μmol ml^{-1} against all fungi tested.

Keywords: Centaurea spruneri; polyphenols; antibacterial activity; antifungal activity.

INTRODUCTION

The genus *Centaurea* L., with nearly 500 species, is mainly distributed around the Mediterranean area and in western Asia.[1] It has been the subject of many chemical investigations, which led to the isolation of various types of compounds, such as sesquiterpene lactones, being the most abundant group, flavonoids, lignans, nor-isoprenoids and volatile constituents. Previous investigations revealed a large number of *Centaurea* species possessing biologically active

* Corresponding author. E-mail: skaltsa@pharm.uoa.gr
doi: 10.2298/JSC100127008C

compounds.[2–15] Sesquiterpene lactones isolated from *C. aschaia*,[2] *C. thessala* subsp. *drakiensis*,[3] *C. attica*,[3] *C. deusta*,[4] *C. chilensis*,[5] and *C. nicolai*[6] were found to possess strong antifungal activity, while those isolated from *C. spinosa* possessed a slight inhibitory effect against Gram-positive bacteria.[7] In addition, flavonoids from *C. raphanina* spp. *mixta* showed moderate antifungal activity,[8] while flavonoids from *C. floccosa*[9] were effective against Gram-positive bacteria.

As a continuation of research on *Centaurea* species,[2–4,7,8,10–17] the secondary metabolites of *C. spruneri* are reported herein.

C. spruneri Boiss. & Heldr. is a perennial species flowering rather late in summer, which grows wild in Greece and Albania. It is classified in the section *Acrocentron* (Cass.) DC.[1] Hitherto, the volatile constituents of the aerial parts were investigated, which were mainly represented by terpenoids and homologous series of alkanes, alkenes, aliphatic alcohols and related aldehydes, as well as fatty acids and fatty acid methyl esters.[16] The present study concerns the non-volatile constituents of the plant. The evaluation of the antimicrobial activity of the isolated compounds was also investigated.

EXPERIMENTAL

Plant material

The plant was collected from the margins of cultivated fields on the foothills of Mt. Pateras (Attiki), 38° 6' N, 23° 14' E, c. 400–500 m, in July, 1998. A voucher specimen of the plant is kept in the Herbarium of the University of Patras (UPA) under the number: Constantinidis 2216.

General procedure

The structures of the isolated compounds were deduced by spectroscopic methods. The UV spectra were recorded on a Shimadzu UV-160A spectrophotometer, according to Mabry *et al.*[18] The IR spectra were obtained on a Perkin-Elmer Paragon 500 FT-IR spectrophotometer. The 1D and 2D NMR spectra were recorded using Bruker DRX 400 and Bruker AC 200 spectrometers. COSY, HMQC, HSQC, HMBC, and NOESY (mixing time 950 ms) were performed using standard Bruker micro programs. Vacuum liquid chromatography (VLC) was performed on silica gel (Merck, Art. 9385) and column chromatography on silica gel (SDS, Art. 2050044), using solvent mixtures indicated in each case. Reversed-phase chromatography was carried out on JASCO HPLC system equipped with a UV detector; preparative HPLC was performed using a C_{18} 25 cm×10 mm Kromasil column. Fractionations were always monitored by ^{1}H-NMR and TLC on silica gel 60 F-254 (Merck, Art. 5554) and cellulose (Merck, Art. 5552) with visualization under UV radiation (254 and 365 nm) and spraying with anisaldehyde–sulfuric acid reagent on silica gel and Neu' s reagent on cellulose.[19]

Extraction and isolation of the bioactive compounds

The fresh plant material (2.26 kg) was ground finely and extracted successively at room temperature with cyclohexane–Et_2O–MeOH (1:1:1) and MeOH–H_2O (5:1). The non-polar extract was washed with brine; the aqueous layer was re-extracted with EtOAc and the organic layer dried with Na_2SO_4 and concentrated under reduced pressure. The latter residue (6.73 g) was pre-fractionated by VLC on silica gel (10.0 cm×8.0 cm), using cyclohexane––EtOAc–Me_2CO mixtures of increasing polarity as eluents to give 12 fractions (**A1**–**A12**).

Column chromatography over silica gel (15 cm×1.0 cm) of fraction **A5** (92.7 mg; eluted with EtOAc, 100 %) afforded 12 fractions (**B1**–**B12**). Fraction **B11** (26.7 mg; eluted with cyclohexane–CH_2Cl_2, 30:70) was subjected to HPLC (MeOH–H_2O with 2 % AcOH, 4:6) and afforded compounds **4** (1.1 mg; t_R 11.4 min) and **5** (0.9 mg; t_R 89.1 min). Fraction **A6** (116.6 mg; eluted with EtOAc–Me_2CO, 90:10) was subjected to column chromatography over silica gel (12 cm×1.5 cm) and afforded 11 fractions (**C1**–**C11**). Further purification of fraction **C8** (64.4 mg; eluted with cyclohexane–CH_2Cl_2, 50:50) by HPLC (MeOH–H_2O with 2 % AcOH, 4:6) yielded compounds **1** (3.1 mg; t_R 22.6 min) and **5** (0.6 mg; t_R 49.1 min). Column chromatography over silica gel (12 cm×1.5 cm) of fraction **A7** (274.3 mg; eluted with EtOAc––Me_2CO, 75:25) afforded 10 fractions (**D1**–**D10**). Fraction **D8** (64.0 mg; eluted with cyclohexane–EtOAc, 30:70) was subjected to HPLC (MeOH–H_2O with 2 % AcOH, 4:6) and afforded compounds **2** (3.0 mg; t_R 22.8 min), **3** (2.0 mg; t_R 13.9 min) and **5** (2.7 mg; t_R 78.3 min).

Antimicrobial activity

The following Gram-negative bacteria were used: *Escherichia coli* (ATCC 35210), *Proteus mirabilis* (clinically isolated), *Pseudomonas aeruginosa* (ATCC 27853) and *Salmonella typhimurium* (ATCC 13311); and the following Gram-positive bacteria: *Bacillus cereus* (clinically isolated), *Micrococcus flavus* (ATCC 10240), *Listeria monocytogenes* (NCTC 7973) and *Staphylococcus aureus* (ATCC 6538). For the antifungal bioassays, eight fungi were used: *Aspergillus niger* (ATCC6275), *Aspergillus versicolor* (ATCC11730), *Aspergillus flavus* (ATCC 9170), *Aspergillus fumigatus* (clinical strain), *Candida albicans* (clinical strain) *Penicillium funiculosum* (ATCC10509), *Penicillium ochrochloron* (ATCC9112) and *Trichoderma viride* (IAM5061). The organisms were obtained from the Mycological Laboratory, Department of Plant Physiology, Institute for Biological Research "Siniša Stanković", Belgrade, Serbia and the Institute of Public Health of Serbia "Dr Milan Jovanović Batut". The micromycetes were maintained on malt agar (Torlak, Serbia) and the cultures were stored at 4 °C and sub-cultured once a month.[20] In order to investigate the antibacterial and antifungal activity of the isolated compounds, a modified microdilution technique was used for both activities.[21,22] Bacterial species were cultured overnight at 37 °C in tryptic soy broth medium (Biolife, Italy). The spore suspension was adjusted with sterile saline to a concentration of approximately 1.0×10^5 spores in a final volume of 100 μL per well. The inocula were stored at 4 °C for further use. Dilutions of the inocula were cultured on Müller–Hinton agar for bacteria and solid malt agar for fungi to verify the absence of contamination and to check the validity of the inoculum. The compounds investigated were dissolved in DMSO (0.1–1 μg mL^{-1}) and added in the broth medium (bacteria)/broth malt medium (fungi) with inocula. The minimum inhibitory concentration (*MIC*) values were determined by a serial dilution technique using 96-well micro titer plates. The micro plates were incubated for 48 h at 37 °C (bacteria) or 72 h at 28 °C (fungi). For the fungi, the lowest concentration without visible growth (using a binocular microscope) was defined as the *MIC*. For the bacteria, the following day, 50 μL of 0.2 mg mL^{-1} solution of INT (*p*-iodonitrotetrazolium violet) was added, and the plates were returned to the incubator for at least 30 min to ensure adequate color reaction. Inhibition of growth was indicated by a clear solution or a definite decrease in the color reaction. This value was taken as the *MIC* value for the bacteria.[23] The minimum bactericidal concentration (*MBC*) and minimum fungicidal concentration (*MFC*) were determined by serial sub-cultivation of a 2 μL sample into microtiter plates containing 100 μL of broth per well and further incubation for 48 h at 37 °C or 72 h at 28 °C for the bacteria and fungi, respectively. The lowest concentration with no visible growth was defined as the *MBC* or *MFC*, respectively, indicating 99.5 % killing of the original inoculum.[20] DMSO was used as the negative control, while the antibiotics strepto-

mycin and amoxicillin and the commercial fungicides bifonazole and ketokonazole were used as the positive controls (0.1–5 μL mL^{-1}). All experiments were performed in triplicate.

RESULTS AND DISCUSSION

The structures of the isolated compounds are given in Fig 1. Their spectroscopic data were according to the literature.[18,24,25]

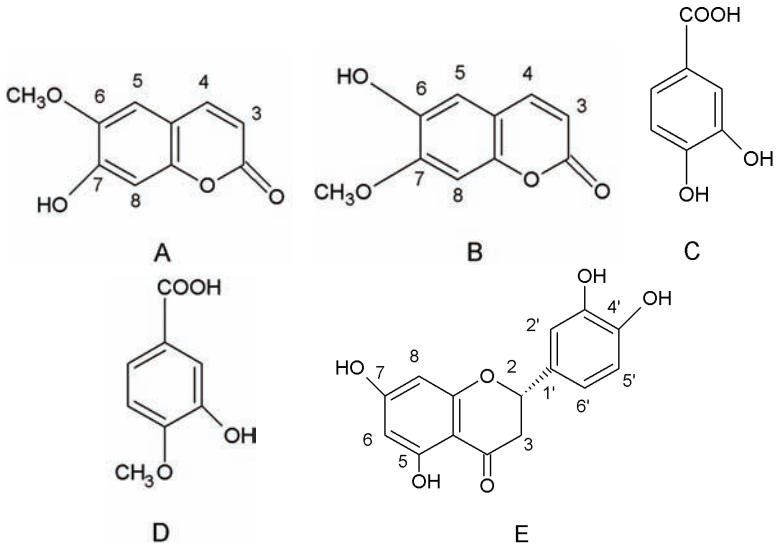

Fig. 1. Structures of the isolated compounds **1**–**5** (A–D, respectively).

The results for the antibacterial activity of compounds **1**–**5** are shown in Table I. The tested compounds possessed moderate antibacterial activity against all the tested bacterial species. The best results were obtained with compound **3**, which showed the strongest antibacterial activity with *MIC* values of 0.65–1.3 μmol ml^{-1} and *MBC* values of 1.3–2.6 μmol ml^{-1}. Compound **4** exhibited the lowest antibacterial activity, with MIC and MBC values in the range 1.19–2.38 μmol ml^{-1}. *B. cereus* was the most sensitive bacterial species (*MIC* 0.65–1.19 μmol ml^{-1}), while *L. monocytogenes* was the most resistant species (*MIC* 1.30––2.38 μmol ml^{-1}).

The results from the antifungal assay are summarized in Table II. Compound **5** possessed the best antifungal activity, with *MIC* and *MFC* values in the range 0.694–1.388 μmol ml^{-1}, while compound **3** showed the lowest antifungal activity. This latter compound inhibited fungal growth at 0.65–1.3 μmol ml^{-1}, while fungicidal activity was achieved at 1.3–2.6 μmol ml^{-1}. The majority of the compounds showed the worst activity against *A. flavus*, while *C. albicans* was the most sensitive species. The commercial drugs possessed lower or similar antifungal activity as the tested compounds, with *MIC* values of 0.322–0.644 μmol

ml^{-1} and *MFC* values of 0.483–0.806 μmol ml^{-1} for bifonazole, and *MIC* values of 0.376–4.70 μmol ml^{-1} and MFC values of 0.64–5.64 μmol ml^{-1} for ketokonazole. Although compound **3** showed the lowest antifungal activity, it exhibited the strongest antibacterial activity. In an effort to explain the different activity profiles of this compound, it was found that phenolic compounds with more hydroxyl groups possess better antibacterial activity,[26] while the antifungal activity was ascribed to the absence of polar groups in the molecule.[27,28]

TABLE I. Minimum inhibitory and bactericidal concentrations (*MIC* and *MBC* / 10^{-2} μmol ml^{-1}, 1st and 2nd row for each bacterium, respectively) of compounds **1**–**5**

Bacterium	**1**	**2**	**3**	**4**	**5**	Streptomycin[a]	Amoxicillin[a]
Bacillus	103.8±0.6	103.8±0.6	65.0±0	119.0±1.5	69.4±0.3	4.3±0.3	27.4±0.6
cereus	103.8±0.6	103.8±0.6	130.0±0.6	119.0±1.5	69.4±0.3	8.6±1.2	54.8±1.7
Micrococcus	103.8±0.6	103.8±0.6	130.0±0.6	119.0±1.0	69.4±0.3	8.6±1.2	6.9±0.3
flavus	207.6±1.2	207.6±1.2	260.0±1.0	238.0±1.0	277.6±1.2	17.2±0.3	13.7±0.3
Staphylococcus	103.8±0.6	207.6±1.2	130.0±0.6	119.0±1.5	69.4±0.3	17.2±0.3	6.9±0.3
aureus	207.6±1.2	415.2±1.7	260.0±1.0	238.0±1.0	277.6±1.2	34.4±0.3	13.7±0.3
Listeria	207.6±1.2	207.6±1.2	130.0±0.6	238.0±2.0	138.8±0.6	34.4±0.3	27.4±0.6
monocytogenes	207.6±1.2	415.2±1.7	260.0±1.0	238.0±2.0	277.6±1.2	68.8±0.6	54.8±0.6
Escherichia	103.8±0.3	103.8±0.6	130.0±0.6	119.0±0.6	69.4±0.3	8.6±1.2	27.4±0.6
coli	103.8±0.3	103.8±0.6	130.0±0.6	119.0±0.6	277.6±1.2	17.2±0.3	54.8±1.7
Pseudomonas	103.8±0.6	103.8±0.3	65.0±0	119.0±1.0	69.4±0.3	17.2±0.3	13.7±0.6
aeruginosa	103.8±0.6	103.8±0.3	130.0±0.6	119.0±1.0	277.6±2.1	34.4±0.3	27.4±1.2
Proteus	103.8±0.6	207.6±1.7	130.0±0.6	238.0±2.0	138.8±1.2	34.4±0.3	27.4±1.2
mirabilis	207.6±1.7	207.6±1.7	260.0±1.0	238.0±2.0	277.6±2.1	68.8±1.2	54.8±1.7
Salmonella	103.8±0.3	103.8±0.3	65.0±0	119.0±1.5	69.4±0.3	17.2±1.7	13.7±0.6
typhimurium	103.8±0.3	103.8±0.3	130.0±0.6	119.0±1.5	277.6±2.1	34.4±1.2	27.4±1.2

[a]Positive control, standard antibiotics

Previous investigations revealed that the antimicrobial potential of *Centaurea* species is mainly due to their high content of sesquiterpene lactones.[2–7,13,14] Thus, sesquiterpene lactones such as cnicin, 4'-acetylcnicin, 8-(3-hydroxy-4-acetoxy-2-methylenebutanoyloxy)-4-*epi*-sonchucarpolide, 8*α*-*O*-(4,5-dihydroxytigloyloxy) esters of salonitenolide, 11,13-dihydromelitensin and 9-*O*-acetyl and 3--*O*-deacetyl-9-O-acetyl derivatives of salograviolide A isolated from various of *Centaurea* species exhibited high or moderate antifungal activities against all the tested fungi with exception of *Trichoderma viride*, for which no inhibition was observed or with the worst activity.[2,3,7] The sesquiterpene lactones: 8*α*-*O*-(4-hydroxy-2-methylenebutanoyloxy)melitensine, melitensin, 11*β*,13-dihydrosalonitenolide, 8*α*-hydroxy-11*β*,13-dihydro-4-*epi*-sonchucarpolide and 8*α*-hydroxy-11*β*,13-dihydroonopordaldehyde isolated from the aerial parts of *C. pullata* showed greater antibacterial and antifungal activities than the positive controls used.[14] The flavonoids, 6-methoxyapigenin, apigenin, 6-methoxyluteolyn-4',7--dimethylether, 6-methoxyluteolyn-3'-methylether, 6-methoxyluteolyn-3',4',7-

trimethylether and C-glycosyl flavonoids characterized from the *C. virgata*, *C. kilea* and *C. intermis* exhibited inhibitory activities on fungal species, Gram-positive and Gram-negative bacteria. None of them was effective against *Staphylococcus aureus* and *S. epidermidis*.[29] The present study revealed that *C. spruneri* is a species poor in sesquiterpene lactones but rich in polyphenols, which were shown to possess antimicrobial activities against all the tested fungi, Gram-positive and Gram-negative bacteria. With respect to the antifungal potential of this latter group, the results obtained in the present study are in agreement with those previously reported for *C. raphanina* ssp. *mixta*[8] and *C. floccosa*.[9]

TABLE II. Minimum inhibitory and fungicidal concentrations (*MIC* and *MFC* / 10^{-2} μmol ml^{-1}, 1st and 2nd row for each fungus, respectively) of compounds **1**–**5**

Fungus	**1**	**2**	**3**	**4**	**5**	Bifonazole[a]	Ketoconazole[a]
Penicillium	103.8±0.3	103.8±0.3	130.0±1.0	119.0±1.0	69.4±0.6	64.4±0.3	37.6±0.6
funiculosum	103.8±0.3	103.8±0.3	130.0±1.0	119.0±1.0	138.8±1.2	80.6±0.6	64.0±1.5
Penicillium	103.8±0.6	103.8±0.6	130.0±0.6	238.0±2.0	138.8±1.2	48.3±0.6	188.0±1.0
ochrochloron	207.6±0.6	207.6±0.6	260.0±1.5	238.0±2.0	138.8±1.2	64.4±1.7	188.0±1.0
Trichoderma	51.9±0.6	51.9±0.6	65.0±0	59.0±0.6	69.4±0.6	64.4±1.2	470.0±2.0
viride	103.8±0.6	103.8±0.6	130.0±1.0	238.0±1.0	138.8±0.6	80.6±0.6	564.0±1.5
Aspergillus	103.8±0.6	103.8±0.6	130.0±0.6	238.0±1.0	138.8±0.6	48.3±0.6	37.6±0.6
fumigatus	103.8±0.6	103.8±0.6	260.0±1.0	238.0±2.0	138.8±0.6	64.4±1.7	94.0±1.0
Aspergillus	103.8±0.6	103.8±0.6	130.0±1.0	238.0±1.0	138.8±0.6	48.3±0.6	37.6±0.6
niger	207.6±1.2	207.6±1.2	260.0±1.5	238.0±1.0	138.8±0.6	64.4±1.7	94.0±1.0
Aspergillus	207.6±1.7	207.6±1.7	130.0±0.6	238.0±2.0	138.8±0.6	48.3±0.6	282.0±2.0
flavus	207.6±1.7	207.6±1.7	260.0±1.0	238.0±2.0	138.8±0.6	64.4±1.7	376.0±1.0
Aspergillus	51.9±0.6	51.9±0.6	65.0±0	59.0±0.6	69.4±0.3	32.2±0.3	37.6±0.6
versicolor	207.6±1.2	207.6±1.2	260.0±1.5	238.0±1.5	138.8±1.2	64.4±1.2	94.0±1.0
Candida	25.9±0.3	51.9±0.6	65.0±0	59.0±0.6	69.4±0.6	32.2±0.3	37.6±0.6
albicans	103.8±0.3	103.8±0.6	130.0±0.6	119.0±1.0	69.4±0.6	48.3±0.6	94.0±1.0

[a]Positive control, standard antibiotics

Together with previously published data, the presented results indicate that *Centaurea* species possess biologically active compounds with different degrees of action. It can be seen that the growth of the tested microorganism responded differently to the investigated compounds, suggesting that different components may have different modes of action or that the metabolism of some microorganisms are better able to overcome the effect of the compound or adapt to it.

Acknowledgments. The authors are grateful to the Ministry of Science and Technological Development of the Republic of Serbia (Project No. 143041) and GSRT (70/3/7714) for financial support. The authors are also grateful to Assistant Prof. Dr. Theophanis Constantinidis (Faculty of Biology, NKUA, Greece) for the identification of the plant material and Milan Radović spec. food microbiology (Institute of Public Health of Serbia "Dr Milan Jovanović Batut", Serbia) for the bacterial strains.

ИЗВОД

АНТИМИКРОБНА АКТИВНОСТ СЕКУНДАРНИХ МЕТАБОЛИТА ИЗОЛОВАНИХ ИЗ *Centaurea spruneri* Boiss & Heldr.

АНА ЋИРИЋ[1], ANASTASIA KARIOTI[2,3], ЈАСМИНА ГЛАМОЧЛИЈА[1], МАРИНА СОКОВИЋ[1] и HELEN SKALTSA[2]

[1]Одељење за биљну физиологију, Миколошка лабораторија, Институт за биолошка истраживања "С. Станковић", Универзитет у Београду, Булевар деспота Стефана 142, 11 000 Београд, [2]Department of Pharmacognosy, School of Pharmacy, University of Athens, Panepistimiopolis, Zografou, 157 71, Athens, Greece и [3]Department of Pharmaceutical Sciences, University of Florence, via Ugo Schiff 6, Polo Scientifico, Sesto Fiorentino, 50019 Florence, Italy

Из надземног дела *Centaurea spruneri* изолована су два кумарина скополетин (**1**) и изоскополетин (**2**), две просте фенолске киселине протокатехуинска киселина (**3**) и изованилинска киселина (**4**) и флавоноид ериодиктиол. Хемијске структуре познатих једињења су утврђене коришћењем 1D и 2D NMR, MS и UV спектроскопских анализа. У *in vitro* тесту за одређивање антимикробне активности изолованих једињења коришћена је микродилуциона метода. Добијена једињења тестирана су на по осам бактеријских и гљивичних врста. Сва једињења су имала умерену антибактеријску и антифунгалну активност. Минимална инхибиторна концентрација тестираних једињења се кретала од 0,655 до 2,38 μmol ml^{-1}, а минимална бактерицидна концентрација 0,694–4,15 μmol ml^{-1}. Тестирана једињења су показала фунгицидну активност од 0,259–2,38 μmol ml^{-1} и фунгистатичку 0,694–2,60 μmol ml^{-1}, на све тестиране гљиве.

(Примљено 27. јануара, ревидирано 19. маја 2010)

REFERENCES

1. J. Mabberley, *The Plant Book*, 2nd ed., Cambridge University Press, Cambridge, 1997, p. 138
2. H. Skaltsa, D. Lazari, B. Gracia, J. Pedro, M. Sokovic, T. Constantinidis, *Z. Naturforsch*. **55c** (2000) 534
3. H. Skaltsa, D. Lazari, C. Panagouleas, E. Georgiadou, B. Gracia, M. Sokovic, *Phytochemistry* **55** (2000) 903
4. A. Karioti, H. Sklatsa, D. Lazari, M. Sokovic, B. Gracia, C. Harvala, *Z. Naturforsch*. **57c** (2002) 75
5. R. Negrete, N. Backhouse, S. Avendano, A. San Martin, *Plant. Med. Phytother*. **18** (1984) 226
6. V. Vajs, N. Todorović, M. Ristić, V. Tešević, B. Todorović, P. Janacković, P. Marin, S. Milosavljević, *Phytochemistry* **52** (1999) 383
7. V. Saroglou, A. Karioti, C. Demetzos, K. Dimas, H. Skaltsa, *J. Nat. Prod*. **68** (2005) 1404
8. C. Panagouleas, H. Skaltsa, D. Lazari, A.-L. Skaltsounis, M. Sokovic, *Pharm. Biol*. **41** (2003) 266
9. R. E. Negrete, N. Backhouse, B. Bravo, S. Erazo, R. Garcia, S. Avendano *Plant. Med. Phytother*. **21** (1987) 168
10. H. Skaltsa, D. Lazari, E. Georgiadou, S. Kakavas, T. Constantinidis, *Planta Med*. **65** (1999) 393
11. E. Koukoulitsa, H. Skaltsa, A. Karioti, C. Demetzos, K. Dimas, *Planta Med*. **68** (2002) 649
12. C. Gousiadou, H. Skaltsa, *Biochem. Syst. Ecol*. **31** (2003) 389

13. S. Djeddi, A. Karioti, M. Sokovic, D. Stojkovic, R. Seridi, H. Skaltsa, *J. Nat. Prod.* **70** (2007) 1796
14. S. Djeddi, A. Karioti, M. Sokovic, C. Koukoulitsa, H. Skaltsa, *Bioorg. Med. Chem.* **16** (2008) 3725
15. S. Djeddi, C. Argyropoulou, H. Skaltsa, *Biochem. Syst. Ecol.* **36** (2008) 336
16. D. Lazari, H. Skaltsa, T. Constantinidis, *Flavour Fragr. J.* **14** (1999) 415
17. D. Lazari, H. Skaltsa, T. Constantinidis, *Flavour Fragr. J.* **15** (2000) 7
18. T. J. Mabry, K. R. Makham, M. B. Thomas, *The Systematic Identification of Flavonoids*, Springer, New York, **1970**
19. R. Neu, *Naturwissenschaften* **44** (1957) 181
20. C. Booth, in *Methods in Microbiology*, J. R. Norris, D. W. Ribbons, Eds., Academic Press, London, 1971, p. 49
21. H. Hanel, W. Raether, *Mycoses* **31** (1998) 148
22. R. K. Daouk, S. M. Dagher, J. E. Sattout, *J. Food Prot.* **58** (1995) 1147
23. J. N. Eloff, *Planta Med.* **64** (1998) 711
24. M. R. Horowitz, J. Leonard, *J. Org. Chem.* **26** (1961) 2446
25. J. B. Harborne, *Phytochemical Methods*, 2nd ed., Chapman & Hall, London, 1984
26. A. Mori, C. Nishino, N. Enoki, S. Tawata, *Phytochemistry* **26** (1987) 2231
27. M. Weidenbörner, H. Hindorf, H. Chandra Jha, P. Tsotsonos, H. Egge, *Phytochemistry* **29** (1990) 1103
28. A. Picman, E. Schneider, J. Picman, *Biochem. Syst. Ecol.* **23** (1995) 683
29. S. Öksüz, H. Ayyildiz, C. Johansson, *J. Nat. Prod.* **47** (1984) 902.

Journal of the Serbian Chemical Society
JSCS-info@shd.org.rs • www.shd.org.rs/JSCS
J. Serb. Chem. Soc. 76 (1) 35–42 (2011) UDC 633.861+543.544.5.068.7:547.814.5:678.048
JSCS–4097 *Original scientific paper*

Quantification of genistein and daidzein in two endemic *Genista* species and their antioxidant activity

ILKAY ERDOGAN ORHAN[1]*, FATMA TOSUN[1], UGUR TAMER[2], AHMET DURAN[3], BURCU ALAN[1] and ALI FUAT KÖK[1]

[1]*Department of Pharmacognosy, Faculty of Pharmacy, Gazi University, 06330, Ankara,* [2]*Department of Analytical Chemistry, Faculty of Pharmacy, Gazi University, 06330 Ankara and* [3]*Department of Biology, Faculty of Education, Selçuk University, Meram 42090, Konya, Turkey*

(Received 8 April, revised 17 June 2010)

Abstract: In the current research, the total and free genistein and daidzein contents were determined in two endemic *Genista* species (*G. sandrasica* and *G. vuralii*) by an HPLC method. The highest amount of total genistein and total daidzein was found in *G. sandrasica*, 0.582 and 0.113 %, respectively, whereas only the free daidzein content of *G. sandrasica* was higher than that of *G. vuralii*. The antioxidant activity of the crude methanol and hydrolyzed extracts of these species was evaluated by three *in vitro* methods; namely DPPH free radical scavenging, ferrous ion-chelating and ferric-reducing antioxidant power (FRAP) tests at 0.25, 0.50, and 1.0 mg ml^{-1}. The hydrolyzed extracts of both species displayed greater antioxidant activity than the crude methanol extracts in all tests. Total phenol and flavonoid contents in the extracts were determined *via* the Folin–Ciocalteau and $AlCl_3$ reagents, respectively. *G. vuralii* was richer in terms of total phenol and flavonoid contents compared to *G. sandrasica*.

Keywords: *Genista* L.; Fabaceae; isoflavones; daidzein; genistein; HPLC; antioxidant.

INTRODUCTION

Daidzein (7,4'-dihydroxyisoflavone) and genistein (5,7,4'-trihydroxyisoflavone) are known as phytoestrogens because they are plant compounds possessing estrogen-like activity. Phytoestrogens are considered to play an important role in the prevention of cancers, cardiovascular diseases, menopausal symptoms and osteoporosis.[1,2] Isoflavones are found in highest amounts in soybeans[3] and soy foods[4,5]; they are also present in other beans and legumes.[6] Dietary supplements containing isoflavones mainly from soybean and red clover were brought

* Corresponding author. E-mail: iorhan@gazi.edu.tr
doi: 10.2298/JSC100408015O

on the market as natural alternatives to conventional hormone replacement therapy.[7]

The genus *Genista* L. (Leguminosae) is represented by thirteen species in the Turkish flora, among these species, *G. involucrata*, *G. aucheri*, *G. burdurensis*, *G. vuralii* and *G. sandrasica* are endemic.[8–10] In previous studies, the aerial parts of eleven *Genista* species growing in Turkey were analyzed for their total and free genistein and daidzein contents.[11,12] The highest amount of total and free genistein was found in *G. tinctoria*, *i.e.*, 1.05 and 0.27 %, respectively,[13] whilst the highest amount of total and free daidzein was found in *G. sessilifolia* and *G. lydia* var. *antiochia*, *i.e.*, 0.0056 and 0.0009 %, respectively.[14] Continuing the investigations on the Turkish *Genista* species,[11–14] the genistein and daidzein contents in *G. vuralii* A. Duran & H. Dural and *G. sandrasica* Hartwig & Strid (Fabaceae), which have not been investigated before, are reported herein. In addition, their antioxidant activities were measured by three *in vitro* methods: 2,2--diphenyl-1-picrylhydrazyl (DPPH) free radical scavenging, ferrous ion-chelating, and ferric-reducing antioxidant power (FRAP) tests at 0.25, 0.50, and 1.0 mg ml^{-1} concentrations. The total phenol and flavonoid contents in the extracts were determined spectrophotometrically *via* the Folin-Ciocalteau and $AlCl_3$ reagents, respectively.

EXPERIMENTAL

Plant materials

G. vuralii (GV) and *G. sandrasica* (GS) were collected at the flowering stage from the Ilgaz Mountain in the Çankırı Province in July 2004 and from the Sandras Mountain in the Muğla Province in July 2006 in Turkey, respectively. The plant materials were identified by one of us (Prof. Dr. Ahmet Duran). Voucher specimens (A. Duran 6735 and A. Duran 7312 & M. Dinç) are kept at the Herbarium in the Department of Biology Education, Faculty of Education, Selçuk University, Konya, Turkey.

Chemicals

Genistein and daidzein standards were purchased from Sigma. (St. Louis, MO, USA). HPLC grade methanol (Merck, Darmstadt, Germany) and deionized water (Millipore) was used for chromatographic and antioxidant activity studies.

Preparation of standards

Five working solutions were prepared for each standard in methanol containing genistein in 1, 2, 3, 4, and 8 mg l^{-1} and daidzein in 4, 8, 10, 12, and 16 mg l^{-1} concentrations.

Extract preparation for HPLC analysis and the antioxidant activity tests

Air-dried and powdered aerial parts of each plant species were extracted following a previously reported method[13,14] for analyzing free and total isoflavones. Each plant was milled homogenously and 1 g was precisely weighed on a digital balancer. The powdered materials were extracted with methanol under ultrasonic vibration. The extracts were analyzed for their free isoflavones. One gram of precisely weighed aerial parts of the plant materials was hydrolyzed by heating with a mixture of an equal volume of methanol and 2 M HCl for 1 h under reflux. After filtering the mixture, 1 ml filtrate was diluted with 9 ml water and loaded

on to a Sep-Pak C18 cartridge (Waters). The isoflavones were retained on the Sep-Pak C18 cartridge, which was then washed twice with 10 ml of water and eluted with 70 % methanol. These extracts were analyzed for their total isoflavones.

HPLC Analysis

The HPLC analyses were realized on a HP 1050 Liquid Chromatograph System equipped with a Hypersil 120-S ODS column (250 mm×4.6 mm, 10 μm) and a UV detector. The mobile phase was methanol:water (70:30, v/v) at a flow rate of 0.7 ml min^{-1}. The temperature of the column was 25 °C. Data were collected at 261 nm for genistein and at 248 nm for daidzein. Each extract and five solutions of each standard were injected three times.

Antioxidant activity

DPPH free radical-scavenging assay. The hydrogen atom or electron donation capacity of the corresponding extracts was computed from the bleaching property of the purple-colored methanol solution of 2,2-diphenyl-1-picrylhydrazyl (DPPH). The stable DPPH radical scavenging activity of the extracts was determined by the Blois method.[15] The samples and reference dissolved in ethanol (75 %) were mixed with DPPH solution (1.5×10^{-4} M). The remaining amount of DPPH was measured at 520 nm using a Unico 4802 UV–visible double beam spectrophotometer (USA). The results were compared to that of gallic acid employed as the reference. The inhibition of DPPH (*I*) in percent was calculated as follows:

$$I\ \% = 100(A_{\text{blank}} - A_{\text{sample}})/A_{\text{blank}} \quad (1)$$

where A_{blank} is the absorbance of the control reaction (containing all reagents except the test sample) and A_{sample} is the absorbance of the extracts/reference. The experiments were run in triplicates and the results are conveyed as average values with the *SEM*. (Standard error mean).

Fe^{2+}–ferrozine test system for iron chelating. The ferrous ion-chelating effect of the extracts by the Fe^{2+}–ferrozine test system was estimated by the method of Chua *et al*.[16] Accordingly, 740 μl of ethanol and the samples were incubated with 2 mM $FeCl_2$ solution. The reaction was initiated by the addition of 40 μl of ferrozine solution into the mixture and left standing at ambient temperature for 10 min. The absorbance of the reaction mixture was measured at 562 nm. The ratio of inhibition of ferrozine–Fe^{2+} complex formation was calculated by Eq. (1).

The control contained only $FeCl_2$ and ferrozine. The analyses were run in triplicates and the results are expressed as average values with the *SEM*.

The ferric-reducing antioxidant power (FRAP). The ferric-reducing antioxidant power (FRAP) of the extracts and reference was tested using the assay of Oyaizu.[17] One ml of different concentrations of the extracts, as well as chlorogenic acid as the reference for comparative purposes, was added to 2.5 ml of phosphate buffer (pH 6.6) and 2.5 ml of potassium ferricyanide. Subsequently, the mixture was incubated at 50 °C for 20 min and then trichloroacetic acid (10 %) was added. After vigorous shaking, this solution was mixed with distilled water and $FeCl_3$ (0.1 %, w/v). After 30 min incubation, the absorbance was read at 700 nm using a Unico 4802 UV–visible double beam spectrophotometer (USA). The analyses were realized in triplicate. An increase in the absorbance of the reaction mixture indicates an increase in the reducing power of the extracts.

Determination of the total phenol and total flavonoid contents of the extracts

Phenolic compounds were determined using Folin-Ciocalteau reagent according to the Singleton and Rossi method.[18] In brief; the samples were mixed with 750 μl of Folin-Cio-

calteau reagent and 600 µl of sodium carbonate in test tubes. The tubes were then vortexed and incubated at 40 °C for 30 min. Subsequently, absorption was measured at 760 nm using a Unico 4802 UV–visible double beam spectrophotometer (USA). The total flavonoid content was determined by the aluminum chloride colorimetric method.[19] In short, a number of dilutions of quercetin were obtained to prepare a calibration curve. Then, the same dilutions from the sample were also prepared and separately mixed with 95 % ethanol, 10 % aluminum chloride, 1 M sodium acetate as well as 2.8 ml of distilled water. Following incubation for 30 minutes at room temperature, the absorbance of the reaction mixture was measured at 415 nm with a Unico 4802 UV–visible double beam spectrophotometer (USA). The total phenolic and flavonoid contents of the extracts are expressed as gallic acid and quercetin equivalents (mg g^{-1} extract), respectively.

RESULTS AND DISCUSSION

The total and free genistein and daidzein amounts found in *G. vuralii* (GV) and *G. sandrasica* (GS) are given in Table I. The amounts of genistein were calculated from the regression equation obtained from a standard curve which was linear within the concentration range 1–8 mg l^{-1}. The amounts of the daidzein were calculated from the regression equation obtained from daidzein standard curve which was linear within the concentration range of 4–16 mg l^{-1}. The regression equation and correlation coefficient determined for genistein and daidzein were $y = 154.8x - 0.12$ ($r^2 = 0.9997$) and $y = 153.2x - 3.90$ ($r^2 = 0.9981$), respectively. The amount of total and free genistein was found in GS and GV to be 0.58 and 0.05 %, respectively (Table I). The total and free daidzein contents of the aerial parts of GS were higher than those of GV and twelve other Turkish *Genista* species studied previously, *i.e.*, *G. acanthoclada*, *G. albida*, *G. anatolica*, *G. aucheri*, *G. burdurensis*, *G. carinalis*, *G. involucrata*, *G. libanotica*, *G. lydia* var. *antiochia*, *G. lydia* var. *lydia*, *G. sessilifolia*, and *G. tinctoria*.[12] On the other hand, the free daidzein content (0.068 %) was much higher than the free genistein content (0.013 %) in GS. In addition, the total genistein content of GS (0.582 %) was higher than those of GV and other *Genista* species previously studied, except for *G. tinctoria* (1.05 %).[11] Considering the formerly studied species, total daidzein contents ranged between 0.0003–0.0056 %, while the total genistein contents were in the range 0.01–1.05 %.[11,12]

TABLE I. Genistein and daidzein contents (mass %) of *G. vuralii* (GV) and *G. sandrasica* (GS)

Species	Total genistein	Free genistein	Total daidzein	Free daidzein
GV	0.363	0.050	0.048	0.016
GS	0.582	0.013	0.113	0.068

The methanol extracts of GS and GV exerted a similar scavenging effect against the DPPH radical at the tested concentrations (Table II), whereas the hydrolyzed extracts of these two species were found to have higher effects in this test. The same tendency for the extracts was also observed in the ferric-reducing

antioxidant power test, in which the hydrolyzed extract of *G. vuralii* (GVH) was much more active than the main methanol extracts (Table III). The hydrolyzed extract of *G. sandrasica* (GSH) could not be tested due to its inadequate amount. In the ferrous ion-chelating capacity test, the extracts did not show a significant effect (Table III).

TABLE II. Total phenol (mg g^{-1} extract as gallic acid equivalent) and total flavonoid (mg g^{-1} extract as quercetin equivalent) contents and DPPH radical scavenging activities of the methanol extracts of *G. vuralii* (GV) and *G. sandrasica* (GS) and their hydrolyzed extracts as well as daidzein and genistein

Extract	Total phenol content±*SEM*[a]	Total flavonoid content±*SEM*	Inhibition±*SEM*, %, against DPPH radical		
			c / μg ml^{-1}		
			250	500	1000
GV	212.24±2.62	203.82±4.08	16.85±1.25	29.91±0.01	50.70±3.87
GS	166.94±3.13	158.06±0.13	15.90±0.42	24.77±3.43	46.16±1.09
GVH[b]	NT[c]	NT	69.80±3.27	85.05±0.25	86.12±0.42
GSH[d]	NT	NT	69.51±2.85	85.64±0.59	87.18±0.08
Daidzein	–	–	–[e]	2.52±0.76	6.99±3.56
Genistein	–	–	–	–	–
Gallic acid (reference)	–	–	87.65±0.28	91.61±0.06	92.57±0.10

[a]Standard error mean; [b]the hydrolyzed extract of GV; [c]not tested; [d]the hydrolyzed extract of GS; [e]no activity

TABLE III. Ferrous ion-chelating capacity (inhibition±*SEM*, %), and ferric-reducing antioxidant power (absorbance at 700 nm±*SEM*) of the methanol extracts of *G. vuralii* (GV) and *G. sandrasica* (GS) and their hydrolyzed extracts, as well as daidzein and genistein

Extracts	Ferrous ion-chelating capacity (inhibition±*SEM*, %)			Ferric-reducing antioxidant power (absorbance at 700 nm±*SEM*)		
				c / μg ml^{-1}		
	250	500	1000	250	500	1000
GV	3.28±1.24	7.47±0.11	10.21±1.78	0.468±0.007	0.627±0.021	1.005±0.018
GS	6.89±0.88	8.29±0.71	8.21±0.42	0.458±0.023	0.652±0.044	0.860±0.046
GVH	8.83±0.89	8.95±0.65	13.90±0.91	1.289±0.016	2.478±0.053	2.829±0.031
GSH	NT[a]	NT	NT	NT	NT	NT
Daidzein	–[b]	–	–	0.206±0.021	0.211±0.023	0.292±0.007
Genistein	–	–	–	0.192±0.005	0.216±0.005	0.340±0.021
Butylated hydroxyanisol (reference for ferric ion-chelating capacity)	NT	21.71±1.10	26.94±1.48			
Chlorogenic acid (reference for FRAP)				2.955±0.09	3.547±0.06	3.618±0.01

[a]Not tested; [b]no activity

For total phenol content, the calibration equation was calculated as y = = 0.9051x + 0.0549 (r^2 = 0.9943) (gallic acid equivalent) and as y = 5.5398x + + 0.1209 (r^2 = 0.9988) (quercetin equivalent) for the total flavonoid content in the methanol extracts (Table II). The total phenol and flavonoid amounts of GSH and GVH could not be established due to their small amounts. The methanol extracts were found to contain total phenol and flavonoid in similar quantities.

On the other hand, there have been a few reports on the antioxidant activity of *Genista* species. For instance; various extracts of *G. tenera* of Portuguese origin were tested for their scavenging activity against the DPPH radical and the ethyl acetate extract was shown to cause the best scavenging activity of 48.7 % at a concentration of 139.1 μg ml^{-1}.[20] In another study, the methanol extracts from the aerial parts of *G. sessilifolia* and *G. tinctoria* were tested on pBR322 DNA cleavage induced by hydroxyl radicals ($^{\bullet}$OH), generated from UV-photolysis of hydrogen peroxide (H_2O_2) and by nitric oxide (NO) and they displayed a protective effect on UV light and nitric oxide-mediated plasmid DNA damage.[21]

In the present antioxidant assays, genistein and daidzein were not active in the DPPH radical scavenging and ferrous ion-chelating capacity tests; whereas they exhibited mild FRAP (Tables II and III). Genistein and daidzein, the well--known isoflavone-type of phytoestrogens, have been studied up to date for their antioxidant activities by various methods and they were reported to be active in some assays. However, no data on the effect of these two isoflavones in the ferrous ion-chelating capacity test were encountered, while one study proved that metabolites of these isoflavones were more active than genistein and daidzein in FRAP.[22] In one recent study,[23] the antioxidant activities of some isoflavonoids, *i.e.*, puerarin and daidzein as well as *Pueraria lobata* and *P. miristica* extracts, were determined using the DPPH radical scavenging test and daidzein was shown to display the same level of antioxidant activity as α-tocopherol. This discrepancy might result from differences in the method used in the present study and in the literature publication. However, in another report,[24] daidzein was concluded to up-regulate the antioxidant enzyme catalase but showed only little antioxidant capacity *per se*. Genistein and daidzein were also found to show strong antioxidant effects against the oxygen radical.[25,26] Arteaga *et al.* suggested that phytoestrogens including genistein and daidzein showed weak antioxidant activity *in vitro* in the low density lipoprotein (LDL) oxidation test.[27]

CONCLUSIONS

To the best of our knowledge, the current study reports the first data on the antioxidant activity of and the genistein and daidzein contents in *G. vuralii* and *G. sandrasica*. The results indicated that the hydrolyzed extracts had higher antioxidant activities. *G. sandrasica* was also shown to contain larger amount of free and total daidzein than *G. vuralii*, which was richer in total phenol and fla-

vonoid than *G. sandrasica*, as well as the other *Genista* species studied previously. However, the daidzein and genistein were found to have no or little effects in the antioxidant assays applied herein.

И З В О Д

ОДРЕЂИВАЊЕ ГЕНИСТЕИНА И ДАИДЗЕИНА У ДВЕ ЕНДЕМСКЕ ВРСТЕ *Genista* И МЕРЕЊЕ ЊИХОВЕ АНТИОКСИДАТИВНЕ АКТИВНОСТИ

ILKAY ERDOGAN ORHAN[1], FATMA TOSUN[1], UGUR TAMER[2], AHMET DURAN[3], BURCU ALAN[1] и ALI FUAT KÖK[1]

[1]*Department of Pharmacognosy, Faculty of Pharmacy, Gazi University, 06330, Ankara,* [2]*Department of Analytical Chemistry, Faculty of Pharmacy, Gazi University, 06330 Ankara u* [3]*Department of Biology, Faculty of Education, Selçuk University, Meram 42090, Konya, Turkey*

У овом истраживању одређиван је садржај укупног и слободног генистеина и даидзеина у две ендемске *Genista* врсте (*G. sandrasica* и *G. vuralii*) методом HPLC. Највећа количина укупног генистеина и даидзеина је нађена у *G. sandrasica*, 0,582 % односно 0,113 %, док је количина слободног даидзеина у *G. sandrasica* била већа од укупног у *G. vuralii*. Антиоксидативна активност сировог метанолног и хидролизованог екстракта ових врста је одређивана применом три *in vitro* методе, методом DPPH за мерење слободних радикала и тестовима хелатирања феро- и фери-јона (FRAP) при концентрацијама 0,25, 0,50 и 1,00 mg ml^{-1}. Хидролизовани екстракти обе врсте су испољили већу антиоксидативну активност у свим тестовима. Садржај укупних фенола и флавоноида је одређиван Folin–Ciocalteau и $AlCl_3$ реагенсом. Врста *G. vuralii* је имала више фенола и флавоноида од *G. sandrasica*.

(Примљено 8. априла, ревидирано 17. јуна 2010)

REFERENCES

1. K. D. R. Setchell, *Am. J. Clin. Nutr.* **68** (1998) 1333
2. F. Kronenberg, A. Fugh-Berman, *Ann. Intern. Med.* **137** (2002) 805
3. E. W. Lusas, M. N. Riaz, *J. Nutr.* **125** (1995) 573S
4. T. Cornwell, W. Cohick, I. Raskin, *Phytochem.* **65** (2004) 995
5. K. Reinli, G. Block, *Nutr. Cancer* **26** (1996) 123
6. C. Terreaux, J. Polasek, K. Hostettmann, *Curr. Org. Chem.* **7** (2003) 1151
7. R. Maul, N. H. Schebb, S. E. Kulling, *Anal. Bioanal. Chem.* **391** (2008) 239
8. P. E. Gibbs, in *Flora of Turkey and the East Aegean Islands*, Vol. 3, P. H. Davis, Ed., Edinburgh University Press, Edinburgh, 1970, p. 24
9. P. H. Davis, R. R. Mill, K. Tan, *Genista L*, in *Flora of Turkey and the East Aegean Islands*, Vol. 10, P. H. Davis, R. R. Mill, K. Tan, Eds., Edinburgh University Press, Edinburgh, 1988, p. 113
10. A. Duran, H. Dural, *Ann. Bot. Fennici.* **40** (2003) 113
11. F. Tosun, C. K. Erdem, Y. Eroglu, *Pharmazie* **58** (2003) 549
12. N. Erdemoğlu, F. Tosun, Y. Eroğlu, *Chem. Nat. Comp.* **42** (2006) 517
13. F. Tosun, A. Tosun, M. Tanker, T. Ozden, *J. Fac. Pharm. Gazi Univ.* **11** (1994) 197
14. F. Tosun, C. Akyuz, *J. Pharm. Pharmacol.* **50** (1998) 236
15. M. S. Blois, *Nature* **181** (1958) 1199
16. M. T. Chua, Y. T. Tung, S. T. Chang, *Biores. Technol.* **99** (2008) 1918
17. M. Oyaizu, *Jap. J. Nutr.* **44** (1986) 307

18. V. L. Singleton, J. A. Rossi Jr., *Am J Enol Viticult* **16** (1965) 144
19. R. Woisky, A. Salatino, *J. Apicol. Res.* **37** (1998) 99
20. A. P. Rauter, A. Martins, R. Lopes, J. Ferreira, M. L. Serralheiro, M. E. Araujo, C. Borges, J. Justino, F. V. Silva, M. Goulart, J. Thomas-Dates, A. J. Rodrigues, E. Edwards, J. P. Noronha, R. Pinto, H. M. F. Hélder, *J. Ethnopharmacol.* **122** (2009) 384
21. D. Rigano, V. Cardile, C. Formisano, M. T. Maldini, S. Piacente, Y. Bevelacqua, A. Russo, F. Senatore, *Chem.-Biol. Inter.* **180** (2009) 211
22. G. Rimbach, S. De Pascual-Teresa, B. A. Ewins, S. Matsugo, Y. Uchida, A. M. Minihane, R. Turner, K. Vafeiadou, P. D. Weinberg, *Xenobiotica* **33** (2003) 913
23. W. Cherdshewasart, W. Sujit, *Phytomed.* **15** (2008) 38
24. A. Kampkotter, Y. Chovolou, A. Kulawika, E. Rohrdanz, N. Weber, P. Proksch, *Nutr. Res.* **28** (2008) 620
25. C. E. Rufer, S. E. Kulling, *J. Agric. Food Chem.* **54** (2006) 2926
26. J. M. Choi, H. J. Ryu, J. H. Chung, J. C. Park, J. K. Hwang, D. B. Shin, S. K. Lee, R. Ryang, *Food Sci. Biotechnol.* **14** (2005) 399
27. E. Arteaga, P. Villaseca, A. Rojas, G. Marshall, M. Bianchi, *Climacteric* **7** (2004) 397.

Journal of the Serbian Chemical Society
JSCS-info@shd.org.rs • www.shd.org.rs/JSCS
J. Serb. Chem. Soc. 76 (1) 43–52 (2011)
JSCS–4098
UDC 546.73'76+544.35:544.537:
57.083.36:577.338
Original scientific paper

A selective laser melted Co–Cr alloy used for the rapid manufacture of removable partial denture frameworks – initial screening of biocompatibility

DANIMIR JEVREMOVIĆ[1], VESNA KOJIĆ[2], GORDANA BOGDANOVIĆ[2], TATJANA PUŠKAR[3], DOMINIC EGGBEER[4], DANIEL THOMAS[4] and ROBERT WILLIAMS[4]*

[1]Clinic for Prosthodontics, School of Dentistry, Pančevo, University Business Academy, Novi Sad, [2]Oncology Institute of Vojvodina, Sremska Kamenica, [3]Clinic for Prosthodontics, School of Medicine, Department of Dentistry, University of Novi Sad, Serbia and [4]Centre for Dental Technology and the National Centre for Product Design and Development Research, University of Wales Institute, Cardiff, United Kingdom

(Received 6 April, revised 28 July 2010)

Abstract: The aim of this study was to determine the cytotoxicity of a Co–Cr alloy used for the rapid manufacture of removable partial denture frameworks using murine fibroblasts L929 cell lines and three test methods: the MTT (3-(4,5-dimethylthiazol-2-yl)-2,5-diphenyltetrazolium bromide, a yellow tetrazole) assay, the agar diffusion test (ADT) and the dye exclusion test (DET). Two groups of disc specimens (5 mm diameter, 1 mm thick) were fabricated. The first group was cast using a conventional method (CM) in a Nautilus CC casting. The second group was fabricated using selective laser melting (SLM) in SLM Realiser The total cell number and viability of cells pre-incubated with CM and SLM alloys were comparable to the control sample. Differences between the growth inhibitory effects of the CM and SLM alloys in the MTT assay were below 30 %. Results of two independent agar diffusion tests with CM and SLM alloys showed neither detectable discoloration around or under the discs nor a detectable difference in staining intensity. As the cell response for both CM and SLM alloys was 0/0, the discs can be rated as non-cytotoxic. The results suggested that the F75 Co–Cr alloy used for the SLM process did not release harmful material that could cause acute effects against L929 cells under the given experimental conditions.

Keywords: dental alloys; selective laser melting; cytotoxicity; removable partial dentures.

* Corresponding author. E-mail: rjwilliams@uwic.ac.uk
doi: 10.2298/JSC100406014J

INTRODUCTION

Over the last decade, there has been a rapid increase in the employment of computer-aided design (CAD) and computer-aided manufacture (CAM) in dental applications. The majority of currently used CAD/CAM systems are based on a milling procedure, whereby requested forms, such as frameworks or full anatomical crowns, are fabricated by milling material from a block. Additive manufacturing (AM), on the other hand, uses a revolutionary layering additive technique, enabling the production of complex customized shapes, such as removable partial denture (RPD) frameworks.

In recent years, the term "additive manufacture" (AM) has been used to describe the fabrication of functional, end use components in a layer-by-layer manner. AM enables the fabrication of geometries unsuitable for alternative methods and can be ideal for low volume or one off production, especially in medical applications.[1,2] In dental technology, research has shown that a combination of CAD and AM may be used to replace laboratory crafting techniques [2–5]. Furthermore, the AM process, selective laser melting (SLM, Realiser GmbH/ /MTT-Group) has been used to fabricate RPD frameworks.[6,7]

The potential advantages of such a process over conventional laboratory techniques can be summarized as reduced manufacture time, inherent repeatability and elimination of inter-operator variation. In addition, CAD could provide some automation of dental processes (for example, cast analysis, undercut elimination and path of insertion identification).

The first steps towards clinical trials have been completed. A RPD framework was made by means of scanning a patient's cast followed by virtual surveying and framework design using CAD, and then CAM production using SLM technology. Conventional finishing and polishing procedures were used to complete the RPD framework.[6] The conclusions of the pilot study were that CAD/ /SLM produced frameworks that were comparable to conventional frameworks in terms of accuracy, quality of fit and function. However, this conclusion was based on a single study and no long-term results are available since there is no known data about the biocompatibility of the specific cobalt-chromium alloy used for the SLM process. Though the basic chemical elements generally match those of the conventional casting alloy, it has been stated that alterations in the composition and pre-treatment can greatly influence the cytotoxicity of an alloy.[8,9] Cell culture studies are the usual starting point when evaluating biocompatibility, providing an investigation of toxicity in a simplified system that minimizes the effect of confounding variables.[10] By using cells from the murine fibroblast cell line, the cytotoxicity of various dental materials, including dental alloys, can be determined. This study used murine fibroblasts (L929) in accordance with the requirements of the ISO standard 7405 (ISO 2008).[11] The aim was to determine the cytotoxicity of the Co–Cr alloy used for the fabrication of

an SLM RPD framework by using L 929 cell line and three test methods: the MTT (3-(4,5-dimethylthiazol-2-yl)-2,5-diphenyltetrazolium bromide, a yellow tetrazole) assay, the agar diffusion test (ADT) and the dye exclusion test (DET). To the best of our knowledge, there are no reports about the cytotoxicity of the selected laser melted Co–Cr alloy used for the rapid manufacture of RPD frameworks.

EXPERIMENTAL

Sample preparation

a) Conventional method (CM) samples. The composition of the commercially available alloy Remanium GM380+ (Dentaurum, Ispringen, Germany) used in this study is presented in Table I.

TABLE I. Composition (mass %) of the Remanium GM 380+ and Sandvik Osprey F75 alloys

Alloy	Co	Cr	Mo	Si	Mn	N	C	Fe	Ni
Remanium 380+	64.6	29	4.5	< 1	< 1	< 1	< 1	–	–
Sandvik Ospreys F75 alloy	Balance	27–30	5–7	<1	<1	–	<0.35	<0.75	<0.5

The alloy is a non-precious Co–Cr alloy containing no Ni, Be or Fe, which is widely used as a cast partial denture alloy. Five disc specimens (5 mm diameter, 1 mm thick) were obtained from wax patterns that were invested and cast according to the manufacturer's instructions. The investment used was Rema dynamic (Dentaurum, Ispringen, Germany), and vacuum casting was performed using a Nautilus CC (Bego, Bremen, Germany). After casting, the discs were divested and blasted with 100 μm aluminium oxide particles, then polished with silicon carbide papers in the sequence 320, 400, 600, 1200, 1500, and 2000. Final polishing was performed using oxide pastes.

b) Selective laser melting (SLM) samples. Five disc specimens (5 mm diameter, 1 mm thick) were first built in a virtual environment (Magics, Materialise, Belgium). The physical specimens were produced using an SLM Realiser (MTT-Group, UK). The powdered alloy used in the process was a Co–Cr type alloy, the composition of which contained a maximum of 0.5 % Ni (F75 alloy, Sandvik Osprey Ltd., UK, Table I.). After the build, the supporting structures were removed, and then the samples were prepared as described above for the cast samples.

Cell lines

L-929 cells were grown in a suitable culture medium, supplemented with antibiotics to prevent the growth of opportunistic microorganisms. The cell population was divided twice a week and placed in fresh media to stimulate growth and development. The tissue was broken into a suspension of single cells by enzymatic digestion in the presence of a chelating agent. The cell lines were cultured in 25 cm^3 flasks at 37 °C in 100 % humidity and 95 % air, 5 % CO_2. Only cells in the rapid or exponential growth phase of development were used for the assays. The cell number and percentage of viable cells were determined by a dye exclusion test (DET) with Trypan Blue.[12] The viability of the cells used in the assay was over 90 %.

Cytotoxicity tests

The cytotoxicity was measured as a percentage of cell growth inhibition using the three tests described below.

a) *Dye exclusion test (DET)*. Petri dishes (50 mm; Falcon, Becton Dickinson and Comp., Franklin Lakes, NJ, USA) containing CM or SLM alloy discs were plated with viable mouse cells and incubated for 24 h at 37 °C in 95 % air and 5 % CO_2. Control samples were also incubated but contained no alloy discs. After incubation, a single cell suspension was obtained by trypsinization. Cell number and viability were assayed by Trypan Blue staining in a counting chamber.[12] (Dead cells take up Trypan Blue whilst living cells do not.). Over 90 % of the cultured cells were viable (*i.e.*, no uptake of Trypan Blue) when assayed.

b) *MTT assay*. Growth inhibition was also evaluated by the tetrazolium colorimetric MTT assay (ISO 2009).[13] The assay depends on the cleavage of the tetrazolium salt MTT to purple formazan crystals by mitochondrial dehydrogenases in viable cells.

Cells (L929) were cultured in Petri dishes containing CM or SLM alloy discs and incubated for 24 h at 37 °C, in air containing 5 % CO_2. The control samples contained no discs. After incubation, the cells were detached from the alloy discs using enzymatic digestion, and counted in a counting chamber using Trypan Blue stain. New cells were cultured for 48, 72 or 96 h at 37 °C in 95 % air and 5 % CO_2. These cells were then cultured for 3 h with yellow MTT solution and the purple formazan product was isolated and dissolved in 100 µl of 0.04 M hydrochloric acid in 2-propanol. The cytotoxicity was expressed as the percentage growth inhibition.

c) *Agar diffusion test (ADT)*. L-929 cells were incubated for 24 h at 37 °C in 95 % air and 5 % CO_2 after plating on Petri dishes (10 mm). The concentration of cells was 10 ml; 2.5×10^5 cells ml^{-1}. Sterile agar was heated and a nutrient medium added. The mouse cells were combined with the agar-nutrient mixture and allowed to solidify over 30 min. The cells were stained with a neutral red solution (or toluylene red, Basic Red 5, or C.I. 50040; IUPAC name: toluylene red) and kept in the dark for 15 min. Two samples of CM or SLM discs were placed into each Petri dish and the dishes incubated for 24 h at 37 °C in 95 % air and 5 % CO_2.

Any interaction between the metal and the cells, causing the cells to die and lose the red dye, was noted using an inverted microscope, Reichert-Jung, Biostar, model 1820E. It is well known that living cells retain the red dye. Thus, the decolourised zones of dead cells were measured using a ruler and analysed according to ISO standards (2008).[11] The results were evaluated according to the zone and lyses index and rated for the severity of the cytotoxicity, as described previously.[12] Each product was tested in quadruplicate and the experiment was repeated twice.

Statistical analysis was realised using the Statgraphics Centurion program. The data were statistically evaluated by the Student's *t*-test. A value of $p < 0.05$ was considered statistically significant.

RESULTS

Rounded, disc-shaped experimental samples are shown in Figs. 1 and 2 (CM and SLM samples, respectively). The unpolished SLM samples exhibited very fine surface roughness, caused by the transition of the laser beam during the manufacturing process. The polished samples correspond to the state of the final alloy under oral environmental conditions.

Fig. 1. CM Samples (left – cast and sandblasted, right – polished).

Fig. 2. F75 SLM Samples (left – untreated, right - polished). Note the fine surface roughness of the untreated sample caused by the laser beam.

The L929 fibroblasts were pre-incubated in culture medium with CM or SLM alloys for 24 h and then the survival rates of the pre-treated cells were evaluated by the standard procedure for the DET or MTT assay. The results of the DET and MTT assays are presented in Figs. 3 and 4, respectively.

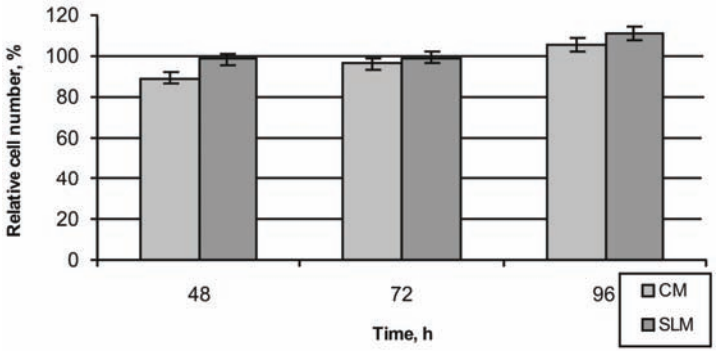

Fig. 3. Dye exclusion test (DET). Recovery of L929 cells pre-incubated with CM and SLM alloys for 24 h. The results show the relative cell number obtained from two independent experiments completed in triplicate. Data are shown as the mean and the bar indicates the standard deviation ($p > 0.05$).

The variation in the cell numbers of pre-incubated cells compared to the control sample was small: 8 percent below and 15 percent above the control value for both the CM and SLM alloys, respectively. The viability of each sample was 99 %.

The cell number steadily increased during the recovery period for both CM and SLM alloys (48–96 h), which indicated that no cytotoxic effects were registered in the several cell generations. There were no statistical significant differences between treatments regardless of the recovery period.

In the MTT assay during the same recovery period, no cytotoxic effects of the CM or SLM alloys against L929 cells were detected (Fig. 4). Differences between the growth inhibitory effects of CM and SLM alloys were found but the growth inhibition level was not statistically significant ($p > 0.05$). Therefore, both alloys can be rated as non-cytotoxic.

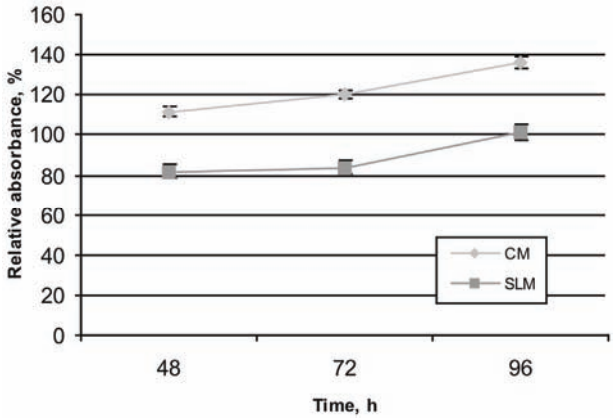

Fig. 4. MTT Assay. Survival of L929 cells pre-incubated with CM and SLM alloys for 24 h. The results represent the relative absorbance of the pre-treated cells obtained from two independent experiments, completed in quadruplicate. The data are shown as the mean and the bar indicates the standard deviation ($p > 0.05$).

The results of two independent ADT with CM and SLM alloys showed a detectable discoloration neither around nor under the discs, or a detectable difference in the staining intensity. As the cell response to both the CM and SLM alloys was 0/0, the discs can be rated as non-cytotoxic.

DISCUSSION

Super-alloys, such as Co–Cr, are suited to the SLM process as the material properties facilitate the process physics, such as melt-pool and temperature gradient control. However, alloys available for AM processes, such as SLM, routinely include nickel. When the specifications for these alloys were developed, there were allowable levels of various elements, which permitted recyclers more flexibility in making low-cost alloys. The alloy used for the tests reported herein contained a maximum of 0.5 % nickel. AM alloys containing a maximum of 0.1 % nickel can be obtained but this adds considerably to the cost.

Among other elements, the use of nickel in dental alloys has often been attacked because of its potential side effects.[14] Severely cytotoxic Co–Cr alloys contained high amounts of Ni, although no general correlation between the overall alloy composition and cytotoxicity was detected.[15] While Co and Cr undergo redox-cycling reactions, the primary Ni route is depletion of glutathione and bonding to sulph-hydryl groups of proteins.[16] However, it can be stated that Ni showed a negative effect in combination with certain other metals and, therefore, does not necessarily contribute to a toxic or allergenic potential.[17]. Generally, element release is not simply proportional to its abundance in the bulk alloy, but is also highly dependent on the inter-ionic interactions within the alloy.[10]

Cytotoxicity tests can implement several cellular parameters, such as cell viability, DNA/RNA/protein synthesis, membrane integrity, *etc*. In this study, cytotoxicity was assessed by three methods, addressed to different ends, *i.e*., viability and cell survival. Viability was determined by short-term (24 h) ADT and DET assays, and cell survival, after cell pre-treatment with the alloys, by DET and MTT assays. Although only the ADT assay has been prescribed as an ISO standard (ISO 2008),[11] the use of different test methods is highly advisable.[18] While the DET and ADT methods rely on the breakdown of membrane integrity, the MTT method focuses mainly on the mitochondrial function (dehydrogenase activity).[19] Although the last test showed a slightly worse outcome for the SLM alloy, cellular proliferation in the subsequent period (48, 72 and 96 h), which covered several cell cycles *i.e*., cell generations, showed no significant damage to the cell function. Replication during an extended contact period with potential toxic substances, however, showed good biocompatible properties of the chosen SLM alloy. Furthermore, membrane lyses was not detected in the ADT or DET assay when L929 fibroblasts were exposed to the examined alloys. The negative effect decreased with time for both examined substances.

The results suggested that the alloys did not release harmful material that could cause acute effects against L929 cells under the given experimental conditions.

In an oral environment, the intimate contact between the alloy and tissues can create microspaces with a high concentration of released metal ions. Alloy surface properties can be of decisive importance in such situations; a point supported by findings suggesting less biocompatibility in under as-cast alloy conditions compared to its highly polished state.[20] Enhanced contact might lead to local adverse tissue reaction.[21] Ensuring that cast or AM-produced frameworks are appropriately finished and that their porosity is low remains dependent on human subjectivity.

The murine L929 fibroblast assays represent sufficient screening models for an investigation of the *in vitro* toxicity of metal cations. They exhibit a similar

response with gingival fibroblasts; hence, it can be assumed that the SLM alloy also does not have cytotoxic effect on gingival tissue.[20,22,23]

Generally, corrosion is characterized by electrochemical phase boundary reactions which cause the liberation of metal ions.[14] The amount and nature of released cations varied depending upon the type of alloy and other parameters, *e.g.*, type of corrosion, composition and chemical characteristics of the corrosive solution-such as pH and ionic composition, artificial saliva, cell culture medium, serum, e*tc*.[25–27] In one study, ion release from cast and SLM Co–Cr alloy was compared.[28] The main ion released was cobalt, as, due to the passivating behaviour or chrome, only a small amount of chromium and molybdenum was detected. Due to the low releases of ions, the corrosion was influenced almost completely by the surface. The SLM test specimens showed lower emissions than the cast specimens did because the laser molten material is more homogeneous, contains fewer pores and has a finer microstructure. However, almost no difference was detected after two weeks between the different variants examined, having concentrations below the detection limit of the analyzing method.

However, oral mucosa could present only an increased resistance towards the leakage of cytotoxic agents, as it becomes keratinized and has a protective mucin layer. On the other hand, it should be emphasized that the oral environment includes severe biological factors, plus interactions such as saliva composition, pH status, *etc*. Nevertheless, based on the obtained data, the SLM alloy shows promising potential to withstand environmental conditions and have a life span comparable to the currently used cast alloy when biocompatible properties are concerned.

Although the lost wax procedure has been a central technique in RPD framework production for a very long time, AM with its link to information technology might be of great interest in dentistry in general.[24] Linking intra-oral scanning to CAD and AM has the potential to remove laborious laboratory techniques and improve accuracy and repeatability.

Future research on the mechanical properties, as well as *in vivo* tests of the SLM or other AM produced dentures are necessary to show whether in reality a revolution is at hand, as it appears.

CONCLUSIONS

Based on the results of the MTT, ADT and DET tests employed in this study, it can be concluded that the Co–Cr alloy routinely in use in AM technologies such as SLM, does not exhibit cytotoxic potential. Further clinical trials should be performed to show the *in vivo* behaviour of this alloy under oral environmental conditions.

ИЗВОД

СЕЛЕКТИВНО ЛАСЕРСКО ТОПЉЕЊЕ Co–Cr ЛЕГУРЕ ЗА СКЕЛЕТИРАНЕ ПРОТЕЗЕ – ИНИЦИЈАЛНА ПРОЦЕНА БИОКОМПАТИБИЛНОСТИ

ДАНИМИР ЈЕВРЕМОВИЋ[1], ВЕСНА КОЈИЋ[2], ГОРДАНА БОГДАНОВИЋ[2], ТАТЈАНА ПУШКАР[3], DOMINIC EGGBEER[4], DANIEL THOMAS[4] и ROBERT WILLIAMS[4]

[1]Клиника за стоматолошку протетику, Стоматолошки факултет Панчево, Универзитет "Привредна академија", Нови Сад, [2]Институт за онкологију Војводине, Сремска Каменица, [3]Клиника за стоматолошку протетику, Медицински факултет – Одсек за стоматологију, Универзитет у Новом Саду и [4]Centre for Dental Technology and the National Centre for Product Design and Development Research, University of Wales Institute, Cardiff, United Kingdom

Циљ студије је да одреди цитотоксичност F75 Co–Cr легуре, која се употребљава током компјутерског процеса производње скелетиране парцијалне протезе, коришћењем L929 ћелијске линије мишјих фибробласта и три методе: MTT теста, агар дифузионог теста (ADT) и теста губљења боје (DET). Направљене су две групе узорака (5 mm пречник, 1 mm дебљина). Прва група је изливена од легуре кобалт–хром конвенционалном методом (CM) у пећи за ливење Nautilus CC. Друга група је направљена коришћењем методе селективног топљења ласером (SLM) у апарату SLM Realiser. Укупан број ћелија, преинкубираних са CM и SLM легуром, као и њихова одрживост упоређени су са контролним узорком. Разлике у инхибиторном ефекту на раст CM и SLM легуре у MTT тесту биле су мање од 30 %. Резултати два независна агар-дифузиона теста са CM и SLM легуром не показују приметно обезбојавање око или испод дискова, нити приметну разлику у интензитету пребојавања. Како је ћелијски одговор за CM и SLM легуру био 0/0, дискови се могу окарактерисати као не-цитотоксични. Резултати сугеришу да F75 Co–Cr легура, која се користи у SLM процесу добијања скелетираних протеза не отпушта штетне материје, које могу проузроковати акутне ефекте на линију L929 ћелија под датим експерименталним условима.

(Примљено 6. априла, ревидирано 28. јула 2010)

REFERENCES

1. R. Bibb, A. Bocca, P. Evans, *J. Maxillofac. Prosthet. Technol.* **5** (2002) 28
2. R. Bibb, D. Eggbeer, R. J. Williams, A. Woodward, *J. Eng. Med.* **220** (2006) 793
3. R. Williams, R. Bibb, T. Rafik, *J. Prosthet. Dent.* **91** (2004) 85
4. R. Williams, D. Eggbeer, R. Bibb, *Quintessence J. Dental Technol.* **2** (2004) 242
5. D. Eggbeer, R. J. Williams, R. Bibb, *Quintessence J. Dental Technol.* **2** (2004) 490
6. R. Williams, R. Bibb, T. Rafik, *J. Prosthet. Dent.* **91** (2004) 85
7. B. Gao, J. Wu, X. Zhao, H. Tan, *Rapid Prototyping J.* **15** (2009) 133
8. G. Sjogren, G. Sletten, J. Dahl, *J. Prosthet Dent.* **84** (2000) 229
9. A. Faria, A. Rosa, R. Rodrigues, R. Ribeiro, *J. Biomed. Mater. Res. B* **85** (2008) 504
10. S.B. Jones, R.L. Taylor, J. S. Colligon, D. Johnson. *Dental Mater.* **26** (2010) 249
11. *International Standard ISO 7405: Dentistry - Evaluation of Biocompatibility of Medical Devices Used in Dentistry – Test Methods for Dental Materials*, International Organisation for Standardisation, Geneva, 2008
12. G. Bogdanović, J. Raletić-Savić, N. Marković, *Arch. Oncol.* **2** (1994) 181
13. *International Standard ISO 10993–5: Biological Evaluation of Medical Devices – Part 5: Tests for* in vitro *cytotoxicity*, International Organisation for Standardisation, Geneva, 2009
14. W. Geurtsen, *Crit. Rev. Oral Biol. Med.* **13** (2002) 71
15. M. Valko, H. Morris, M. T. Cronin, *Curr. Med. Chem.* **12** (2005) 1161

16. J. C. Wataha, C. T. Hanks, Z. Sun, *Dental Mater.* **10** (1994) 156
17. J. C. Wataha, P. E. Lockwood, S. K. Nelson, *J. Oral Rehabil.* **26** (1999) 798
18. R. Al, J. Dahl, E. Morisbak, G. Polyzois, *Gerodontology* **22** (2005) 177
19. A. Naji, M. F. Harmand, *J. Biomed. Mater. Res.* **24** (1990) 861
20. G. Smaltz, D. Arenholt-Bindslev, S. Pfueller, H. Schweikl, *ATLA.* **25** (1997) 323
21. K. Arvidson, M. Cottler-Fox, E. Hammarlund, U. Friberg, *Scand. J. Dent. Res.* **95** (1987) 356
22. A. Schedle, P. Samorapoompichit, X. H. Rausch-Fan, A. Franz, W. Füreder, W. R. Sperr, W. Sperr, A. Ellinger, R. Slavicek, G. Boltz-Nitulescu, P. Valent *J. Dent. Res.* **74** (1995) 1513
23. A. Franz, F. Konig, A. Skolka, W. Sperr, P. Bauer, T. Lucas, D. C. Watts, A. Schedle, *Dent. Mater.* **23** (2007) 1438
24. R. J. Williams, D. Eggbeer, R. Bibb, *Quintessence J. Dental Technol.* **1** (2008) 42
25. J. S. Covington, M. A. McBride, W. F. Slagle, A. L. Disney, *J. Prosthet Dent.* 54 (1985) 127
26. S. K. Nelson, J. C Wataha, A. M. Neme, A. M. Cibirka, P. E. Lockwood, *J. Prosthet Dent.* **81** (1999) 591
27. S. K. Nelson, J. C. Wataha, P. E. Lockwood, *J. Prosthet Dent.* **81** (1999) 715
28. B. Vandenbroucke, J. P. Kruth, *Rapid Prototyping J.* **13** (2007) 196.

Journal of the Serbian Chemical Society
JSCS-info@shd.org.rs • www.shd.org.rs/JSCS
J. Serb. Chem. Soc. 76 (1) 53–61 (2011) UDC 546.962+547.821–32:57.083.36:543.422.25
JSCS–4099 *Original scientific paper*

X-Ray structure and cytotoxic activity of a picolinate ruthenium(II)–arene complex

IVANKA IVANOVIĆ[1], SANJA GRGURIĆ-ŠIPKA[1*#], NEVENKA GLIGORIJEVIĆ[2], SINIŠA RADULOVIĆ[2], ALEXANDER ROLLER[3], ŽIVOSLAV LJ. TEŠIĆ[1#] and BERNHARD K. KEPPLER[3]

[1]*Faculty of Chemistry, University of Belgrade, Studentski trg 12-16, 11 000 Belgrade* [2]*Institute of Oncology and Radiology of Serbia, Pasterova 14, 11000 Belgrade, Serbia and* [3]*Institute of Inorganic Chemistry, University of Vienna, Währinger Str. 42, 1090 Vienna, Austria*

(Received 17 May, revised 17 August 2010)

Abstract: A ruthenium(II)–arene complex with picolinic acid, [(η^6-*p*-cymene)RuCl(pico)]·H_2O, was prepared by the reaction of [(η^6-*p*-cymene)$RuCl_2$]$_2$ with picolinic acid in a 1:2 molar ratio in 2-propanol. The compound was characterized by elemental analysis, and IR and NMR spectroscopy. X-ray diffraction analysis showed that the molecule adopts a "three-leg piano-stool" geometry, which is common for this type of complexes. The cytotoxic activity of the complex was tested in two human cancer cell lines HeLa (cervix) and FemX (melanoma) by MTT assay. The IC_{50} values were at 82.0 and 36.2 μmol dm^{-3} for HeLa and FemX cells, respectively.

Keywords: ruthenium(II)–arene; picolinic acid; cytotoxic activity.

INTRODUCTION

The structures and chemical properties of metal complexes of some pyridine carboxylates have been widely investigated.[1–5] Picolinic acid (2-pyridinecarboxylic acid) is a biologically important ligand incorporated into some enzymes, and it is an active agent in some drugs as well.[6–11] It is also catabolite of L-tryptophan detected in the human body.[12,13] Picolinates are used as dietary supplements. In particular, the chromium(III) complex reduces diabetes risk and therefore is used as a dietary supplement for obese people.[14] Zinc picolinate revealed an effect in the oxidant–antioxidant balance in patients with chronic obstructive pulmonary disease.[15] Alkaline picolinates inhibit the growth of *Escherichia coli*.[16,17] Platinum complexes with picolinic acid have been synthesized and screened for cytotoxic activity.[18]

* Corresponding author. E-mail: sanjag@chem.bg.ac.rs
# Serbian Chemical Society member.
doi: 10.2298/JSC100517017I

In recent years, ruthenium complexes have gained much attention[19–23] in attempts to overcome the downsides of platinum complexes. Organometallic complexes and half-sandwich complexes of Ru(II) emerged as promising scaffolds for anticancer drug design.[24–35] They often show aqueous solubility along with the necessary lipophilicity. The electronic system of the arene ligand stabilizes the metal in its lower oxidation state and also provides a hydrophobic face in the complex, which might enhance transport of ruthenium through cell membranes. In addition, ruthenium compounds possess good cytotoxic activity, while not notably affecting normal cells.[36,37] One aspect of the action of ruthenium complexes is their ability to bind with the serum proteins: transferrin and albumin.[38] Tumor cells are more susceptible to ruthenium complexes due to an increased demand for iron and therefore there is an increased number of transferrin receptors on their surface.[39,40] In addition, because ruthenium can mimic iron in binding to carrier proteins, its excess can be removed from cells, which is the reason for lower toxicity of ruthenium complexes compared to platinum complexes.[39]

Recently, two series of Ru(II)-arene complexes with functionalized pyridines were described of the general formulae [(η^6-*p*-cymene)Ru(XY)Cl] and [(η^6-*p*--cymene)Ru(X)Cl_2], where XY were the mono-anionic N,O-bidentates 2,3-pyridine-, 2,4-pyridine-, 2,5-pyridine- and 2,6-pyridine-dicarboxylate, while X were monodentate ligands 3-acetylpyridine, 4-acetylpyridine, 2-amino-5-chloropyridine, isonicotinic or nicotinic acid bound to ruthenium(II) *via* the pyridine nitrogen.[41]

Herein the X-ray diffraction structure of [(η^6-*p*-cymene)Ru(pico)Cl] and its antiproliferative activity in two human cancer cell lines (cervix HeLa and melanoma Femx) are reported. Since the introduction of picolinate into a metal complex can result in enhanced activity,[42,43] the aim of this work was to compare the activities of the prepared complex with previously described analogue complexes.[41] It should be noted that the complex was previously described but its X-ray diffraction structure has not hitherto been reported.[44]

EXPERIMENTAL

Materials and measurements

Picolinic acid was purchased from Acros Organics and used without further purification. [(η^6-*p*-Cymene)$RuCl_2$]$_2$ was prepared according to a published procedure.[45] Elemental analysis was realized using an Elemental Vario EL III microanalyzer. The infrared spectra were recorded on a Nicolet 6700 FT-IR spectrometer using the attenuated total reflectance (ATR) technique. The ^{1}H- and ^{13}C-NMR spectra of the ligand and the complex were recorded on a Varian Gemini 200 instrument. Chemical shifts were referenced to residual ^{1}H and ^{13}C present in deuterated dimethyl sulfoxide.

Synthesis of the complex

To a warm solution of [(η^6-*p*-cymene)$RuCl_2$]$_2$ (0.100 g, 0.16 mmol) in 2-propanol (25 cm^3) was added a solution of picolinic acid (0.046 g, 0.35 mmol) in 2-propanol (5 cm^3). The

mixture was stirred at room temperature for 7 days and then kept in refrigerator until the product precipitated. The yellow-orange product was filtered off, washed with several drops of 2-propanol and then diethyl ether and dried in air. A crystal suitable for X-ray analysis was obtained by the slow evaporation of the mother liquor.

Crystallographic structure determination

The measurement was performed on a Bruker X8 APEXII CCD diffractometer. A single crystal was positioned at 35 mm from the detector and 941 frames were measured, each for 30 s over a 1° scan width. The data were processed using SAINT-Plus software.[46] The crystal data, data collection parameters and structure refinement details are given in Table I. The structure was solved by direct methods and refined by full-matrix least-squares techniques. Non-hydrogen atoms were refined with anisotropic displacement parameters. The H atoms were placed at calculated positions and refined as riding atoms in the subsequent least-squares model refinements. The isotropic thermal parameters were estimated to be 1.2 or 1.5 times (methyl groups) the values of the equivalent isotropic thermal parameters of the non-hydrogen atoms to which the hydrogen atoms were bonded. The following software programs, personal computer and tables were used: structure solution, SHELXS-97,[47] refinement, SHELXL-97,[48] molecular diagrams, ORTEP,[49] Pentium IV, Tables 4.2.6.8 and 6.1.1.4 for the scattering factors were taken from the literature.[50]

TABLE I. Crystal data and details of data collection for **1**·H_2O

Empirical formula	$C_{16}H_{20}ClNO_3Ru$
FW	410.85
Space group	*Pn*
a / Å	8.9150(4)
b / Å	8.6498(4)
c / Å	10.6539(4)
β / °	91.853(3)
V / Å^3	821.12(6)
Z	2
λ / Å	0.71073
ρ_{calcd} / g cm^{-3}	1.662
Crystal size, mm^3	0.50×0.05×0.01
T / K	100
μ / mm^{-1}	1.128
R_1[a]	0.0381
wR_2[b]	0.0687
GOF[c]	0.979

[a]$R_1 = \Sigma||F_o| - |F_c||/\Sigma|F_o|$; [b]$wR_2 = \{\Sigma[w(F_o^2 - F_c^2)^2]/\Sigma[w(F_o^2)^2]\}^{1/2}$; [c]$\text{GOF} = \{\Sigma[w(F_o^2 - F_c^2)^2]/(n - p)\}^{1/2}$, where *n* is the number of reflections and *p* is the total number of parameters refined.

Cytotoxicity

Cell culture. Human cervix carcinoma cells (HeLa) and human melanoma cells (FemX) were maintained as monolayer cultures in Roswell Park Memorial Institute (RPMI) 1640 nutrient medium (Sigma Chemicals Co, USA). The RPMI 1640 nutrient medium was prepared in sterile deionized water, supplemented with penicillin (192 U ml^{-1}), streptomycin (200 μg ml^{-1}), 4-(2-hydroxyethyl)piperazine-1-ethanesulfonic acid (HEPES) (25 mM), L-glutamine (3 mM) and 10 % heat-inactivated fetal calf serum (FCS) (pH 7.2). The cells were grown at 37 °C in a 5 % CO_2 humidified air atmosphere.

Cytotoxicity assay. The drug-induced cytotoxicity was determined using the 3-(4,5-dimethylthiazol-2yl)-2,5-diphenyltetrazolium bromide (MTT, Sigma) assay.[51] Cells were seeded in 96-well cell culture plates (NUNC), HeLa (2000 c/w) and FemX (2000 c/w), in culture medium and grown for 24 h. A stock solution of the complex was prepared in DMSO at a concentration of 30 mM and subsequently diluted with nutrient medium to the desired final concentrations (in the range up to 300 μM).

Solutions of various concentrations of the examined compound were added to the wells, except for the control wells where only the nutrient medium was added. All samples were prepared in triplicate. Nutrient medium with corresponding agent concentrations but without the target cells was used as the blank, also in triplicate. The cells were incubated with the test compound for 48 h at 37 °C, in a 5 % CO_2 humidified air atmosphere. After incubation, 20 μl of MTT solution, 5 mg mL^{-1} in phosphate buffer solution (PBS), pH 7.2, were added to each well. The samples were incubated for 4 h at 37 °C in a 5 % CO_2 humidified air atmosphere. Formazan crystals were dissolved in 100 μL 10 % sodium dodecyl sulfate (SDS) in 0.01 M HCl. The absorbance was recorded on an enzyme-linked immunosorbent assay (ELISA) reader after 24 h at a wavelength of 570 nm. The IC_{50} (μM) was defined as the concentration of drug producing 50 % inhibition and was determined from cell survival diagrams.

RESULTS AND DISCUSSION

Synthesis

The reaction of $[(\eta^6\text{-}p\text{-cymene})RuCl_2]_2$ with picolinic acid in a 1:2 molar ratio in 2-propanol at room temperature leads to the formation of the complex $[(\eta^6\text{-}p\text{-cymene})RuCl(pico)]\cdot H_2O$ in high yield (Scheme 1). Crystals precipitated directly from the reaction mixture. The complex is soluble in water, methanol, ethanol, acetonitrile and dimethyl sulfoxide.

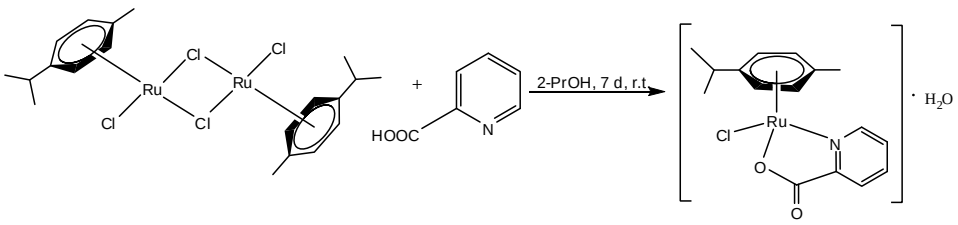

Scheme 1. Synthesis of the complex $[(\eta^6\text{-}p\text{-cymene})RuCl(pico)]\cdot H_2O$

Analytic and spectral data

Yield: 0.1 g, 76.9 %. Anal. Calcd. for $C_{16}H_{20}O_3NRuCl$ (M_r = 410.86): C, 46.77; H, 4.91; N, 3.41 %. Found: C, 46.70; H, 4.98; N, 3.39. IR (ATR, cm^{-1}): 3536, 3467 (*m*), 3069, 2955 (*w*), 1637 (*s*), 1601 (*w*). ^{1}H-NMR (199.97 MHz, DMSO-d_6, δ / ppm): 1.12 (6H, *dd*, –CH(C**H**$_3$)$_2$, J = 2.2 and 7 Hz), 2.15 (3H, *s*, –CH_3), 2.72 (1H, *m*, –C**H**(CH$_3$)$_2$, J = 6.8 Hz), 5.88 and 5.65 (4H, 2*t*, CH (arene), J = 4.6 and 7.8 Hz), 7.74 (1H, *m*, H^4, J = 7.3 Hz), 7.79 (1H, *m*, H^3), 8.09 (1H, *td*, H^5, J = 7.5 Hz), 9.26 (1H, *d*, H^6, J = 5.6 Hz). ^{13}C-NMR (50.28 MHz, DMSO-d_6, δ / / ppm) 18.27 (CH_3), 22.00 (CH(**C**H$_3$)$_2$), 30.65 (**C**H(CH$_3$)$_2$), 80.23, 81.21, 82.60,

82.78, 98.38 and 101.17 (CH (arene)), 125.59 (C3), 128.30 (C5), 139.86 (C4), 150.73 (C2), 154.01 (C6), 170.70 (C1).

Spectroscopy

[(η^6-*p*-Cymene)RuCl(pico)]·H_2O exhibits an asymmetric stretching vibration $\nu_{as}(COO^-)$ at 1637 cm^{-1}. Picolinic acid revealed an analogous vibration of the free carboxylic group at 1718 cm^{-1}. The difference in frequency is due to coordination of the ligand through one of the oxygen atoms of the carboxylic group and nitrogen atom of the pyridine ring, and is consistent with the X-ray diffraction structure.

The ^{1}H NMR spectrum of the complex contains a characteristic pattern for the *p*-cymene moiety. A methyl group singlet is seen at 2.15 ppm, the resonance signal of –C**H**$(CH_3)_2$ appears as a multiplet at 2.72 ppm and -CH(C**H**$_3)_2$ as a doublet at 1.12 ppm. The resonances of the arene ring protons were found at 5.64 and 5.88 ppm. Aromatic region of the ^{1}H-NMR spectrum of the complex also shows four resonances (7.74 (1H), 7.78 (1H), 8.09 (1H), 9.26 (1H)) of coordinated picolinate. Concerning the pyridine protons, H^3 and H^4 are shifted downfield by 0.3 and 0.27 ppm, respectively, while H^5 and H^6 are shifted upfield by 0.44 and 0.52 ppm, respectively, compared with the free ligand as a consequence of picolinate coordination to the ruthenium(II) atom.

The ^{13}C-NMR spectrum displays resonances at 18.27 ppm from the methyl group attached to the cymene moiety, 22.00 ppm from –CH(**C**$H_3)_2$, while the signal at 30.65 ppm is due to the **C**H$(CH_3)_2$ group. The aromatic carbons from cymene display resonances within 80.23–101.17 ppm. Five pyridine carbon resonances were observed at 125.59 (C^3), 128.30 (C^5), 139.86 (C^4), 150.73 (C^2), 154.01 (C^6) and carboxylate carbon at 170.67 ppm (C^1).

X-Ray crystallography

The structure of [(η^6-*p*-cymene)RuCl(pico)]·H_2O was confirmed by X-ray diffraction. The complex crystallized in the monoclinic space group *Pn* and has the typical "three-leg piano-stool" geometry well-documented for a large number of ruthenium(II) and osmium(II) arene complexes, and in particular, for the closely related compounds [(η^6-1,3,5-$Me_3C_6H_3$)RuCl(pico)][52] and [(η^6-*p*-cymene)$_2$OsCl(pico)],[42] with the η^6 π-bound arene ring forming the seat and the picolinate ligand bound *via* a nitrogen and one carboxylic oxygen, with one chloride ligand as the legs of the piano-stool. Selected bond lengths and angles are given in the legend to Fig. 1. The bond lengths Ru–ring centroid, Ru–Cl, Ru–O1 and Ru––N1 in [(η^6-*p*-cymene)Ru^{II}Cl(pico)]·H_2O of 1.665(9), 2.4225(9), 2.085(2) and 2.101(3) Å, respectively, are slightly longer than similar bonds 1.652(2), 2.4048(13), 2.080(3) and 2.090(4) Å in [(η^6-*p*-cymene)Os^{II}Cl(pico)].[42] The shortening of the Ru–N and Ru–O bonds in *mer*-[Ru^{III}(pico)$_3$]·H_2O (2.052(3), 2.064(3), 2.052(3)

and 2.002(3), 2.024(3), 1.996(2) Å, respectively)[53] is even more evident. The Ru–Cl, Ru–N1 and Ru–O1 bonds in [(η^6-1,3,5-$Me_3C_6H_3$)RuCl(pico)][52] are at 2.420(1), 2.102(4) and 2.101(4) Å, respectively. Two hydrogen bonding interactions between the co-crystallized water molecule and **1** of the type O3−H···O2 (O3−H, 0.86, H···O2, 1.94, O3···O2, 2.78 Å, O3−H···O2, 168.5°) and O3−H···Cl1^{i} (x + 0.5, −y + 1, z + 0.5) (O3−H, 0.87, H···O2, 1.94, O3···Cl1^{i}, 2.78 Å, O3−H···Cl1^{i}, 172.6°) are evident in the crystal structure of **1**·H_2O.

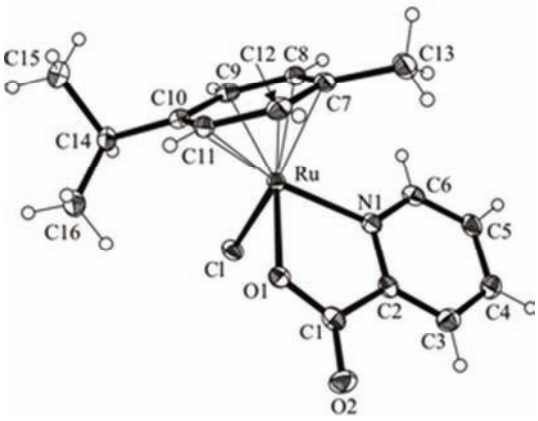

Fig. 1. ORTEP view of a molecule of **1** with atom-labeling scheme and thermal ellipsoids drawn at the 50 % probability level. Selected bond distances (Å) and angles (°): Ru−O1 2.085(2), Ru––N1 2.101(3), Ru−Cl 2.4225(9), Ru––C7 2.195(3), Ru−C8 2.186(3), Ru−C9 2.175(4), Ru−C10 2.211(4), Ru−C11 2.192(4) and Ru−C12 2.176(4), O1––Ru−N1 77.96(10).

Cytotoxic activity

The antiproliferative activity of the prepared complex was assayed in two human cancer cell lines HeLa (cervix) and FemX (melanoma) by the MTT assay. The tumor cells were incubated for 48 h with the investigated complex. The results of these tests indicate that the complex after 48 h of incubation exhibited cytotoxic activity with IC_{50} 81.97 μM for HeLa cells and 36.23 μM for FemX cells. These values are the mean of 2 to 3 independent experiments, whereby the standard deviations were less than 15 %. The results of representative experiments are shown in Fig. 2.

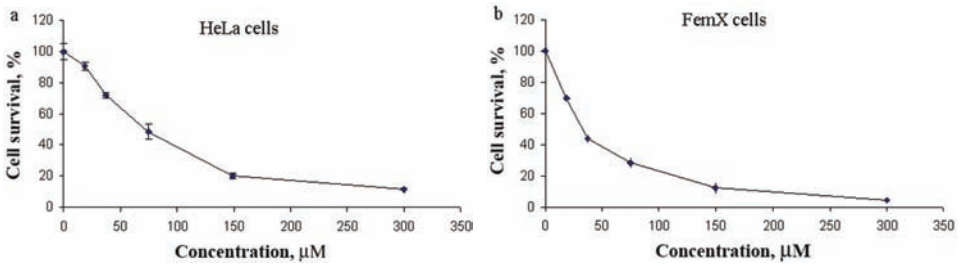

Fig. 2. Diagram of (a) HeLa and (b) FemX cells survival after 48 h of continual agent action. Data are representative for one out of two to three separate experiments with standard deviation.

CONCLUSIONS

In this paper, the synthesis and characterization of the organoruthenium complex, [(η^6-*p*-cymene)RuCl(pico)]·H_2O is described. Although in a previous work, structurally related complexes were found to have limited antiproliferative activity in tumor cells, the complex reported herein exhibits much higher cytotoxicity in cervix HeLa and melanoma FemX human cancer cell lines. This implies that the presence of picolinate coordinated to a metal center had a notable effect on cytotoxic activity. This makes this new ruthenium complex of interest for further investigation.

SUPPLEMENTARY MATERIAL

Crystallographic data for **1** has been deposited with the Cambridge Crystallographic Data Center as supplementary publication No. CCDC 775760. Copies of the data can be obtained free of charge on application to The Director, CCDC, 12 Union Road, Cambridge CB2 1EZ, UK (fax: +44 1223 336 033; e-mail: deposit@ccdc.cam.ac.uk).

Acknowledgements. This work was supported by the Ministry of Science and Technological Development of the Republic of Serbia, Grant Nos. 142010, 142062 and 145035.

И З В О Д

РЕНДГЕНСКА СТРУКТУРНА АНАЛИЗА И ЦИТОТОКСИЧНА АКТИВНОСТ ПИКОЛИНАТО РУТЕНИЈУМ(II)–АРЕНСКОГ КОМПЛЕКСА

ИВАНКА ИВАНОВИЋ[1], САЊА ГРГУРИЋ-ШИПКА[1], НЕВЕНКА ГЛИГОРИЈЕВИЋ[2], СИНИША РАДУЛОВИЋ[2], ЖИВОСЛАВ Љ. ТЕШИЋ[1], ALEXANDER ROLLER[3] и BERNHARD K. KEPPLER[3]

[1]Хемијски Факултет,Универзитет у Београду, Студентски трг 12–16, 11 000 Београд, [2]Институт за онкологију и радиологију Србије, Пастерова 14, 11000 Београд и [3]Institute of Inorganic Chemistry, University of Vienna, Währinger Str. 42, 1090 Vienna, Austria

Рутенијум(II)–аренски комплекс са пиколинском киселином [(η^6-*p*-цимен)RuCl(пиколинато)]·H_2O синтетисан је у реакцији [(η^6-*p*-цимен)$RuCl_2]_2$ комплекса са пиколинском киселином у молском односу 1:2 у изопропанолу. Једињење је окарактерисано елементалном анализом, ИЦ и NMR спектроскопијом. Анализа дифракцијом X-зрацима показала је да молекул има тзв. "*three-leg piano-stool*" геометрију која је карактеристична за овај тип комплекса. Цитотоксична активност комплекса је одређена на две хумане туморске ћелијске линије, HeLa (грлића материце) и FemX (меланома), MTT тестом. IC_{50} вредности су биле 82,0 и 36,2 μmol dm^{-3} за HeLa и FemX ћелије, редом.

(Примљено 17. маја, ревидирано 17. августа 2010)

REFERENCES

1. O. Jøns, E.S. Johansen, *Inorg. Chim. Acta* **151** (1988) 129
2. S.C. Dixit, R. Sharan, R.N. Kapoor, *Inorg. Chim. Acta* **109** (1989) 113
3. E. Libby, R.J. Webb, W.E. Streib, K. Folting, J.C. Huffman, D.N. Hendrickson, G. Christou, *Inorg. Chem.* **28** (1989) 4037
4. D.M. Strearns, W.H. Armstrong, *Inorg. Chem.* **31** (1992) 5178
5. W. Li, M.M. Olmstead, D. Miggins, R.H. Fish, *Inorg. Chem.* **35** (1996) 51
6. H. Ding, L.K. Olson, J.A. Caruso, *Spectrochim. Acta B* **51** (1996) 1801

7. G.S. Morris, K.A. Guindry, M. Hegsted, D.L. Hasten, *Nutr. Res.* **15** (1995) 1045
8. N.E. Chakov, R.A. Collins, J.B. Vincent, *Polyhedron* **18** (1999) 2891
9. Y. Liang, L.K. Noda, O. Sala, *J. Mol. Struct.* **554** (2000) 271
10. D.M. Stearns, S.M. Silveira, K.K. Wolf, A.M. Luke, *Mutat. Res.* **513** (2002) 135
11. D.D. Hepburn, J.M. Burney, S.A. Woski, J.B. Vincent, *Polyhedron* **2** (2003) 455
12. M. Hidalgo, S.G. Eckhardt, *J. Natl. Cancer Inst.* **93** (2001) 178
13. S. Cai, K. Sato, T. Shimizu, S. Yamabe, M. Hiraki, C. Sano, H. Tamioka, *J. Antimicrob. Chemother.* **57** (2006) 85
14. J. R. Komorowski, D. Greenberg, V. Juturu, *Toxicol. In Vitro* **22** (2008) 819
15. G. Kirkil, M. Hamdi Muz, D. Seckin, K. Sahin, O. Kucuk, *Respiro. Med.* **102** (2008) 840
16. P. Koczoń, J. Piekut, M. Borawska, R. Świslocka, W. Lewandowski, *Spectrochim. Acta A* **61** (2005) 819
17. P. Koczoń, J. Piekut, M. Borawska, R. Świslocka, W. Lewandowski, *Anal. Bioanal. Chem.* **384** (2006) 302
18. R. Song, K. M. Kim, Y. S. Sohn, *Inorg. Chim. Acta* **292** (1999) 238
19. S. Grguric-Sipka, C. R. Kowol, S.-M. Valiahdi, R. Eichinger, M. A. Jakupec, A. Roller, S. Shova, V. B. Arion, B. K. Keppler, *Eur. J. Inorg. Chem.* (2007) 2870
20. C. R. Kowol, R. Eichinger, M. A. Jakupec, M. Galanski, V. B. Arion, B. K. Keppler, *J. Inorg. Biochem.* **101** (2007) 1946
21. W. F. Schmid, S. Zorbas-Seifried, R. O. John, V. B. Arion, M. A. Jakupec, A. Roller, M. Galanski, I. Chiorescu, H. Zorbas, B. K. Keppler, *Inorg. Chem.* **46** (2007) 3645
22. I. Bratsos, G. Birarda, S. Jedner, E. Zangrando, E. Alessio, *Dalton Trans.* (2007) 4048
23. C. Streu, P. J. Carroll, R. K. Kohli, E. Meggers, *J. Organomet. Chem.* **693** (2008) 551
24. W. F. Schmid, R. O. John, V. B. Arion, M. A. Jakupec, B. K. Keppler, *Organometallics* **26** (2007) 6643
25. W. F. Schmid, R. O. John, G. Mühlgassner, P. Hefeter, M. A. Jakupec, M. Galanski, W. Berger, V. B. Arion, B. K. Keppler, *J. Med. Chem.* **50** (2007) 6343
26. R. Schuecker, R. O. John, M. A. Jakupec, V. B. Arion, B. K. Keppler, *Organometallics* **27** (2008) 6587
27. L. K. Filak, G. Mühlgassner, M. A. Jakupec, P. Heffeter, W. Berger, V. B. Arion, B. K. Keppler, *J. Biol. Inorg. Chem.* **15** (2010) 903
28. S. M. Guichard, R. Else, E. Reid, B. Zeitlin, R. Aird, M. Muir, M. Dodds, H. Fiebig, P. J. Sadler, D. I. Jodrell, *Biochem. Pharm.* **71** (2006) 408
29. T. Bugarcic, A. Habtemariam, J. Stepankova, P. Heringova, J. Kasparkova, R. J. Deeth, R. D. L. Johnstone, A. Prescimone, A. Parkin, S. Parsons, V. Brabec, P. J. Sadler, *Inorg. Chem.* **47** (2008) 11470
30. T. Bugarcic, A. Habtemariam, R. J. Deeth, F. P. A. Fabbiani, S. Parsons, P. J. Sadler, *Inorg. Chem.* **48** (2009) 9444
31. T. Bugarcic, O. Nováková, A. Halámiková, L. Zerzánková, O. Vrána, J. Kašpárková, A. Habtemariam, S. Parsons, P. J. Sadler, V. Brabec, *J. Med. Chem.* **51** (2008) 5310
32. M. Gras, B. Therrien, G. Süss-Fink, P. Štěpnička, A. K. Renfrew, P. J. Dyson, *J. Org. Chem.* **693** (2008) 3419
33. M. Auzias, J. Gueniat, B. Therrien, G. Süss-Fink, A. K. Renfrew, P. J. Dyson, *J. Org. Chem.* **694** (2009) 855
34. C. Scolaro, C. G. Hartinger, C. S. Allardyce, B. K. Keppler, P. J. Dyson, *J. Inorg. Biochem.* **102** (2008) 1743

35. S. Grgurić-Šipka, M. M. Alshtewi Al. Arbi, D. Jeremić, G. N. Kaluđerović, S. Gomez-Ruiz, Ž. Žižak, Z. Juranić, T. J. Sabo, *J. Serb. Chem. Soc.* **73** (2008) 619
36. V. Rajendiran, M. Murali, E. Suresh, S. Sinha, K. Somasundaram, M. Palaniandavar, *Dalton Trans.* (2008) 148
37. V. Djinovic, M. Momcilovic, S. Grguric-Sipka, V. Trajkovic, S. M. Mostarica, D. Miljkovic, T. Sabo, *J. Inorg. Biochem.* **98** (2004) 2168
38. A. Bergamo, L. Messori, F. Piccioli, M. Cocchietto, G. Sava, *Invest. New Drug.* **21** (2003) 401
39. A. R. Timerbaev, C. G. Hartinger, S. S. Aleksenko, B. K. Keppler, *Chem. Rev.* **106** (2006) 2224
40. W. H. Ang, P. J. Dyson, *Eur. J. Inorg. Chem.* **20** (2006) 8153
41. S. Grgurić-Šipka, I. Ivanović, G. Rakić, N. Todorović, N. Gligorijević, S. Radulović, V. B. Arion, B. K. Keppler, Ž. Lj. Tešić, *Eur. J. Med. Chem.* **45** (2010) 1051
42. A. F. A. Peacock, S. Parsons, P. J. Sadler, *J. Am. Chem. Soc.* **129** (2007) 3348
43. S. H. van Rijt, A. F. A. Peacock, R. D. L. Johnstone, S. Parsons, P. J. Sadler, *Inorg. Chem.* **48** (2009) 1753
44. D. Camm, A. El-Sokkary, A. L. Gott, P. G. Stockley, T. Belyaeva, P. C. McGowan, *Dalton Trans.* (2009) 10914
45. S. B. Jensen, S. J. Rodger, M. D. Spicer, *J. Organomet. Chem.* **556** (1998) 151
46. *SAINT-Plus*, version 7.56a, Bruker AXS Inc., Madison, WN, 2008
47. G. M. Sheldrick, *SHELXS-97, Program for Crystal Structure Solution*, University Göttingen, Göttingen, 1997
48. G. M. Sheldrick, *SHELXL-97, Program for Crystal Structure Refinement*, University Göttingen, Göttingen, 1997
49. G. K. Johnson, *Report ORNL-5138*, Oak Ridge National Laboratory, Oak Ridge, TN, 1976
50. *International Tables for X-Ray Crystallography*, Vol. C, A. J. C. Wilson, Ed., Kluwer Academic Press, Dodrecht, 1992, Tables 4.2.6.8 and 6.1.1.4.
51. R. Surpino, in *Methods in Molecular Biology*, in Vitro *Toxicity Testing Protocols*, S. O'Hare, C.K. Atterwill, Eds., Humana Press, New York, 1995, p. 137
52. L. Carter, D. L. Davies, J. Fawcett, D. R. Russell, *Polyhedron* **12** (1993) 1599
53. M. C. Barrel, R. Jimenez-Aparicio, E. C. Royer, M. J. Sancedo, F. A. Urbanos, E. Gutierrez-Pueblo, C. Ruiz-Valero, *J. Chem. Soc. Dalton Trans.* (1991) 1609.

Journal of the Serbian Chemical Society
JSCS-info@shd.org.rs • www.shd.org.rs/JSCS
J. Serb. Chem. Soc. 76 (1) 63–74 (2011)
JSCS–4100
UDC 542.913+542.9+547.571+547.551+546.792'562'47+54–71–034:547.415.1'631.6
Original scientific paper

Tetradentate Schiff base ligands of 3,4-diaminobenzophenone: Synthesis, characterization and thermodynamics of complex formation with Ni(II), Cu(II) and Zn(II) metal ions

MOZAFFAR ASADI[1]*, HAJAR SEPEHRPOUR[1] and KHOSRO MOHAMMADI[2]

[1]*Chemistry Department, College of Sciences, Shiraz University, Shiraz 71454 and* [2]*Chemistry Department, Faculty of Sciences, Persian Gulf University, Bushehr 75169, I. R. Iran*

(Received 4 January , revised 12 July 2010)

Abstract: Some new symmetrical diimino tetradentate Schiff base ligands were synthesized by the reaction of 3,4-diaminobenzophenone with salicylaldehyde derivatives, such as [3,4-bis(((2-hydroxy-4-methoxyphenyl)methylene)amino)-phenyl]phenylmethanone (L^1), [3,4-bis(((2-hydroxy-5-methoxyphenyl)methylene)amino)phenyl]phenylmethanone (L^2), [3,4-bis(((5-bromo-2-hydroxyphenyl)methylene)amino)phenyl]phenylmethanone (L^3) and [3,4-bis(((2-hydroxy--5-nitrophenyl)methylene)amino)phenyl]phenylmethanone (L^4). Additionally, a tetradentate Schiff base ligand [3,4-bis(((2-hydroxy-3-methoxyphenyl)methylene)amino)phenyl]phenylmethanone (L^5) was synthesized. All the Schiff bases and their Ni(II), Cu(II) and Zn(II) complexes were characterized using elemental analysis and infrared, electronic, mass and ^{1}H-NMR spectroscopy. The formation constants of the complexes were measured using UV–Vis spectroscopic titration at constant ionic strength 0.10 M ($NaClO_4$), at 25 °C in dimethylformamide (DMF) as solvent.

Keywords: synthesis; tetradentate Schiff base; metal complex; diaminobenzophenone; formation constant.

INTRODUCTION

Tetradentate Schiff base ligands were synthesized by the reaction of diamines with the corresponding salicylaldehyde derivative. These reactions are important due to the great number of molecules that can be generated and the well--known ability of these tetradentate ligands to form stable complexes with different metal cations.[1]

The literature clearly shows that the study of Schiff base ligand systems is linked with many of the key advances made in inorganic chemistry.[2–4] They played a seminal role in the development of modern coordination chemistry.[5] Se-

* Corresponding author. E-mail: asadi@susc.ac.ir
doi: 10.2298/JSC100104004A

veral metal chelates of the ONNO donor class of Schiff bases were studied as oxygen carrier and they were found to be useful models for bioinorganic processes.[6,7] Schiff bases are effective inhibitors and could be adsorbed on the surface of metals.[8] Symmetric tetradentate Schiff base complexes have been extensively used as macrocycle models.[9] These compounds have received considerable attention because of their potential use as catalysts,[10–14] and their antibacterial,[5,15,16] antifungal,[17] antitumour[18,19] and herbicidal activities.[20]

The main goals of this study were the synthesis and characterization of some new tetradentate Schiff bases and their complexation with Ni(II), Cu(II) and Zn(II) metals. These compounds were characterized by elemental analysis, and FT–IR, ^{1}H-NMR, mass and UV–Vis techniques. In addition, the formation constants, K_f, were determined spectrophotometrically and the free energy changes, $\Delta G^{\ominus}$, at 25 °C, were calculated for the complexes. The effects of the electronic and steric nature of substituents on the Schiff base type ligands on the formation constants and free energy changes resulting from complex formation were studied.

EXPERIMENTAL

Materials and instruments

The materials, 3,4-diaminobenzophenone, 3-methoxysalicylaldehyde, 4-methoxysalicylaldehyde, 5-methoxysalicylaldehyde, 5-bromosalicylaldehyde, 5-nitrosalicylaldehyde, dimethylformamide, methanol, chloroform, nickel acetate tetrahydrate, zinc acetate dihydrate and copper acetate monohydrate were purchased from Merck and Fluka, Germany. Spectrograde solvents were used for the spectral measurements.

C, H, N analysis data were obtained using a Thermo Finningan Flash EA-1112 elemental analysis instrument. Melting points were measured in capillary tubes using a Buchi 535 melting point apparatus. The infrared spectra were recorded on a Shimadzu FTIR-8300 spectrophotometer using the KBr pellet technique. The UV–Vis spectra were obtained in DMF on a Perkin Elmer Lambda 2-UV/Vis spectrophotometer. The ^{1}H-NMR spectra were recorded on a Bruker Avance DPX-250 MHz spectrometer with TMS as internal standard and the mass spectra were obtained on a Perkin-Elmer R MU-6E instrument.

Synthesis of the Schiff base ligands and their complexes

All the new tetradentate Schiff base ligands (L^1–L^4) were prepared by condensation of a derivative of salicylaldehyde (2 mmol) with 3,4-diaminobenzophenone (1 mmol) by refluxing in MeOH (30 cm^3) for 2 h. The final products were analytically pure solids after recrystallization from 1:1 chloroform/methanol mixed solvent for L^1, L^2 and L^3, and dimethylformamide/methanol mixture (1:1) for L^4. The products were dried at 50 °C under vacuum for 24 h. The L^5 Schiff base ligand was prepared according to a previously published method.[21]

Ni(II), Cu(II) and Zn(II) complexes of L^1, L^2 and L^3 were prepared by the addition of 1.5 mmol of the appropriate metal acetate hydrates dissolved in 10 cm^3 of methanol to a hot mixture of methanol (20 cm^3) and chloroform (15 cm^3) containing 1 mmol of the required Schiff base ligand. The mixture was then refluxed for 3 h for L^1, L^2 and L^3. The precipitated solids were recrystallized from methanol and dried under vacuum. The Ni(II), Cu(II) and Zn(II) complexes of L^4 were prepared in a similar way but the Schiff base ligand was dissolved in a hot mixture of methanol (15 cm^3) and DMF (20 cm^3). The same metal complexes of L^5 were also prepared by a similar method but dissolved in methanol at room temperature (Scheme 1).

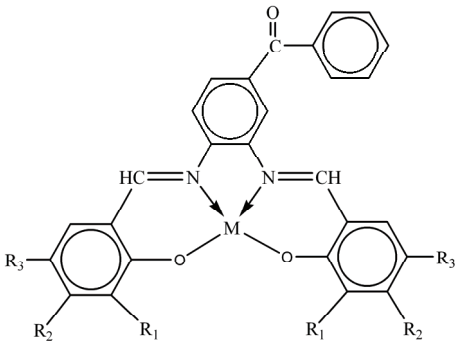

M = Ni^{2+}, Cu^{2+}, Zn^{2+}
L^1: $R_1 = R_3 = H$, $R_2 = OMe$
L^2: $R_1 = R_2 = H$, $R_3 = OMe$
L^3: $R_1 = R_2 = H$, $R_3 = Br$
L^4: $R_1 = R_2 = H$, $R_3 = NO_2$
L^5: $R_2 = R_3 = H$, $R_1 = OMe$

Scheme 1. A structural representation of the Schiff base complexes.

Thermodynamic studies

The formation constants, K_f, were determined by UV–Vis absorption spectroscopy through titration of a fixed concentration (3×10^{-5} M) of the ligands with various concentrations of the metal ions (10^{-4}–10^{-5} M) at constant ionic strength (0.1 M $NaClO_4$) and at 25 °C. The interaction of $NaClO_4$ with the ligands in dimethylformamide was negligible. The absorption measurements were performed at various wavelengths, where the difference in the absorption was the maximum after equilibrium. The formed product exhibited different absorptions from those of the free ligand, while the metal ion solution showed no absorption at these wavelengths.

RESULTS AND DISCUSSION

The elemental analyses and some physical properties of the synthesized ligands and their complexes are collected in Table I.

TABLE I. The analytical and the physical data of the ligands and their complexes

Compound	Empirical formula	Formula weight	Yield %	Colour	M.p. °C	Found (Calcd.), %		
						C	H	N
L^1	$C_{29}H_{24}N_2O_5$	480.62	78	Yellow	127	72.71 (72.49)	5.17 (5.03)	5.75 (5.83)
L^2	$C_{29}H_{24}N_2O_5$	480.62	70	Yellow	152	72.79 (72.49)	5.18 (5.03)	5.62 (5.83)
L^3	$C_{27}H_{18}N_2Br_2O_3$	578.36	80	Yellow	169	55.74 (56.08)	3.16 (3.14)	4.99 (4.84)
L^4	$C_{27}H_{18}N_4O_7$	510.63	83	Yellow	237	63.60 (63.53)	3.73 (3.55)	11.03 (10.98)
CuL^1	$C_{29}H_{22}N_2O_5Cu$	542.15	70	Brown	>250	64.35 (64.26)	4.12 (4.09)	5.15 (5.17)

TABLE I. Continued

Compound	Empirical formula	Formula weight	Yield %	Colour	M.p. °C	Found (Calcd.), %		
						C	H	N
CuL^2	$C_{29}H_{22}N_2O_5Cu$	542.15	70	Brownish red	>250	64.21 (64.26)	3.95 (4.09)	5.12 (5.17)
CuL^3	$C_{27}H_{16}N_2Br_2O_3Cu$	639.88	54	Brown	>250	50.58 (50.69)	2.53 (2.52)	4.32 (4.38)
CuL^4	$C_{27}H_{16}N_4O_7Cu$	572.15	45	Green	>250	56.65 (56.70)	2.84 (2.82)	9.85 (9.80)
CuL^5	$C_{29}H_{22}N_2O_5Cu$	542.15	53	Brown	>250	64.10 (64.26)	4.14 (4.09	5.20 (5.17)
NiL^1	$C_{29}H_{22}N_2O_5Ni$	537.30	45	Brownish red	>250	64.71 (64.84)	4.18 (4.13)	5.04 (5.21)
NiL^2	$C_{29}H_{22}N_2O_5Ni$	537.30	71	Brownish red	>250	64.53 (64.84)	4.02 (4.13)	4.90 (5.21)
NiL^3	$C_{27}H_{16}N_2Br_2O_3Ni$	635.03	50	Brownish red	>250	50.80 (51.07)	2.45 (2.54)	4.44 (4.41)
NiL^4	$C_{27}H_{16}N_4O_7Ni$	567.30	55	Brownish red	>250	57.25 (57.18)	2.72 (2.84)	9.62 (9.76)
NiL^5	$C_{29}H_{22}N_2O_5Ni$	537.30	58	Brownish red	>250	64.62 (64.84)	4.23 (4.13)	5.11 (5.21)
ZnL^1	$C_{29}H_{22}N_2O_5Zn$	543.99	37	Yellow	>250	64.12 (64.04)	4.06 (4.08)	5.24 (5.15)
ZnL^2	$C_{29}H_{22}N_2O_5Zn$	543.99	70	Red	>250	64.14 (64.04)	4.10 (4.08)	4.29 (5.15)
ZnL^3	$C_{27}H_{16}N_2Br_2O_3Zn$	641.72	45	Orange	>250	56.42 (56.51)	2.46 (2.51)	4.29 (4.37)
ZnL^4	$C_{27}H_{16}N_4O_7Zn$	573.99	72	Yellow	>250	62.15 (62.19)	2.78 (2.81)	9.62 (9.76)
ZnL^5	$C_{29}H_{22}N_2O_5Zn$	543.99	40	Red	245	64.15 (64.04)	4.02 (4.08)	4.95 (5.15)

Spectral characterization

^{1}H-NMR spectra. The ^{1}H-NMR spectra of the compounds were obtained in DMSO-d_6 and $CDCl_3$ at room temperature using TMS as the internal standard. The ^{1}H-NMR assignments of the compounds are presented in Table II. The chemical shift observed for the OH protons in the ligands (12.27–13.88 ppm) were not observed in any of the complexes. This confirms the bonding of the oxygen atoms to the metal ions (C–O–M).The presence of a sharp singlet for the –C(H)=N proton in the Schiff bases (7.99–9.15 ppm) clearly indicates that the magnetic environments for all such protons were similar, suggesting the presence of a planar ligand in these complexes.[22] The multiplets of the aromatic protons appeared within the range 6.15–8.63 ppm. In ligands L^1, L^2, L^5 and their complexes, the protons peak of O–CH_3 appeared in 3.69–3.86 ppm region.

TABLE II. ^{1}H-NMR data of the Schiff bases and their complexes (δ / ppm)

Compounds	OH	H–C=N	Ar–H	OMe
L^{1a}	12.27	8.63	6.45–7.77	3.81
L^{2a}	13.37	7.99	6.96–7.77	3.79
L^{3a}	12.75	8.61	6.92–7.76	–
L^{4b}	13.88	9.01	6.82–8.25	–
NiL^{1b}	–	8.14	6.31–7.80	3.80
NiL^{2b}	–	8.95	6.82–8.50	3.71
NiL^{3b}	–	8.46	6.77–8.10	–
NiL^{4b}	–	9.15	6.53–8.52	–
NiL^{5a}	–	9.15	6.53–8.50	3.75
ZnL^{1b}	–	8.91	6.15–8.16	3.73
ZnL^{2b}	–	9.08	6.63–8.25	3.69
ZnL^{3b}	–	8.25	6.63–7.97	–
ZnL^{4b}	–	8.96	6.73–8.63	–
ZnL^{5b}	–	9.04	6.40–8.21	3.73

[a]$CDCl_3$; [b]DMSO-d_6

IR spectra. The IR spectra provided valuable information regarding the nature of the functional groups attached to the metal atom. The main infrared bands and their assignments are listed in Table III. The strong broad band in the IR spectra of the ligands in the range 3375–3463 cm^{-1} is assigned to O–H stretching vibrations, which is affected by the intramolecular hydrogen bond to the azomethine group (O–H···N=C). These bands disappeared through complexation with the metal ions.[23] The weak bands at 2823–3062 cm^{-1} are related to (C–H) vibrations. The band in the region 1643–1666 cm^{-1} is attributed to ($\nu_{C=O}$). The spectra of the ligands showed two different (–C=N) bands in the region 1527–1620 cm^{-1}, which were shifted to lower frequencies in the spectra of all the complexes, indicating the involvement of the –C=N nitrogen in the coordination to the metal ions. [24] The ring skeletal vibrations (C=C) were observed in the region 1427–1546 cm^{-1}. The phenolic C–O stretching vibrations appeared in the region 1188–1292 cm^{-1}. The assignment of the proposed coordination sites was further supported by the appearance of bands at 489–574 cm^{-1} and 412–493 cm^{-1}, which could be attributed to $\nu_{N–M}$ and $\nu_{O–M}$, respectively. All the IR data suggest that the metal was bonded to the Schiff bases through the phenolic oxygen and the imino nitrogen.[25]

Electronic spectra. The electronic spectra of the free ligands $L^{1–3}$ and L^5 show a weak band, as a shoulder in the region of 415–485 nm, which is assigned to $n\rightarrow\pi^*$ transition involving molecular orbitals of the C=N chromophore and the benzene ring.[26–29] L^4 shows a sharp peak at 428 nm. The band in the range of 320–404 nm for $L^{1–3}$ and L^5 is assigned to $\pi\rightarrow\pi^*$ type transition, which involves molecular orbitals essentially localized on the C=N group and the benzene ring; thus, the transition involves the azomethine group. This type of transition in L^4 is

a sharp peak at 375 nm. These differences in shape and position of the band in L^4 are probably due to the presence of the NO_2 chromophore in the ligand (See Table IV).

TABLE III. The IR bands of the ligands and their complexes, cm^{-1} (*s* – strong, *m* – medium, *w* – weak)

Compounds	ν_{O-H}	ν_{C-H}	$\nu_{C=O}$	$\nu_{C=N}$	$\nu_{C=C}$	ν_{C-O}	ν_{N-M}	ν_{O-M}
L^1	3444	3047(*w*)	1647(*s*)	1612(*s*)	1546(*s*)	1234(*m*)	–	–
		2927(*w*)		1584(*s*)	1508(*s*)			
L^2	3463	3209(*w*)	1647(*s*)	1604(*s*)	1488(*s*)	1269(*m*)	–	–
		2823(*w*)		1577(*s*)	1461(*s*)			
L^3	3402	3047(*w*)	1643(*s*)	1620(*s*)	1469(*s*)	1276(*m*)	–	–
		2927(*w*)		1554(*s*)	1446(*s*)			
L^4	3382	3055(*w*)	1647(*s*)	1620(*s*)	1533(*s*)	1292(*m*)	–	–
		2850(*w*)		1589(*s*)	1481(*s*)			
CuL^1	–	2935(*w*)	1647(*s*)	1612(*s*)	1515(*s*)	1199(*m*)	516(*w*)	439(*w*)
		2835(*w*)		1573(*s*)	1461(*s*)			
CuL^2	–	2931(*w*)	1654(*s*)	1600(*s*)	1523(*s*)	1215(*m*)	505(*w*)	451(*w*)
		2835(*w*)		1581(*s*)	1465(*s*)			
CuL^3	–	3047(*w*)	1643(*s*)	1608(*s*)	1504(*s*)	1242(*m*)	516(*w*)	443(*w*)
		2912(*w*)		1577(*s*)	1454(*s*)			
CuL^4	–	2912(*w*)	1666(*s*)	1608(*s*)	1542(*s*)	1272(*m*)	524(*w*)	443(*w*)
		3058(*w*)		1581(*s*)	1492(*s*)			
CuL^5	–	2927(*w*)	1658(*s*)	1620(*s*)	1537(*s*)	1238(*m*)	520(*w*)	443(*w*)
		2835(*w*)		1600(*s*)	1475(*s*)			
NiL^1	–	2935(*w*)	1647(*s*)	1612(*s*)	1504(*s*)	1207(*m*)	528(*w*)	435(*w*)
		2835(*w*)		1573(*s*)	1431(*s*)			
NiL^2	–	2835(*w*)	1654(*s*)	1577(*s*)	1461(*s*)	1215(*m*)	509(*w*)	451(*w*)
		2827(*w*)		1527(*s*)	1427(*s*)			
NiL^3	–	3058(*w*)	1654(*s*)	1608(*s*)	1512(*s*)	1245(*m*)	516(*w*)	412(*w*)
		2908(*w*)		1577(*s*)	1446(*s*)			
NiL^4	–	3062(*w*)	1658(*s*)	1604(*s*)	1542(*s*)	1276(*m*)	516(*w*)	455(*w*)
		2923(*w*)		1581(*s*)	1504(*s*)			
NiL^5	–	3000(*w*)	1647(*s*)	1608(*s*)	1539(*s*)	1242(*m*)	574(*w*)	493(*w*)
		2920(*w*)		1581(*s*)	1461(*s*)			
ZnL^1	–	2923(*w*)	1647(*s*)	1608(*s*)	1519(*s*)	1188(*m*)	509(*w*)	466(*w*)
		2854(*w*)		1577(*s*)	1427(*s*)			
ZnL^2	–	2890(*w*)	1649(*s*)	1604(*s*)	1527(*s*)	1211(*m*)	489(*w*)	443(*w*)
		2831(*w*)		1581(*s*)	1469(*s*)			
ZnL^3	–	3047(*w*)	1651(*s*)	1612(*s*)	1515(*s*)	1245(*m*)	547(*w*)	497(*w*)
		2908(*w*)		1581(*s*)	1461(*s*)			
ZnL^4	–	2997(*w*)	1654(*s*)	1612(*s*)	1546(*s*)	1272(*m*)	505(*w*)	439(*w*)
		2923(*w*)		1585(*s*)	1485(*s*)			
ZnL^5	–	2997(*w*)	1647(*s*)	1608(*s*)	1539(*s*)	1230(*m*)	501(*w*)	439(*w*)
		2920(*w*)		1577(*s*)	1465(*s*)			

Shifts were observed in the visible spectra of the metal complexes when compared with those of the corresponding free ligands. The formation of the metal–nitrogen bond stabilizes the electron pair on the nitrogen atom, *i.e.*, the energy of the non-bonding orbital is lowered and the transition occurs at a lower wavelength. This band is obscured by a strong band which can be assigned to $\pi \rightarrow \pi^*$ type transitions involving the metal–ligand bonds.[30,31] The d–d band was not observed, as it was masked by the metal to ligand charge transfer (MLCT) band.

TABLE IV. The electronic spectral data of the Schiff bases and their complexes (nm) in DMF

Compounds	π–π^*	n–π^*	Charge transfer transition
L^1	393	450(*sh*)	–
L^2	338	485(*sh*)	–
L^3	344	477(*sh*)	–
L^4	375	428	–
L^5	331	415(*sh*)	–
NiL^1	390	–	452
NiL^2	390	–	478
NiL^3	386	–	484
NiL^4	323	–	392
NiL^5	395	–	467
ZnL^1	395	–	454
ZnL^2	382	–	481
ZnL^3	330	–	420
ZnL^4	330	–	390
ZnL^5	330	–	431
CuL^1	404	–	462
CuL^2	380	–	494
CuL^3	320	–	427
CuL^4	325	–	390
CuL^5	371	–	475

In the compounds, bands of the ligands were observed in the 331–393 nm and 415–485 nm ranges, as shoulders. In their complexes, the bands were shifted to lower energy. The spectral changes were observed in DMF solution when up to 3.5 equivalents of $Ni(OAc)_2$ were added relative to L^2. In the absence of the metal ion, the L^2 solution showed absorption bands at 338 and 485 nm as shoulders. As the metal ion solution was added, the signals of L^2 decreased and those of the new complex, NiL^2, at 390 and 478 nm increased in intensity with isosbestic points at 370 and 700 nm. After the addition of 3.5 equivalents of the metal ion, the solution showed only the signals for NiL^2. The same was valid for the other systems.

The electronic spectra of the complexes formed during the titration were the same as those of the separately synthesized complexes. The UV–Vis spectra of

L^2, NiL^2 from the titration and the synthesized NiL^2 product are shown in Fig. 1. The data show that the synthesized complex and the product of the titration are same. The results were same for the other systems.

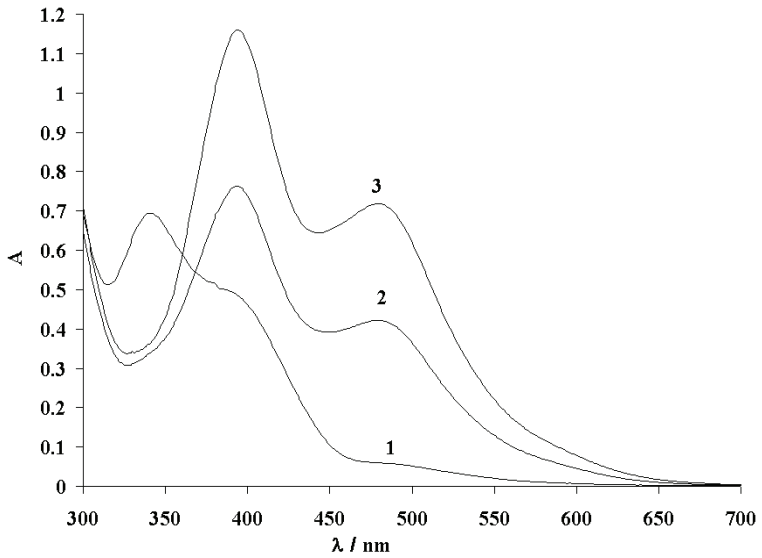

Fig. 1. UV–Vis spectra of the ligand L^2 (1), the end point of the titration of the ligand with Ni^{2+} (2), and the synthesized NiL^2 (3) in DMF.

Mass spectra. The mass spectra of the ligands and complexes show intense molecular ion peaks *m*/*z* M^+/$(M+H)^+$. In addition to these peaks, they show some peaks due to elimination of phenyl or benzyl derivative species from the molecular ion. The mass spectra of the compounds also show some prominent peaks corresponding to *m*/*z* $(M–Ar)^+$, $(M–Ar–CH)^+$, $(Ar)^+$, $(Ar–CH)^+$ and $(PhCO)^+$ (Table V). The fragmentation of the mass spectrum of the L^2 ligand is: 480 (M+, 9.9), 344 ($C_6H_5COC_6H_3N{=}CHC_6H_3OHOMeN$, 70.6), 239 ($C_6H_3N{=}CHC_6H_3OHOMeN$, 4.6), 221 ($C_6H_5COC_6H_3N{=}CHN$, 5.0), 180 ($C_6H_5COC_6H_3$, 3.2), 123 ($C_6H_3OHOMe$, 11.5), 105 ($C_6H_5CO$, 95.0), 77($C_6H_5$, 100.0) (Table V).

The formation constants

Complexes were obtained from the reaction of the metals with the Schiff base donors according to Eq. (1):

$$H_2L^x + M(OAc)_2 \rightleftharpoons [ML^x] + 2HOAc \quad (1)$$

The formation constants were determined by UV–Vis absorption spectroscopy through titration of the ligands with various concentrations of the metal ions at a constant ionic strength 0.1 M ($NaClO_4$) at 25 °C. The complex formation constants, K_f, were calculated using the SQUAD computer program,[32] designed

to calculate the best values for formation constants by employing a non-linear, least squares approach. The free energy change $\Delta G^{\ominus}$ of the formed complexes were calculated from $\Delta G^{\ominus} = -RT \ln K_f$ at 25 °C, where K_f is the complex formation constant, R the gas constant and T the thermodynamic temperature (Table VI).

TABLE V. The mass spectra of the ligands and their complexes

Compound	*m*/*z*								
L^1	480	344	239	221	180	105	77		
L^2	480	344	240	181	105	77			
L^3	578	392	283	220	185	124	105	77	
L^4	510	360	253	178	105	77	57		
NiL^1	537	401	343	298	239	183	122	105	77
NiL^2	537	403	338	280	236	180	124	105	77
NiL^3	635	448	393	345	285	169	77		
NiL^4	567	418	345	240	183	137	105	77	
NiL^5	537	400	295	238	179	124	105		
ZnL^1	543	407	343	302	238	185	105	77	
ZnL^2	543	406	347	301	243	180	77		
ZnL^3	641	456	393	351	287	170	105	77	
ZnL^4	573	424	344	318	240	177	137	105	77
ZnL^5	543	407	342	239	180	123	77		
CuL^1	542	406	343	303	185	123	105	77	
CuL^2	542	408	302	179	122	105	77		
CuL^3	639	453	392	377	169	105	77		
CuL^4	572	406	345	301	183	105	77		
CuL^5	542	343	330	180	124	105	77		

TABLE VI. The formation constants, log K_f, and the thermodynamic free energy for the complexes of the ligands with the metal ions at 25 °C, in DMF and at I = 0.1 mol dm^{-3} ($NaClO_4$)

Ligand	Cu^{2+}		Ni^{2+}		Zn^{2+}	
	log K_f	$\Delta G^{\ominus}$ / kJ mol^{-1}	log K_f	$\Delta G^{\ominus}$ / kJ mol^{-1}	log K_f	$\Delta G^{\ominus}$ / kJ mol^{-1}
L^1	5.42(0.48)	–30.92(1.11)	5.63(0.04)	–32.10(0.32)	5.33(0.24)	–30.39(0.12)
L^2	5.84(0.43)	–33.30(0.76)	6.13(0.22)	–34.96(0.19)	5.11(0.30)	–29.14(0.74)
L^3	5.31(0.26)	–30.28(0.19)	5.41(0.04)	–30.85(0.37)	4.14(0.02)	–23.61(0.44)
L^4	3.67(0.01)	–20.93(0.07)	4.85(0.01)	–27.66(0.44)	2.42(0.63)	–13.80(1.31)
L^5	5.60(0.30)	–31.93(0.09)	5.79(0.06)	–33.02(0.19)	5.20(0.32)	–29.65(0.74)

The metal effect

The trend of the complex formation of the metal ions with a given ligand is as follows: $Ni^{2+} > Cu^{2+} > Zn^{2+}$.

The crystal field stabilization energy, *CFSE*, affects the stability of the produced complexes. Ni^{2+} has the highest *CFSE*; hence, it has the highest formation constant. The coordination around nickel is essentially square planar with a small tetrahedral distortion. The molecular structure of [Ni(salen)],[33] [Ni(cd_5Clsalen)][34]

and [Ni(cdsalen)][35] were determined previously and may be compared with the structure of the present complexes $NiL^{1–5}$.

Zn(II), with a d^{10} configuration, has more potency to take a tetrahedral configuration; hence, it has the smallest formation constant, while Cu(II), with a d^9 configuration, tends to have a distorted square planar geometry because of the Jahn–Teller effect[36] (Table VI).

The electronic effect of para*-substituted Schiff base ligands*

For studying the electronic effect of *para* substitution on the Schiff base ligands, some different substituents were used. In the *para*-substituted Schiff base ligands, the formation constants vary as could be expected according to the electronic effect of the substituents at the *para* position. Thus, the formation constants decrease according to the sequence OMe > Br > NO_2. An electron-withdrawing functional group, such as NO_2, makes the Schiff base a poorer donor ligand and decreases the formation constant, while an electron-donor group, such as OMe, increases the formation constant. Therefore, the ligands having Br and NO_2 groups, (L^3) and (L^4), respectively, have the smallest formation constants, while the ligands with an OMe group have the highest (Table VI).[37,38]

The effect of the position of the methoxy substituent on the Schiff base

The results show the following trend of complex formation of either nickel(II) and copper(II) with the Schiff bases (Table VI): 5-OMe (L^2) > 3-OMe (L^5) > > 4-OMe (L^1).

In the case of L^2, the methoxy group was situated in the *para* position to the phenolic oxygen of the N_2O_2 backbone, which can release an electron directly to the phenyl ring compared with that of the *meta* and *ortho* positions in L^1 and L^5, respectively.[39]

The trend of the formation constant for the Zn^{2+} complexes is as follows: 5--OMe (L^2) < 3-OMe (L^5) < 4-OMe (L^1).

It seems, due to the preference of Zn^{2+} for a tetrahedral geometry, the steric factor predominates over the electronic factor.

CONCLUSIONS

Some new symmetrical di-imino tetradentate Schiff base ligands and their complexes with Ni(II), Cu(II) and Zn(II) were synthesized and characterized. The thermodynamic formation constants, K_f, were determined spectrophotometrically at 25 °C. By considering the formation constants and the free energy changes, the following conclusions were drawn.

The complex formation constant for Ni(II) was higher than Cu(II) and Zn(II) has the smallest formation constant: Ni(II) > Cu(II) > Zn(II).

An electron-donor group increases the formation constant, while an electron--withdrawing functional group decreases it. The trend of the formation constant is as follows: $ML^{1,2,5} > ML^3 > ML^4$, M = Cu(II), Zn(II) and Ni(II).

Acknowledgements. We are grateful to the Shiraz University Research Council for their financial support.

ИЗВОД

СИНТЕЗА ТЕТРАДЕНТАТНИХ ЛИГАНАДА ТИПА ШИФОВИХ БАЗА ПОЛАЗЕЋИ ОД 3,4-ДИАМИНОБЕНЗОФЕНОНА: СИНТЕЗА, КАРАКТЕРИЗАЦИЈА И ТЕРМОДИНАМИЧКЕ КОНСТАНТЕ ФОРМИРАЊА КОМПЛЕКСА Ni(II), Cu(II) И Zn(II)

MOZAFFAR ASADI[1], HAJAR SEPEHRPOUR[1] и KHOSRO MOHAMMADI[2]

[1]*Chemistry Department, College of Sciences, Shiraz University, Shiraz 71454 и* [2]*Chemistry Department, Faculty of Sciences, Persian Gulf University, Bushehr 75169, I. R.. Iran*

У реакцији између 3,4-диаминобензофенона и деривата салицилалдехида, као што су [3,4-бис(((2-хидрокси-4-метоксифенил)метилен)амино)фенил]фенилметанон (L^1), [3,4-бис-(((2-хидрокси-5-метоксифенил)метилен)амино)фенил]фенилметанон (L^2), [3,4-бис(((5-бромо-2-хидроксифенил)метилен)амино)фенил]фенилметанон (L^3) и [3,4-бис(((2-хидрокси-5--нитрофенил)метилен)амино)фенил]фенилметанон (L^4), синтетисани су нови тетрадентатни лиганди типа Шифових база. Поред тога, у овом раду описана је синтеза тетрадентатног лиганда [3,4-бис(((2-хидрокси-3-метоксифенил)метилен)амино)фенил]фенилметанона (L^5), који такође припада типу Шифових база. Добијени лиганди су употребљени за синтезу одговарајућих Ni(II), Cu(II) и Zn(II) комплекса. За карактеризацију ових комплекса употребљени су елементарна микроанализа, инфра-црвени, електронски, масени спектри. Поред тога, за карактеризацију комплекса, осим за Cu(II) комплексе, употребљени су и њихови ^{1}H-NMR спектри. Дате су вредности за константе грађења комплекса, као и вредности за неке термодинамичке параметре, који су одређени помоћу UV–Vis спектрофотометрије у 0,10 M $NaClO_4$ на 25 °C у диметилформамиду (DMF) као растварачу.

(Примљено 4. јануара, ревидирано 12. јула 2010)

REFERENCES

1. S. Akine, T. Nabeshima, *Dalton Trans*. (2009) 10377
2. S. Hazra, R. Koner, P. Lemoine, E. C. Sanudo, S. Mohanta, *Eur. J. Inorg. Chem*. (2009) 3458
3. B. Y. Li, Y. M. Yao, Y. R. Wang, Y. Zhang, Q. Shen, *Inorg. Chem. Commun*. **11** (2008) 349
4. J. Chakraborty, A. Ray, G. Pilet, D. Luneau, R. F. Ziessel, L. J. Chabonnier, L. Carrella, E. Rentschler, M. S. El Fallah, S. Mitra, *Dalton Trans*. (2009) 4923
5. A. Burkhardt, H. Görls, W. Plass, *Carbohyd. Res*. **343** (2008) 1266
6. P. Adao, I. Pessoa, R. T. Henrlques, M. L. Kuznetsov, F. Aveclla, M. R. Maurya, U. Kumar, I. Correla, *Inorg. Chem*. **48** (2009) 3542
7. M. Valko, R. Klement, P. Pelikan, R. Boca, L. Dlhan, A. Boettcher, H. Elias, L. Mueller, *J. Phys. Chem*. **99** (1995) 137
8. N. Soltani, M. Behpour, S. M. Ghoreishi, H. Naeimi, *Corros. Sci*. **52** (2010) 1351

9. M. K. Taylor, K. D. Trotter, J. Reglinski, L. E. A. Beriouis, A. R. Kennedy, C. M. Spickett, R. J. Sowden, *Inorg. Chim. Acta* **361** (2008) 2851
10. S. Rayati, N. Torabi, A. Chamei, S. Mohebbi, A. Wojtczak, A. Kozakiewicz, *Inorg. Chim. Acta* **361** (2008) 1239
11. K. E. Edmund, *Polyhedron* **26** (2007) 2559
12. N. S. Youssef, E. El. Zahany, A. M. A. Seidy, B. N. Barsoum, *Transition Met. Chem*. **34** (2009) 905
13. K. C. Gupta, A. Kumar Sutar, C. Chieh Lin, *Coord. Chem. Rev*. **523** (2009) 1926
14. R. Zhang, J. Ma, W. Wang, B. Wang, R. Li, *J. Electroanal. Chem.* **643** (2010) 31
15. P. Lix, J. Shi, Q. Tong, Y. Feng, H. Huang, L. Jia, *Inorg. Chim. Acta* **362** (2009) 229
16. H. Bayrak, A. Demirbas, S. A. Karaoglu, N. Demirbas, *Eur. J. Med. Chem*. **44** (2009) 1057
17. N. A. Negm, M. F. Zaki, M. A. I. Salem, *Colloids Surf. B* **77** (2010) 96
18. N. Demirbas, R. Ugurluoglu, *Turk. J. Chem*. **28** (2004) 679
19. V. X. Jin, S. I. Tan, J. D. Ranford, *Inorg. Chim. Acta* **358** (2005) 677
20. S. Samadhiya, A. Halve, *Orient. J. Chem*. **17** (2001) 119
21. A. A. Jarrahpour, M. Zarei, *Molbank* (2004) M374
22. R. Siddiqui, A. P. Raj, A. K. Saxena, *Synth. React. Inorg. Met.-Org. Chem*. **26** (1996) 1189
23. M. Tumer, M. H. Koksal, M. K. Sener, S. Serin, *Transition Met. Chem*. **24** (1999) 414
24. M. Tumer, M. H. Koksal, M. K. Sener, S. Serin, *Synth. React. Inorg. Met.-Org. Chem*. **26** (1996) 1589
25. G. Wang, J. C. Chang, *Synth. React. Inorg. Met.-Org. Chem*. **24** (1994**)** 1091
26. J. R. Zamian, E. R. Dockal, *Transition Met. Chem*. **21** (1996) 370
27. R. C. Felicio, G. A. da Silva, L. F. Ceridorio, E. R. Dockal, *Synth. React. Inorg. Met.-Org. Chem*. **29** (1999**)** 171
28. E. R. Signorini, G. Dockal, O. G. Castellano, *Polyhedron* **15** (1996) 245
29. B. Bosnich, *J. Am. Chem. Soc*. **90** (1968) 627
30. M. Silverstein, G. C. Bassler, T. C. Morril, *Spectrometric Identification of Organic Compounds*, Wiley, New York, 1991, p. 289
31. S. V. Sheat, T. N. Waters, *J. Inorg. Nucl. Chem.* **26** (1964) 1221
32. D. L. Leggett, *Computational Methods for the Determination of Formation Constants*, Plenum Press, New York, 1985
33. R. C. Holm, *J. Am. Chem. Soc*. **82** (1960) 5632
34. M. Asadi, K. Mohammadi, S. Esmaielzadeh, B. Etemadi, H. Kun Fun, *Polyhedron* **28** (2009) 1409
35. B. Castro, E. Pereiral, L. Gomes, *Inorg. Chim. Acta* **271** (1998) 83
36. M. Asadi, K. Mohammadi, S. Esmaielzadeh, B. Etemadi, H. Kun Fun, *Polyhedron* **362** (2009) 4913
37. M. Asadi, A. H. Sarvestani, M. Abbasi, *J. Chem. Res*. (2007) 56
38. M. Asadi, M. Mohammadikish, K. Mohammadi, *Cent. Eur. J. Chem.* **8** (2010) 291
39. A. H. Sarvestani, S. Mohebbi, *J. Iran. Chem. Soc*. **4** (2007) 215.

Journal of the Serbian Chemical Society
JSCS-info@shd.org.rs • www.shd.org.rs/JSCS
J. Serb. Chem. Soc. 76 (1) 75–83 (2011)
JSCS–4101
UDC 547–304.9+542.9+547.571+547.551+66.094.3.097:615.281
Original scientific paper

Transition metal complexes of 5-bromosalicylidene-4-amino-3--mercapto-1,2,4-triazine-5-one: Synthesis, characterization, catalytic and antibacterial studies

AYALOOR SUBRAMANIAN RAMASUBRAMANIAN, BADEKAI RAMACHANDRA BHAT*, RAMAKRISHNA DILEEP and SANDYA RANI

Department of Chemistry, National Institute of Technology Karnataka, Surathkal, Srinivasnagar – 575025, Karnataka State, India

(Received 12 February, revised 1 June 2010)

Abstract: Transition metal complexes of 5-bromosalicylidene-4-amino-3-mercapto-1,2,4-triazine-5-one with metal precursors, such as Cu(II), Ni(II), Co(II) and Pd(II), were synthesized and characterized by physico–chemical and spectroscopic techniques. All the complexes are of the ML type. Based on analytical, spectral data and magnetic moments, the Co(II) and Ni(II) complexes were assigned octahedral geometries, while the Cu (II) and Pd(II) complexes square planar. A study on the catalytic oxidation of benzyl alcohol, cyclohexanol, cinnamyl alcohol, 2-propanol and 2-methyl-1-propanol was performed with N-methylmorpholine-*N*-oxide (NMO) as co-oxidant. All the complexes and their parent organic moiety were screened for their biological activity on several pathogenic bacteria and were found to possess appreciable bactericidal properties.

Keywords: triazine; Schiff base; catalytic oxidation; antibacterial studies.

INTRODUCTION

Catalytic oxidation of alcohols is an important industrial process due to the wide variety of products synthesized by this route. Many systems have been reported for the oxidation of alcohols, mainly involving catalysts containing transition metals such as bivalent Co,[1], Pd,[2] Ni[3] and Ru.[4] The ability of transition metals to assume a wide range of oxidation states and coordination geometries provides unique opportunities for catalysis. The development of highly efficient transition metals-based catalysts is also driven by their tolerance towards functional groups, their ease of synthesis and their versatility. Schiff bases and their transition metal complexes are still found to be of great interest in inorganic

* Corresponding author. E-mail: chandpoorna@yahoo.com
doi: 10.2298/JSC100212136R

chemistry, although this subject has been studied extensively.[5,6] Schiff bases and their metal complexes show biological activity as antibiotics, antiviral and anti-tumour agents because of their specific structures.[7,8]

Triazole chemistry is becoming more important due to its excellent biological activity. The triazole antifungal drugs include fluconazole, isavuconazole, itraconazole, voriconazole, pramiconazole and posaconazole. The triazole plant protection fungicides include epoxiconazole, triadimenol, propiconazole, metconazole, cyproconazole, tebuconazole, flusilazole and paclobutrazol. Studies have been reported on the synthesis and characterization of metal complexes of Schiff base involving 1,2,4-mercapto triazoles with salicylaldehyde, p-nitrobenzaldehyde, *o*-nitrobenzaldehyde, *p*-toluylaldehyde and cimmamaldehyde.[9–11] Transition metal complexes of polydentate ligands involving five donor atoms have also been reported.[12] These ligands were reported to coordinate through deprotonated oxygen, thio-enolic sulphur and azomethine nitrogen atoms.

In the present study, the synthesis and characterization of transition metal complexes of 5-bromosalicylidene-4-amino-3-mercapto-1,2,4-triazine-5-one (BrSAMT) were undertaken and their applications as catalysts for the oxidation of benzyl alcohol, cyclohexanol, cinnamyl alcohol, 2-propanol and 2-methyl-1--propanol. Their possible anti-bacterial activity was also explored.

EXPERIMENTAL

Methods

The metal content of these complexes were estimated using a Varian AA 55B atomic absorption spectrometer. The infrared spectrum was recorded on an ABB BOMEM FT-IR spectrophotometer. Carbon, hydrogen, nitrogen and sulphur were analyzed using a Thermo Flash EA 1112 series CHN analyzer. The magnetic susceptibilities were determined using a Sherwood Scientific magnetic susceptibility meter (Cambridge, UK). The electronic spectra of the complexes in DMF were recorded on a GBC model UV–Vis spectrophotometer. Thermogravimetric analysis was realised using an SII Exstar 6000 model TGA analyzer. Gas chromatographic analysis was performed on a Shimadzu 2014 model instrument. The ^{1}H-NMR spectra were recorded on a Bruker AV 400 instrument using TMS as the internal standard. The conductivity measurements were performed on an Elico 32 model instrument.

Synthesis of the ligand

The ligand was synthesized in two steps. In the first step, 4-amino-3-mercapto-1,2,4-triazine-5-one was synthesized according to a literature procedure.[13] In the second step, a solution of 0.10 mol of 4-amino-3-mercapto-1,2,4-triazine-5-one in 10 ml of ethanol and 0.10 mol of 5-bromo salicylaldehyde was refluxed for 4 h, cooled, filtered, washed with water, dried and then recrystallized from absolute alcohol. The yellow coloured 5-bromosalicylidene-4-amino-3-mercapto-1,2,4-triazine-5-one (BrSAMT) was dried in a desiccator.

Synthesis of the complexes

To a hot solution of 40 mmol of BrSAMT in 20 ml alcohol, 0.002 mol of the respective transition metal chlorides in water (minimum quantity 2 ml) was added and the mixture refluxed for 2 h and then cooled. The different coloured complexes were filtered, washed with

water, ethanol, diethyl ether and dried in a desiccator. The resultant complexes were brown coloured for the Cu(II) and Co(II) complexes, orange brown for the Pd(II) complex and reddish orange for the Ni(II) complex.

Catalytic oxidation experiments with N-*methyl morpholine*-N-*oxide (NMO)*

To a solution of the required alcohol (0.060–0.12 mL, 1.0 mmol) in dichloromethane (20 mL), NMO (0.35 g, 3.0 mmol) and the required metal-complex (0.01 mmol) were added and the solution was heated under reflux for 2 h. The mixture was then filtered and the filtrate was dried over anhydrous Na_2SO_4. It was then evaporated to dryness and extracted with diethyl ether. The diethyl ether extract was filtered and evaporated to give the corresponding aldehyde.[14,15] The products were identified using gas chromatography by comparing their retention time with those of authentic samples.

Biological tests

The synthesized complexes of BrSAMT were screened for their *in vitro* antibacterial activity against pathogenic strains of gram-negative bacteria, *i.e*., *Escherichia Coli*, *Pseudomonas aeruginosa*, *Salmonella typhi* and *Shigella flexneri* using the plate technique. The bacteria were cultured in previously sterilized Mueller Hinton agar medium in a petri dish. Solutions of the ligand and its complexes in DMF were plated onto the cultured agar medium and incubated for a period of 24 h at 37 °C. Solutions of the ligand and its complexes in DMF were plated on cultured agar medium and incubated for a period of 24 h at 37 °C. The components to be tested were dissolved in DMF to a final concentration of 0.5 and 1% and soaked in filter paper discs of 5 mm diameter and 1 mm thickness. Nicotinic acid was used as reference material. After the incubation period the plates were observed for zones of inhibition (in cm).

RESULTS AND DISCUSSION

Analytic and spectral data

Ligand. Yield: 60 %; Anal. Calcd. for $C_{10}H_6BrN_4O_2S$: C, 36.4; H 2.1; N, 17.0; S 9.7 %. Found: C, 36.5, H, 2.1, N, 17.2, S, 9.7 %. IR (KBr, cm^{-1}): 1690 *s* (–C=O stretching of –CO in the triazole group), 1650 (C=N– stretching of the azomethine group), 1455 (thioamide group). ^{1}H-NMR (200 MHz, DMSO-d_6, δ / / ppm): 11.20 (1H, *s*, –SH), 8.7 (1H, *s*, –CH=N–), 6.24–8.76 (3H, *m*, aromatic, J = 7.8 Hz).

Ni(II) complex. Yield: 60 %; Anal. Calcd. for $C_{10}H_{10}BrClN_4NiO_4S$: C, 26.29; H, 2.15; N, 12.15; S, 7.01 %. Found: C, 26.32, H, 2.15, N, 12.28, S, 7.03 %. IR (KBr, cm^{-1}): 3500, 900 (–OH stretching of H_2O), 1730 *s* (–C=O stretching of –CO in triazole group), 1620 (C=N– stretching of the azomethine group), 1450 (thioamide group), 490 (Ni–O), 440 (Ni–N). ^{1}H-NMR (200 MHz, DMSO-d_6, δ / / ppm): 11.24 (1H, *s*, –SH), 8.5 (1H, *s*, –CH=N–), 6.24–8.76 (3H, *m*, aromatic, J = 7.8 Hz). Magnetic moment, μ_{eff} / μ_B: 2.73.

Co(II) complex. Yield: 60 %; Anal. Calcd. for $C_{10}H_{10}BrClCoN_4O_4S$: C, 26.25; H, 2.20; N, 12.20; S, 7.01 %. Found: C, 26.31, H, 2.21, N, 12.27, S, 7.02 %. IR (KBr, cm^{-1}): 3500, 905 (–OH stretching of H_2O), 1740 *s* (–C=O stretching of –CO in the triazole group), 1610 (C=N– stretching of the azomethine group),

1445 (thioamide group), 495 (Co–O), 445 (Co–N). ^{1}H-NMR (200 MHz, DMSO–d_6, δ / ppm): 11.10 (1H, *s*, –SH), 8.55 (1H, *s*, –CH=N–), 6.24–8.76 (3H, *m*, aromatic, J = 7.8 Hz). Magnetic moment, μ_{eff} / μ_B: 3.72.

Cu(II) complex. Yield: 60 %; Anal. Calcd. for $C_{10}H_6BrClCuN_4O_2S$: C, 28.15; H, 1.36; N, 13.09; S, 7.41 %. Found: C, 28.25, H, 1.42, N, 13.18, S, 7.54 %. IR (KBr, cm^{-1}): 1745 *s* (–C=O stretching of –CO in the triazole group), 1620 (C=N– stretching of the azomethine group), 1452 (thioamide group), 490 (Cu–O), 440 (Cu–N). ^{1}H-NMR (200 MHz, DMSO-d_6, δ / ppm): 11.55 (1H, *s*, –SH), (1H, *s*, –CH=N–), 6.24–8.76 (3H, *m*, aromatic, J = 7.8 Hz). Magnetic moment, μ_{eff} / / μ_B: 1.73.

Pd(II) complex. Yield: 60 %; Anal. Calcd. for $C_{10}H_6BrClCuN_4O_2S$: C, 25.58; H, 1.28; N, 11.75; S, 7.01 %. Found: C, 25.66, H, 1.29, N, 11.97, S, 7.02 %. IR (KBr, cm^{-1}): 1744 *s* (–C=O stretching of –CO in the triazole group), 1615 (C=N– stretching of the azomethine group), 1448 (thioamide group), 491 (Pd–O), 446 (Pd–N). ^{1}H-NMR (200 MHz, DMSO-d_6, δ / ppm): 11.35 (1H, *s*, –SH), 8.45 (1H, *s*, –CH=N–), 6.24–8.76 (3H, *m*, aromatic, J = 7.8 Hz).

Infrared spectra

The ligands showed an infrared band at 2900 cm^{-1}, indicating the absorptions ν(C–H). The ligand also showed the presence of four thioamide bands I, II, III and IV at 1500–1600, 1270, 900, and 800 cm^{-1}, respectively, indicating the presence of the thioamide moiety in the ligand molecule. No systematic shifts of these bands in the complexes were observed. The band at around 1700 cm^{-1}, corresponding to ν(C=O) of the carbonyl group in the ligand, was altered in the complexes. This shows the possibility of carbonyl group participation in the bonding. The bands at 1650 and 1600 cm^{-1} in the ligand and the complexes correspond to ν(C=N) of the azomethine linkage[16] and the shift in frequency to lower wave numbers indicates the coordination of the nitrogen of this group with the metal ions. In the complexes, the band at 1300 cm^{-1}, due to the phenolic group, was shifted to higher wave numbers, indicating the involvement of the phenolic oxygen in the coordination with the metal. The broad band at around 3500 and 890 cm^{-1}, corresponding to ν(O–H) in cases of the Co(II) and Ni(II) complexes indicates the presence of coordinated water molecules in these complexes. The presence of a band at 669 cm^{-1} in the spectrum of the BrSAMT ligand and its complexes, due to C–Br stretching, remained unchanged, indicating that the bromo group was not involved in the bonding.

Electronic spectra

In the case of six coordinated octahedral and pseudo-octahedral Ni(II) complexes, the three spin allowed transitions from $^3A_{2g}$(F) to $^3T_{2g}$(F), $^3T_{1g}$(F) and $^3T_{1g}$(P) generally fall within the regions 7000–13000 cm^{-1}, 11000–20000 cm^{-1}

and 19000–27000 cm^{-1}, respectively. The ratio of the frequencies of the second to the first transitions would be around 1.8.[17] The first transition, corresponding to $^3A_{2g}(F)$ to $^3T_{2g}(F)$ was not recorded in the electronic spectra. For high spin octahedral complexes of Co(II), three transitions are expected in the electronic spectra and they are $^4T_{1g}(F) \rightarrow {}^4T_{2g}(F)$, $^4T_{1g}(F) \rightarrow {}^4A_{2g}$ and $^4T_{1g}(F) \rightarrow {}^4T_{1g}(P)$ in order of increasing energy. The first transition was not recorded but the position was calculated from the second transition. For the complexes of Cu (II), only one transition was observed, assigned to $^2E_{1g}(F) \rightarrow {}^2T_{2g}(F)$.

^{1}H-NMR Spectra

The ^{1}H-NMR spectra of the free ligand and the complexes were recorded in DMSO. The ligand exhibit a singlet at 11.24. This signal in the spectra of the complexes remained as such, suggesting the non-participation of sulphur in the coordination. The singlet at 8.7 ppm in the ligand due to the azomethine proton was shifted to 8.5 ppm in the complexes. In the spectrum of the ligand, multiplets due to aromatic protons appeared in the range δ 6.24–8.76 ppm. These resonance signals remain unchanged in the spectra of the complexes, suggesting their non-involvement in bonding. The peak corresponding to –OH at 10.8 ppm in the free ligand was not observed in the spectra of the complexes. This clearly shows deprotonation of –OH during complex formation.

Magnetic susceptibility

The magnetic susceptibility results indicate that the complexes of Co(II), Ni(II) and Cu(II) are paramagnetic, while the Pd(II) complex is diamagnetic in nature. Ni(II) being a d^8 in an octahedral field contains two unpaired electrons and hence shows paramagnetism. The value of 2.73 μ_B is close to the theoretical value of 2.83 for octahedral Ni(II) complexes. Co(II) is a d^7 system, thus its complexes show paramagnetism equivalent to three unpaired electrons in octahedral geometry. Since the orbital contribution of tetrahedral Co(II) is much less than that of octahedral complexes, tetrahedral Co(II) complexes generally have lower values of magnetic moments, as compared to that of octahedral complexes. This high degree of orbital contribution for octahedral complexes is due to the three--fold degeneracy of the $^4T_{1g}$ ground state. The observed value of 3.72 μ_B is close to the theoretically calculated values of 3.83 μ_B for octahedral Co(II) complexes. Cu(II), being a d^9 system, shows paramagnetism in square planar complexes. The value of 1.74 μ_B is close to theoretical value of 1.73 BM for Cu(II) square planar complexes.

Molar conductance

The results of molar conductance, which were less than 30 μS m^2 mol^{-1} in DMF solution, indicate that all the formed complexes were non-electrolytes, electrically neutral and non-ionic in nature.[18]

Thermogravimetric analysis

It was observed that the complexes of Ni(II) and Co(II) show a loss in weight between 150–200 °C, indicating that crystal water molecules and coordinated water molecules are present in the complexes. The TG curves in the 200––310 °C range suggest that the loss in weight for all complexes corresponds to decomposition of the ligand. In the range above 310 °C, the loss in weight corresponded to the remaining organic ligand molecules. In all cases, the remaining residues were the corresponding metal oxide. These results are in accordance with the composition of the complexes.

Catalytic studies

The catalytic activity of the newly synthesized complexes was examined in the presence of NMO as a co-oxidant for the oxidation of primary and secondary alcohols in CH_2Cl_2. The results are presented in Table I. The reaction was initially conducted using molecular oxygen. Results of the present investigation suggest that the complexes are able to react more efficiently with NMO than with molecular oxygen, as indicated by the low product yield when molecular oxygen was employed as the co-oxidant. This is in accordance with a previous observation[19]. *N*-Methylmorpholine and water were the by-products during the course of the reactions. An important characteristic of the transition metal–NMO system

TABLE I. Oxidation of alcohols by the synthesised metal(II) complexes

Complex	Substrate	Product	Yield[a], %	*TON*[b]
Ni(II) BrSAMT	Benzyl alcohol	Benzaldehyde	85	87
	Cyclohexanol	Cyclohexanone	80	82
	Cinnamyl alcohol	Cinnamaldehyde	88	89
	2-Propanol	Acetone	73	75
	2-Methyl-1-propanol	2-Methylpropanal	76	77
Co(II) BrSAMT	Benzyl alcohol	Benzaldehyde	87	89
	Cyclohexanol	Cyclohexanone	92	93
	Cinnamyl alcohol	Cinnamaldehyde	89	90
	2-Propanol	Acetone	76	78
	2-Methyl-1-propanol	2-Methylpropanal	72	74
Pd(II) BrSAMT	Benzyl alcohol	Benzaldehyde	90	92
	Cyclohexanol	Cyclohexanone	91	92
	Cinnamyl alcohol	Cinnamaldehyde	85	87
	2-Propanol	Acetone	74	76
	2-Methyl-1-propanol	2-Methylpropanal	79	81
Cu(II) BrSAMT	Benzyl alcohol	Benzaldehyde	86	88
	Cyclohexanol	Cyclohexanone	88	89
	Cinnamyl alcohol	Cinnamaldehyde	93	94
	2-Propanol	Acetone	77	78
	2-Methyl-1-propanol	2-Methylpropanal	78	79

[a]Yield based on substrate; [b]turn-over number, moles of product per mole of catalyst

results in the selective oxidation at the alcoholic group of the unsaturated cinnamyl alcohol to cinnamaldehyde, while the double bond remained unaffected. Saturated aliphatic alcohols, such as 2-propanol and 2-methyl-1-propanol, were converted to the corresponding aldehydes with high conversion.

Biological tests

The Cu(II), Co(II) and Ni(II) complexes of BrSAMT showed a greater zone of inhibition compared to the uncomplexed Schiff base, indicating that these complexes possess more antibacterial activity against pathogenic strains of gram negative bacteria, such as *E. Coli*, *P. aeruginosa*, *S. typhi* and *S. flexneri*.[20,21] The results are given in Table II.

TABLE II. Antibacterial activity of the synthesised metal(II) complexes (Zone inhibition in cm)

Compound	*S. Typhi*		*P. aeruginosa*		*E. Coli*		*S. Flexneri*	
	Amount, µg							
	30	50	30	50	30	50	30	50
Ligand	–	0.9	0.8	1.2	0.7	1.2	0.7	0.9
Ni(II) BrSAMT	1.3	1.7	1.4	1.9	1.3	1.8	0.9	1.4
Co(II) BrSAMT	1.0	1.2	0.8	1.1	0.9	1.4	0.8	1.2
Cu(II) BrSAMT	1.2	1.6	1.3	1.8	0.9	1.1	0.9	1.4
Pd(II) BrSAMT	–	–	–	–	–	–	–	–
Nicotinic acid	1.8	2.0	2.4	2.6	2.4	2.7	1.3	1.8
DMF	–	–	–	–	–	–	–	–

CONCLUSIONS

Based on the above characterization data and keeping in mind the preferred geometries, octahedral structures are proposed for the Co(II) and Ni(II) complexes (Fig. 1) and square planar geometries for the Cu(II) and Pd(II) complexes (Fig. 2). The newly synthesized complexes are good catalysts for the oxidation of alcohols to the corresponding carbonyl compounds. The catalytic efficiency was high when NMO was employed as the co-oxidant. The Cu(II), Ni(II) and Co(II) complexes exhibited antibacterial activity against gram-negative bacteria, such as *E. Coli*, *P. aeruginosa*, *S. typhi* and *S. flexneri.* Further studies on the catalytic and biological applications are in progress.

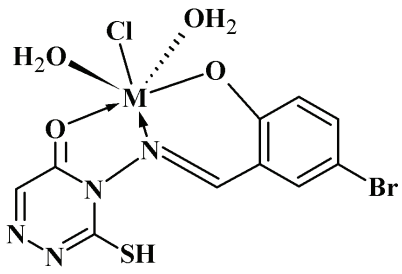

Fig. 1. Proposed structure for the Ni(II) and Co(II) complexes.

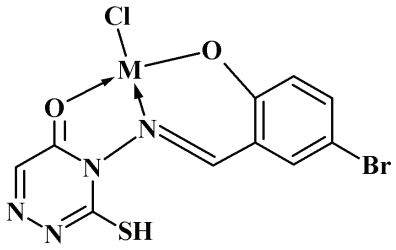

Fig. 2. Proposed structure for the Cu(II) and Pd(II) complexes.

Acknowledgements. The authors are grateful to the Indian Institute of Science, Bangalore, for the NMR analysis.

И З В О Д

КОМПЛЕКСИ ПРЕЛАЗНИХ МЕТАЛА СА 5-БРОМОСАЛИЦИЛИДЕН-4-АМИНО-3--МЕРКАПТО-1,2,4-ТРИАЗИН-5-ОН ЛИГАНДОМ: СИНТЕЗА, КАРАКТЕРИЗАЦИЈА, КАТАЛИТИЧКА И АНТИБАКТЕРИЈСКА ИСПИТИВАЊА

A.S. RAMASUBRAMANIAN, BADEKAI RAMACHANDRA BHAT, RAMAKRISHNA DILEEP и SANDYA RANI

Department of Chemistry, National Institute of Technology Karnataka, Surathkal, Srinivasnagar – 575025, Karnataka State, India

Описана је синтеза, физичко-хемијска и спектроскопска карактеризација комплекса Cu(II), Ni(II), Co(II) и Pd(II) са 5-бромосалицилиден-4-амино-3-меркапто-1,2,4-тризин-5-он лигандом. Нађено је да су сви добивени комплекси ML-типа. На основу аналитичких података, IR спектросопије и магнетних мерења закључено је да комплекси Co(II) и Ni(II) имају октаедарску, а комплекси Cu (II) и Pd(II) квадратно-планарне геометрију. Помоћу *N*-метилформолин-*N*-оксида и молекулског кисеоника као оксиданаса, у присуству наведених комплекса као каталитичких агенаса, испитивана је оксидација бензил-алкохола, циклохексанола, цинамил алкохола, 2-пропанола и изобутил-алкохола. Нађено је да неки од добијених комплекса показују антибактеријске особине.

(Примљено 12. фебруара, ревидирано 1. јуна 2010)

REFERENCES

1. S. Das, T. Punniyamurthy, *Tetrahedron Lett.* **44** (2003) 6033
2. T. L. Stuchinskaya, I. V. Kozhevnikov, *Catal. Commun.* **4** (2003) 417
3. K. O. Xavier, J. Chacko, K. K. Mohamed Yusuff, *J. Mol. Catal. A* **178** (2002) 275
4. S. A. Chimatadar, T. Basavaraj, K. A Thabaj, S. T. Nandibewoor, *J. Mol. Catal. A* **267** (2007) 65
5. M. Sekerci, C. Alkan, A. Cukurovali, S. Saydam, in *Proceedings of XIII National Chemistry Congress*, Samsun, Turkey, 1999, p. 182
6. M. Sekerci, in *Proceedings of XIV National Chemistry Congress*, Diyarbakir, Turkey, 2000, p. 414
7. D. R. Williams, *Chem. Rev*. **72** (1972) 203
8. H.-J. Sun, X.-Y. Li, X.-G. Cui, D.-X. Liu, G. Xuexiao, H. Xuebao, *Chem. Abstr*. **13** (1992) 1168
9. J. Singh, N. K. Singh, *Proc. Indian Acad. Sci. (Chem. Sci.)* **93** (1984) 125
10. S. A. Patil, B. M. Badiger, S. M. Kudari, V. H. Kulkarn, *Trans. Met. Chem.* **8** (1983) 238

11. K. S. Dhaka, J. Mohan, V. K. Chadha, H. K. Pujari, *Indian J. Chem. A* **12** (1974) 288
12. R. G. Pearson, *J. Am. Chem. Soc.* **85 (**1963) 3533
13. B. Ramachandra, B. Narayana, *Indian J. Chem. A* **38** (1999) 1297
14. A. I. Vogel, *Text book of practical organic chemistry*, 5th ed., Longman, London, 1989
15. C. Jayabalakrishnan, R. Karvembu, K. Natarajan, *Trans. Met. Chem.* **27** (2002) 790
16. V. K. Sharma, A. Srivastava, *Indian J. Chem. A* **46** (2007) 1963
17. J. D. Lee, *Concise Inorganic Chemistry*, 5th ed., Wiley, New York, 2007
18. R.-H. Hui, P. Zhou, Z.-L. You. *Ind. J. Chem. A* **48** (2009) 663
19. P. Paraskevopoulou, N. Psaroudakis, S. Koinis, P. Stavropoulos, K. Mertis, *J. Mol. Catal. A* **240** (2005) 27
20. S. A. Sallam, *Trans. Met. Chem*. **30** (2005) 341
21. Y.-H. Li, Z.-Y. Yang, B.-D. Wang, *Trans. Met. Chem*. **31** (2006) 598.

Journal of the Serbian Chemical Society
JSCS-info@shd.org.rs • www.shd.org.rs/JSCS
J. Serb. Chem. Soc. 76 (1) 85–99 (2011)
JSCS–4102
UDC 547.575'461.5:66.097.8+
519.711+54–124:57–188
Original scientific paper

MTD–CoMSIA modelling of HMG-CoA reductase inhibitors

DANIEL M. DUDA-SEIMAN[1], SPERANȚA AVRAM[2], SILVIA MANCAȘ[1], VALENTIN CAREJA[3], CORINA DUDA-SEIMAN[4]*, MIHAI V. PUTZ[4] and DAN CIUBOTARIU[5]

[1]Department of Medical Ambulatory, Medical Emergencies, University of Medicine and Pharmacy "Victor Babes", Timisoara, [2]Department of Physiology and Biophysics, University of Bucharest, Faculty of Biology, Bucharest, [3]Institute of Chemistry "Coriolan Drăgulescu" of the Romanian Academy, Timisoara, [4]Department of Chemistry, University of West Timisoara, Faculty of Chemistry-Biology-Geography, Timişoara and [5]Faculty of Pharmacy, University of Medicine and Pharmacy "Victor Babeş", Timisoara, Timisoara, Romania

(Received 1 June, revised 23 August 2010)

Abstract: The 3D quantitative structure–activity relationship for a series of hydroxymethylglutaryl-CoA (HMG-CoA) reductase inhibitors based on the pyrrolylethyl-tetrahydropyranone scaffold was examined using the Minimal Topological Difference (MTD) method and comparative molecular similarity index analysis (CoMSIA). The studied compounds were of the tetrahydro-4-hydroxy--6-[2-(1*H*-pyrrol-1-yl)ethyl]-2*H*-pyran-2-one type. In clinical practice, HMG--CoA reductase inhibitors are usually referred to by the generic name statins. The analysis performed using the MTD method showed that voluminous substituents produce a significant biological activity (R^2_{CV} = 0.677 > 0.5; *SEECV* = = 0.319), while the CoMSIA method added useful information regarding the influence of the steric, electrostatic, hydrophobic, hydrogen bond donor, and acceptor properties on biological activity (R^2_{CV} = 0.60; r^2 = 0.98).

Keywords: statins; molecular modelling; correlations; 3D-quantitative structure–biological activity.

INTRODUCTION

Among cholesterol-lowering drugs, statins (hydroxymethylglutaryl-CoA reductase inhibitors) manage effectively artherogenic dyslipidemia,[1] with immediate and long-term consequences on cardiovascular morbidity and mortality.[2]

Statins inhibit competitively the enzyme hydroxymethylglutaryl-CoA reductase (HMG-CoA-reductase)[3] and they play a fundamental role in the modern concept of artherothrombotic cardiovascular disease prevention.[4] Statins have realized a significant reduction of global cardiovascular risk, as well as of cardio-

* Corresponding author. E-mail: cori_mam@yahoo.com
doi: 10.2298/JSC100601019D

vascular mortality.[2] The absolute vascular benefit of statins is obtained when the level of low-density-lipoproteins (LDL – "bad cholesterol") is reduced below 70 mg dL^{-1}.[5,6] Thus, in the ARBITER trial, one-year aggressive statin therapy led to a 48.5 % reduction in LDL-cholesterol to 76 mg dL^{-1}, being associated with a significant regression of the carotid intima-medial thickness (p = 0.03).[5,7] Achieving the above mentioned LDL goals with aggressive statin therapies, HDL-cholesterol levels improved significantly and coronary arteriosclerosis may regress.[8]

The HMG-CoA-reductase inhibition has a double action mechanism: decreasing hepatic cholesterol synthesis and increasing LDL catabolism.[9]

Besides correcting the lipid fractions, statins show other beneficial effects on the arterial wall: they modulate the endothelial function and they have anti-inflammatory and anti-proliferative effects, thereby stabilizing the atheroma plaque and preventing thrombogenesis.[10] Due to these now well-established effects of statins, it has been suggested that they could be a choice of treatment in a large variety of diseases, including dementia and autoimmune disorders.[11]

Hydroxymethylglutaryl-CoA reductase inhibitors were well established as the cornerstone of pharmacoprevention of atherosclerotic and atherothrombotic arterial disease by means of primary and secondary cardiovascular prevention trials.[12]

Molecular modelling requires not only good algorithms but also a close integration with experiment and a better understanding of the underlying physical and biological principals involved.[13] Thus, molecular modelling studies would allow a more profound documentation of ligand (L)–receptor (R) interactions and a better specification of optimal structural requirements. The present study investigates the biologic activity of HMG-CoA reductase under the interaction with a representative series of statins by employing the 3D-minimal topological difference (3D-QSAR MTD)[14] and comparative molecular similarity indices analysis (CoMSIA) methods.[15]

Background methods

The MTD method. The MTD method aims to provide a description of the molecular stereochemistry (of both receptor and effectors, *i.e.*, drug molecules) by indicating the presence or absence of atoms from the considered M_i molecule, i = 1,...,N, in the vertices of the hypermolecule, H (which describes the receptor).[14,16,17] The hypermolecule is obtained by an approximately atom-by-atom superposition of all M_i molecules, neglecting the hydrogen atoms. The hypermolecule H can be considered as a topological network in which the vertices correspond to atoms, while the edges are derived from the corresponding chemical bonds. If molecule i occupies vertex j, this may be accounted for by x_{ij} = 1,

while otherwise $x_{ij} = 0$. Then, the minimal steric difference, MTD_i, of molecule i with respect to the receptor is calculated according to the formula:[14]

$$MTD_i = s + \sum_j \varepsilon_j x_{ij} \quad (1)$$

with $\varepsilon_j = -1$, 0 or +1 for vertices attributed to the receptor cavity (beneficial), to the exterior (irrelevant) and to the receptor walls (detrimental), respectively; s is the total number of cavity vertices. Thus, the degree of steric misfit for the molecule M_i with respect to the receptor, *i.e.*, MTD_i, is defined as the sum of the number of unoccupied cavity vertices of H and the number of occupied wall vertices of H.

The attributions of $\varepsilon_j = -1$, 0 or +1 to the vertices j are performed according to an optimization procedure (see below). One starts from an initial attribution of j vertices, ε_j^0, and changes these ε_j settings towards an increase in the correlation coefficient, r^2, by measuring the degree of residues minimization for a predicted equation of the type:

$$A_i = \alpha - \beta MTD_i \quad (2)$$

The resulting picture of H (meaning cavity, wall and irrelevant zone) obtained by the optimization procedure constitutes a hypothetical predicted steric receptor map.

The CoMSIA method. The CoMSIA method was developed to improve the limitations of the steric and electrostatic fields in comparative molecular field analysis (CoMFA).[15] Being an extension of the CoMFA approach, the CoMSIA method incorporates five different property fields: steric, electrostatic, hydrophobic, and hydrogen bond donor and acceptor properties. In CoMSIA, the screening interactions between the inhibitors and a probe atom having a radius of 1 Å, charge of +1 and hydrophobicity of +1 are considered. Using the CoMSIA method, similarly to the CoMFA method, the aim is to divide the contribution of the steric, electrostatic, hydrophobic, and hydrogen bond donor and acceptor properties and to evaluate these contributions with respect to the biological activity. This indicates which factors have the largest influence on the receptor binding affinities.[15,18]

The aim of the CoMSIA method employed here is to use predictive 3D QSAR models in order to understand the enzyme inhibitor interaction at the active site of HMG-CoA reductase and, in particular, to pinpoint which structural features are responsible for its selectivity. Future work based on the models developed here will therefore allow the design of selective inhibitors of HMG-CoA reductase with superior clinical profiles for the treatment of cardiovascular diseases.

The CoMSIA method was employed to evaluate various descriptors in the context of inhibition of HMG-CoA reductase, such as the electrostatic, steric,

hydrophobic and donor effects. As opposed to MTD (and other QSAR methods), the CoMSIA method enables the determination of the individual contribution of each descriptor to the biological activity of HMG-CoA reductase inhibitors.

COMPUTATIONAL DETAILS

The general structure of the studied series of hydroxymethylglutaryl-CoA reductase inhibitors is shown in Fig. 1.

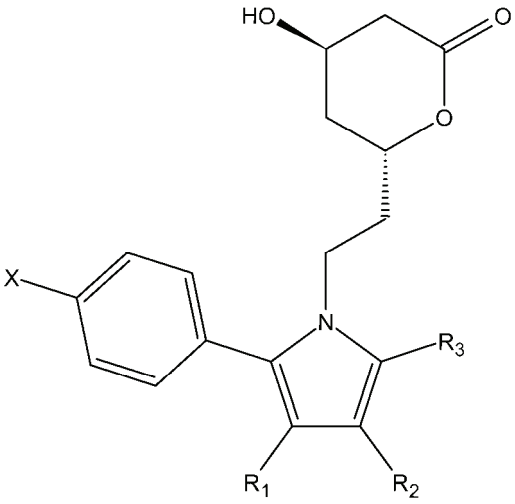

Fig 1. General structure of the statins.

The statins inhibitory activity data were selected considering the criteria of low values for the biological activity, IC_{50}, and through the existence of a high number of different substituent groups (*e.g.*, phenyl, CO_2CH_3, 2-pyridyl, 3-pyridyl, methyl, *etc*.).[19]

HMG-CoA reductase was expressed using the common logarithm, log ($1/IC_{50}$), for the inverse of experimental concentration of a compound leading to 50 % inhibition (IC_{50}), see Table I.

Note that the absolute *R*/*S* configurations for the compounds listed in Table I were not considered for the MTD calculations.

The local minimum potential energy was determined within Polack-Ribiere conjugate--gradient method with a convergence of the total root-mean-square (*RMS*) gradient as 0.01 kcal $mol^{-1} \cdot Å^{-1}$. The method allows geometry optimization (energy minimization) through finding the Cartesian coordinates $\mathbf{r}_i$ of a molecular structure that represent the potential energy minimum, $\partial V / \partial \mathbf{r}_i = 0$, *i.e.*, when the interatomic forces are minimum. This is searched by cycles with default conjugate gradient directions having the *RMS* of the current configuration of atoms that is close to zero on local minimums (see above); the geometry optimization results in a new structure at a minimum for which the atomic coordinates and energy can be examined. After energy minimization, the Gasteiger–Marsili partial charges[15,20,21] were used for the CoMSIA methodology.

The steric field, the electrostatic field energies, as well as the hydrophobic and donor characters of each inhibitor were calculated at the intersection points of a regularly spaced grid (2Å) in a grid box surrounding the molecules. Sybyl/CoMSIA software was used to

calculate the electrostatic and steric potential functions within the Tripos force field,[15] while using an sp^3 carbon atom with a +1 charge as the probe atom.

TABLE I. The series of tetrahydro-4-hydroxy-6-[2-(1*H*-pyrrol-1-yl)ethyl]-2*H*-pyran-2-one molecules with the experimental 50 % inhibition concentrations, IC_{50}, on the HMG-CoA reductase together with the employed $A_{observed} = -\log (IC_{50} / \mu mol\ dm^{-3}) = 6 - \log (IC_{50} / mol\ dm^{-3})$ activity in the actual study[19]

Molecular labels[a]	Substituents				IC_{50} μmol dm^{-3}	A_{obs}
	X	R_1	R_2	R_3		
1	F	H	H	*i*-Pr	0.230	6.638
3a	H	Ph	CO_2Et	CH_3	4.000	5.398
3b	H	Ph	CO_2Et	Et	0.890	6.051
3c	H	Ph	CO_2Et	*i*-Pr	0.170	6.77
3d	F	CO_2CH_3	CO_2CH_3	*i*-Pr	0.180	6.745
3e	F	CO_2Et	CO_2Et	*i*-Pr	0.350	6.456
3f	F	CO_2Et	Ph	*i*-Pr	0.050	7.301
3g	F	Ph	CO_2Et	*i*-Pr	0.200	6.699
3h	F	Ph	CO_2CH_2Ph	*i*-Pr	0.040	7.398
3i	F	Ph	CONHPh	*i*-Pr	0.025	7.602
3j	F	4-CN-Ph	CO_2Et	*i*-Pr	0.280	6.553
3k	F	CH_3	CH_3	*i*-Pr	0.140	6.854
3l	F	Ph	H	*i*-Pr	0.347	6.46
3m	F	2-pyridyl	H	*i*-Pr	0.046	7.337
3n	F	3-pyridyl	H	*i*-Pr	0.071	7.149
3o	F	4-pyridyl	H	*i*-Pr	0.310	6.509
3p	F	H	Ph	*i*-Pr	0.120	6.921
30a	F	Cl	Cl	*i*-Pr	0.028	7.553
30b	F	Br	Br	*i*-Pr	0.028	7.553
30c	F	$COCF_3$	H	*i*-Pr	0.800	6.097
33	F	Ph	CONHPh	*i*-Pr	0.007	8.155

[a]nomenclature from ref. 19

The geometry of the statin molecules under study was optimized using molecular mechanics and quantum chemistry methods. The structures obtained by minimizing the internal energy with the aid of the MM+ force field were used as input data for the program AM1 (Austin Model 1).[13] An energy cut-off of 30 kcal mol^{-1} was used for both electrostatic and steric contributions. The relatively high rigidity of the statins structure justified the molecular construction in bi-dimensional space (2D) using the classic formulas, where the optimized structures **1** to **33** were overlain with the HyperChem programme package, using molecular mechanics techniques of the MTD algorithm in the superposition process for designing the hypermolecule H.

The hydrogen atoms were not considered and common vertices of the 3D molecular graphs in Fig. 2b were specified in the parent structure of the hypermolecule (numbered vertices).

In the superposition process, those conformations from the minimal step interval +1 kcal assuring a maximal coverage, *i.e.*, a minimal number of considered (numbered) vertices, were considered.

Regression analysis was performed by the Partial Least Squares (PLS) algorithm within Sybyl 7.2. The cross-validation procedure was also used in order to assess the reliability of the

obtained results. This allows for the separation of steric factors (measured by MTD_i values) from the others, such as hydrophobic, electrical, *etc*., which possibly control the biological response. The leave-one-out cross-validation method using the SAMPLS (a program created by Brucle Bush at DuPont which vastly accelerates cross-validation calculations for PLS analyses involving COMFA, COMSIA fields) was used.[22] The optimal number of components for the final 3D-QSAR equation was chosen based on the highest q_2 (cross-validated r^2) value.[16] Field points with a standard deviation below 2.0 were dropped from the PLS calculation. The statistical results q_2 (cross-validated r^2),[23,24] fitted correlation coefficient r^2, Fisher test (F), SEE (standard error of estimate)[23,25] and the electrostatic, steric, hydrophobic and donor contributions[15,25] were calculated as implemented in Sybyl 7.2.

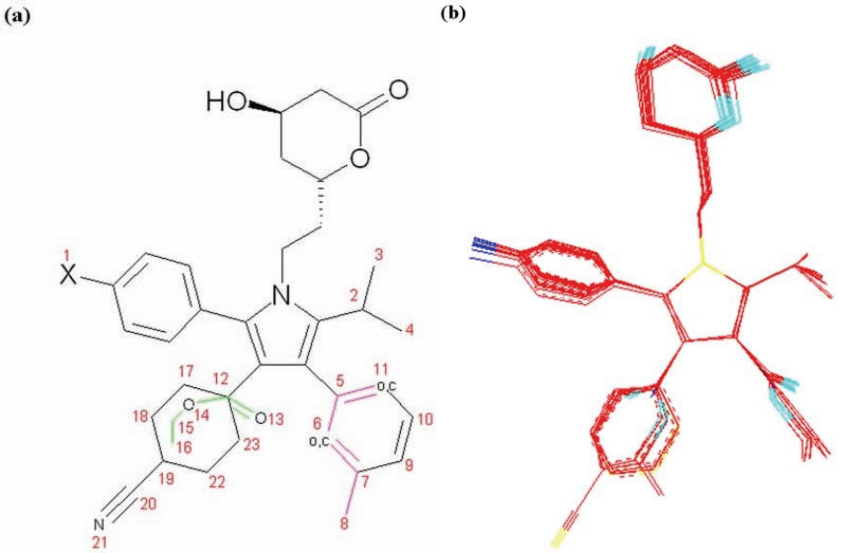

Fig. 2. a) 2D-Hypermolecule for the superimposed statins of Table I, excepting **3h**, (±)-**3i**, **30c**, (+)-**33** and (–)-**33** molecules, with the marked vertices. The green lines indicate a carboxyl or ester group which in space is located in a perpendicular plane to the benzene hexagon plane, while with pink lines, the same group type partially superposed (on vertices 5, 6, 7, 11) upon the benzene hexagon plane is indicated. The molecules with higher flexibility (**3a**, **3b**, **3d** and **3e** of Table I) had a position outside the benzene plane and could introduce supplementary vertices. However, they were partly "laid down" upon benzene and after the rotations, they become the conformers **3a70**, **3b70**, **3d70** and **3e70** (see Table II); consequently, the number of vertices decreased and the hypermolecule was realized. A similar procedure could not be applied to the molecules in the green zone because of steric misfit and of increased rotation impediments. b) The same hypermolecule as in a) but as a 3D-representation.

RESULTS AND DISCUSSION

The starting map S^0 for the MTD optimization procedure,[17] which was obtained by an inspection of vertices found preferentially in molecules with high and respectively low activity for all the compounds given in Table I, looks like:

$$S^0 = \begin{cases} -1: 1,2,3,4,5,12 \\ 0: 9,10,13,14,15,16,20,21 \\ +1: 6,7,8,11,17,18,19,22,23 \end{cases} \quad (3)$$

It is based on the 2D-representation of the standard benchmark molecule **3a** in Table I.

In MTD, the starting map S^0 is automatically chosen using the interquartile interval. The structures were sorted by their inhibitory potency in parallel with descending activity, given in Table I: occupied vertices in all (or in almost all) the most active molecules (usually the first quarter) are considered in the cavity (–1), and those in the last quarter (molecules with the weakest activity) are considered in the wall (+1). The others, in the middle of the series, are irrelevant (0). Note that the S^0 coefficients were set at the beginning according to the recorded activity (the most/least influential), while the S^* coefficients paralleling the cross-validation process are automatically delivered.

The studied series of statins shows an increased conformational degree of liberty. Thus, initially, the obtained hypermolecule contained the superposition of all 21 molecules in the series; some of them introduced in a disadvantageous way many more supplementary vertices. These facts imposed the removal of four molecules from the studied series, namely **3h**, **3i**, **30c** and **33**.

In this way, the obtained results are based on a statins series containing the remaining 17 compounds; from them four did not superpose well, namely the molecules **3a**, **3b**, **3d** and **3e** in Table I, see Fig. 2a.

However, on closer inspection, it was observed that some bonds in the mentioned molecules, due to their high conformational flexibility, could undergo some rotations. Hence they may be forced to better superimpose on others when appropriate torsions are applied; actually, referring to just one valence angle, which was changed by about 21–34° in each molecule the energy required in the torsion process was computed, see Table II.

TABLE II. The four molecules of Table I for which smooth low energy torsion were performed in order to overlap with the rest of the minimal energy conformations of molecules in the hypermolecule of Fig. 2

Molecule	Angle, °	Torsion, °	Heat of formation, kcal/mol	Energy difference, kcal/mol
3a	36.18	33.82	–6674.52	0.96
3a70	70	–	–6673.56	–
3b	35.79	34.21	–6955.2	0.86
3b70	70	–	–6954.34	–
3d	42.2	27.8	–6403.09	0.73
3d70	70	–	–6402.36	–
3e	48.71	21.29	–6965.08	0.77
3e70	70	–	–6964.31	–

If the resulting torsion energy were appreciable, say over 1.0 kcal mol^{-1}, the respective molecule must be excluded from the computation series, since it would represent a departed conformation from the congeneric series in focus. Accordingly, the results in Table II clearly indicate that the above-mentioned molecules with high conformational flexibility may be superposed upon the others when slightly rotated. In this way, the 3D-hypermolecule of Fig. 2b was built.

The optimized 3D structures were used for overlapping. From this point of view, the methodology of the MTD method may be considered as 2.5D. Such a superposition procedure is the basis for the description of molecular stereochemistry in the MTD method. Equivalent atoms with inter-distances less than 0.5 Å are considered to occupy the same vertex; the inter-distance 0.5 Å limit was justified by an analysis of the dependence of the Van der Waals interaction energies on the interatomic distances.[17]

Vertices occupancy x_{ij} (the junctions) of each molecule in the hypermolecule H of Fig. 2a, together with resulting molecular MTD parameters, are provided in Table III.

TABLE III. Vertices occupancy x_{ij} (junctions), together with the MTD parameters computed with Eq. (1), MTD-predicted activities, MTD residual values, with respect to those observed from Table I, for all 17 molecules of the hypermolecule H of Fig. 2

Molecule	Vertex																							*MTD*	A_{MTD}	A_{obs}–A_{MTD}
	01	02	03	04	05	06	07	08	09	10	11	12	13	14	15	16	17	18	19	20	21	22	23			
1	1	1	1	1	0	0	0	0	0	0	0	0	0	0	0	0	0	0	0	0	0	0	0	8	6.648	–0.0102
3a	0	1	0	0	1	1	1	1	0	0	1	1	0	0	0	0	1	1	1	0	0	1	1	11	5.691	–0.2942
3b	0	1	0	1	1	1	1	1	0	0	1	1	0	0	0	0	1	1	1	0	0	1	1	10	6.01	0.0398
3c	0	1	1	1	1	1	1	1	0	0	1	1	0	0	0	0	1	1	1	0	0	1	1	9	6.329	0.4398
3d	1	1	1	1	1	1	1	0	0	0	1	1	1	1	1	0	0	0	0	0	0	0	0	8	6.648	0.0958
3e	1	1	1	1	1	1	1	1	0	0	1	1	1	1	1	1	0	0	0	0	0	0	0	9	6.329	0.1258
3f	1	1	1	1	1	1	1	0	1	1	1	1	1	1	1	1	0	0	0	0	0	0	0	6	7.286	0.0148
3g	1	1	1	1	1	1	1	1	0	0	1	1	0	0	0	0	1	1	1	0	0	1	0	8	6.648	0.04982
3j	1	1	1	1	1	1	1	1	0	0	1	1	0	0	0	0	1	1	1	1	1	1	1	8	6.648	–0.0962
3k	1	1	1	1	1	0	0	0	0	0	0	1	0	0	0	0	0	0	0	0	0	0	0	6	7.286	–0.4332
3l	1	1	1	1	0	0	0	0	0	0	0	1	0	0	0	0	1	1	1	0	0	1	1	7	6.967	–0.5082
3m	1	1	1	1	0	0	0	0	0	0	0	1	0	0	0	0	1	1	1	0	0	1	1	7	6.967	0.3698
3n	1	1	1	1	0	0	0	0	0	0	0	1	0	0	0	0	1	1	1	0	0	1	1	7	6.967	0.1808
3o	1	1	1	1	0	0	0	0	0	0	0	1	0	0	0	0	1	1	1	0	0	1	1	7	6.967	–0.4592
3p	1	1	1	1	1	1	1	0	1	1	1	0	0	0	0	0	0	0	0	0	0	0	0	7	6.967	–0.0472
30a	1	1	1	1	1	0	0	0	0	0	0	1	0	0	0	0	0	0	0	0	0	0	0	6	7.286	0.2658
30b	1	1	1	1	1	0	0	0	0	0	0	1	0	0	0	0	0	0	0	0	0	0	0	6	7.286	0.2658

As such, the MTD method reveals the structural requirements necessary to have a significant biological activity[26,27] as the hypothetically hypermolecule H of Fig. 2 is predicted. Through conformational analysis calculations, the MTD

method prescribes that the optimized map at the receptor level should maximally fit with the statins ligand map:

$$S^* = \begin{cases} -1: 3,4,5,9,10,12,17,18,20 \\ 0: 1,6,13,14,15,16,19,21 \\ +1: 2,7,8,11,22,23 \end{cases} \quad (4)$$

whereas the predicted activity correlation equation unfolds as:

$$A_i = 9.2 - 0.319 MTD_i,\ i = 1,...,N = 17 \quad (5)$$

with the statistical factors: $r = 0.853$, $r^2 = 0.728$, $EV = r_{adj}^2 = 0.70984$, $PRESS = 1.288$, $SEE = 0.293$ and $F = 40.142$, as the correlation, squared correlation, explained variance (or adjusted correlation), prediction sum of squares, standard error of estimate and the Fisher test, respectively.

The values given in Table III qualify the actual MTD approach among acceptable 3D-QSAR models since both the observed and predicted values provide the same mean value of 6.761, while the mean of the residual activities goes to zero. Moreover, aiming for the internal validation procedure, the leave-half--out procedure (*i.e.*, splitting the original set of data into even and odd sets and considering, alternatively, one as the observed data and computing the remaining data leading to the final cross-validation scores) was undertaken, leading to the results:

$$PRESS_{CV} = \sum_{i=1}^{N} \left(A_i^{obs} - A_i^{MTD\text{-}CV} \right)^2 = 1.529$$

$$R_{CV}^2 = 1 - \frac{PRESS_{CV}}{\sum_{i=1}^{N} \left(A_i^{obs} - \overline{A^{obs}} \right)^2} = 0.677 > 0.5 \quad (6)$$

$$SEE_{CV} = \sqrt{\frac{PRESS_{CV}}{N-2}} = 0.319 \cong \frac{1}{9}\left(A_{obs}^{max} - A_{obs}^{min} \right)$$

suggesting the present MTD analysis is of significant value since the R_{CV}^2 value lies above the threshold of 0.5 for the statistical limit of cross-validation, while the cross-validation standard error of estimate behaves like the 9th part of all the observed activity range of the HMG-CoA reductase inhibitors in Table I.

However, it may be argued that the MTD regression seems to be over-determined: while each vertex in H represents a degree of freedom, there are 23 vertices considered against only 17 correlated molecules. In this regards, it is worth noting that since the MTD method is based on the non-null occupancies of the vertices of the hypermolecule, the maximum cardinal of occupancy among the series does not exceed the number of molecules in the series, see Table I and Eq. (4), from which it appears that the non-zero attributions (ε_j) do not exceed 15

out of 23 possibilities, revealing in fact only 15 degrees of freedom for 17 molecules, thereby confirming that the present approach is well-defined.

For completion of the 3D-activity analysis, the inhibitors listed in Table I were further used to design a CoMSIA model, the results of which are presented in Table IV. This time, the statistical significance of the model was assessed throughout by the leave-one-out cross-validated PLS analysis running with four principal components, which lead to a R^2_{CV} cross-validated correlation coefficient as high as 0.60, of comparable order with that obtained in a previous MTD analysis.

TABLE IV. The predicted and residual biological CoMSIA activities of the statin derivatives of Table I, grouped in training and test sets

Compound index	A_{CoMSIA} (predicted)	A_{obs}–A_{CoMSIA} (residual)
Training set		
1	6.57	0.06
3a	5.46	–0.07
3b	5.96	0.09
3d	6.77	–0.03
3f	7.33	–0.03
3g	6.71	–0.02
3h	7.33	0.06
3i	7.52	0.08
3j	6.58	–0.03
3k	6.84	0.01
3l	6.49	–0.04
3o	6.53	–0.03
3p	7.01	–0.09
30a	7.36	0.19
30b	7.63	–0.08
30c	6.08	0.01
33	8.23	–0.08
Testing set		
3c	6.03	0.73
3e	6.94	–0.49
3m	6.28	1.05
3n	6.34	0.8

Taking into account that the HMG-CoA reductase inhibitors display large molecular diversity through the many types of chemical substituents, the leave-one-out cross-validation method is here found to be the appropriate statistical technique. In addition, for a non-cross-validated PLS analysis, a suitable fitted correlation coefficient (r^2) of 0.98 was obtained, as revealed in Table V.

However, by comparing the statistical parameters of the CoMSIA and MTD methods, *i.e.*, $R^2_{CV\text{-}MTD}$ = 0.677106 with $R^2_{CV\text{-}CoMSIA}$ = 0.6, although the first was based on the leave-half-out, whereas the second on the leave-one-out algo-

rithm, permits the conclusion that the MTD method gives a similar robust model as the CoMSIA method. Such a comparison is justified by the fact that both models were computed on the same training set, *i.e.*, with 17 molecules, albeit slightly different, because the CoMSIA method did not discriminate the molecules **3h**, **3i**, **30c** and **33**, leading to their exclusion from training set, while the MTD analysis did it due to the revealed geometrical reasons. In this way, the MTD analysis was somewhat superior from the computational point of view; this superiority was also emphasized by the considerable lower standard error of estimate for CoMSIA with respect to the MTD analysis, see Table V and the statistical factor for Eq. (5), respectively. Nevertheless, the MTD method gains because of the starting configuration of the intuitive 3D hypermolecule, producing in the end similar statistical results. Yet, for CoMSIA analysis, the value of R^2_{CV} =0.60 is by over 0.3 units different to the determination coefficient of the model r^2 = 0.98 , compared to the difference of 0.05 between the same quantities in the case of the MTD model. Such a behaviour indicates that the present CoMSIA description could suffer either from an over-fitted circumstance by the presence of irrelevant independent variables and/or by the presence of outliers; at the same time, the MTD algorithm, although employing a 2.5D analysis, provides better self-consistent statistical factors, this being an argument for further MTD development in molecular design.

TABLE V. Synopsis of the statistical CoMSIA-PLS analysis used to evaluate the predictive quality for the biological activity of the statins derivatives of Table III used as HMG-CoA reductase inhibitors

Statistical quantity	Value
Number of molecules in the training set	17
Cross-validated R^2_{CV}	0.6
r^2	0.98
SEE (standard error of estimate)	0.08
Fisher test	249.58

Furthermore, the predictive power of CoMSIA was tested on the inhibitors included in the molecular test set given in Table IV.

From residuals given in Table IV, it is clear that the predictive power of CoMSIA was quite poor outside the training range. These results limit the usefulness of the CoMSIA analysis to the sample molecules under consideration. However, useful information from the training set is revealed, indicating the development of new inhibitors starting from **3k** and **30c** as templates with considerable low residuals with respect to those predicted by MTD analysis, see Tables IV and III, respectively.

Moreover, because the CoMSIA method predicts biological activity using electrostatic, steric, hydrophobic and donor descriptors, it is important to con-

sider their contributions to the inhibitory activities of the statins. The contribution of steric, electrostatic and donor descriptors to the inhibitory activities of the statins were just 0.154, 0.153 and 0.287 respectively, while hydrophobic contribution was found significantly higher, 0.407.

Finally, in order to properly compare the biostatistics of the MTD and CoMSIA methods, the recent Steiger test is considered here.[28] It is based on checking whether the null hypothesis according to which the dispersions of the (molecular) populations investigated by MTD and CoMSIA are equal:

$$\sigma_{\mathrm{MTD}} = \sigma_{\mathrm{CoMSIA}} \tag{7a}$$

(against the alternative $\sigma_{\mathrm{MTD}} \neq \sigma_{\mathrm{CoMSIA}}$) parallels inclusion in the confidence interval of the root-mean-square standardized effect (*RMSSE*),

$$\Psi = \sqrt{\frac{\lambda}{(p-1)n}} \tag{7b}$$

of the non-central Fisher-related statistics:

$$f_{\mathrm{CoMSIA}}^{\mathrm{MTD}} = \frac{SEE_{\mathrm{MTD}}}{SEE_{\mathrm{CoMSIA}}} \tag{7c}$$

in terms of the non-centrality parameter λ, when n observations per group (p) are statistically performed. In the present case, p = 17 molecules (as the whole group) and n = 1 (as the individual members studied for their bioactivity); while noting that for the Fisher test:

$$F_{\mathrm{CoMSIA}}^{\mathrm{MTD}} = \left(f_{\mathrm{CoMSIA}}^{\mathrm{MTD}} \right)^2 = 13.414$$

with the degrees of freedom $v_1 = v_2 = 16$, the 95 % interval for λ ranges from 70.617 to 385.227. Hence, the application of the confidence interval transformation in accordance with the inversion confidence interval principles,[28] provides the validation result:

$$f_{\mathrm{CoMSIA}}^{\mathrm{MTD}} \in \left(\Psi_{\mathrm{lower}}, \Psi_{\mathrm{upper}} \right), \tag{8a}$$

with:

$$f_{\mathrm{CoMSIA}}^{\mathrm{MTD}} = 3.66; \ \Psi_{\mathrm{lower}} = 2.1; \ \Psi_{\mathrm{upper}} = 4.91. \tag{8b}$$

In this way, the hypothesis (7a) is confirmed and therefore the bioequivalence in assessing the activity modelling by both the MTD and CoMSIA approaches on the series of molecules given in Table I.

CONCLUSIONS

QSAR studies enable the identification and removal of molecular structures with no therapeutic potential. The provided data allow structural features es-

sential for an increased biological activity to be identified, suggesting that there are certain structural requirements for a statin to have an increased biological potential. The present 3D-QSAR study modelled a series of 21 molecules of the tetrahydro-4-hydroxy-6-[2-(1*H*-pyrrol-1-yl)ethyl]-2*H*-pyran-2-one type against the HMG CoA-reductase enzyme by MTD and CoMSIA algorithms.

The 3D-QSAR MTD-CoMSIA study was performed in order to obtain a more detailed insight into the structure–activity relationships of HMG-CoA reductase inhibitors, beyond the usual features apparent from pharmacophore models. The observed biological activities of HMG CoA-reductase inhibitors were selected from a published report. Molecular modelling of the inhibitors was performed in Sybyl 7.2. The minimum potential energy for statins derivatives was calculated by the conjugate–gradient method, convergence of 0.01, Tripos force field. Finally, Gasteiger–Marsili partial charges were loaded. The partial least squares (PLS) algorithm within Sybyl 7.2 was used to evaluate the statistic parameters R^2_{CV}, *PRESS*, *SEE*, r^2, Fisher test (*F*). Statistically significant models were derived within both the MTD and CoMSIA models: while MTD allows a better geometrical description and control of the optimum hypermolecular 3D structure, CoMSIA provides better residuals for the identified template molecules. Moreover, it was demonstrated by the recently established Steiger test that both provide compatible biostatistics.

However, it is noteworthy that the present study enriches in some respect a previous report on the 3D-QSAR-CoMSIA approach for studying the inhibitory activity of statin moieties,[29] through performing molecular alignment by systematic MTD analysis, while imposing more restrictive convergence criteria on the gradient fields and yielding smoother better MTD-statistics.

While, generally, it is difficult to propose a clear conclusion regarding the steric configuration because of the diversity of the studied compounds, it appears that a better activity is predicted for substitutes that are more voluminous. The study showed that the relative activity in the studied series is given not only by the presence of the substituents on the nitrogen atom of the main ring, but also by the presence of 4-fluorophenyl and isopropyl substituents in positions 2 and 5 of the same ring, see Fig. 1. In addition, the activity is strongly influenced by the presence and the type of the substituents in positions 3 and 4 of the main ring: electrophilic atoms or groups of atoms determine a variation of the activity depending on the electrophilic potential and on the geometry (steric conformation) of the substitute.

It is believed that these results could be very useful for the development of new HMG-CoA reductase inhibitors belonging to statins classes, if good superposition (employing the MTD method) and minimization (employing the CoMSIA method) of the molecules belonging to the statistic model are achieved.

Acknowledgements. The authors are truly indebt to the anonymous referees for their constructive criticisms that considerably refined the initial arguments in the manuscript.

И З В О Д

MTD–CoMSIA МОДЕЛОВАЊЕ ИНХИБИТОРА HMG-CoA РЕДУКТАЗЕ

DANIEL M. DUDA-SEIMAN[1], SPERANŢA AVRAM[2], SILVIA MANCAŞ[1], VALENTIN CAREJA[3], CORINA DUDA-SEIMAN[4], MIHAI V. PUTZ[4] и DAN CIUBOTARIU[5]

[1]*Department of Medical Ambulatory, Medical Emergencies, University of Medicine and Pharmacy "Victor Babes", Timisoara,* [2]*Department of Physiology & Biophysics, University of Bucharest, Faculty of Biology, Bucharest,* [3]*Institute of Chemistry "Coriolan Drăgulescu" of the Romanian Academy, Timisoara,* [4]*Department of Chemistry, University of West Timisoara, Faculty of Chemistry-Biology-Geography, Timişoara и* [5]*Faculty of Pharmacy, University of Medicine and Pharmacy "Victor Babeş", Timisoara, Timisoara, Romania*

Испитиване су 3Д квантитативне релације између структуре и активности за серију инхибитора хидроксиметилглутарил-CoA (HMG-CoA)-редуктазе, базираној на основу пиролилетил-тетрахидропиранона. Радило се применом методе минималне тополошке разлике (*Minimal Topological Difference*, MTД) и анализом индекса компаративне молекулске сличности (CoMSIA). Проучавана су једињења тетрахидро-4-хидрокси-6-[2-(1*H*-пирол-1-ил)етил]--2*H*-пиран-2-она. У клиничкој пракси, инхибитори HMG-CoA-редуктазе се обично називају статинима. Анализа MTD методом показала је да волуминозни супституенти имају знатну биолошку активност (R^2_{CV} = 0,677 > 0,5; *SEECV* = 0,319), док метода CoMSIA даје корисне додатне информације о утицају на биолошку активност стерних, електростатичких и хидрофобних особина, као и донорских и акцепторских утицаја водоничне везе (R^2_{CV} = 0,60; r^2 = = 0.98).

(Примљено 1. јуна, ревидирано 23. августа 2010)

REFERENCES

1. R. Y. A. Mukhtar, J. Reid, J. P. D. Reckless, *Int. J. Clin. Practice* **59** (2005) 239
2. B. Genser, W. März, *Clin. Res. Cardiol*. **95** (2006) 393
3. D. J. Maron, S. Fazio, M. F. Linton, *Circulation* **101** (2000) 207
4. C. J. Vaughan, A. M. Gotto, *Circulation* **110** (2004) 886
5. C. L. Grines, *J. Interven. Cardiol*. **19** (2006) 3
6. C. I. Ardern, P. T. Katzmarzyk, I. Janssen, T. S. Church, S. N. Blair, *Circulation* **112** (2005) 1478
7. A. J. Taylor, S. M. Kent, P. J. Flaherty, C. L. Coyle, T. T. Markwood, M. N. Vernalis, *Circulation* **106** (2002) 2055
8. S. E. Nissen, S. J. Nicholls, I. Sipahi, P. Libby, J. S. Raichlen, C. M. Ballantyne, J. Davignon, R. Erbel, J. C. Fruchart, J. C. Tardif, P. Schoenhagen, T. Crowe, V. Cain, K. Wolski, M. Goormastic, E. M. Tuzcu, *J. Am. Med. Assoc*. **295** (2006) E1
9. J. A. Tobert, *Circulation* **76** (1987) 534
10. J. G. Robinson, B. Smith, N. Maheshwari, H. Schrott, *J. Am. Coll. Cardiol*. **46** (2005) 1855
11. J. C. LaRosa, *J. Am. Coll. Cardiol*. **46** (2005) 1863
12. A. J. Taylor, S. M. Kent, P. J. Flaherty, L. C. Coyle, T. T. Markwood, M. N. Vernalis, *Circulation* **106** (2002) 2055
13. A. R. Leach, *Molecular Modelling Principles and Applications*, 2nd ed., Pearson Prentice Hall, Harlow, 2001

14. Z. Simon, A. Chiriac, S. Holban, D. Ciubotariu, I. Mihalas, *Minimum Steric Difference. The MTD Method for QSAR Studies*, Wiley Res. Stud. Press, Letchworth, NY, 1984
15. G. Klebe, U. Abraham, T. Mietzner, *J. Med. Chem*. **34** (1994) 4130
16. I. Niculescu-Duvăz, D. Ciubotariu, Z. Simon, N. Voiculetz, in *Modeling of Cancer Genesis and Prevention*, N. Voiculetz, A. T. Balaban, I. Niculescu-Duvăz, Z. Simon, Eds., CRC Press, Boca Raton, FL, 1991, p. 157
17. D. Ciubotariu, V. Gogonea, M. Medeleanu, in *QSAPR/QSAR Studies by Molecular Descriptors*, M. V. Diudea, Ed., NOVA Science, Huntington, NY, 2001, p. 281
18. E. R. Malinowski, D. G. Howery, *Factor Analysis in Chemistry*, Wiley, New York, 1980
19. B. D. Roth, C. J. Blankley, A. W. Chucholowski, E. Ferguson, M. L. Hoefle, D. F. Orwine, R. S. Newton, C. S. Sekerke, D. R. Sliskovic, C. D. Stratton, M. W. Wilson, *J. Med. Chem*. **34** (1991) 357
20. M. E. Suh, S.-Y. Park, H.-J. Lee, *Bull. Korean Chem. Soc*. **23** (2002) 417
21. J. Boström, M. Böhm, K. Gundertofte, G. Klebe, *J. Chem. Inf. Comput. Sci*. **43** (2003) 1020
22. T. I. Oprea, in *Quantitative chemical structure–biological activity relationships. The MTD method*, A. Chiriac, D. Ciubotariu, Z. Simon, Eds., Mirton Publishing House, Timisoara, 1996, p. 221 (in Romanian)
23. M. Akamatsu, *Curr. Top. Med. Chem*. **2** (2002) 1381
24. S. J. Cho, A. Tropsha, *J. Med. Chem*. **38** (1995) 1060
25. *SYBYL Theory Manual*, version 6.4, Tripos Associates Inc., 1699 South Hanley Road, St. Louis, MO, 1988
26. C. Duda-Seiman, D. Duda-Seiman, D. Dragoş, M. Medeleanu, V. Careja, M. V. Putz, A. M. Lacrămă, A. Chiriac, R. Nuţiu, D. Ciubotariu, *Int. J. Mol. Sci*. **7** (2006) 537
27. C. Duda-Seiman, D. Duda-Seiman, M. V. Putz, D. Ciubotariu, *Digest. J. Nanomat. Biostruct*. **2** (2007) 207
28. J. H. Steiger, *Psychological Methods* **9** (2004) 164
29. R. Thilagavathi, R. Kumar, V. Aparna, M. E. Sobhia, B. Gopalakrishnan, A. K. Chakraborti, *Bioorg. Med. Chem. Lett.* **15** (2005) 1027.

Journal of the Serbian Chemical Society
JSCS-info@shd.org.rs • www.shd.org.rs/JSCS
J. Serb. Chem. Soc. *76* (1) 101–112 (2011)
JSCS–4103
UDC 679.91+66.081:549.25:544.4:536.7
Original scientific paper

Sorption of Cu^{2+} and Co^{2+} from aqueous solutions onto sepiolite: an equilibrium, kinetic and thermodynamic study

SLAVICA LAZAREVIĆ[1*#], IVONA JANKOVIĆ-ČASTVAN[1#], ŽELJKO RADOVANOVIĆ[1#], BRANISLAV POTKONJAK[2#], DJORDJE JANAĆKOVIĆ[1#] and RADA PETROVIĆ[1#]

[1]*Faculty of Technology and Metallurgy, University of Belgrade, Karnegijeva 4, 11000 Belgrade and* [2]*Institute of Chemistry, Technology and Metallurgy, Njegoševa 12, 11000 Belgrade, Serbia*

(Received 18 January, revised 10 September 2010)

Abstract: The efficiency of natural sepiolite for the removal of Cu^{2+} and Co^{2+} from aqueous solution was determined using the batch method. The sorption experiments were performed as a function of the initial metal concentration, the equilibration time and temperature. Thermodynamic parameters, such as enthalpy, free energy and entropy, were calculated from the temperature dependent sorption isotherms and these values showed that the sorption of the investigated metals onto sepiolite was endothermic. The pseudo-second order kinetic model provides the best correlation of the experimental kinetic data.

Keywords: sepiolite; sorption; heavy metals; kinetics; thermodynamic.

INTRODUCTION

Wastewaters from many industries, such as metallurgy, tannery, mining, battery-production, insecticide, fungicide, paint and coating manufacture, *etc*., pollute the environment with heavy metals, which is of very serious environmental concern for all living organisms, especially for humans. Heavy metal ions, such as copper and cobalt, accumulated through the food chain; even at low concentrations, have damaging effects on human health because there are no adequate mechanisms for their elimination from the body.[1]

The most important technologies developed to remove and recovery heavy metals from wastewaters include chemical precipitation, ion exchange, electrochemical removal, membrane separation, microbe separation, sorption by activated carbon, *etc*. Heavy metals sorption by low-cost sorbents is currently of great interest. The employment of clay minerals, such as kaolinite,[2,3] vermicu-

* Corresponding author. E-mail: slazarevic@tmf.bg.ac.rs
# Serbian Chemical Society member.
doi: 10.2298/JSC100118005L

lite,[4] montmorilonite,[5] bentonite[6] and sepiolite[7–9] has recently received increasing attention because they showed high sorption capacities and are abundant in nature, inexpensive and environmental friendly.

Sepiolite is a hydrous magnesium silicate ($Si_{12}O_{30}Mg_8(OH)_4(H_2O)_4 \cdot 8H_2O$) characterized by its fibrous morphology and intracrystalline channels. Due to its sorptive, rheological and catalytic properties, sepiolite is widely used in a variety of industrial applications. Sepiolite is used as a catalyst and catalyst support,[10] a filler in polymer composites,[11] a membrane for ultrafiltration[12] and as molecular sieves.[13] Sepiolite is an effective and economical sorbent material, a bleaching and clarifying agent, a filter aid, an industrial sorbent and the spectrum of its utilization ranges from cosmetics to paints and fertilizers.

The aims of this study were: to investigate the effectiveness of natural sepiolite in the removal of Cu^{2+} and Co^{2+} by sorption from aqueous solution; to examine the dominant mechanisms of the interaction of these ions with sepiolite; to investigate the influence of the equilibrium time and temperature on the sorption capacity of sepiolite; to determine the thermodynamic parameters of sorption (free energy change, enthalpy and entropy change).

EXPERIMENTAL

The natural sepiolite sample was obtained from the deposit Andrići (Serbia). The chemical composition, X-ray diffraction, differential thermal and FTIR analyses of the sample and the point of zero charge of 7.4±0.1 were reported previously.[14]

Sorption procedure

The batch equilibration method was used to investigate the removal of Cu^{2+} and Co^{2+} by the natural sepiolite sample. The sorption of ions onto the sepiolite was studied based on the shift of the point of zero charge, determination of sorption isotherms and the correlation between the quantity of Mg^{2+} released from, and the quantity of Cu^{2+} and Co^{2+} sorbed onto the sepiolite sample. The experiments were performed using solutions of $Cu(NO_3)_2$ and $Co(NO_3)_2$ in high quality water (18 MΩ) obtained from a Mill-Q water purification system.

The shift of the point of zero charge was investigated using 0.01 and 0.001 mol dm^{-3} solutions of $Cu(NO_3)_2$ and $Co(NO_3)_2$. The measurements were performed using 25 cm^3 of metal ion solutions (concentration 0.01 or 0.001 mol dm^{-3}) in poly(vinyl chloride) (PVC) vessels. The initial pH value (pH_i) of the electrolytes was adjusted by the addition of small quantities of a 0.1 mol dm^{-3} HCl or KOH solution. Then, 0.050 g of sepiolite was added to each sample. Equilibration was attained by shaking for 24 h in a water bath thermostated at 298 K. The dispersions were then filtered and the final pH of the solutions (pH_f) was determined. The point of zero charge was found from a plot of pH_f *vs.* pH_i. The sorption of Co^{2+} was examined in the pH range from approx. 3.5 to approx. 8, whereas the sorption of Cu^{2+} was investigated from approx. 3.5 to approx. 6 in order to avoid ion hydrolysis at higher pH values and the dissolution of sepiolite at lower pH values.

For the determination of the sorption isotherms, solutions of Cu^{2+} (initial concentrations from 30 to 250 mg dm^{-3}) and Co^{2+} (initial concentrations from 30 to 200 mg dm^{-3}) in demineralized water were prepared. The initial pH values of the solutions were 5.6±0.1. Aliquot of 25 cm^3 of each solution was equilibrated for 24 h with 0.05 g of sepiolite, with shaking. The

metal ions remaining unabsorbed in the supernatant, as well as the concentration of Mg^{2+}, were determined using AAS (Perkin Elmer 730). All the sorption studies were repeated twice; the reported value is the average of two measurements.

Effect of contact time

The removal of Cu^{2+} and Co^{2+} by the sepiolite sample was also investigated as a function of the contact time. Solutions of the metal ions (25 cm^3) with an initial ion concentration of 100 mg dm^{-3} and a pH value of 5.6±0.1 were equilibrated with 0.05 g sepiolite at a temperature of 298 K for contact times ranging from 1 h to 24 h. After separation of the solid from liquid phase, the final concentration of Cu^{2+}, Co^{2+} and Mg^{2+} were measured as dependent variables of time.

Effect of temperature

In order to investigate the influence of the temperature on the sorption process, sorption experiments were also performed at temperatures of 318, 328 and 338 K. The M^{2+} solutions with different initial concentrations were adjusted to a pH value of 5.6±0.1. Aliquot of 25 cm^3 of each solution was equilibrated for 24 h with 0.05 g of sepiolite, with shaking in a water bath thermostated at the desired temperature.

RESULTS AND DISCUSSION

Sorption of Cu^{2+} and Co^{2+} onto sepiolite

The specific sorption of cations onto a solid surface leads to a shift in the point of zero charge to lower values. This shift is more pronounced, the greater the amount of specifically sorbed ions is.[15]

The results of the determination of the point of zero charge for sepiolite in $Cu(NO_3)_2$ and $Co(NO_3)_2$ solutions, of concentrations 0.01 and 0.001 mol dm^{-3}, are presented in Figs. 1 (for Cu^{2+}) and 2 (for Co^{2+}). From the dependences pH_f *vs.* pH_i, the value of the point of zero charge was obtained as the pH value at which the plateau of the curve, *i.e.*, the inflexion point of the curve, appeared.

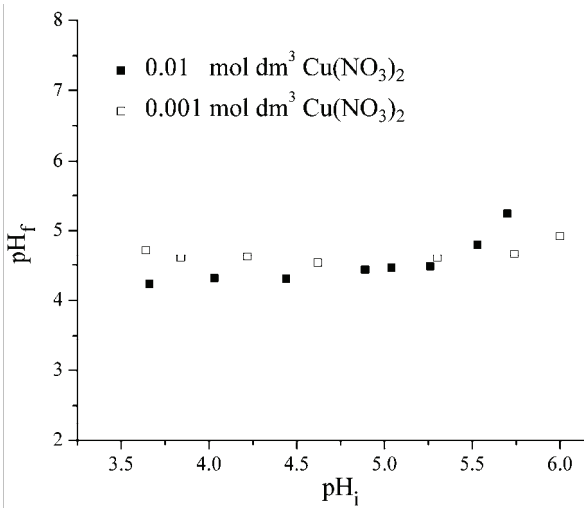

Fig. 1. Dependences of pH_f on pH_i during the equilibration of sepiolite with 0.01 and 0.001 mol dm^{-3} $Cu(NO_3)_2$ solutions.

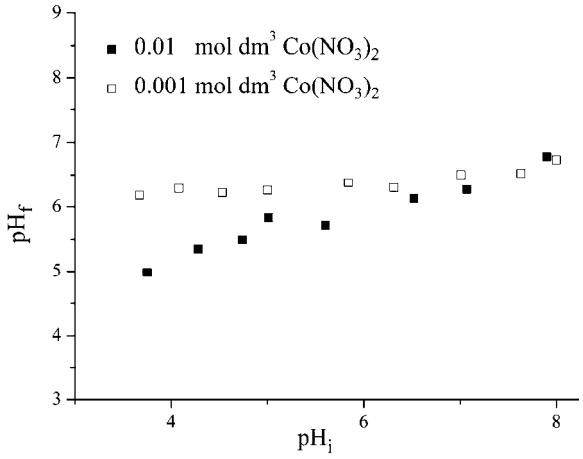

Fig. 2. Dependences of pH_f on pH_i during the equilibration of sepiolite with 0.01 and 0.001 mol dm^{-3} $Co(NO_3)_2$ solutions.

The pH of the point of zero charge, pH_{pzc}, values of the sepiolite determined in solutions of M^{2+} of concentration 0.01 mol dm^{-3} were 4.4±0.1 and 6.2±0.1 for the solutions of Cu^{2+} and Co^{2+}, respectively, whereas the respective values obtained in solutions of concentration 0.001 mol dm^{-3} were 4.6±0.1 and 6.5±0.1.

During the equilibration of sepiolite with $Cu(NO_3)_2$ and $Co(NO_3)_2$ solutions, the plateau position shifted towards lower pH values compared to the pH_{pzc} of 7.4±0.1, obtained under the same conditions for KNO_3 solutions (concentration of 0.1, 0.01 and 0.001 mol dm^{-3}, in the pH range from approx. 3.5 to approx. 10),[14] indicating that specific sorption of Cu^{2+} and Co^{2+} onto the sepiolite occurred. For the same initial ion concentration, the shift of the plateau was more pronounced with Cu^{2+} than with Co^{2+}, suggesting that Cu^{2+} have a higher affinity for specific sorption onto sepiolite sample than Co^{2+}. The shift of pH_{pzc} in the solutions of M^{2+} was higher when the initial concentration was 0.01 mol dm^{-3} as a result of increased specific sorption.

The quantity of specifically sorbed ions onto the surface of solids[16] is strongly dependent of the radii of the hydrated ions, the electron charge, the metal electronegativity, the hydrolysis constant, *etc*. The electric charge of the investigated ions are the same and the radii of the hydrated ions (Co^{2+}, 0.423 nm and Cu^{2+}, 0.419 nm)[17] and metal electronegativities (Cu, 1.90 and Co, 1.88) are similar. There are, however, differences in the hydrolysis constant: Cu^{2+} ($10^{-7.53}$) > > Co^{2+} ($10^{-9.6}$).[18] The higher the hydrolysis constant of a given ion is, the higher is the tendency of the ion to specific sorption.

The sorption isotherms (with the same solid/liquid ratio as in the determination of the pH_{pzc}) and the dependences of the quantity of Mg^{2+} released into the solution as a result of the ion exchange process on the equilibration concentration of the sorbed ions, c_e, are presented in Figs. 3 (for Cu^{2+}) and 4 (for Co^{2+}).

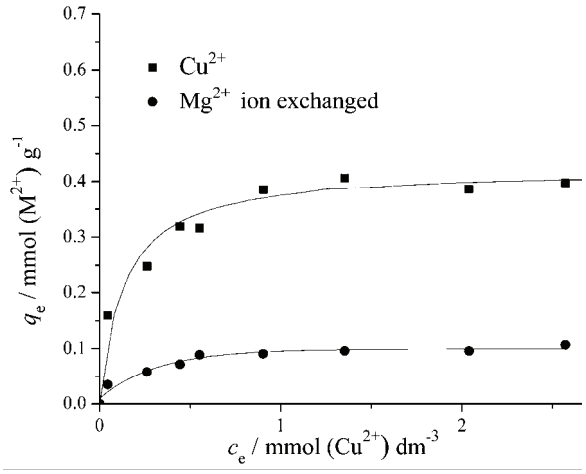

Fig. 3. Sorption isotherm for Cu^{2+} onto sepiolite and dependence of q_e / mmol (Mg^{2+}) g^{-1} on c_e / mmol (Cu^{2+}) dm^{-3}.

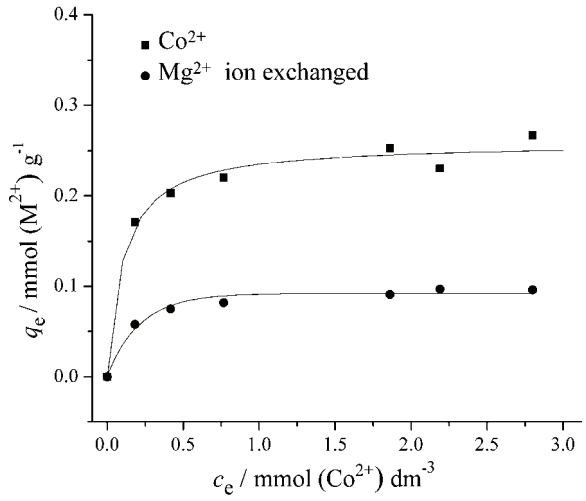

Fig. 4. Sorption isotherm for Co^{2+} onto sepiolite and dependence of q_e / mmol (Mg^{2+}) g^{-1} on c_e / mmol (Co^{2+}) dm^{-3}.

The total amount of Mg^{2+} present in the solution after equilibration of the solution with sepiolite is the result of two processes: the ion exchange of Mg^{2+} from the sepiolite structure with Cu^{2+} and Co^{2+}, and dissolution of the sepiolite. The exchangeable Mg^{2+} were determined as the difference between the total amount and amount of Mg^{2+} released into the solution due to dissolution of sepiolite (0.09 mmol g^{-1}, determined during the determination of the pH_{pzc}).[14] The difference between the values of q_e (mmol (M^{2+}) g^{-1}) and q_e (mmol (Mg^{2+}) g^{-1}) corresponds to the quantity of M^{2+} removed from the solution by other mechanisms: specific sorption, ion exchange with exchangeable ions from the sepiolite structure, *etc*. The mechanism of precipitation of hydroxides of these ions ($M(OH)_2$) could not be involved considering the pH values of the solutions. The occurrence of specific sorption of Cu^{2+} and Co^{2+} onto the sepiolite was con-

firmed by the shifts of the pH_{pzc} towards lower pH values, proportional to the quantity of specifically sorbed ions.

During the ion exchange of Cu^{2+} and Co^{2+}, Mg^{2+} are displaced from the sepiolite lattice, releasing them into solution and replacing them within the structure. This process does not influence the change of the pH_{pzc} because H^+ ions are not involved in the ion exchange process.

The process of ion exchange depends of the similarity of crystallographic radii of Mg^{2+} and the M^{2+}. The values of crystallographic radii of Cu^{2+}, Co^{2+} and Mg^{2+} of 0.073, 0.075 and 0.072 nm, respectively, suggest that the affinity of the investigated ions for ion exchange with Mg^{2+} should be very similar.[19] The results of the present investigation showed that quantity of M^{2+} exchanged was almost the same for Cu^{2+} and Co^{2+}.

According to the results presented in Figs. 3 and 4, obtained at a temperature of 298 K, the sepiolite sample showed the higher sorption capacity for Cu^{2+} then for Co^{2+}.

Effect of contact time

The effect of contact time on the amounts of Cu^{2+} and Co^{2+} sorbed onto sepiolite is shown in Fig. 5. It can be seen that the removal of Cu^{2+} and Co^{2+} using sepiolite as the sorbent is a two-step process. Most of the metal ion sorption was achieved within 400 min for both investigated ions. The initial faster metal ion uptake may be explained by the high number of available active sites on the sepiolite surface. Thereafter, a slower increase of the amount of cations sorbed can be observed in the second stage, due to the gradual occupancy of the active sites and the decrease of the metal ion concentrations in the solutions; thus the sorption became less efficient.

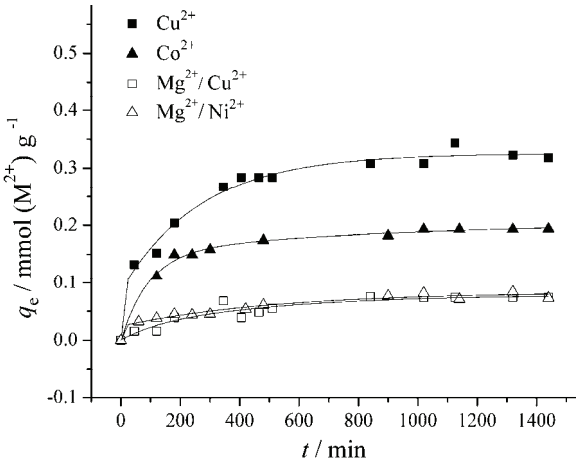

Fig. 5. Effect of contact time on the amounts of Cu^{2+} and Co^{2+} sorbed and Mg^{2+} exchanged (initial ion concentration of 100 mg dm^{-3}, at a temperature of 298 K and pH of 5.6±0.1).

In addition to Cu^{2+} and Co^{2+} sorption, the quantity of Mg^{2+} released into the solution as result of the ion exchange process was also examined (Fig. 5). The obtained data confirmed that the affinity for ion exchange was similar for Cu^{2+} and Co^{2+}, and that sorption of the investigated ions included a high amount of specific sorption on the sepiolite surface.

In order to investigate the mechanism of sorption and the potential rate-controlling steps, the two most widely applied kinetic models were used to fit the experimental data: the pseudo-first-order equation proposed by Lagergren[20] and the pseudo-second-order kinetic model proposed by Ho and G. McKay.[21] The linear forms of the pseudo-first-order and pseudo-second-order equations are given by the following equations:

$$\log(q_e - q_t) = \log q_e - \frac{k_1 t}{2.303} \quad (1)$$

$$\frac{t}{q_t} = \frac{1}{k_2 q_e^2} + \frac{t}{q_e} \quad (2)$$

where t is the contact time (min), q_e and q_t are the amounts of sorbed M^{2+} (mmol g^{-1}), at equilibrium and time t and k_1 and k_2 are the rate constants of the pseudo-first-order (min^{-1}) and pseudo-second-order kinetics (g $mmol^{-1}$ min^{-1}), respectively.

The initial sorption rate h (mmol g^{-1} min^{-1}) can be obtained using calculated values of the pseudo-second-order rate constant and the equilibrium sorbed amounts from the following expression:

$$h = k_2 q_e^2 \quad (3)$$

The pseudo-first-order and pseudo-second-order model for the sorption of Cu^{2+} and Co^{2+} onto sepiolite are shown in Figs. 6 and 7, respectively. Based on

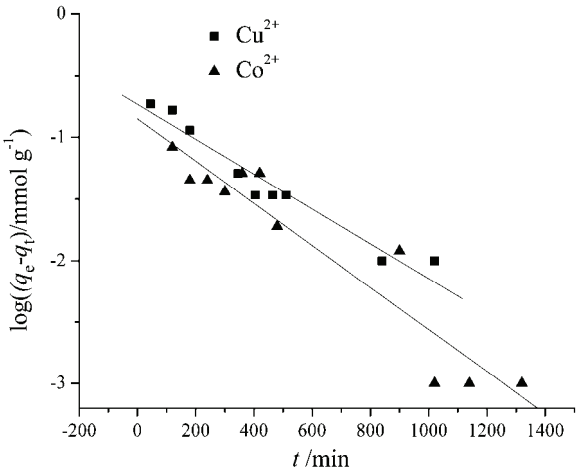

Fig. 6. Linear fitting of the kinetic data by the pseudo-first-order kinetic model.

the above two kinetic models, the obtained parameters for the sorption kinetics are given in Table I.

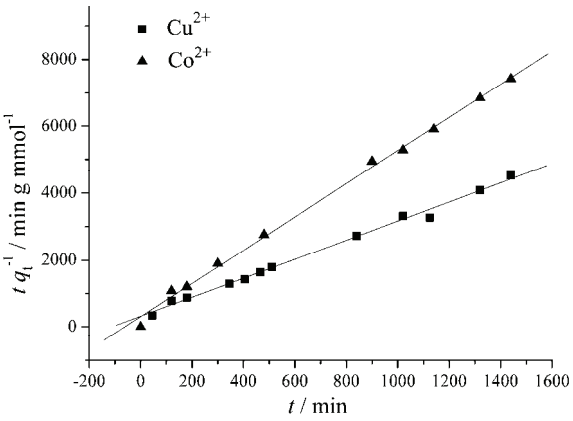

Fig. 7. Linear fitting of the kinetic data by the pseudo-second-order kinetic model.

It can be concluded that the pseudo-second-order equation is the model that best describes the experimental data, since the q_e values estimated by this model are in good agreement with the experimental results and the values of the correlation coefficients are close to 1.

TABLE I. Kinetic parameters for Cu^{2+} and Co^{2+} sorption onto sepiolite

Metal Ion	Pseudo-first-order			Pseudo-second-order			
	k_1 min^{-1}	q_e mmol g^{-1}	R^2	k_2 g mmol^{-1} min^{-1}	q_e mmol g^{-1}	R^2	h mmol g^{-1} min^{-1}
Cu^{2+}	0.00322	0.184	0.972	0.025	0.352	0.995	0.0031
Co^{2+}	0.00398	0.147	0.947	0.078	0.201	0.997	0.0030

According to the literature, the pseudo-second-order kinetic model includes different sorption mechanisms, such as surface complexation, ion-exchange, *etc*. The model is based on the assumption that the rate-limiting step may be chemical sorption or chemisorption involving valence forces through the sharing or exchange of electrons between the sorbent and the sorbate and that the sorption rate depends on the concentration of sorbate at the sorbent surface.[21,22] As the correlation coefficients are very high (Table I), it may also be assumed that sorption of Cu^{2+} and Co^{2+} onto sepiolite occurs through chemisorption, which confirms that the main mechanisms of sorption onto the sepiolite sample are specific sorption and ion exchange of Mg^{2+} from the sepiolite structure with Cu^{2+} and Co^{2+} from the solutions.

Effect of temperature

The relationship between the amount of Cu^{2+} and Co^{2+} sorbed per unit mass of sepiolite q_e (mmol (M^{2+}) g^{-1}) and the equilibrium concentration c_e (mmol

(M^{2+}) dm^{-3}) for four series of experiments at different temperatures are shown in Figs. 8 and 9. The quantity of sorbed ions increased with increasing temperature. This indicates that a higher temperature favors metal ion removal by sepiolite, *i.e.*, that the sorption of Cu^{2+} and Co^{2+} onto sepiolite are endothermic processes. The increase of sorption with increasing temperature may be attributed to either an increase in the number of active surface sites on the sorbent surface or the desolvation of the sorbing species and a decrease in the thickness of the boundary layer surrounding the sorbent; hence the mass transfer resistance of the sorbate in the boundary layer decreases.[23]

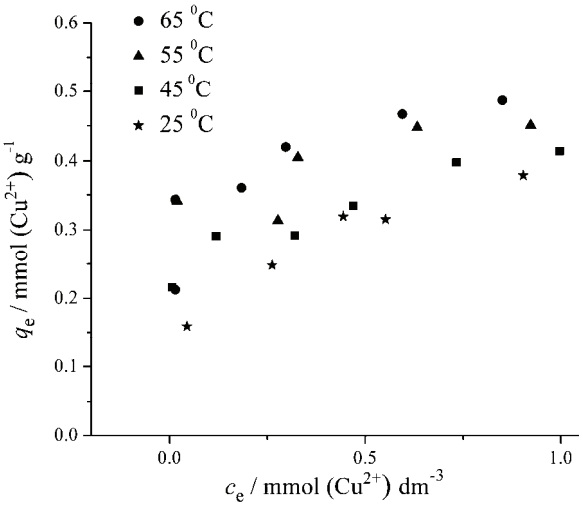

Fig. 8. Sorption isotherms of Cu^{2+} onto sepiolite at different temperatures.

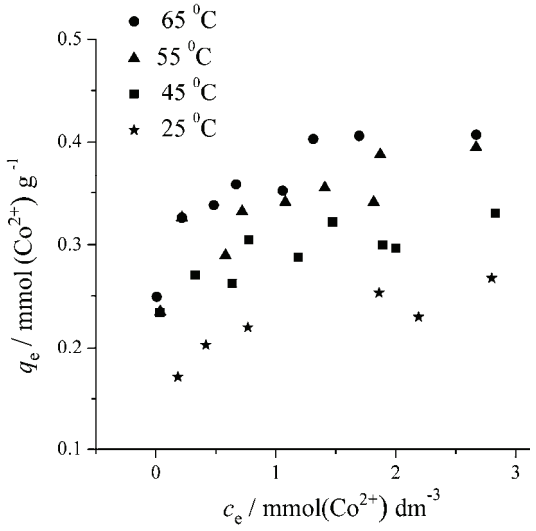

Fig. 9. Sorption isotherms of Co^{2+} onto sepiolite at different temperatures.

Thermodynamics of sorption

In order to investigate the effect of temperature on the sorption of Cu^{2+} and Co^{2+} onto sepiolite, the distribution coefficient, K_d, was calculated at the temperatures 298, 318, 328 and 338 K using the equation:

$$K_d = \frac{q_e}{c_e} \quad (4)$$

The thermodynamic parameters, the enthalpy change (ΔH), the entropy change (ΔS), and the Gibbs free energy change (ΔG) were calculated using the following equations:

$$\ln K_d = \Delta S/R - \Delta H/(RT) \quad (5)$$

$$\Delta G = \Delta H - T\Delta S \quad (6)$$

The enthalpy change and the entropy change were determined graphically from the slope and intercept of the straight line plots of $\ln K_d$ *versus* $1/T$ (Fig. 10). The values of the thermodynamic parameters are presented in Table II.

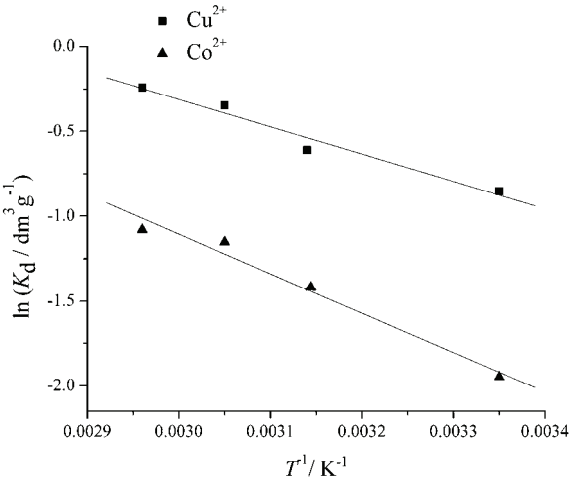

Fig. 10. Effect of temperature on the distribution coefficients for Cu^{2+} and Co^{2+} sorption onto sepiolite.

The positive enthalpy change indicates that the process of Cu^{2+} and Co^{2+} removal from solution by sepiolite is endothermic. The free energy values are small and positive and decrease with increasing temperature. This indicates that the sorption is more efficient at higher temperatures and that the reaction requires a small amount of energy. The ΔG values will be negative if the solution temperature becomes higher than 338 K. This indicates the presence of an energy barrier in the sorption process.[24] Considering the positive values of ΔG, it has been suggested that this is quite common with the sorption of metal ions by the ion-exchange mechanism because of the activated complexation of the metal ion formed with the sorbent in the excited state.[25]

TABLE II. Thermodynamic parameters of the sorption of Cu^{2+} and Co^{2+} by sepiolite

Metal Ion	ΔH / kJ mol^{-1}	ΔS / J mol^{-1} K^{-1}	ΔG / kJ mol^{-1}			
			T / K			
			298	318	328	338
Cu^{2+}	13.45	37.77	2.24	1.48	1.06	0.728
Co^{2+}	19.34	48.80	4.80	3.81	3.32	2.84

The positive values of entropy change may be explained by structural changes of both the sorbates and sorbents during the sorption process.[3,26] According some authors, the positive values of ΔS indicate an increase in randomness at the solid/liquid interface during the sorption of metal ions by clays.[27]

CONCLUSIONS

The sorption capacity shown by the sepiolite suggests that this mineral, as a natural low-cost sorbent, can be successfully employed for the removal of Cu^{2+} and Co^{2+} from highly polluted waters.

The retention occurred dominantly by specific sorption and exchange of Mg^{2+} from the sepiolite structure. The occurrence of specific sorption was confirmed by shifts of the pH_{pzc} towards lower pH values, proportional to the quantity of specifically sorbed ions.

The sorption kinetic study showed that the pseudo-second-order model described best the experimental data, indicating that the sorption may be controlled by chemical sorption.

The thermodynamic analysis showed that the process of sorption of Cu^{2+} and Co^{2+} onto sepiolite was endothermic. The small and positive ΔG values suggest that the sorption process requires a small amount of energy.

Acknowledgements. Financial support through the Ministry of Science and Technological Development of the Republic of Serbia, Project No. III 45019 and EUREKA Project E! 4141 is gratefully acknowledged.

ИЗВОД

СОРПЦИЈА ЈОНА БАКРА И КОБАЛТА ИЗ ВОДЕНИХ РАСТВОРА НА СЕПИОЛИТУ, ИСПИТИВАЊЕ РАВНОТЕЖЕ, КИНЕТИКЕ И ТЕРМОДИНАМИКЕ СОРПЦИЈЕ

СЛАВИЦА ЛАЗАРЕВИЋ[1], ИВОНА ЈАНКОВИЋ-ЧАСТВАН[1], ЖЕЉКО РАДОВАНОВИЋ[1], БРАНИСЛАВ ПОТКОЊАК[2], ЂОРЂЕ ЈАНАЋКОВИЋ[1] и РАДА ПЕТРОВИЋ[1]

[1]Технолошко–металуршки факултет, Карнегијева 4, 11 000 Београд и [2]Институт за хемију, технологију и металургију, Његошева 12, 11001 Београд

У раду је испитана ефикасност уклањања јона бакра и кобалта из водених раствора на природном сепиолиту применом методе уравнотежавања посебних проба. Испитан је утицај почетних концентрација Cu^{2+} и Co^{2+}, као и времена уравнотежавања и температуре на процес сорпције. Вредности термодинамичких параметара сорпције (промене енталпије, промене ентропије, промене слободне енергије сорпције), одређене на основу зависности сорпционог капацитета од температуре, указују на то да је процес сорпције Cu^{2+} и Co^{2+} на сепиолиту

ендотерман. Поређењем експерименталих резултата са кинетичким моделима утврђено је да се кинетика сорпције Cu^{2+} и Co^{2+} на сепиолиту може описати кинетичким моделом псеудо--другог реда.

(Примљено 18. јануара, ревидирано 10. септембра 2010)

REFERENCES

1. M. Arora, B. Kiran, S. Rani, A. Rani, B. Kaur, N. Mittal, *Food Chem*. **111** (2008) 811
2. K. G. Bhattacharyya, S. S. Gupta, *Appl. Clay Sci*. **41** (2008) 1
3. O. Yavuz, Y. Altrunkayanak, F. Guzel, *Water Res*. **37** (2003) 948
4. M. Malandrino, O. Abollino, A. Giacomino, M. Aceto, E. Mentasti**,** *J. Colloid Interface Sci.* **299** (2006) 537
5. O. Abollino, A. Giacomino, M. Malandrino, E. Mentasti, *Appl. Clay Sci*. **38** (2008) 153
6. E. Alvares-Ayuso, A. Garcia-Sanchez, *Clay Clay Miner*. **51** (2003) 475
7. S. Kocaoba, *Desalination* **244** (2009) 24
8. N. Bektas, B. Akman Agim, S. Kara, *J. Hazard. Mater*. **112** (2004) 115
9. M. Kara, H. Yuzer, E. Sabah, M. S. Celik, *Water Res.* **37** (2003) 224
10. A. Corma, H. Garcia, A. Leyva, A. Primo, *Appl. Catal. A* **257** (2004) 77
11. L. González, A. Rodríguez, A. Marcos-Fernández, A. del Campo, *J. Appl. Polym. Sci.* **79** (2001) 714
12. Q. K. Wang, T. Matsuura, C. Y. Feng, M. R. Weir, C. Detellier, E. Rutadinka, R. L. Van Mao, *J. Membr. Sci*. **184** (2001) 153
13. E. Ruiz-Hitzky, *J. Mater. Chem.* **11** (2001) 86
14. S. Lazarević, I. Janković-Častvan, D. Jovanović, S. Milonjić, Dj. Janaćković, R. Petrović, *Appl. Clay Sci.* **37** (2007) 47
15. B. M. Babić, S. K. Milonjić, M. J. Polovina, S. Čupić, B. V. Kaludjerović, *Carbon* **40** (2002) 1109
16. M. B. McBride, *Chemisorption and precipitation of inorganic ions in Environmental Chemistry of Soils*, Oxford Univ. Press, New York, 1994, p. 121
17. E. R. Nightingale Jr., *J. Phys. Chem.* **63** (1959) 1381
18. C. F. Baes, R. E. Mesmer, *The hydrolysis of cations*, Wiley-Interscience, New York, 1976.
19. Y. M. Chiang, D. Birnie, W. D. Kingery, *Physical ceramics principles for ceramic science and engineering, In: Structure in ceramics*, Wiley, New York, 1997, p. 1
20. S. Lagergren, *K.* Sven, *Vetenskapsakad. Handl*. **24** (1898) 1
21. Y. S. Ho, G. McKay, *Process Biochem*. **34** (1999) 451
22. H. Chen, A. Wang, *J. Colloid Interface Sci*. **307** (2007) 309
23. A. K. Meena, G. K. Mishra, P. K. Rai, C. Rajagopal, P. N. Nagar, *J. Hazard. Mater*. **122** (2005) 161
24. T. Shi, S. Jia, Y. Chen, Y. Wen, C. Du, H. Guo, Z. Wand, *J. Hazard. Mater*. **169** (2009) 838
25. A. S. Ozcan, A. Ozcan, *J. Colloid Interface Sci.* **276** (2004) 39
26. Q. Fan, D. Shao, Y. Lu, W. Wu, X. Wang, *Chem. Eng. J*. **15** (2009) 188
27. H. Baker, *Desalination* **244** (2009) 48.

Journal of the Serbian Chemical Society
JSCS-info@shd.org.rs • www.shd.org.rs/JSCS
J. Serb. Chem. Soc. 76 (1) 113–123 (2011) UDC 547.262+577.15+541.135.5–039.26:66.087
JSCS–4104 *Original scientific paper*

Sensitive determination of dihydronicotinamide adenine dinucleotide and ethanol with a nano-porous carbon electrode

XIAOQIN LIU, BUHAI LI and CHUNYA LI*

Key Laboratory of Analytical Chemistry of the State Ethnic Affairs Commission, College of Chemistry and Materials Science, South-Central University for Nationalities, Wuhan 430074, China

(Received 27 January, revised 6 July 2010)

Abstract: A nano-porous carbon electrode, fabricated in 0.1 mol L^{-1} NaOH by the electrochemical technique, was used for the electrochemical detection of dihydronicotinamide adenine dinucleotide, NADH, with an overpotential decrease of about 270 mV and a linear range from 1.0×10^{-6} to 1.0×10^{-4} mol L^{-1}. Amperometric sensing of ethanol cooperating with alcohol dehydrogenase and nicotinamide adenine dinucleotide was successfully demonstrated. A linear response in the range from 5.0×10^{-5} mol L^{-1} to 1.0×10^{-2} mol L^{-1} was obtained, with a detection limit of 1.0×10^{-5} mol L^{-1}. The method was successfully employed to determine ethanol in beer with high precision.

Keywords: nano-porous carbon; NADH; ethanol; electrochemical process; amperometry.

INTRODUCTION

The electrochemical oxidation of dihydronicotinamide adenine dinucleotide, NADH, to the enzymatically active NAD^+ in aqueous solution has attracted considerable interest due to its significance as a cofactor for dehydrogenase enzymes and in the development of biosensors. NAD^+ as a co-enzyme can catalyze the oxidation of various compounds of great interest in analytical chemistry, such as alcohols, aldehydes and carbohydrates, in cooperation with enzymes, including dehydrogenases and oxidoreductases, to generate NADH. Therefore, the electrochemical detection of NADH and a highly selective and sensitive NADH transducer is desired.[1] However, the direct electrochemical oxidation of NADH at a bare glassy carbon electrode requires a high overpotential. Although the reversible potential of the NADH/NAD^+ couple is estimated to be –0.56 V (*versus* SCE) in neutral pH, the direct oxidation of NADH at unmodified electrodes often occurs at a potential of about 1.0 V.[2] The large overpotential always

* Corresponding author. E-mail: lcychem@yahoo.com
doi: 10.2298/JSC100127007L

results in interferences from the real samples. In addition, the electrode surface is often fouled by the adsorption of reaction intermediates that are generated during the oxidation of NADH.[3] Hence, considerable effort has been made to modify the electrode surface to decrease the overpotential for the oxidation of NADH and to minimize the surface passivation effects.

Many methods have been adopted to immobilize the mediator on the electrode surface to reduce the overpotential for NADH oxidation. Electrodes modified with carbon nanotubes,[4,5] CdS nanoparticles,[6] nanostructured TiO_2,[7] boron--doped diamond[8] and conducting polymer nanotubes[9] have been developed for the electrochemical detection of NADH. However, the stability of the mediator limits the reproducibility and the operational lifetime of these modified electrodes. Therefore, sensitively and selectively in the electrochemical detection of NADH are still challenging tasks.

Various kinds of activation methods, such as mechanical polishing,[10] ultrasonification,[11] vacuum heating,[12] laser irradiation and electrochemical pretreatment[13] have been developed to improve the electrochemical performance of glassy carbon electrodes. Among these activation methods, electrochemical pretreatment is one of the most commonly used methods to improve the electrochemical responses to biological compounds, due to its good reproducibility and simple operation. The higher density of functional groups produced on the surface of glassy carbon electrodes by electrochemical activation have been characterized by various techniques, including X-ray photoelectron spectroscopy (XPS), scanning electron microscopy (SEM) and electrochemical impedance spectra (EIS).[14] The results indicate that the existence of carboxyl groups on the electrode surface can accelerate electron transfer between the electrode surface and the solution.[15,16] These conclusions initiated this investigation on the electrochemical performance of an electrochemically-treated glassy carbon electrode in the determination of NADH.

In this study, a glassy carbon electrode was treated in 0.1 mol L^{-1} NaOH by electrochemical oxidization at 1.80 V for 3 min followed by reduction at –1.00 V for 1 min. This electrochemical process resulted in the formation of nano-porous cavities on the electrode surface. This nano-porous carbon electrode exhibited excellent electro-catalytic activity towards the oxidation of NADH at a low potential in phosphate buffer at pH 7.0. Furthermore, an electrochemical method for ethanol determination at the nano-porous carbon electrode in presence of alcohol dehydrogenase, ADH, and NAD^+ using amperometry was developed.

EXPERIMENTAL

Apparatus and reagents

The electrochemical measurements were performed with an EC 550 electrochemical workstation (Gaoss Union Technology Co., Ltd, Wuhan, China) in an electrochemical cell containing 10.0 mL of 1/15 mol L^{-1} phosphate buffer solution at a pH of 7.0. A conventional three-

-electrode system was used with a pretreated glassy carbon electrode, GCE (diameter 3 mm), as the working electrode, a Pt wire as the auxiliary electrode and a saturated calomel electrode (SCE) as the reference electrode (all potentials are expressed *vs*. SCE) . All experiments were realized at room temperature. AVG Multilab 2000F X-ray photoelectron spectroscope (Thermo Electron Corp., USA) and a JSM-6700F field emission scanning electron microscope (JEOL Ltd., Japan) were applied for surface analysis of the nano-porous carbon electrode. The electrochemical impedance spectra (EIS) measurements were performed in a 0.5 mol L^{-1} KCl solution containing 2.0 mmol L^{-1} $K_4[Fe(CN)_6]/K_3[Fe(CN)_6]$ at a measuring potential of 0.19 V.

Nicotinamide adenine dinucleotide (NAD^+), nicotinamide adenine dinucleotide reduced form (NADH) and alcohol dehydrogenase ADH (EC 1.1.1.1) from baker's yeast in the form of a lyophilized powder were obtained from Sigma. All other chemicals were of analytical grade and all of the solutions were prepared with ultrapure water obtained from a molecular water purification system.

Preparation of the nano-porous carbon electrode

A glassy carbon electrode was polished with fine emery paper and alumina slurries followed by rinsing thoroughly with distilled water. The electrodes were successively sonicated in nitric acid, ethanol, and distilled water, and then allowed to dry at room temperature. A freshly polished electrode was electrochemically treated in 0.1 mol L^{-1} NaOH at 1.80 V for 3 min, and then reduced at –1.0 V for 1 min, whereby a nano-porous carbon electrode was obtained. After successive cyclic voltammetric scanning for 20 cycles in phosphate buffer solution in the potential range from 0.0 to 0.80 V, the nano-porous carbon electrode was taken out and washed thoroughly with ultrapure water. The same procedure was employed for the electrochemical treatment of a glassy carbon electrode in acid, only 0.1 mol L^{-1} H_2SO_4 solution was used instead of NaOH solution. The density and diameter of the formed nano-porous cavities could be modulated easily by the adjustment of the potential and the time of electrochemical treatment.

Electrochemical measurements

NADH detection was performed under stirring using amperometric batch analysis in an electrochemical cell containing 10 mL of 1/15 mol L^{-1} phosphate buffer solution (PBS) at pH 7.0 with an applied potential of 350 mV. The nano-porous carbon electrode was dipped in the buffer solution, then, after a stable background current was observed, NADH was successively added and a fast current response was obtained.

RESULTS AND DISCUSSION

Characterization of the nano-porous carbon electrode

Scanning electron microscopy was used to characterize the morphology of the obtained nano-porous carbon electrode surface. The SEM images of the glassy carbon electrode before (a) and after (b) electrochemical treatment in 0.1 mol L^{-1} NaOH are presented in Fig. 1. A slide surface was observed for the glassy carbon electrode before treatment. However, many cavities of nano-meter size were found on the surface of the electrochemically treated electrode. The rough and lacunose construction of the nano-porous carbon electrode offers more electroactive sites and a larger surface area, which is responsible for easier electron-transfer processes and the enhancement of the current response.

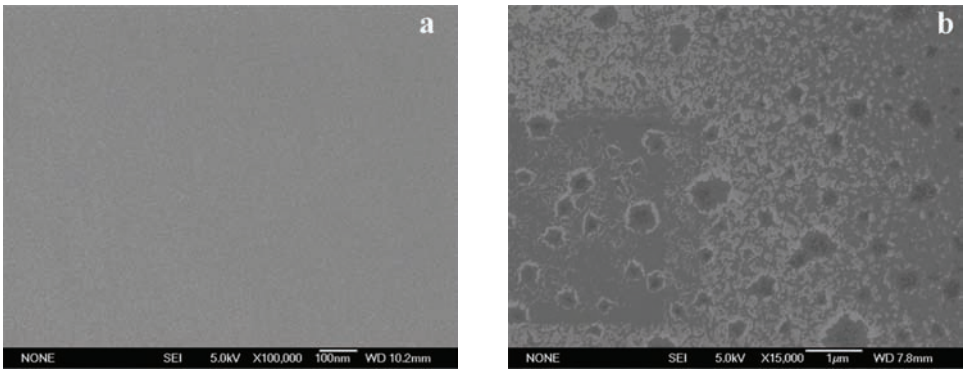

Fig. 1. Morphology of the glassy carbon electrode a) before and b) after electrochemical treatment in 0.1 mol L^{-1} NaOH solution.

It was found that electrodes that had been freshly polished with emery paper and alumina showed relatively poor activity toward the oxidation of NADH, compared to electrodes that had been electrochemically pretreated. It was suggested that pretreatment introduces or alters the nature of functional groups on the electrode surface and that such groups might serve as mediators of electrons between the electrode and the electroactive species. After electrochemical oxidation, phenolic, quinoidal, and carboxyl functional group were generated on the electrode surface. According to an early report,[14] carboxyl groups on the surface of a GCE treated by an electrochemical process can mediate charge transfer reactions. Thus, in the present, XPS was used to determine the carbon and oxygen content of the electrochemically treated electrode surface, and the results are shown in Fig. 2, from which it was found that the oxygen-to-carbon (O/C) ratios

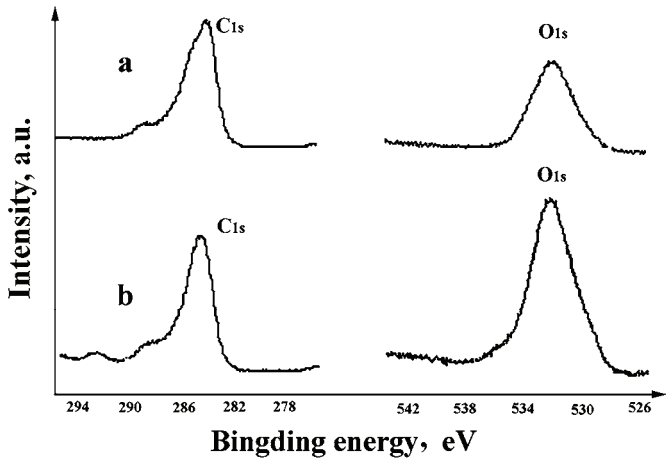

Fig. 2. XPS Spectra of the O (1s) and C (1s) regions: a) bare GCE; b) nano-porous carbon electrode.

of the surface of the bare GCE and the nano-porous carbon electrode were 0.27 and 0.46, respectively. The increase in the O/C ratio indicated that the electrochemical process could increase the number of oxygen-containing functional groups on the GCE surface, especially those groups which were negatively charged, which would experience an electrostatic repulsion towards NADH, which is negatively charged in PBS at pH 7.0.

Electrochemical impedance spectroscopy (EIS) is a powerful tool for studying the interface properties of nano-porous carbon electrodes and can provide information on the impedance changes between the interface between the electrode surface and electrolyte solution. Nyquist plots are presented in Fig. 3 for the bare GCE (a) and the nano-porous carbon electrode (b) in 0.5 mol L^{-1} KCl solution containing 2.0 mmol L^{-1} $K_4[Fe(CN)_6]$ /$K_3[Fe(CN)_6]$ using an amplitude of 0.005 V and a frequency range of 1 mHz–100 kHz. The Randles circuit (inset of Fig. 3) was chosen to fit the obtained impedance data. The resistance to charge transfer (R_{ct}) and the diffusion impedance (W) were both in parallel to the interfacial capacitance (C_{dl}). The diameter of the semicircle corresponded to the interfacial electron-transfer resistance (R_{ct}). By fitting the data, R_{ct} was estimated to be 1081 Ω at the bare GCE, the R_{ct} decreased to 103.8 Ω at the nano-porous carbon electrode. This result demonstrates that the nano-porous surface of the carbon electrode could function as an efficient electron conducting tunnel between the electrode surface and electrolyte solution due to the enormous numbers of nano-cavities and electroactive sites.

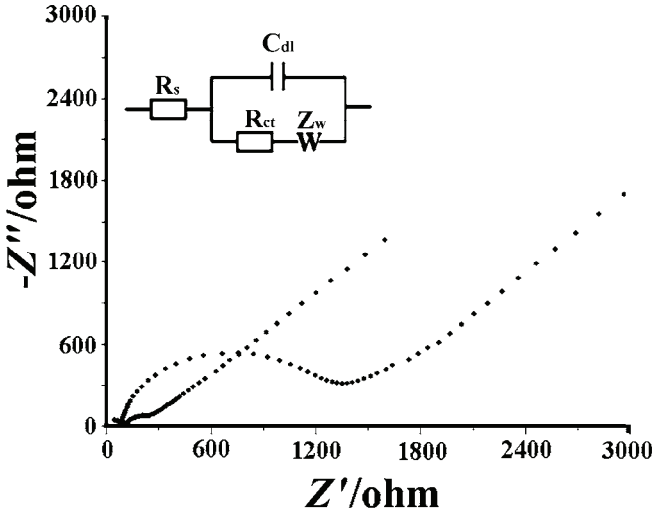

Fig. 3. Nyquist plots for the bare GCE (a) and nano-porous (b) carbon electrode in the presence of 2.0 mmol L^{-1} $K_4[Fe(CN)_6]/K_3[Fe(CN)_6]$ in 0.5 mol L^{-1} KCl solution. The inset is the Randle equivalent circuit used to fit the EIS measurements.

Electrochemical behavior of NADH

Considering the higher surface density of functional groups on the nano-porous carbon electrode, the electrochemical oxidation of NADH could be reasonably catalyzed.[15,16] Accordingly, the electrochemical behavior of 1.0 mmol L^{-1} NADH at the nano-porous carbon electrode was investigated in 1/15 mol L^{-1} PBS (pH 7.0) by differential pulse voltammetry (DPV). The obtained voltammograms are shown in Fig. 4. When the GCE was electrochemically treated in different supporting electrolyte solutions, the change in the structure of the electrode surface was different, which resulted in different decreases in the overpotential for electrochemical oxidation. For the bare GCE, the recorded difference pulse voltammogram shows an oxidation peak at 0.62 V (curve a). After electrochemical treatment in 0.1 mol L^{-1} H_2SO_4 solution (curve b), the oxidation peak was negatively shifted to 0.42 V. However, after electrochemical treatment in 0.1 mol L^{-1} NaOH solution, the oxidation peak appeared at 0.35 V (curve c). No peak at 0.35V was observed at the nano-porous carbon electrode in the absence of NADH (curve d). Therefore, the oxidation peak at 0.35 V can be assigned to the catalytic oxidation of NADH by functional groups on the nano-porous carbon electrode. It can be seen that the response of the carbon electrodes to NADH depended on the nature of the pretreatment. The main difference in the electrochemical pretreatment process was the composition of the electrolyte solution, which includes both the pH of the solution and the nature and concentration of the electrolyte ions besides H^+. Thus, it can be concluded that the functional groups obtained on the electrode surface by pretreatment in a 0.1 mol L^{-1} NaOH solution were different from that in 0.1 mol L^{-1} H_2SO_4 solution. It can also be seen from Fig. 4 that the oxidation overpotential of NADH was decreased by 270 mV and the oxidation peak current was improved significantly after the glass carbon electrode had been electrochemically treated.

Chronocoulometry is useful for measuring electrode surface areas, diffusion coefficients, the time window of an electrochemical cell, adsorption of electroactive species, and the mechanisms and rate constants for chemical reactions coupled to electron transfer reactions. The chronocoulometry for the bare GCE and the nano-porous carbon electrode in 0.5 mmol L^{-1} $K_3[Fe(CN)_6]$ solution containing 0.1 mol L^{-1} KCl were investigated with a potential step from 0.0 to 0.40 V, a pulse width of 0.25 s and sample interval of 0.00025 s. The results showed that the effective surface areas of the nano-porous carbon electrode and the bare GCE were 0.023 cm^2 and 0.018 cm^2, respectively. The increase in the effective surface area of electrode should be partly responsible for the current increase in the oxidation of NADH,[17] but the large number of functional groups on the electrode surface is the most important factor leading to the decrease of the overvoltage for the oxidation of NADH. This result indicated that the electrochemical treatment in 0.1 mol L^{-1} NaOH solution can improve the electroche-

mical activity of the electrode, which facilitates electron transfer between the electrode surface and the NADH solution.

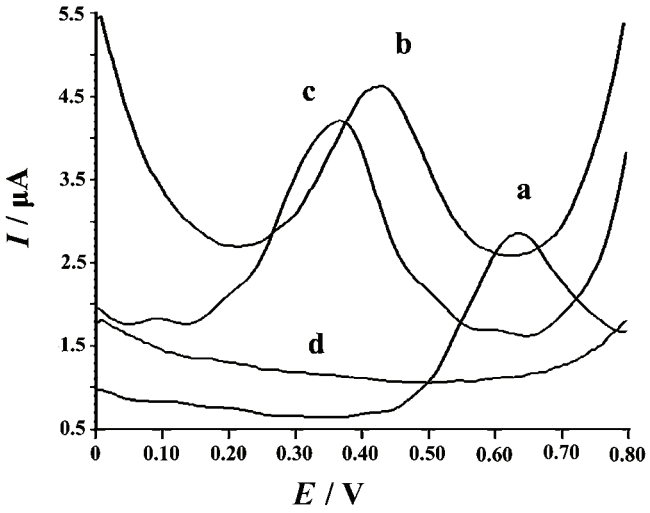

Fig. 4. Differential pulse voltammograms of 1.0 mmol L^{-1} NADH at a) the bare GCG, the nano-porous carbon electrode obtained in b) 0.1 mol L^{-1} H_2SO_4 solution and c) 0.1 mol L^{-1} NaOH solution, and d) the nano-porous carbon electrode obtained in 0.1 mol L^{-1} NaOH solution in the absence of NADH.

NADH determination

The advantageous effect of the functional groups leading to a decrease in the overvoltage for the oxidation of NADH on the surface of the pretreated electrode was successfully used for NADH detection. The amperometric responses of NADH recorded with an initial potential at 0.35 V (*vs*. SCE) in a stirred buffer solution were investigated. It was found that the increment of the current response at the nano-porous carbon electrode was almost the same for successive injections of 10 μL of 1.0 mmol L^{-1} NADH into 10 mL PBS at pH 7.0, indicating a good reproducibility. The mechanism of NADH oxidation reaction, which has already been extensively investigated, is that NADH undergoes a two--electron and one proton process to yield the corresponding enzymatic active NAD^+. Direct electrochemical oxidation of NADH only occurs at high overpotentials and is accompanied by rapid poisoning of the reaction because the electrode surface is fouled by polymeric products of side reactions which occur because of the one-electron oxidation intermediates formed in the reaction. Then, the oxidation current of NADH decreases and the reaction becomes unstable. After a glass carbon electrode was pretreated by electrochemical polarization, many functional groups were generated on the electrode surface that could act as transfer electron oxidants, which were used to lower the overpotential of NADH

and decrease the polymeric products of the one-electron oxidation intermediates.[18] Figure 5 shows the amperometric response of the nano-porous carbon electrode to successive additions of different concentrations of NADH into a stirred buffer solution. After each injection of NADH, the current response (I) increased immediately and reached a steady state quickly. It exhibited a linear range from 1.0×10^{-6} to 1.0×10^{-4} mol L^{-1} according to the equation:

$$I\ (\mu A) = 0.00591c\ (\mu mol\ L^{-1}) + 0.00271,\ r = 0.993 \quad (1)$$

where c is the NADH concentration.

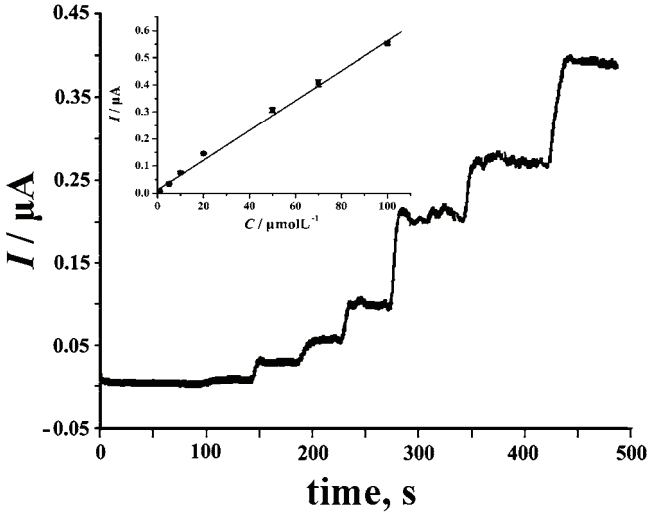

Fig. 5. Amperometric response of NADH at various concentrations in the range from 1.0×10^{-6} mol L^{-1} to 1.0×10^{-4} mol L^{-1} in phosphate buffer solution (pH 7.0) at the nano-porous carbon electrode. The inset is the calibration curve for NADH determination.

It is also important to emphasize that an NADH concentration as low as 1.0×10^{-6} mol L^{-1} was detected with high accuracy, indicating that the nano-porous carbon electrode could be used as a sensitive sensor for NADH.

Application to ethanol determination

Electrochemical sensing of ethanol was performed in a phosphate buffer solution using the nano-porous carbon electrode in the presence of ADH and NAD^+. The enzymes, together with their principal cofactor NAD^+, were initially used free in solution at their optimum pH. The reaction that occurs in the solution was consistent with an earlier report,[19] and can be described as follows:

$$\text{ethanol} + NAD^+ + \text{ADH} \rightarrow \text{acetaldehyde} + \text{NADH} + H^+ \quad (2)$$

After the background current had reached a steady state, 10 μL of 0.05 mol L^{-1} ethanol were successively added and the subsequent formation of NADH was

measured as described above. The amperometric response of the nano-porous carbon electrode towards different concentrations of ethanol is shown in Fig. 6. The insert curves are the calibration curves for ethanol determination. It was found that amperometric current (I) was linearly related to ethanol concentration (c) in the concentration range from 1.0×10^{-5} mol L^{-1} to 1.0×10^{-3} mol L^{-1} and 1.0×10^{-3} mol L^{-1} to 1.0×10^{-2} mol L^{-1} according to the equations:

$$I_1 \text{ (nA)} = 56.510c_1 \text{ (mmol L}^{-1}\text{)} + 3.580,\ r = 0.995 \quad (3)$$

and

$$I_2 \text{ (nA)} = 8.941c_2 \text{ (mmol L}^{-1}\text{)} + 49.26,\ r = 0.996 \quad (4)$$

At higher concentrations, the slope of the curve decreases, most likely because of control by the enzymatic reaction. A similar behavior was reported previously.[8]

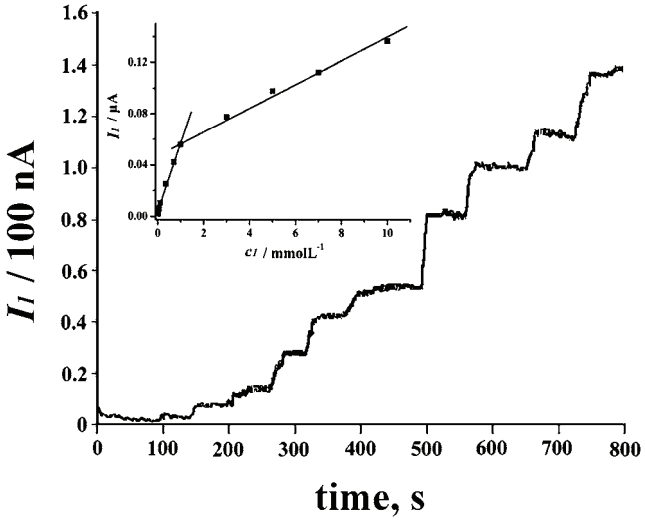

Fig. 6. Amperometric response of ethanol at various concentrations in the range from 1.0×10^{-5} mol L^{-1} to 1.0×10^{-2} mol L^{-1} in phosphate buffer solution containing 1 mg mL^{-1} ADH and 3.0 mmol L^{-1} NAD^+ at the nano-porous carbon electrode. The inset shows the calibration curves for ethanol determination.

The concentration of ethanol in Budweiser beer was measured using the nano-porous carbon electrode. 10 mL of phosphate buffer solution at pH 7.0 was spiked with 2.0 μL of beer. Five parallel determinations were performed to determine the ethanol content. The average ethanol content was determined to be 3.7±0.3 (vol. %), which is close to the ethanol nominal of 3.7 (vol. %), showing a good accuracy and high precision as the obtained relative standard deviation was 0.24 %.

CONCLUSIONS

In this present work, a nano-porous carbon electrode was fabricated by electrochemically treatment in NaOH solution with oxidation at 1.80 V following by reduction at –1.00 V. The electrochemical performances of the obtained nano--porous carbon electrode towards NADH were investigated thoroughly by voltammetry and amperometry. The overpotential for the oxidation of NADH was decreased substantially and the current response was improved significantly. In cooperation with NAD^+ and ADH, the nano-porous carbon electrode was successfully utilized for ethanol determination, which indicates that the obtained electrode can potentially be applied in the analysis of ethanol in real samples.

Acknowledgements. The authors gratefully acknowledge the financial supports from the Natural Science Foundation of Hubei Province (No. 2007ABA127), the State Ethnic Affairs Commission (No. 07ZN06) and the Nature Science Foundation of South-Central University for Nationalities (XTZ09005) and the special fund for Basic Scientific Research of Central Colleges, South-Central University for Nationalities (No. ZZZ10002).

И З В О Д

ОСЕТЉИВА МЕТОДА ОДРЕЂИВАЊА NADH И ЕТАНОЛА КОРИШЋЕЊЕМ НАНО-ПОРОЗНЕ УГЉЕНИЧНЕ ЕЛЕКТРОДЕ

XIAOQIN LIU, BUHAI LI и CHUNYA LI

Key Laboratory of Analytical Chemistry of the State Ethnic Affairs Commission, College of Chemistry and Materials Science, South-Central University for Nationalities, Wuhan 430074, China

Нано-порозна угљенична електрода је формирана електрохемијским поступком у раствору 0,1 mol L^{-1} NaOH, а затим је коришћена за електрохемијску детекцију NADH уз смањење пренапетости од 270 mV и линеарни опсег од $1{,}0\times10^{-6}$ до $1{,}0\times10^{-4}$ mol L^{-1}. Такође је демонстрирана могућност амперометријског одређивања етанола уз алкохол дехидрогеназу и никотинамид аденин динуклеотид. Добијен је линеарни одговор у опсегу од $5{,}0\times10^{-5}$ до $1{,}0\times10^{-2}$ mol L^{-1}. Метода је успешно примењена за одређивање етанола у пиву и показала је велику прецизност.

(Примљено 27. јануара, ревидирано 6. јула 2010)

REFERENCES

1. C. R. Raj, S. Behera, *Biosens. Bioelectron.* **21** (2005) 949
2. A. Barzegar, A. A. Moosavi-Movahedi, M. R. Ganjali, *J. Appl. Electrochem.* **39** (2009) 1111
3. P. C. Pandey, S. Upadhyay, B. C. Upadhyay, H. C. Pathak, *Anal. Biochem.* **260** (1998) 195
4. X. H. Kang, Z. B. Mai, X. Y. Zou, P. X. Cai, J. Y. Mo, *Anal. Biochem.* **369** (2007) 71
5. H. N. Choi, Y. K. Lyu, J. H. Han, W. Y. Lee, *Electroanal.* **19** (2007) 1524
6. W. Vastarella, R. Nicastri, *Talanta* **66** (2005) 627
7. A. Curulli, E. Valentini, G. Padeletti, M. Viticoli, D. Caschera, G. Palleschi, *Sens. Actuators B* **111–112** (2005) 441
8. T. N. Rao, I. Yagi, T. Miwa, D. A. Tryk, A. Fujishima, *Anal. Chem.* **71** (1999) 2506
9. F. Valentini, A. Salis, A. Curulli, G. Palleschi, *Anal. Chem.* **76** (2004) 3244

10. G. N. Kamau, W. S. Willis, J. F. Rusling, *Anal. Chem.* **57** (1985) 545
11. H. H. Zhang Jr., L. A. Coury, *Anal. Chem.* **65** (1993) 1552
12. D. T. Fagan, I. F. Hu, T. Kuwana, *Anal. Chem.* **57** (1985) 2759
13. R. J. Bowling, R. T. Packard, R. L. McCreery, *J. Am. Chem. Soc.* **111** (1989) 1217
14. Q. L. Zhao, Z. L. Zhang, L. Bao, D. W. Pang, *Electrochem. Commun.* **10** (2008) 181
15. R. C. Engstrom, *Anal. Chem.* **54** (1982) 2310
16. N. Cenas, J. Rozgaite, A. Pocius, J. Kulys, *J. Electroanal. Chem.* **154** (1983) 121
17. L. J. Kepley, J. A. Bard, *Anal. Chem.* **60** (1988) 1459
18. M. Musameh, J. Wang, A. Merkoci, Y. H. Lin, *Electrochem. Commun.* **4** (2002) 743
19. Z. H. Dai, F. X. Liu, G. F. Lu, J. C. Bao, *J. Solid State Electrochem.* **12** (2008) 175.

Journal of the Serbian Chemical Society
JSCS-info@shd.org.rs • www.shd.org.rs/JSCS
J. Serb. Chem. Soc. *76* (1) 125–127 (2011)
JSCS–4105
UDC 620.193+541.138:681.32:091.5
Extended abstract

EXTENDED ABSTRACT

In-line digital holography for the study of localized corrosion and dynamic processes of electrochemical reactions•

SHENHAO CHEN*

Department of Chemistry, Shandong University, Jinan 250100, P. R. China and State Key Laboratory for Corrosion and Protection, Shenyang 110015, P. R. China

(Received 18 May 2010)

Abstract: Digital holographic reconstruction has been used to map the transient concentration field within the diffusion layer, detect the dynamic processes of localized corrosion, such as pitting corrosion, crevice corrosion and scratch corrosion crack. It has been used with an attempt to identify the actual mechanism through observing the dynamic changes of the diffusion layer near the electrode/electrolyte interface during anodic processes of copper.

Keywords: digital holographic reconstruction; concentration change; diffusion layer; localized corrosion.

Digital holography is a new technique applied in electrochemistry and corrosion science. It has many advantages compared with traditional photographic holography.[1] In digital holography, holograms are recorded by a CCD camera and image reconstruction is performed by a computer. It saves the trouble of photographic processing and delivers the distributions of both intensity and phase directly.[2,3] Since the distributions of not only intensity but also phase can be calculated, object displacement can be directly detected from the difference of the reconstructed phases before and after object deformation.[4,5]

In our laboratory, digital holographic reconstruction has been employed in studies of dynamic changes of the concentration and the diffusion layer and for the detection of some types of localized corrosion.

a) Digital holographic reconstruction was employed in studies of the dynamic changes of the concentration and diffusion layer at the $Cu/CuSO_4$ interface. A two-dimensional concentration distribution was presented to illustrate the diffusion layer and the concentration changes.[5]

• Invited Lecture of the Electrochemical Section of the Serbian Chemical Society held on 16 April 2010, Belgrade.

* E-mail: shchen@sdu.edu.cn

doi: 10.2298/JSC100518018C

b) It was used to observe the dynamic pitting processes of X70 carbon steel in neutral solution containing chloride ions.[6] It was employed in an attempt to identify the actual mechanism through observing the dynamic changes of the diffusion layer at the electrode/electrolyte interface during the anodic processes of copper in 0.5 mol dm^{-3} NaCl solution.[7] The results confirmed that in the initial stage, the cuprous ion is formed first, which then reacts to produce cuprous chloride and/or cuprous chloride-complexes. The two-dimensional concentration images were also used to study the dynamic concentration changes during current oscillations in an acidic solution of iron.

c) Recently, the dynamic processes of crack corrosion during the anodic dissolution of a cracked electrode in a 0.5 mol dm^{-3} NaCl solution[8] were investigated. The localized scratch-induced corrosion process of Alloy 690 in 0.5 mol dm^{-3} H_2SO_4 containing 0.1 mol dm^{-3} NaCl solution[9] and stress corrosion cracking of stainless steel have also been studied by digital holographic reconstruction. This method was shown to be an effective *in situ* technique for detecting changes in concentration at the interface of localized corrosion regions.

Acknowledgements. Special thanks to the Special Funds for the Major State Basic Research Projects (2006CB605004, G19990650) and the Chinese National Science Fund (No. 20373038, 20573069). The author also thanks Dr. Chao Wang, Dr. Xuegeng Yang, Dr. Liang Li, Mr. Boyu Yuan, Mr. Henglei Jia and Mr. Liang Wang.

ИЗВОД

IN-LINE ДИГИТАЛНА ХОЛОГРАФИЈА ЗА ИСИТИВАЊЕ ЛОКАЛИЗОВАНЕ КОРОЗИЈЕ И ДИНАМИЧКИХ ПРОЦЕСА У ЕЛЕКТРОХЕМИЈСКИМ РЕАКЦИЈАМА

SHENHAO CHEN

Department of Chemistry, Shandong University, Jinan 250100, P. R. China and u State Key Laboratory for Corrosion and Protection, Shenyang 110015, P. R. China

Приказано је коришћење дигиталне холографске реконструкције за мапирање транзијентног концентрационог поља унутар дифузионог слоја и за детекцију динамичких процеса локализоване корозије, као што су питинг корозија, корозија у пукотинама и корозија у огреботинама. Помоћу ове методе праћене су динамичке промене дизузионог слоја на граници фаза електрода/електролит у циљу успостављања механизма анодних процеса на бакру.

(Примљено 18 маја 2010)

REFERENCES

1. E. Cuche, F. Bevilacgua, C. Depeursinge, *Opt. Lett.* **24** (1999) 291
2. X. Yang, S. Chen, C. Wang, L. Li, *Electrochem. Commun.* **6** (2004) 643
3. C. Wang, S. Chen, X. Yang, L. Li, *Electrochem. Commun.* **6** (2004) 1009
4. J. D. Rudnicki, G. M. Brisard, H. A. Gasteiger, R. E. Russo, F. R. McLarnon, E. J. Gairns, *J. Electroanal. Chem.* **362** (1993) 55
5. B. Yuan, S. Chen, X. Yang, C. Wang, L. Li, *Electrochem. Commun.* **10** (2008) 392
6. L. Li, C. Wang, B. Yuan, S. Chen, *Electrochem. Commun.* **10** (2008) 103

7. B. Yuan, C. Wang, L. Li, S. Chen, *Electrochem. Commun.* 11(2009) 1373.
8. H. Jia, S. Chen, B. Yuan, C. Wang, L. Li, *J. Serb. Chem. Soc.* **74** (2009) 197.
9. L. Wang, S. Chen, B. Yuan, F. Meng, J. Wang, C. Wang, L. Li, *J. Serb. Chem. Soc.* **75** (2010) 505.

Journal of the Serbian Chemical Society
JSCS-info@shd.org.rs • www.shd.org.rs/JSCS
J. Serb. Chem. Soc. *76* (1) 129–142 (2011)
JSCS–4106
UDC 547.466.24:532.14:532.13:541.25+54–145.2
Original scientific paper

A volumetric and viscometric study of 4-aminobutyric acid in aqueous solutions of metformin hydrochloride at 308.15, 313.15 and 318.15 K

KRISHA RAJAGOPAL[1] and S. S. JAYABALAKRISHNAN[2]*

[1]*Department of Physics, Government College of Engineering, Tirunelveli-627007 Tamil Nadu and* [2]*Department of Physics, P. S. R. Engineering College, Sivakasi, Tamil Nadu, India*

(Received 16 June 2009, revised 21 September 2010)

Abstract: Density (ρ) and viscosity (η) measurements were performed for 4-aminobutyric acid in 0.05, 0.10 and 0.15 M aqueous metformin hydrochloride at 308.15, 313.15 and 318.15 K. The measured values of density and viscosity were used to estimate some important parameters, such as the partial molal volume, V_ϕ, the standard partial molal volume, $V_\phi^\ominus$, the standard partial molal volume of transfer, $\Delta V_\phi^\ominus$, the hydration number, n_H, the second derivative of the infinite dilution of the standard partial molal volume with temperature $\partial^2 V_\phi^\ominus/\partial T^2$, the viscosity *B*-coefficients, variation of *B* with temperature, d*B*/d*T*, the free energy of activation per mole of solvent $\Delta\mu_1^{\ominus *}$ and solute $\Delta\mu_2^{\ominus *}$ of the amino acid in a ternary system. These parameters were interpreted in terms of solute–solute and solute–solvent interactions and structure making/breaking ability of solutes in the given solution.

Keywords: density; viscosity; standard partial molal volume; hydration number; viscosity *B*-coefficient; free energy activation parameters.

INTRODUCTION

Since several biological processes involve expansion and contraction of proteins molecules resulting from temperature and pressure variations in the living systems, resulting from fever, hypothermia, anaesthesia, *etc*., the study of these processes requires fundamental information about the volumetric properties of proteins.

Amino acids (AA) were considered as model compounds instead of proteins in the presence of aqueous salt solutions to obtain thermodynamic information, as the structure of proteins are highly complicated.[1–5] Some amino acids in the presence of aqueous minerals, such as $CaCl_2$ and NaCl, are available in literature.[6,7]

* Corresponding author. E-mail: krishnanpsr@yahoo.com
doi: 10.2298/JSC090616002R

As pointed out by Iqbal *et al*.,[8] although a great amount of volumetric data for amino acids has been reported in literature, they were obtained at 25 °C; it is understandable that much more relevance and significance can be achieved by studying compounds of biological importance (amino acids) at temperatures close to physiological temperatures, namely 35 °C (308.15 K), which is close to the optimum temperature of several living species. Recently, the results of volumetric and viscometric studies of 4-aminobutyric acid in aqueous solutions of salbutamol sulphate at various temperatures were reported.[9]

A literature survey shows that the study of amino acids in the presence of aqueous metformin hydrochloride has not hitherto been reported. Thus, in this paper, the volumetric and viscometric data of 4-aminobutyric acid in aqueous metformin hydrochloride solutions at three different temperatures (308.15 to 318.15 K) are reported.

Metformin hydrochloride ($C_4H_{11}N_5HCl$) is an antidiabetic and antihyperglycemic agent[10,11] that covers both basal and postprandial elevated blood glucose in patients with non-insulin dependant diabetes mellitus (type 2 diabetes), whose hyperglycemia cannot be satisfactorily managed by diet alone. In continuation of an earlier work on metformin hydrochloride,[12] in this paper, the density (ρ) and viscosity (η) data of 4-aminobutyric acid in aqueous metformin hydrochloride solutions at three different molar concentrations are reported. As hydration effects are known to be very sensitive to temperature,[13–16] both volumetric and viscometric studies are reported at three temperatures, *i.e*., 308.15, 313.15 and 318.15 K. Different physical parameters, such as partial molal volume, $V_\phi^\ominus$, standard partial molal volume, standard partial molal volume of transfer, $\Delta V_\phi^\ominus$, hydration number, n_H, second derivative of infinite dilution of the standard partial molal volume with temperature $\partial^2 V_\phi^\ominus/\partial T^2$ and the viscosity *B* coefficient were calculated using the Jones–Dole equation[17] and the free energies of activation of viscous flow $\Delta\mu_1^{\ominus *}$ and $\Delta\mu_2^{\ominus *}$ per mole of solvent and solutes[18] were, respectively, estimated. All these parameters are used to discuss the solute–solute and solute–solvent interactions occurring in the ternary (4-aminobutyric acid + metformin hydrochloride + water) system as well as the structure making/breaking tendency of the solute (AA) in the given solution.

EXPERIMENTAL

The 4-aminobutyric acid (Otto Chemicals Ltd., Bangalore, minimum assay +99 %) employed in this study was of analytic grade and was used without further purification. However, it was dried over P_2O_5 in a desiccator for 72 h before use. Analytic grade metformin hydrochloride (Accuumen Pharmaceuticals, Pondichery, minimum assay 99.5 %) was used as such without any pre-treatment. Doubly distilled, deionised water with a conductivity of 1.5×10^{-4} Ω^{-1} m^{-1} was used in the experiments and was degassed prior to making the solutions. The densities of the solutions were measured using a single stem pycnometer (Pyrex glass) of bulb capacity of 8×10^{-3} dm^3 having a graduated stem with 5×10^{-7} dm^3 divisions. The marks on the stem were calibrated with doubly distilled water. The weighings were realized

by taking the samples in airtight bottles on a high precision electronic balance (A & D model HR300, Japan) with a precision of ±0.1 mg. The reproducibility of the density measurements was $\pm 2.8\times10^{-5}$ kg m^{-3}.[9] Uncertainty values related to measured density data are calculated based JCGM 100:2008. The viscosities were measured by means of a suspended level Ubbelohde viscometer with a flow time of approximately 161 s for distilled water at 308.15 K. The time of flow was measured with a stopwatch capable of recording ±0.01 s. An average of three to four sets of flow times for each solution was taken for the calculation of the viscosity. The overall experimental reproducibility was estimated to be $\pm 1.9\times10^{-3}$ mPa s.[9] As the flow times were greater than 100 s, kinetic energy corrections were not necessary.[19] The pycnometer filled with air bubble free solutions and Ubbelohde viscometer filled with test solutions were allowed to stand for about 30 min in a thermostatic water bath so as to minimize thermal fluctuations. The temperatures of the solutions were maintained to an accuracy of ±0.01 K (Eurotherm, Mittal Enterprises, New Delhi, India) in an electronically controlled thermostated water bath. The data on the density and viscosity for doubly distilled water at the studied temperatures were compared with the literature values (Table I).[20] The fair agreement between the measured and the literature values validated the experimental procedures.

TABLE I. Comparison of experimental density, ρ, and viscosity, η, of water at different temperatures with literature values

T/K	ρ / 10^3 kg m^{-3}		η / mPa s	
	Present work	Literature[20]	Present work	Literature[20]
308.15	0.9940	0.994031	0.718	0.71903
313.15	0.9922	0.992217	0.653	0.65263
318.15	0.9902	0.990216	0.597	0.59716

RESULTS AND DISCUSSION

The experimental densities of the solutions at 308.15, 313.15 and 318.15 K are shown in Table II. The partial molal volumes, V_ϕ of the amino acid were calculated using the following equation:

$$V_\phi = (M/\rho) - 1000(\rho - \rho_0)/(m\rho\rho_0) \quad (1)$$

where M, m, ρ and ρ_0 are the molar mass of the solute, the molality of the solute, and the densities of the solution and solvent (aqueous solution of metformin hydrochloride and water), respectively. The calculated values of V_ϕ are also included in Table II.

The reported values of the apparent molal volume data for amino acids may generally be represented by the linear equation:[21]

$$V_\phi = V_\phi^\ominus + S_V m \quad (2)$$

where $V_\phi^\ominus$ is the standard partial molal volume at infinite dilution ($V_\phi^\ominus = \overline{V}_\phi^\ominus$) and S_V is the experimental slope. However, in those cases where there is a non-linear dependence of V_ϕ on m, as in the present case, the $V_\phi^\ominus$ values are calculated by taking the average of all the data points.[22,23]

The values of $V_\phi^\ominus$ of the amino acid in water at the studied temperatures are given in Table III, together with literature values for comparison. It can be seen from Table III that there is close agreement of the $V_\phi^\ominus$ values of the amino acids

in water reported in this report with the literature values, which further validates the employed experimental procedures.

TABLE II. Values of density, ρ, and partial molal volume, V_ϕ, of 4-aminobutyric acid in aqueous metformin hydrochloride (m_H – molality of metformin hydrochloride; m_A – molality of the amino acid $\delta\rho$ – uncertainty value for density)

m_A / mol kg^{-1}	ρ / 10^3 kg m^{-3}	$V_\phi^\ominus$ / 10^{-6} m^3 mol^{-1}	m_A / mol kg^{-1}	ρ / 10^3 kg m^{-3}	$V_\phi^\ominus$ / 10^{-6} m^3 mol^{-1}
T = 308.15 K					
m_H = 0.00 mol kg^{-1}, $\delta\rho$ = 4.58×10^{-4} kg m^{-3}			m_H = 0.05 mol kg^{-1}, $\delta\rho$ = 3.92×10^{-4} kg m^{-3}		
0.00	0.9940	–	0.00	0.9975	–
0.02	0.9946	73.33	0.02	0.9981	73.18
0.04	0.9952	73.29	0.04	0.9986	75.66
0.06	0.9958	73.25	0.06	0.9991	76.46
0.08	0.9964	73.20	0.08	0.9996	76.83
0.10	0.9970	73.16	0.10	1.0001	77.05
m_H = 0.10 mol kg^{-1}, $\delta\rho$ = 3.99×10^{-4} kg m^{-3}			m_H = 0.15 mol kg^{-1}, $\delta\rho$ = 3.89×10^{-4} kg m^{-3}		
0.00	0.9991	–	0.00	1.0002	–
0.02	0.9996	78.13	0.02	1.0007	78.07
0.04	1.0002	75.58	0.04	1.0013	75.53
0.06	1.0007	76.38	0.06	1.0018	76.32
0.08	1.0012	76.75	0.08	1.0023	76.70
0.10	1.0017	76.97	0.10	1.0027	77.91
T = 313.15 K					
m_H = 0.00 mol kg^{-1}, $\delta\rho$ = 4.58×10^{-4} kg m^{-3}			m_H = 0.05 mol kg^{-1}, $\delta\rho$ = 4.16×10^{-4} kg m^{-3}		
0.00	0.9922	–	0.00	0.9960	–
0.02	0.9928	73.41	0.02	0.9965	78.29
0.04	0.9934	73.37	0.04	0.9971	75.73
0.06	0.9940	73.32	0.06	0.9976	76.53
0.08	0.9946	73.28	0.08	0.9982	75.65
0.10	0.9952	73.24	0.10	0.9987	76.11
m_H = 0.10 mol kg^{-1}, $\delta\rho$ = 3.89×10^{-4} kg m^{-3}			m_H = 0.15 mol kg^{-1}, $\delta\rho$ = 3.91×10^{-4} kg m^{-3}		
0.00	0.9972	–	0.00	0.9988	–
0.02	0.9977	78.23	0.02	0.9993	78.14
0.04	0.9983	75.67	0.04	0.9998	78.11
0.06	0.9988	76.47	0.06	1.0004	76.39
0.08	0.9993	76.85	0.08	1.0009	76.77
0.10	0.9997	78.07	0.10	1.0013	77.99
T = 318.15 K					
m_H = 0.00 mol kg^{-1}, $\delta\rho$ = 4.58×10^{-4} kg m^{-3}			m_H = 0.05 mol kg^{-1}, $\delta\rho$ = 3.89×10^{-4} kg m^{-3}		
0.00	0.9902	–	0.00	0.9943	–
0.02	0.9908	73.50	0.02	0.9948	78.38
0.04	0.9914	73.45	0.04	0.9954	75.81
0.06	0.9920	73.41	0.06	0.9959	76.61
0.08	0.9926	73.37	0.08	0.9964	77.00
0.10	0.9932	73.32	0.10	0.9968	78.23

TABLE II. Continued

m_A / mol kg^{-1}	ρ / 10^3 kg m^{-3}	V_ϕ^0 / 10^{-6} m^3 mol^{-1}	m_A / mol kg^{-1}	ρ / 10^3 kg m^{-3}	V_ϕ^0 / 10^{-6} m^3 mol^{-1}
T = 318.15 K					
m_H = 0.10 mol kg^{-1}, $\delta\rho$ = 3.91×10^{-4} kg m^{-3}			m_H = 0.15 mol kg^{-1}, $\delta\rho$ = 3.82×10^{-4} kg m^{-3}		
0.00	0.9955	–	0.00	0.9972	–
0.02	0.9960	78.32	0.02	0.9977	78.23
0.04	0.9965	78.28	0.04	0.9982	78.19
0.06	0.9971	76.55	0.06	0.9987	78.15
0.08	0.9976	76.94	0.08	0.9992	78.11
0.10	0.9980	78.16	0.10	0.9997	78.07

TABLE III. Values of standard partial molal volume, $V_\phi^\ominus$ / 10^{-6} m^3 mol^{-1}, of 4-aminobutyric acid in aqueous metformin hydrochloride (m_H – molality of metformin hydrochloride; standard error is given in parentheses)

T / K	m_H / mol kg^{-1}				Literature
	0.0	0.05	0.10	0.15	
308.15	73.25	75.84	76.76	76.91	74.18[24,25], 71.6[26]
	(0.00)	(0.85)	(1.10)	(1.29)	
313.15	73.32	76.46	77.06	77.48	74.1[27], 72.8[26]
	(0.00)	(0.99)	(1.30)	(0.09)	
318.15	73.41	77.21	77.65	78.15	–
	(0.00)	(1.31)	(0.96)	(0.00)	

The standard partial molal volume of transfer, $\Delta V_\phi^\ominus$, for 4-aminobutyric acid for pure water and for the metformin hydrochloride–water mixtures were calculated using Eq. (3):

$$\Delta V_\phi^\ominus = \Delta V_\phi^\ominus \text{ (in a mixture)} - \Delta V_\phi^\ominus \text{ (in pure water)} \quad (3)$$

The results are given in Table IV. It can be seen from Tables III and IV that the values of $V_\phi^\ominus$ and $\Delta V_\phi^\ominus$ for 4-aminobutyric acid are positive and increase monotonically with the molal concentration of metformin hydrochloride and temperature.

TABLE IV. Values of the standard partial molal volume of transfer, $\Delta V_\phi^\ominus$ / 10^{-6} m^3 mol^{-1}, of 4-aminobutyric acid in aqueous metformin hydrochloride solutions (m_H –molality of metformin hydrochloride)

T / K	m_H / mol kg^{-1}		
	0.05	0.10	0.15
308.15	2.59	3.51	3.66
313.15	3.14	3.74	4.16
318.15	3.80	4.24	4.74

The value of $V_\phi^\ominus$ is by definition free from solute–solute interaction and therefore provides information regarding solute–solvent interactions.[28] The posi-

tive $\Delta V_\phi^\ominus$ may be qualitatively interpreted as follows. It is well known that solute–solute interactions are absent at infinite dilution and therefore the observed standard partial molal volume of transfer $\Delta V_\phi^\ominus$ are due to the solute–solvent interactions. The nature of interactions between amino acids and metformin hydrochloride can be classified as follows:[29,30]

i) Ion–ion interactions between $C_4H_{11}N_5H^+$ of the co-solute and the COO^- group of AAs.

ii) Ion–ion interactions between Cl^- of the co-solute and the NH_3 group of AAs.

iii) Ion–non polar group interactions between the co-solute and AAs.

According to the co-sphere overlap model,[31] the first two types of interactions will produce positive $\Delta V_\phi^\ominus$ values, whereas the last type of interactions results in negative $\Delta V_\phi^\ominus$. The observed positive $\Delta V_\phi^\ominus$ values in this work can thus be related to the predominance of first two types of ion–ion interactions over the last ion–non polar interactions. Similar conclusions were drawn by Yan *et al.*[4] in their studies of AAs in aqueous $CaCl_2$ solutions. Due to the interactions between the ions in metformin hydrochloride and the zwitterionic centres of 4-aminobutyric acid, the electrostriction of the water molecules lying in the proximity of the NH_3^+ and the COO^- centres of the amino acids would be diminished and consequently lead to a positive volume contribution.[32,33] Alternatively the standard partial molal volume of the amino acid may be considered[34] to be the sum of van der Waal's volume (V_{VW}) and the volume associated with voids (V_S) or empty space minus the volume due to shrinkage (V_S) that arises due to the electrostriction of solvent caused by the hydrophilic groups present in the amino acid. The presence of metformin hydrochloride in water decreases the extent of the electrostriction caused by the amino acid, which results in a decrease in the shrinkage volume. Assuming that V_{VW} and V_V are not significantly affected by the presence of metformin hydrochloride, an increase in the $V_\phi^\ominus$ values and, hence, in the $\Delta V_\phi^\ominus$ values may be attributed to a decrease in the electrostriction effect. This electrostriction effect is reflected in the values of the hydration number, calculated using the standard equations in the literature,[35–38] which are listed in Table V. It should be noted here that the difference between the molal volume of electrostricted water, $V_E^\ominus$, and molar volume of bulk water, $V_B^\ominus$, at 308.15 K reported by Lark *et al.*[36] and Romero *et al.*[39] was used in the present calculations of n_H at all the studied temperatures. It can be seen from Table V that the hydration number n_H of the amino acid decreases with increasing concentration of metformin hydrochloride and of temperature, which again substantiate an increase in solute-co-solute interactions. Furthermore, this establishes the fact that metformin hydrochloride has a dehydration effect on 4-aminobutyric acid. Wadi and Ramasami[3] reported a similar decrease in n_H values for a few amino acids with increasing concentration of sodium sulphate and temperature.

TABLE V. Values of hydration number, n_H, of 4-aminobutyric acid in aqueous metformin hydrochloride solutions (m_H –molality of metformin hydrochloride; a – using $V_\phi^\ominus$(int) = = (0.7/0.6)$V_\phi^\ominus$(cryst); b – using $V_\phi^\ominus$(int) = (0.7/0.634) $V_\phi^\ominus$(cryst))

T / K	m_H / mol kg^{-1}					
	0.05		0.10		0.15	
	a	b	a	b	a	b
308.15	3.62	2.33	3.39	2.10	3.36	2.06
313.15	3.47	2.17	3.32	2.02	3.21	1.92
318.15	3.28	1.98	3.17	1.87	3.05	1.75

The transfer volumes of 4-aminobutyric acid may also be expressed by the McMillan Mayer theory[40] of solutions, which permits the formal separation of the effects due to interactions between pairs of solute molecules and those due to interactions between three or more solute molecules by the following equation.

$$\Delta V_\phi^\ominus = 2V_{AH}m_H + 3V_{AHH}m_H^2 + \ldots \quad (4)$$

where A stands for the amino acid and H stands for metformin hydrochloride. V_{AH} and V_{AHH} are the pair and triplet volumetric interaction parameters, respectively. Using the above equation, the volumetric interaction parameters were estimated and are given in Table VI. It can be seen that the V_{AH} values are positive while the V_{AHH} values are negative. The large positive V_{AH} values suggest domination of pair interactions for 4-aminobutyric acid over triplet volumetric interaction parameters. Similar reports are available in the literature by for some amino acids in aqueous solutions of $MgCl_2 \cdot 6H_2O$.[37]

TABLE VI. Values of pair and triplet interaction coefficients, V_{AH} and V_{AHH}, of 4-aminobutyric acid in aqueous metformin hydrochloride solutions

T / K	V_{AH} / 10^{-6} m^3 kg mol^{-2}	V_{AHH} / 10^{-6} m^3 kg^2 mol^{-2}
308.15	4.7542	–0.0405
313.15	4.8720	–0.0280
318.15	5.2224	–0.0192

The structure making/breaking property of the solute (AA) in aqueous metformin hydrochloride may be determined from the temperature dependence of the standard partial molal volume at infinite dilution. This study was further used to interpret the effect of the hydrocarbon chain on the structure of water using the general hydrophobicity criteria proposed by Hepler.[41] According to the criteria, the behaviour of the second derivative of the infinite dilution standard partial molal volume with temperature is related to the hydrophobic or hydrophilic character of the solute. When $\partial V_\phi^\ominus/\partial T > 0$ and $\partial^2 V_\phi^\ominus/\partial T^2 < 0$, the solute has hydrophilic character. However when $\partial V_\phi^\ominus/\partial T > 0$ and $\partial^2 V_\phi^\ominus/\partial T^2 < 0$, the solute has hydrophobic character.[42] In order to obtain the hydrophilic or hydrophobic character of 4-aminobutyric acid in aqueous metformin hydrochloride solutions, the

experimental values of $V_\phi^\ominus$ were related to temperature T using the following quadratic equation:[43]

$$V_\phi^\ominus = a + bT + cT^2 \quad (5)$$

The coefficients a, b and c were determined and Eq. (5) has the following forms for the amino acid at three concentrations of metformin hydrochloride reported in this work.

$$\begin{aligned} V_\phi^\ominus &= 288.52 - 1.4914\,T + 0.0026\,T^2 \text{ (for } m_H = 0.05) \\ V_\phi^\ominus &= 617.95 - 3.5435\,T + 0.0058\,T^2 \text{ (for } m_H = 0.10) \\ V_\phi^\ominus &= 234.78 - 1.1286\,T + 0.0020\,T^2 \text{ (for } m_H = 0.15) \end{aligned} \quad (6)$$

Thus, from Eq. (6), it can be observed that the values of $\partial^2 V_\phi^\ominus/\partial T^2$ are positive for all three concentrations of metformin hydrochloride, indicating the structure-making ability of 4-aminobutyric acid in aqueous metformin hydrochloride solutions.[44] This further supports the supposition that the charged end groups of amino acids are the predominant factors for the temperature dependence of $V_\phi^\ominus$ values of amino acid.

The viscosity data obtained in both water and aqueous metformin hydrochloride solutions as a function of the amino acid concentration and the temperature:

$$\eta_r = \eta / \eta_0 \quad (7)$$

are given in Table VII, where η and η_0 are the viscosities of the solution and solvent, respectively.

The viscosity B-coefficients were evaluated by fitting the η_r values to the Jones–Dole Equation by the least squares method[17] as follows:

$$\eta_r = \eta / \eta_0 = 1 + Bc \quad (8)$$

where c is the molar concentration (calculated from the molality data). The values of viscosity B-coefficient are summarized in Table VIII.

TABLE VII. Values of viscosity (η / mPa s) of 4-aminobutyric acid in aqueous metformin hydrochloride solutions (m_H – molality of metformin hydrochloride; m_A – molality of amino acid)

m_A / mol kg^{-1}	m_H / mol kg^{-1}			
	0.00	0.05	0.10	0.15
	T = 308.15 K			
0.00	0.718	0.728	0.739	0.750
0.02	0.723	0.730	0.741	0.752
0.04	0.728	0.737	0.749	0.760
0.06	0.731	0.740	0.752	0.764
0.08	0.735	0.744	0.756	0.768
0.10	0.742	0.750	0.762	0.773

TABLE VII. Continued

m_A / mol kg^{-1}	m_H / mol kg^{-1}			
	0.00	0.05	0.10	0.15
		T = 313.15 K		
0.00	0.653	0.661	0.675	0.680
0.02	0.655	0.663	0.678	0.683
0.04	0.660	0.669	0.684	0.689
0.06	0.662	0.672	0.687	0.692
0.08	0.666	0.676	0.690	0.696
0.10	0.672	0.681	0.696	0.701
		T = 318.15 K		
0.00	0.597	0.607	0.613	0.622
0.02	0.599	0.609	0.615	0.625
0.04	0.603	0.613	0.620	0.630
0.06	0.605	0.617	0.623	0.633
0.08	0.609	0.620	0.626	0.636
0.10	0.614	0.624	0.631	0.641

TABLE VIII. Values of the viscosity B-coefficient (B / 10^{-3} m^3 mol^{-1}) of 4-aminobutyric acid in water and in aqueous metformin hydrochloride (m_H – molality of metformin hydrochloride; standard error is given in parentheses)

T / K	m_H / mol kg^{-1}				Literature
	0.00	0.05	0.10	0.15	
308.15	0.315	0.3187	0.3236	0.3330	0.299[45],
	(0.023)	(0.027)	(0.021)	(0.025)	0.316[46]
313.15	0.310	0.3143	0.3187	0.3283	0.285[46]
	(0.028)	(0.020)	(0.028)	(0.017)	
318.15	0.306	0.3096	0.3142	0.3247	–
	(0.024)	(0.009)	(0.019)	(0.021)	

The literature viscosity B-coefficient values for 4-aminobutyric acid in water are also given in Table VII for comparison. There is close agreement between the viscosity B-coefficient values reported in this work with literature values.

Viscosity B-coefficients are important for a number of reasons.[47] Their application in two research areas is of interest. First, the viscosity B-coefficient provides information about the solvation of solutes and its effects on the structure of the solvent in the near environment of the solute molecules. Furthermore, some activation parameters of viscous flow can be obtained using the viscosity B-coefficient. The viscosity B-coefficient, originally introduced as an empirical term, was found to depend on solute–solvent interactions and on the relative size of the solute and solvent molecules.[48] Larger and positive viscosity B-coefficient values indicate a structure making action (hydrophobic and hydrogen bonded actions) of the solute on solvents.[22] It can be seen from Table VIII that the viscosity B-coefficient values are positive, indicating the structure-making ability of

4-aminobutyric acid and the presence of strong ion–solvent interactions. The viscosity *B*-coefficient values decrease with increasing temperature; hence, their temperature derivatives[49], *i.e.*, d*B*/d*T*, are negative. The sign of d*B*/d*T* gives the information of structure making/breaking property of the solute in the solvent media,[50] rather than simply the viscosity *B*-coefficient. It can be seen from Table VIII that d*B*/d*T* are negative for 4-aminobutyric acid, thereby showing the structure-making ability of amino acid. Thus, 4-aminobutyric acid can be classified as a structure maker in aqueous metformin hydrochloride solutions. The charged groups of the amino acid in the present investigation electrostatically influenced the surrounding water, resulting in the formation of a solvent structure through hydrophobic hydration. These conclusions are in excellent agreement with the conclusions drawn from $\partial^2 V_\phi^\ominus/\partial T^2$ discussed earlier.

In order to obtain the relationship between the viscosity *B*-coefficient and free energy activation parameters, the Eyring simple model[51] was followed, wherein the molecules move one-by-one from their equilibrium positions through their transition-states, in which intermolecular bonds are stretched, to other equilibrium positions. For a pure liquid, it was found that:[51]

$$\eta_0 = (hN_A/\overline{V}_1^\ominus)\exp(\Delta\mu_1^{\ominus *}/RT) \quad (9)$$

where h is the Planck constant, N_A is the Avogadro's number, η_0 is the viscosity of the solvent, R is the gas constant and $\Delta\mu_1^{\ominus *}$ is the contribution per mole of solvent to the free energy of activation for viscous flow of the solution. When a solution flows, both the solute and the solvent molecules move under the shearing force. The activation energy per mole of solution can be written:

$$\Delta G^{\ominus *} = x_1\Delta\mu_1^{\ominus *} + x_2\Delta\mu_2^{\ominus *} \quad (10)$$

where x_1 and x_2 are the mole fraction of the solvent and solute, respectively. $\Delta\mu_2^{\ominus *}$, as defined by Eq. (10), includes any change in the free energy of activation of the solvent molecules caused by the presence of the solute, as well as the contribution from the movement of the solute itself. According to the Feakins *et al.*,[52] the viscosity *B*-coefficient is related to $\Delta\mu_2^{\ominus *}$ by Eq. (11):

$$B = (\overline{V}_1^\ominus - \overline{V}_2^\ominus)/1000 + (\overline{V}_1^\ominus/1000)(\Delta\mu_2^{\ominus *} - \Delta\mu_1^{\ominus *})/\mathrm{RT} \quad (11)$$

Eq. (11) can be rearranged to give:

$$\Delta\mu_2^{\ominus *} = \Delta\mu_1^{\ominus *} + RT/(1000B - (\overline{V}_1^\ominus - \overline{V}_2^\ominus)) \quad (12)$$

where $\overline{V}_1^\ominus = \Sigma x_i M_i/\rho$ is the mean volume of the solvent and $\overline{V}_2^\ominus$ ($V_\phi^\ominus$) is the standard partial molal volume of the solute at infinite dilution. The terms x_i and M_i denote the mole fractions and molecular weights of water (1) and metformin hydrochloride (2). The calculated values of $\Delta\mu_1^{\ominus *}$, $\Delta\mu_2^{\ominus *}$and $\overline{V}_1^\ominus$ are given in Table IX.

TABLE IX. Values of activation free energy of the solvent, $\Delta\mu_1^{\ominus *}$, solute, $\Delta\mu_2^{\ominus *}$, and mean molal volume of the solvent $V_\phi^\ominus$ of aqueous metformin hydrochloride solutions (m_H – molality of metformin hydrochloride)

m_H / mol kg^{-1}	$\Delta\mu_1^{\ominus *}$/ kJ mol^{-1}	$\Delta\mu_2^{\ominus *}$/ kJ mol^{-1}	$V_\phi^\ominus$/ 10^{-6} m^3 mol^{-1}
		T = 308.15 K	
0.00	26.629	78.955	18.123
0.05	26.671	79.574	18.193
0.10	26.723	80.136	18.296
0.15	26.776	81.277	18.409
		T = 313.15 K	
0.00	26.814	79.180	18.156
0.05	26.858	80.047	18.220
0.10	26.908	80.415	18.331
0.15	26.961	81.623	18.434
		T = 318.15 K	
0.00	27.013	79.534	18.193
0.05	27.064	80.391	18.251
0.10	27.106	80.879	18.363
0.15	27.161	82.015	18.464

It may be seen from Table IX that the values of $\Delta\mu_2^{\ominus *}$ are positive and larger than $\Delta\mu_1^{\ominus *}$, indicating the structure-making ability of the solute[52] (namely the amino acid) in aqueous metformin hydrochloride, again supplementing the earlier findings through the $\partial^2 V_\phi^\ominus/\partial T^2$ and dB/dT studies. Furthermore, the larger $\Delta\mu_2^{\ominus *}$ values indicate the presence of stronger ion–solvent interactions. In other words, the formation of the transition state is less favoured in the presence of the amino acid. This means that the formation of the transition state is accompanied by the rapture and distortion of the intermolecular forces in the solvent structure. Similar results were obtained by Mishra *et al.*[53] for glycine in aqueous solutions of transition metal chlorides.

According to transition state theory,[46] every solvent molecule in one mole of solution must pass through the transition state and interact more or less strongly with solute molecules. The activation free energy $\Delta\mu_2^{\ominus *}$ includes the free energy of transfer of solute from the ground state to the transition state solvents ($\Delta G_2^\ominus(1\rightarrow 1')$) and the free energy of the solute through its own viscous transition state ($\Delta G_2^\ominus(2\rightarrow 2')$). The values ($\Delta G_2^\ominus(1\rightarrow 1')$) may be calculated using methods similar to those reported elsewhere.[18,52] These values are given in Table X.

The positive $\Delta\mu_2^{\ominus *}$ and $\Delta G_2^\ominus(1\rightarrow 1')$ values are larger than the $\Delta\mu_2^{\ominus *}$ values. Furthermore, both $\Delta\mu_2^{\ominus *}$ and $\Delta G_2^\ominus(1\rightarrow 1')$ increase with increasing concentration of the co-solute, as well as with increasing temperature. This suggests that the formation of transition state is less favoured in the presence of amino acids. This is due to the breaking and distortion of intermolecular bonds, which effectively means that more solute–solvent bonds must be broken to form the transition

state. Similar reports are available in literature for α-amino acids in aqueous sodium acetate solution.[53]

TABLE X. Values of the thermodynamic activation parameter transfer ($\Delta G_2^{\ominus}(1\rightarrow1')$ / kJ mol^{-1}) of 4-aminobutyric acid from the ground state to the transition state in aqueous metformin hydrochloride solutions

T / K	m_H / mol kg^{-1}			
	0.00	0.05	0.10	0.15
308.15	52.326	52.903	53.413	54.501
313.15	52.366	53.189	53.507	54.662
318.15	52.521	53.327	53.773	54.854

CONCLUSION

In summary, volumetric and viscometric data are reported for 4-aminobutyric acid in different concentrations of aqueous metformin hydrochloride solutions. The standard partial molal volume $V_{\phi}^{\ominus}$, standard partial molal volume of transfer $V_{\phi}^{\ominus}$, hydration number n_H, second derivative of the standard partial molal volume at infinite dilution with temperature $\partial^2 V_{\phi}^{\ominus}/\partial T^2$ were determined and are reported. These results showed that 4-aminobutyric acid acts as structure maker in aqueous metformin hydrochloride solutions and that strong solute–solvent interactions occur in the reported systems. The viscosity B-coefficient, variation of the viscosity B-coefficient with temperature, dB/dT and the free energy of activation per mole of solute, $\Delta\mu_2^{\ominus *}$, values were also calculated and reported. These results also confirmed the structure-making ability of 4-aminobutyric acid in aqueous metformin hydrochloride.

NOMENCLATURE

List of symbols

B	Viscosity B-coefficient (dm^3 mol^{-1})
C	Molarity of the amino acid (mol dm^{-3})
h	The Planck constant
m	Molality of the amino acid
M	Molar mass of the amino acid
n_H	Hydration number
N_A	Avogadro's number
R	Universal gas constant (8.31441m^3 Pa mol^{-1} K^{-1})
S_V	Slope in Eq. (2)
t	Flow time of solution in viscometer
T	Temperature (K)
V_{ϕ}	Partial molal volume of the amino acid
$V_{\phi}^{\ominus}$	Standard partial molal volume of the amino acid
$V_1^{\ominus}$	Standard mean volume of the solvent
$V_2^{\ominus}$	Standard partial molal volume of the solute
$V_B^{\ominus}$	Standard partial molal volumes of water in the hydration shell of a solution

$V_E^{\ominus}$ Standard partial molal volumes of water in the bulk state
$\Delta V_\phi^{\ominus}$ Standard partial molal volume of transfer for the amino acid

Greek letters

η Viscosity (mPa s)
ρ Density (kg m^{-3})
$\Delta\mu_1^{\ominus *}$ Standard free energy of activations for viscous flow of solvent
$\Delta\mu_2^{\ominus *}$ Standard free energy of activations for viscous flow of solution

Subscripts

1 Binary solvent property
2 Solute property

ИЗВОД

ВОЛУМЕТРИЈСКЕ ОСОБИНЕ И ВИСКОЗНОСТ 4-АМИНОБУТЕРНЕ КИСЕЛИНЕ У ВОДЕНОМ РАСТВОРУ МЕТФОРМИН ХИДРОХЛОРИДА НА 308,15, 313,15 И 318,15 K

K. RAJAGOPAL[1] и S.S. JAYABALAKRISHNAN[2]

[1]*Department of Physics, Government College of Engg. Tirunelveli-627007 Tamil Nadu и*
[2]*Department of Physics, P.S.R. Engg. College, Sivakasi, Tamil Nadu, India*

Извршена су мерења густина (ρ) и вискозности (η) 4-аминобутерне киселине у 0,05, 0,10 и 0,15 M воденом раствору метформин хидрохлорида на 308,15, 313,15 и 318,15 K. Измерене вредности густина и вискозности су коришћене за израчунавање особина смеса, као што су парцијална моларна запремина V_ϕ, стандардна парцијална моларна запремина $V_\phi^{\ominus}$, стандардне парцијалне моларне запремине прелаза $\Delta V_\phi^{\ominus}$, хидрацијског броја n_H, другог извода парцијалне моларне запремине при бесконачном разблажењу са температуром $\partial^2 V_\phi^{\ominus}/\partial T^2$, коефицијента вискозности B, промену B са температуром dB/dT, слободне енергије активације по молу растварача $\Delta\mu_1^{\ominus *}$ и растворене амино киселине $\Delta\mu_2^{\ominus *}$ у тернерном систему. Резултати су интерпретирани са аспекта интеракција растворак–растворак и растворак–растварач и могућности настанка/разградње структура растворка у испитиваним растворима.

(Примљено 16. јуна 2009, ревидирано 21. септембра 2010)

REFERENCES

1. A. Ali, S. Hyder, S. Sabir, D. Chand, A. K. Nain, *J. Chem. Thermodyn.* **38** (2006) 136
2. A. Ali, S. Khan, F. Nabi, *J. Serb. Chem. Soc.* **72** (2007) 495
3. R. K. Wadi, P. Ramasami, *J. Chem. Soc. Faraday. Trans.* **93** (1997) 243
4. Z. Yan, J. Wang, W. Kong, J. Lu, *Fluid Phase Equilib.* **215** (2004) 143
5. T. S. Banipal, G. Sehgal, *Thermochim. Acta* **265** (1995) 175
6. Z. Yan, J. Wang, W. Kong, J. Lu, *Fluid Phase Equilib.* **215** (2004) 130
7. A. Soto, A. Arce, K. Mohammed, *Biophys. Chem.***74** (1998) 165
8. M. Iqbal, T. Ahmed, *Indian J. Chem.* **32A** (1993) 119
9. K. Rajagopal, S. S. Jayabalakrishnan, *Chin. J. Chem. Eng.* **17** (2009) 796
10. L. D. Hu, Y. Liu, X. Tang, Q. Zhang, *Eur. J. Pharm. Sci.* **64** (2006) 185
11. G. Corti, M. S. Lirri, F. Maestrelli, N. Manine, P. Mura, *Eur. J. Pharm. Sci.***68** (2008) 303
12. K. Rajagopal, S. S. Jayabalakrishnan, *J. Pure. Appl. Ultrason.* **28** (2006) 81
13. D. P. Kharakoz, *Biophys. Chem.* **34** (1989) 115

14. D. P. Kharakoz, *Biochem.* **36** (1997) 10276
15. M. Sakurai, T. Nakumaura, N. Takenaka, *Bull. Chem. Soc. Jpn.* **67** (1994) 352
16. M. Kikuchi, M. Sakurai, N. Nitta, *J. Chem. Eng. Data* **41** (1996) 1439
17. G. Jones, M. Dole, *J. Am. Chem. Soc*. **51** (1929) 2950
18. B. S. Lark, P. Patyar, T. S. Banipal, *J. Chem. Thermodyn.* **39** (2007) 344
19. Z. Yan, J. Wang, J. Lu, *Biophys. Chem.* **99** (2002) 199
20. A. Pal, S. Kumar, *Indian J. Chem.* **44A** (2005) 469
21. J. A. Reddick, W. B. Bunger, T. K. Sakano, *Organic solvents*, Vol. II, 4th ed., Wiley Interscience, New York, 1986
22. X. Ren, X. Hu, R. Lin, H. Zong, *J. Chem. Eng. Data* **43** (1998) 700
23. Z. Yan, J. Wang, W. Kong, J. Lu, *Fluid Phase Equilib.* **215** (2004) 143
24. R. Bhat, J. C. Ahulwalia, *J. Phys. Chem.* **89** (1985) 1099
25. M. N. Islam, R. K. Wadi, *Phys. Chem. Liq.* **41** (2003) 533
26. R. K. Wadi, R. K. Goyal, *J. Solution Chem*. **21** (1992) 163.
27. M. M. Bhattaacharyya, M. Sengupta, *J. Indian Chem. Soc.* **62** (1985) 959
28. T. V. Chalikian, A. V. Sarvazyan, K. J. Breslauer, *J. Phys. Chem.* **97** (1993) 13017
29. K. Belibagli, E. Ayranci, *J. Solution. Chem.* **19** (1990) 867
30. R. Bhat, N. Kishore, J. C. Ahluwalia, *J. Chem. Faraday Trans. 1* **84** (1988) 2651
31. S. Li, W. Sang, R. Lin, *J. Chem. Thermodyn.* **34** (2002) 1761
32. H. L. Friedman, C. V. Krishnan, in *Water: A comprehensive Treatise*, Vol. 3, F. Franks, Ed., Plenum Press, New York, 1973, p. 1
33. Q. Liu, X. Hu, R. Lin, W. Sang, S. Li, *J. Chem. Eng. Data* **46** (2001) 522
34. C. Zhao, P. Ma, J. Lu, *J. Chem. Thermodyn.* **37** (2005) 37
35. M. Natarajan, R. K. Wadi, H. C. Gaur, *J. Chem. Eng. Data* **35** (1990) 87
36. F. Franks, M. A. Quickenden, D. S. Reid, B. Watson, *Trans Faraday. Soc.* **66** (1970) 582
37. B. S. Lark, P. Patyar, T. S. Banipal, *J. Chem. Thermodyn.* **38** (2006) 1592
38. A. Pal, K. Kumar, *J. Mol. Liq.* **121** (2005) 148
39. F. J. Millero, G. K. Ward, F. K. Lepple, E. V. Hoff, *J. Phys. Chem.* **78** (1974) 1636
40. C. M. Romero, F. Negrete, *Phys. Chem. Liq.* **42** (2004) 261
41. W. G. McMillan, J. E. Mayer, *J. Chem. Phys.* **13** (1945) 276
42. L. Hepler, *Can. J. Chem.* **47** (1969) 4613
43. *Water A: Comprehensive Treatise*, Vol. IV, F. Franks, Ed., Plenum Press, New York, 1978
44. A. Pal, S. Kumar, *J. Mol. Liq.* **109** (2004) 23
45. B. S. Lark, P. Patyar, T. S. Banipal, N. Kishore, *J. Chem. Eng. Data* **49** (2004) 553
46. R. K. Wadi, R. K. Goyal, *J. Chem. Eng. Data* **37** (1992) 377
47. M. M. Bhattacharyya, M. Sengupta, *Z. Phys. Chem. (N.F.)* **133** (1982) 79
48. H. D. B. Jenkins, Y. Marcus, *Chem. Rev.* **95** (1995) 2695
49. T. C. Bai, G. B. Yan, *Carbohydr. Res.* **338** (2003) 2921
50. J. M. Tsangins, R. B. Martin, *Arch. Biochem. Biophys.* **112** (1965) 267
51. T. S. Sharma, J. C. Ahluwalia, *Chem. Soc. Rev.* **2** (1973) 203
52. S. Glasstone, K. Laidler, H. Eyring, *The Theory of Rate Processes*, McGraw Hill, New York, 1941, p. 477
53. D. Feakins, F. M. Bates, W. E. Waghorne, K. G. Lawrence, *J. Chem. Soc. Faraday Trans.* **89** (1993) 3381
54. A. P. Mishra, S. K. Gautam, *Indian J. Chem. A* **40** (2001) 100.

Journal of the Serbian Chemical Society
JSCS-info@shd.org.rs • www.shd.org.rs/JSCS
J. Serb. Chem. Soc. *76* (1) 143–153 (2011) UDC 633.822+546.76+541.183+543.421:615.9
JSCS–4107 *Original scientific paper*

Analysis of the bioavailability of Cr(III) and Cr(VI) based on the determination of chromium in *Mentha piperita* by graphite furnace atomic absorption spectrometry

SVETLANA ĐOGO[1]*#, SLAVICA RAŽIĆ[1]#, DRAGAN MANOJLOVIĆ[2]# and LATINKA SLAVKOVIĆ[3]#

[1]*Institute of Analytical Chemistry, Faculty of Pharmacy, University of Belgrade, P. O. Box 146, 11211 Belgrade,* [2]*Faculty of Chemistry, University of Belgrade, 11000 Belgrade and* [3]*The Vinča Institute of Nuclear Sciences, P. O. Box 522, 11522 Belgrade, Serbia*

(Received 1 April, revised 12 July 2010)

Abstract: *Mentha piperita* L. (*Lamiaceae*) was cultivated under the controlled laboratory conditions in the presence of varying levels of trivalent and hexavalent chromium in order to determine its capacity to control chromium uptake and its tolerance limit. The plants were grown in pots at 25 °C with controlled soil moisture (about 80 % of the water retention capacity). The soil was treated with increasing concentrations of $Cr(NO_3)_3$ (40, 80, 120, and 200 mg kg^{-1}) and $K_2Cr_2O_7$ (2.5, 5, 10, and 15 mg kg^{-1}). A control group of plants was grown without the addition of chromium to the soil. For each concentration, three acidity levels were tested: natural, one pH unit below and one above the natural acidity of the soil (pH_2 6, pH_1 5 and pH_3 7). The plant samples were digested according to the standard procedure and chromium content was determined by GFAAS. For all plants, the transportation index was calculated and the results (expressed in mg kg^{-1}) at pH_1, pH_2 and pH_3, respectively, were: 0.21–0.80, 0.06–1.06 and 0.04–0.52. The recoveries were good (72.73–115.3 %) as evidenced by the analysis of certified reference materials (NIST SRM 8433 – Corn Bran and NIST SRM 1547 – Peach Leaves). The mobility of chromium through the plants tissues is discussed in regard to its competition with iron and manganese for transport binding sites; hence Mn and Fe were also determined.

Keywords: chromium; GFAAS; uptake; translocation; toxicity; *Mentha piperita*.

INTRODUCTION

Environmental protection is of global importance and could be generally discussed in terms of anthropological and natural sources of pollution. Identification of sources followed with a systematic analytical approach is an acceptable mode

* Corresponding author. E-mail: sdjogo@pharmacy.bg.ac.rs
# Serbian Chemical Society member.
doi: 10.2298/JSC100401130D

of action, from which a real contribution could be expected. When chromium is concerned, anthropogenic sources are dominant and significantly contribute to environmental pollution.

The chemistry of chromium is very complex and its solubility and mobility in soils and its bioavailability strongly depend on the various oxidation states of this metal (from 0 to +6), its concentration, soil acidity, redox potential and salinity. Depending on its oxidation state and concentration, chromium acts as toxic or as an essential element for animals and humans. The two most common chromium species are Cr(III) and Cr(VI) in its anionic forms as chromate, dichromate and hydrochromate ions. Cr(III) is essential for animals and humans at low concentrations. It is very stabile in soils, but commonly well immobilized on iron and manganese oxides and hydroxides or complexed to organic matter. The toxicity of Cr(VI) depends strongly on its concentration in the soil as its uptake mechanism is based mainly on passive diffusion. It is still questionable if the trivalent chromium is essential for plants, but at high concentrations it definitely inhibits plants growth while a certain decrease in the activity of the immune system was observed in humans.[1] Toxicity is connected with solubility and, from this point of view, ammonium and alkaline metal salts of chromic acid, as very soluble species in the soil, should be recognized These species are toxic for plants, animals and humans. Symptoms of Cr(VI) toxicity in humans include skin irritation, gastric distress and liver damage. In addition some species formed in the reduction process from hexavalent to trivalent chromium contribute to the cytotoxicity, genotoxicity and carcinogenicity of Cr(VI). The uptake mechanism of this chromium species is active transport, probably correlated with the sulfate transport system of plasma membrane.[3,4]

In plants, chromium reduces the content of proteins, inhibits the activity of enzymes activity, decreases plant growth, and causes chlorosis and necrosis.[5] Barcelo *et al.* found a high correlation between the concentration of chlorophyll pigments and iron uptake in chromium stressed plants.[6] Many authors have reported about the negative effects of chromium on iron and manganese absorption.[2,7–10] Chromium is known to compete with both these metals for transport binding sites.

The relationships between chromium concentrations and contamination of the soil and its concentration in plants are extremely important, not only from the aspect of its influence on plant growth and capacity of plant accumulation, but also for potential toxicity for humans. Chromium accumulated in medical plants enters the food chain and, in this way, increases the potential health risk.

The main objectives of this study were to analyze the bioavailability of two chromium species (Cr^{3+} and the chromate) in contaminated soil and its potential uptake by *Mentha piperita*. Additionally, the influence of the two species on iron and manganese absorption was also investigated. The importance of soil acidity

to chromium mobilization and accumulation was recognized and a systematic empirical approach in the experimental design was developed. For this purpose, *M. piperita* was cultivated under controlled laboratory conditions, on the soils at different acidity levels, treated with Cr^{3+} and $Cr_2O_7^{2-}$. The conducted study was also aimed at elucidating the accumulation and translocation of chromium from the root to the upper plants parts. The obtained results were expected to enable the determination of the tolerance levels for *M. piperita* and also the chromium concentrations when the symptoms of toxicity become visible.

EXPERIMENTAL

Solutions and reagents

All employed reagents were of analytical grade. Single and multi-element calibrant solutions were prepared from 1.0 g L^{-1} *p.a.* stock solutions (Merck, Germany). For the microwave-assisted acid digestion, HNO_3 65 %, *p.a.* (Baker, Holland) and H_2O_2 30 %, *p.a.* (Merck, Germany) were used. The chromium solutions were prepared from reagent grade salts, $Cr(NO_3)_3$ (Fluka, Switzerland) and $K_2Cr_2O_7$ (Merck, Germany). All solutions were prepared with deionized water (Milli-Q system: resistivity 18.2 MΩ cm, TOC < 10 μg L^{-1}).

Soil characterization and preparation procedure

Soil was collected from the plantation of the Institute "Dr Josif Pančić" in Pančevo. The sampling procedure, as well as the measurement of acidity (model HI 9017 pH Meter, Hanna Instruments) were realized according to a procedure presented elsewhere.[11] The measured natural acidity was pH 5.98. The analyzed soil was poorly calcareous. Carbonates were determined by the Scheibler test* and calculated as $CaCO_3$, 0.16 %. The humus content (2.67 %) was determined by the method described by Tjurin and modified by Simakov[12] and total organic carbon (*TOC*) (2.97 %) by an official procedure for waste, sludge and sediments.**

Additionally, the retention water capacity (*RWC*) and the amount of acid (0.10 M HCl) and alkaline (0.10 M NaOH) required to adjust the pH by ±1, using the corresponding buffer curves for soil, were determined.

About 1.5 kg of air-dried soil was weighed and kept in plastic pots with a hole in the bottom to enable drainage. Then, *M. piperita* was planted in each pot.

Plant cultivation and treatment

The rhizomes of *M. piperita L. (Lamiaceae)* were sampled in a field of the Institute for Medical Plant Research "Dr Josif Pančić" in Pančevo. The plants were cultivated at a temperature of about 25 °C under laboratory conditions and natural light. The soil moisture was maintained at about 80 % of the retention water capacity (*RWC*). When the plant specimens had developed and were about 10 cm in height, the soil was treated with increasing concentrations of $Cr(NO)_3$ (40, 80, 120, and 200 mg kg^{-1}) and $K_2Cr_2O_7$ (2.5, 5, 10, and 15 mg kg^{-1}). These concentration levels were selected to obtain two levels below and two above the maximal allowable concentration (*MAC*) for Cr(III) and additionally two levels below and two above the toxic level of 5 mg kg^{-1} for plants.[5,8] Control plants were grown in soil without the

* NEN5757, 1991. The Scheibler test determination of carbonate concentration in soils. Volumetric method (in Dutch). Normalisatie Instituut, Delft, The Netherlands.

** Draft European Standard procedure (chemical analyses – determination of total organic carbon (*TOC*) in waste, sludges and sediments, Method B (direct method), document type: Draft European Standard, STD Version 2.1a (20020903), 2004.

addition of chromium. For each concentration level, sets of three additional samples were prepared at three acidity levels: natural, one pH-unit below and one above the natural acidity of the soil using buffer curves obtained for acid (0.10 M HCl) and alkaline (0.10 M NaOH) conditions.[13] With a natural acidity of pH 5.98, pH 5.00 and pH 7.00 were selected for the experiments.

Sample preparation

After sampling, the plants were separated into herbal parts and roots. Each part was washed, first with tap and then with distilled water and dried. Further sample preparation was applied as described elsewhere.[11,13] For the microwave-assisted acid digestion of the plant samples, the SW-846 EPA Method 3052 was applied.[14] A mixture of an accurately weighed amount of plant sample (*ca*., 0.4 g), 12 ml of 65 % HNO_3 and 4 ml of 30 % H_2O_2, after waiting 10 min for the first vigorous chemical reaction to subside, were digested according to the temperature program presented elsewhere.[11,13] After cooling, the samples were filtered through 0.45 µm Millipore filters. The solutions were quantitatively transferred into 50-ml volumetric flasks and diluted to volume with deionized water.

Instrumental and operating conditions

The determinations of iron and manganese were performed on a Perkin–Elmer Model 5000 atomic absorption spectrophotometer, under optimized measurement conditions using suitable hollow cathode lamps. The signals were measured with background correction (deuterium lamp) at the optimal flame (A–Ac) height.[11,13]

The determination of Cr in all soil and plants extracts was performed using a Perkin–Elmer model 5000 atomic absorption spectrophotometer with a graphite furnace HGA 400 Automatic Burner Control, with pyrollytic graphite tubes and temperature programs presented elsewhere.[11,13]

External calibration was applied for the determination of the metals and the corresponding regression equations were calculated as follows: for Cr, $y = 0.0033x + 0.062$; for Fe, $y = = 0.0437x + 0.0001$ and for Mn, $y = 0.1567x + 0.0016$. The correlation coefficients were in the r^2 range 0.989–0.999.

The good reproducibility of results was proved by the relative standard deviations (*RSD*) values of up to 2 %. All the results presented in Table I represent the average of five sample measurements. The results were rounded up to the last figure associated with random error. The significance level, α, was 0.05. Data analysis was realized using Office Excel 2007.

Analysis of the certified reference materials

The accuracy of the methods applied for determination of Cr, Mn and Fe, after microwave-assisted acid digestion of plants and soil samples, was checked by analysis of SRMs and the obtained results are presented in Table I.

TABLE I. Analysis of the certified references materials

Element	NIST SRM 8433 – Corn Bran			NIST SRM 1547 – Peach Leaves		
	Found mg kg^{-1}	Certified value mg kg^{-1}	Recovery %	Found µg kg^{-1}	Certified value µg kg^{-1}	Recovery %
Cr	0.08	0.11	72.73	890	1000	89.0
Mn	2.10±0.42	2.55±0.29	82.35	113±8	98±3	115.3
Fe	15.7±1.7	14.8±1.8	106.08	199±12	218±14	91.28

Transportation index

The transportation index (*TI*, average Cr content in the herbal plant part, mg kg^{-1}/Cr content in the roots, mg kg^{-1}) was calculated to evaluate the ability of the plants to translocate metal from roots to the upper part of the plant.[13,15–17]

RESULTS AND DISCUSSION

Visible symptoms of chromium toxicity

Decreases in growth and symptoms of toxicity were observed after 18 days in plants cultivated on the soils treated with 120 and 200 mg kg^{-1} Cr(III) and 10 and 15 mg kg^{-1} Cr(VI) under all acidity conditions. After an additional 20 days, the leaves became brownish-red and a reduction of the number and size of leaves was also noticed. In the next 8 days, small necrotic areas were registered on the plants cultivated on the soil treated with 15 mg kg^{-1} Cr(VI). After an additional 5 days, the plant species became dry. In all plants, a poorly developed root system was found.

These observations are in accordance with some reported data.[5,7,9] With concentrations higher than 5 mg kg^{-1}, the hexavalent chromium damaged the root membranes because of its high oxidation power and caused changes in metabolic processes, such as a decrease in chlorophyll synthesis, chlorosis and inhibition of root and plant growth.[5,8,10]

Metal analysis

The concentrations of metals (Cr, Fe and Mn) in *M. piperita* plant samples cultivated on untreated and treated soils are presented in Figs. 1a–1c and in Tables II and III.

The obtained results (Figs. 1a–1c) show that uptake of chromium by *M. piperita* as relatively low from all soils treated with Cr(III) and Cr(VI), at all investigated pH values. This could be explained by the very good immobilization of chromium in the soil by iron and manganese hydroxides and oxides.[8,13] The total chromium content in the herbal part of the plants grown on soil with the native pH of ranged 0.137 to 2.425 mg kg^{-1} for Cr(III) and from 0.334 to 5.025 mg kg^{-1} for Cr(VI), and generally increased with increasing concentration of this metals in the soil (Fig. 1b).

The total Cr content in the roots of *M. piperita* at the native pH value of the soil was from 1.780 to 4.715 mg kg^{-1} for Cr(III) and from 2.201 to 4.304 mg kg^{-1} for Cr(VI). The analysis of *M. piperita* showed several times higher concentrations of chromium in the roots than in the upper plant parts cultivated on soil treated with Cr(III) or Cr(VI), with exception of plants grown on the 10 mg kg^{-1} hexavalent chromium treated soil (Figs. 1a–1c). Zayed and Terry came to a similar conclusion about the ability of plants to hold more than 90 % of chromium in their roots.[8] The obtained results showed a better capacity of *M. piperita* to accumulate Cr in the roots than in the upper plant parts.

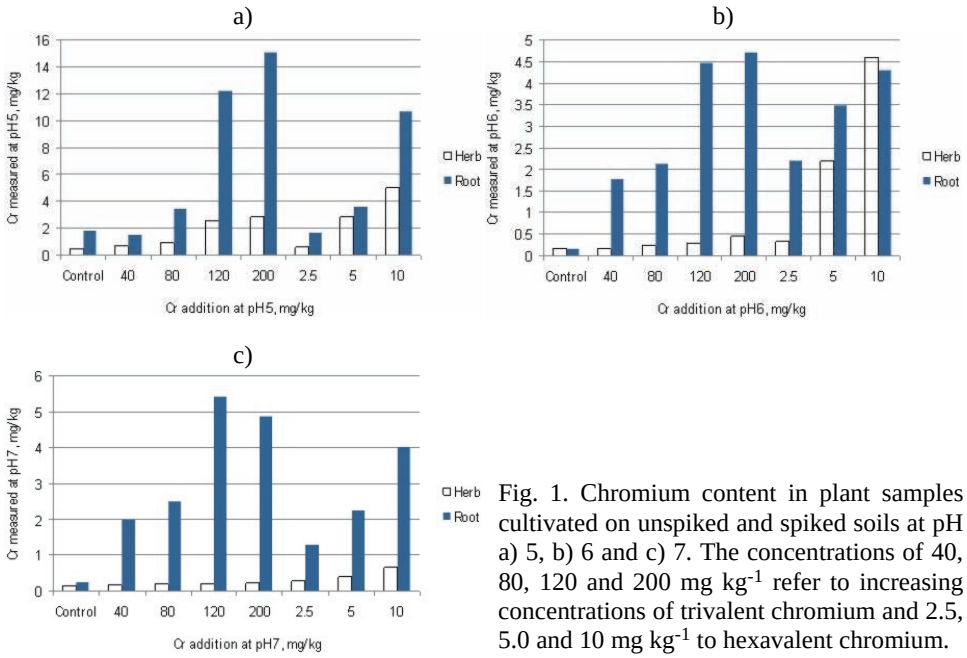

Fig. 1. Chromium content in plant samples cultivated on unspiked and spiked soils at pH a) 5, b) 6 and c) 7. The concentrations of 40, 80, 120 and 200 mg kg^{-1} refer to increasing concentrations of trivalent chromium and 2.5, 5.0 and 10 mg kg^{-1} to hexavalent chromium.

TABLE II. Iron and manganese contents in the herbal part of *M. piperita* cultivated on treated and untreated soils at three acidity levels, expressed in mg kg^{-1}

Sample	pH					
	Mn			Fe		
	6	5	7	6	5	7
$H_{(Control)}$	46.17	44.23	47.39	322.5	354.3	376.3
$H_{(40)}$[a]	44.64	45.32	30.95	320.2	355.6	383.0
$H_{(80)}$	42.68	69.00	29.48	297.4	320.9	356.4
$H_{(120)}$	49.24	68.82	27.57	297.4	318.2	349.9
$H_{(200)}$	52.96	41.78	32.75	263.0	367.3	333.3
$H_{(2.5)}$	42.80	43.88	21.42	345.6	356.4	367.7
$H_{(5)}$	53.15	36.14	34.59	320.0	378.2	358.0
$H_{(10)}$	61.25	51.89	30.05	408.6	368.4	374.3

[a]H(40)–H(200) and H(2.5)–H(10) – herbal (H) samples from the plants cultivated on soils spiked with increasing concentrations of trivalent chromium (40, 80, 120 and 200 mg kg^{-1}) and hexavalent chromium (2.5, 5.0 and 10 mg kg^{-1})

It is important to stress that plants cultivated on untreated soil at pH 6 had almost the same concentration in the roots and in the herbal part (Fig. 1b), but with increasing concentration of chromium in the soil, the transfer efficiency decreased which is in accordance with reported data.[8–110,15,18]

The calculated transportation indexes additionally supported the found poor translocation of chromium from the roots to the upper plant parts (Table IV). The

calculated values for *TI* were five times lower in the plants cultivated on the soil treated with Cr(III) than those cultivated on soil treated with Cr(VI). Higher values for *TI* were calculated for the plants cultivated on the soils treated with concentrations of 5 and 10 mg Cr(IV) kg^{-1}, when the symptoms of oxidative stress were observed. These results support a higher mobility of Cr(VI) through the plant tissues.

TABLE III. Iron and manganese contents the in root part of *M. piperita* cultivated on treated and untreated soils on three acidity levels, expressed in mg kg^{-1}

Sample	pH					
	Mn			Fe		
	6	5	7	6	5	7
$R_{(Control)}$	95.41	76.10	85.24	3363.7	4621.8	3778.4
$R_{(40)}$[a]	141.4	49.39	55.18	4588.0	4752.1	3834.6
$R_{(80)}$	118.0	71.14	55.19	3947.2	4509.4	3698.4
$R_{(120)}$	85.67	100.41	35.65	3329.4	4655.9	3714.6
$R_{(200)}$	75.22	59.84	48.86	2780.2	4312.3	3708.2
$R_{(2.5)}$	89.64	78.61	36.72	3457.9	4218.4	4017.1
$R_{(5)}$	44.64	49.55	47.55	4683.3	4682.6	3896.2
$R_{(10)}$	78.26	93.61	42.15	3785.9	4278.2	4103.5

[a]R(40)–R(200) and R(2.5)–R(10) – root (R) samples from the plants cultivated on the soils spiked with increasing concentrations of trivalent chromium (40, 80, 120 and 200 mg kg^{-1}) and hexavalent chromium (2.5, 5.0 and 10 mg kg^{-1})

TABLE IV. Transportation index (*TI*) for chromium in plants cultivated on untreated and spiked soils with chromium

Chromium species	Content, mg kg^{-1}	*TI*		
		pH		
		6	5	7
Control	0	0.99	0.23	0.52
Cr(III)	40	0.09	0.45	0.08
Cr(III)	80	0.12	0.27	0.07
Cr(III)	120	0.06	0.21	0.04
Cr(III)	200	0.10	0.19	0.05
Cr(IV)	2.5	0.15	0.34	0.23
Cr(IV)	5.0	0.63	0.80	0.18
Cr(IV)	10	1.06	0.47	0.17

Chromium uptake and transport are dependent on its chemical form and the hexavalent species is more mobile than the trivalent one.[1,2,17,18] Torrestday *et al.* reported that accumulation of chromium in the upper plant parts is 12 to 18 times higher for hexavalent than for trivalent chromium.[1] These two species have an independent mechanisms of uptake.[17] The uptake of Cr(III) is passive diffusion and this ion interacts with cell walls through cation-exchange sites.[2,18] Absorption of hexavalent chromium depends on metabolic energy of plants.[2] Cr(VI)

moves more easily from the roots to upper plants tissues because of the absorption, especially of its $Cr_2O_4^{2-}$ form, as an active process, probably correlates with the sulfate transport system located in the plasma membrane.[3,4,19] It is important to stress that despite of the easy way of Cr(VI) absorption, the fact that the *TI* values were not very high is probably due to the ability of the plant to reduce Cr(VI) to the less toxic Cr(III) form at the roots level.[1,10,20] The reduction could be catalyzed by Fe-3-reductase enzymes.[8] This is probably one of the natural plant mechanisms enabling tolerance to high concentrations of chromium.

Bearing in mind possible slight changes of acidity in the environment, it is important to stress that the *TI* values of Cr(III) showed no changes with increasing pH from natural 6 to 7 (Table IV) at all investigated concentration levels in the soil.

However, an increasing tendency of *TI* was noticed at pH 5 (Table IV), which suggests a changed ability of roots and herbal parts to accumulate chromium. From the obtained results, a higher mobility of chromium in the soil at lower acidity could be assumed.[13,21] This is in accordance to other findings that oxidation of Cr(III) to much more mobile Cr(VI) in soil is increased at pH 5.[8] This process is generally very slow under conditions of natural normal acidity.

Being a non-essential element and also toxic for plants, there is no specific mechanism for chromium transport through plants and this metal is known to compete with iron and manganese for transport binding sites.[10] The concentration of manganese generally decreased with increasing Cr levels.[10] The present results (Figs. 1a–1c, Tables II and III) do not show significant correlations between the Cr(III) and Cr(VI) contents in the roots and herbal parts and the concentrations of manganese at the investigated acidity levels. Dube *et al*. came to a similar conclusion.[7] However, comparing the Cr(III) concentrations with the concentrations of Fe (Table II), a negative correlation (R^2 = 0.9851) was noticed in the herbal part of *M. piperita* (Fig. 2). Torrestday *et al*. reported a decrease of the iron concentration in leaf tissue in response to chromium toxicity.[1]

The similarity of the ionic radii of Cr^{3+} and Fe^{3+} species may enable the replacement of iron with chromium in the heme proteins.[3,8,9] It has been found a high correlation between chlorophyll pigments and Fe uptake in chromium stressed plants was found.[6] Despite the similar chemical characteristics of Fe(III) and Cr(III), much higher concentrations of iron (263.0 to 408.6 mg kg^{-1}) than chromium (0.161 to 2.825 mg kg^{-1}) were present in the investigated samples (Table II; Figs. 1a–1c).There is a reasonable explanation for the high immobility of chromium in soil–plant systems: no reduction of Cr(III) to Cr(II) is observed under natural conditions while a relatively easy reduction of Fe(III) to Fe(II) can occur.[5,8,13] A comparison with the control plant samples showed that the concentrations of Fe in the roots was not significantly affected.

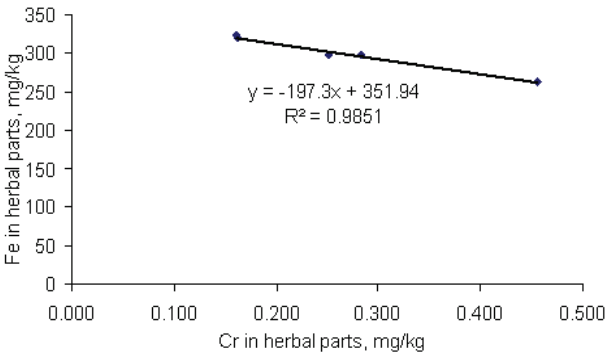

Fig. 2. Correlation graphs of the chromium and iron content in the herbal parts of *M. piperita*.

CONCLUSIONS

In this study, the capacity of the medicinal plant *Mentha piperita* (*L. Lamiaceae*) to control chromium uptake and its tolerance limit on soils treated with different chromium concentrations under conditions of three different pH levels were analyzed.

In order to realize this, *M. piperita* was cultivated under controlled laboratory conditions on soils treated with different concentrations of trivalent and hexavalent chromium.

The obtained results showed relatively low uptakes of chromium by *M. piperita* for all types of soils, treated with both trivalent and hexavalent chromium, at all the investigated pH values, probably due to the good immobilization of chromium in the soil matrix. The total chromium content in the plant, in general, increased with increasing soil concentration of the metal. These concentrations were several times higher in the roots than in the herbal parts of plant which indicated a very good root holding capacity (around 90 %). Exceptions were noticed with plants grown on the more acidic soils (pH 5) because of a poorer holding capacity of roots, probably as a result of damage to the membranes of the root cells.

The translocation indexes calculated for Cr(III)-contaminated plants showed low mobility of this chromium species, which is in correlation with its passive mechanism of uptake. In addition, the negative correlation between the Cr(III) and the Fe concentrations in the herbal plant parts confirms their competition for the transport binding sites.

The obtained results for Cr(VI) showed a very high mobility of hexavalent chromium through the plants tissues, which is in correlation with active uptake mechanism of this chromium species.

The medicinal plant *M. piperita* L. *(Lamiaceae*) analyzed in this work had a large capacity for binding chromium in the root system, which is a very important protection mechanism of the plant from the toxic action of this metal.

Acknowledgements. This work was supported by the Ministry of Science and Technological Development under Project No. 142039. The authors wish to thank Dr Radoslav Jevđović from the "Dr Josif Pančić" Institute for Medical Plant Research in Pančevo, Serbia, for helpful advice in the experimental work.

И З В О Д

АНАЛИЗА БИОДОСТУПНОСТИ Cr(III) И Cr(VI) ЗАСНОВАНА НА ОДРЕЂИВАЊУ ХРОМА У БИЉЦИ *Mentha piperita* МЕТОДОМ АТОМСКЕ АПСОРПЦИОНЕ СПЕКТРОМЕТРИЈЕ СА ГРАФИТНОМ КИВЕТОМ

СВЕТЛАНА ЂОГО[1], СЛАВИЦА РАЖИЋ[1], ДРАГАН МАНОЈЛОВИЋ[2] и ЛАТИНКА СЛАВКОВИЋ[3]

[1]Институт за аналитичку хемију Фармацеутског факултета Универзитета у Београду, п. пр. 146, 11211 Београд, [2]Хемијски факултет Универзитета у Београду, Студентски трг 12–16, 11000 Београд и [3]Институт за нуклеарне науке Винча, п. пр. 522, 11522 Београд

Циљ овог рада је био анализа лимита толеранције за усвајање Cr(III) и Cr(VI) из загађеног земљишта и одређивање капацитета медицинске биљке *Mentha piperita* (*L. Lamiaceae*) ради контроле уноса овог метала. Биљке су узгајане у пластичним посудама, при собној температури од 25 °C и одржаваној влажности земљишта на око 80 % ретенционог воденог капацитета. Земљиште на коме су биљке узгајане контаминирано је раствором Cr(III)-нитрата (40, 80, 120, и 200 mg kg^{-1}) и $K_2Cr_2O_7$ (2,5; 5; 10; и 15 mg kg^{-1}). Контролна група биљака је расла под истим условима без додавања хрома. За сваку концентрацију хрома у земљишту припремане су серије узорака на три нивоа киселости: природни и за по једну јединицу киселији и базнији (pH_2 6, pH_1 5 and pH_3 7). Узорци биљака су припремани за анализу према стандардној процедури и хром је одређиван методом атомске апсорпционе спектрометрије са графитном кивету, GFAAS. За узорке на сва три нивоа киселости израчунат је транспортациони индекс и добијене вредности су у следећим интервалима: 0,21–0,80; 0,06–1,06; 0,04––0,52. Тачност методе (72,73–115,3 %) је потврђена анализом хрома у узорцима стандардних референтних материјала (NIST SRM 8433 – Corn Bran and NIST SRM 1547 – Peach Leaves). Мобилност хрома из кореновог система у надземни део биљке је дискутована и са аспекта компетиције са гвожђем и манганом за иста транспортна места, па су у том смислу у узорцима одређене и концентрације ових метала.

(Примљено 1. априла, ревидирано 12. јула 2010)

REFERENCES

1. J. L. Gardea-Torresdey, G. de la Rosa, J. R. Peralta-Videa, M. Montes, G. Cruz-Jimenez, I. Cano-Aguilera, *Arch. Environ. Contam. Toxicol.* **48** (2005) 225
2. A. Zayed, C. M. Lytle, J. H. Qian, N. Terry, *Planta* **206** (1998) 293
3. N. Pandey, C. P. Sharma, *Environ. Exp. Bot.* **49** (2003) 195
4. Y. J. Kim, J. H. Kim, C. E. Lee, Y. G. Mok, J. S. Choi, H. S. Shin, S. Hwang, *FEBS Lett.* **580** (2006) 206
5. A. Kabata-Pendias, H. Pendias, *Trace Elements in Soils and Plants*, 3rd ed., CRC Press, Boca Raton, FL, 2001, p. 253
6. J. Barcelo, C. Poschenrieder, *J. Plant Natur.* **8** (1985) 211
7. B. K. Dube, K. Tewari, J. Chatterjee, C. Chatterjee, *Chemosphere* **53** (2003) 1147
8. A. M. Zayed, N. Terry, *Plant Soil* **249** (2003) 139
9. J. R. Peralta-Videa, M. L. Lopez, M. Narayan, G. Saupe, J. Gardea-Torresdey, *Int. J. Biochem. Cell B* **41** (2009) 1665

10. A. K. Shanker, C. Cervantes, H. Loza-Tavera, S. Avudainayagam, *Environ. Int.* **31** (2005) 739
11. S. Ražić, A. Onjia, S. Đogo, L. Slavković, *J. Serb. Chem. Soc.* **71** (2006) 1095
12. V. N. Simakov, Pochvovedenie **8** (1957) 72 (in Russian)
13. S. Ražić, S. Đogo, *Chemosphere* **78** (2010) 451
14. *SW-846 EPA Method 3051A, Microwave Assisted Acid Digestion of Sediments, Sludges, Soils and Oils*, in *Test Methods for Evaluating Solid Waste*, 3rd ed., 1994
15. M. J. I. Mattina, W. Lannucci-Berger, C. Musante, J. C. White, *Environ. Pollut.* **124** (2003) 375
16. M. Gosh, S. P. Singh, *Appl. Ecol. Environ. Res.* **3** (2005) 67
17. L. Jean, F. Bordas, C. Gautier-Moussard, P. Vernay, A. Hitmi, J. C. Bollinger, *Environ. Pollut.* **153** (2008) 555
18. F. X. Han, B. B. Maruthi Sridhar, D. L. Monts, Y. Su, *New Phytologist* **162** (2004) 189
19. P. A. Mangabeira, K. L. Gavrilov, A. A. Furtado de Almeida, A. H. Oliveira, M. I. Severo, T. S. Rosa, D. da Costa Silva, L. Labejof, F. Escaig, R. Levi-Setti, M. S. Mielke, F. G. Loustalot, P. Galle, *Appl. Surf. Sci.* **252** (2006) 3488
20. J. Khairiah, Y. H. Yin, K. N. Ibrahim, A. W. Wee, A. Aminah, A. Maimon, M. K. Zalifah, G. A. Giber, *Pak. J. Biol. Sci.* **5** (2002) 471
21. D. C. Adriano, *Trace Elements in the Terrestrial Environment: Biogeochemistry, Bioavailability and Risks of Metals*, Springer-Verlag, New York, Berlin, Heidelberg, 2001, p. 315.